PORE STRUCTURE AND OIL FLOW THROUGH HARDENED CEMENT PASTE, MORTAR AND CONCRETE

by

DANIEL CHIEDU OKPALA

B.Eng Hons (Benin-Nigeria) M.Eng (Sheffield)

Thesis submitted to the
University of Sheffield
for the Degree of
Doctor of Philosophy
in the Faculty of Engineering

Department of Civil and Structural Engineering

October 1982

TO MY MOTHER

WITH

LOTS OF LOVE AND RESPECT

SUMMARY

Increased oil exploration necessitates building of concrete structures for its production and storage. The effects of crude oil on concrete properties are not well known and little data is available in the published works.

This investigation covers HCP, mortar and concrete. First, it studies the effects of cracking and direction of casting on the flow of water or oil of different constitutions through concrete storage tanks. Secondly, it studies the relationships between the pore structure and permeability of HCP, mortar and concrete as influenced by w/c ratio, hydration and aggregate content. OPC was used for the tests.

Experimental results show that, in concrete specimens, the flow of water through cracks is generally greater than the flow of crude oil through the same type of cracks. Sorptivity can predict reasonably accurately the flow of liquids and is useful in characterizing the flow of various oil types through HCP, mortar and concrete. No specific oil property appears to control the oil flow through cement composites. Concrete tanks should be lined when used for storing diesel and parafin. Crude oil flow through concrete tank wall was found to be 1.06 - 1.81 times flow through the tank floor.

Increasing the w/c ratio, increases the total porosity, pore surface area and threshold radius but decreases the density and does not effect the hydraulic radius. Increasing the age of HCP (w/c = 0.7) from 7 days to 6 months decreases the total porosity, pore surface area, threshold radius and hydraulic radius by 12%, 19%, 71% and 9% respectively, but increases the density by 13%. Adding sand to HCP, reduces the total pore volume and the pore surface area but increases the density. Wax deposits from the crude oils blocked all pore radii <650Å, which is called the "critical pore radius" (P_{cr}). Saturation in crude oil appears to alter

the internal structure of the cement composites. Dry curing increased most pore parameters but decreased the strength of the mortars.

Permeability of mortar and concrete increases with w/c ratio, applied pressure, aggregate volume concentration and drying temperature but decreases with the test period and hydration. Permeability was found to relate reasonably accurately to pore structure using Kozeny's theory provided the pore parameters are for pores of radii >650Å.

ACKNOWLEDGEMENTS

The author wishes to thank Professor T. H. Hanna and the Department of Civil and Structural Engineering of the University of Śheffield for providing the facilities for conducting this research.

His greatest gratitude goes to Dr. A. J. Watson, for his constant encouragement, criticisms and supervision throughout the period of the research. My thanks go also to Dr. B Rand and the Department of Ceramics, Glasses and Polymers for providing the mercury porosimeter for the pore structure analysis.

The author also acknowledges the assistance of both the clerical and technical staffs in this department, in particular, Messrs. R. Newman, A. R. Hook, Dick Smith, D. Derek, G. Anthony and to Mr. M. Procter of the Electronics Department for his assistance. Acknowledgements are due to Mr. Wright in the Department of Chemistry for analysing the crude oil samples and Mrs. N. Parkes for her careful typing of the manuscripts.

My thanks go to my wife, Obiageli for her understanding and encouragement at difficult times and to my elder brother, Mr Becco Okpala for his financial support.

CONTENTS

LIST OF FIGURES

LIST OF TABLES

LIST OF PLATES

NOTATIONS AND ABBREVIATIONS

$\mathring{A}$	Angstrom Unit = 10^{-10} metre
C	Cement Weight (kg)
I_o	Loss on ignition (gm/gm)
K	Coefficient of Permeability (m/sec)
m	Degree of Hydration (%)
ϵ	Porosity (cc/cc or cc/gm)
r	Regression Coefficient
r_h	Hydraulic Radius (A)
W_n	Non-evaporable Water content (gm)
W_o	Non-evaporable Water of fully hydrated HCP
ΔP	Pressure Difference (N/m^2)
Q	Volume Flow Rate (m^3/s)
A	Cross-Sectional Area (m^2)
V	Velocity (m/s)
S	Sorptivity $(m/s^{\frac{1}{2}})$
V_p	Pore Volume cm^3/cm^3
S_e	Effective Surface Area $(m^2/gm$ or $m^2/m^3)$
RH	Relative Humidity
OPC	Ordinary Portland Cement
w/c	Water/Cement Ratio
c/s	Cement/Sand Ratio
C.T.R.	Constant Temperature Room $16 \pm 0.5^{\circ}C$, $50 \pm 1\%$ RH
C.O.V.	Coefficient of Variation
exp	Exponent
C-S-H	Calcium Silicate Hydrate
HCP	Hardened Cement Paste
CIRC	Circular Cracks
STRA	Straight Trough Cracks
SINUTH	Cracks Sinusoidal Across the Thickness
SINUDIA	Cracks Sinusoidal Along the Diameter
NATU	Natural Cracks
A.C.I.	American Concrete Institute
A.S.T.M.	American Society for Testing and Materials
cs	Centistokes
SSD	Saturated Surface Dry
I.C.E.	Institution of Civil Engineers
A.S.C.E.	American Society of Civil Engineers

NOTE: Other notations and abbreviations used in this thesis are described at the appropriate places.

CHAPTER 1

INTRODUCTION

1.1 General Introduction

The increasing production of crude oil and its distillates requires increased storage facilities and both steel and concrete tanks are presently being used for this purpose. A literature survey of published work relevant to this study is given in Chapter 2. A survey of tanks in use[1], reveals that steel tanks have a lower initial cost than concrete tanks but concrete tanks offer much better economy through their service life. In some developing countries, where the production of steel is very low, concrete tanks offer greater economy both in the short and long term. Other advantages of concrete tanks over steel tanks include durability and safety especially when used as underground tanks, sea tanks and floating drilling platforms, with underwater storage facilities.

The use of concrete tanks for the storage of petroleum products started as early as 1914[2], but without much success because the concrete was permeable and its use was discontinued. However during World War II, concrete was again used because steel was in short supply. Many concrete tanks were used for storing aviation gasoline, which is a very light crude oil distillate, and as a result severe leakage occurred. To obviate this problem therefore, protective linings were introduced [3, 4]. Currently many concrete tanks for storing crude oil are in use. These include the Ekofisk Oil Field[5] and the Shell-Esso Brent Offshore Oil Field[6, 7].

Marion and Mehfouz[8], without giving much detail, stated that there was no noticeable deterioration of the concrete in contact with the crude oil and no significant penetration of the oil into the concrete. It was also mentioned[9], though without any substantiation, that concrete tanks without any form of lining or coating are adequate for the storage

of heavy petroleum products having a specific gravity not less than 0.875. These views however were not shared by all the researchers. Meissner and Pearson[10] observed a reduction in compressive strength of concrete specimens soaked in aviation gasoline for 180 days. This was supported by Hansen[11] who also stated that creep rate of concrete, saturated with parafin oil after 5 years increased much faster than those in air or water. Lea[12] found out that petroleum distillates, with a low sulphur content, have no general effect on the mature concrete, but that the steel reinforcements were heavily corroded and on heating burnt fiercely.

It is a well accepted fact that if full utilization and exploitation of any material is to be realized, a great deal should be known of its basic structure and properties. Work related to the use of concrete oil storage tanks has been continuing in this department for the past nine years[13-17]. Matti[13, 14] and Faiyadh[15, 16] investigated the effects of crude oil on some material and mechanical properties of concrete and also studied the permeability of concrete to crude oil. Oyeka[17], investigated the pore structure, using a water absorption method, and the effect of pore parameters on the permeability of Hardened Cement Paste (HCP) and concrete. This work is continued in the present investigation and Chapter 3 describes the experimental programme, materials and preparation of specimens.

1.2 Purpose of the Present Research

This investigation is divided into two major parts.

1. To study the influence of cracking and direction of casting on the permeability and the performance of concrete storage tanks containing oils of different constitution.

(a) Chapter 4 describes the experiments to measure North Sea crude oil and water flow through cracks of different width and shape. The

purpose of the tests was to estimate limiting values for oil impermeability. Crack widths from 0.05 to 0.3mm were tested for oil and water flow at liquid pressure head of between 8.30 and 83.0 metres. The following crack patterns were studied, circular cracks (CIRC), cracks sinusoidal along the diameter of specimens (SINUDIA), cracks sinusoidal across the thickness of specimen (SINUTH), straight through cracks (STRA) and natural cracks (NATU).

(b) Chapter 5 describes experiments to measure oil permeability and absorption parallel and perpendicular to the direction of casting. This is to ascertain the performance of the floor and the wall of a tank. The oil properties such as density, molecular size, wax content and viscosity were varied to determine their influence on the absorption and permeability of HCP, mortar and concrete.

2. To study the internal structure of cement paste, mortar and concrete, to determine if there is a definable relationship between the pore parameters and permeability.

(a) Chapter 6 describes the experimental determination of some pore parameters such as total porosity, intruded pore volume, surface area, hydraulic radius etc, for variation in w/c ratio, period of hydration and fine and coarse aggregate inclusions. It also incorporates the study of the effect of saturating HCP, mortar and concrete in various types of oil such as crude oil, diesel and parafin, and the effect of curing condition on the pore structure.

(b) Chapter 7 describes the experimental determination of permeability for mortar and concrete specimens for various mix parameters, period of hydration and specimen dimension. In Chapter 8, relationships between the measured pore parameters and permeability are presented. An attempt is also made to identify the most reliable pore structure parameters that could describe the flow of oil through mortar and concrete. Interpretations of some functional relationships between the measured parameters

of pore structure are deduced and a method of determining the permeability from the measured parameters is suggested.

The conclusions from the work are presented in Chapter 9, together with some suggestions for further investigation.

CHAPTER 2

LITERATURE REVIEW

2.1 Introduction

The review consists of three main sections.

Section 2.2 summarizes the nature of crack formation in cement paste, mortar and concrete (plain and reinforced). Mathematical formulations relating flow to crack characteristics were also reviewed.

Section 2.3 reviews the literature dealing with the internal structure of HCP, mortar and concrete. Models of HCP were cited and methods of determining pore parameters investigated.

Section 2.4 deals with permeability of HCP, mortar and concrete. Theories associated with permeability were reviewed. Theoretical models of pore systems, designed to enable permeability through the system to be ascertained were looked into. Permeability results for cement and its composites were cited and semi-empirical relations correlating pore structure and permeability investigated. Finally a summary of methods of permeability determination is given.

2.2 Fluid flow through cracks in concrete

Crack formation in concrete has been studied vigorously[18-20] since the pioneering work of Richart, Brandtzaer and Brown[21] in 1928. However despite this enormous work, precise details of the process of crack initiation and propagation are still not clear, especially the fracture mechanics of the process and the microstructural characteristics. In a recent paper by Mindess and Diamond[22], some deductions which may be of value to the determination of fluid flow through cracks were presented. These include

(a) The crack is tortuous.

(b) Branch cracks exist, but these are fairly widely spaced and do not appear to form a continuous network.

(c) Discontinuities or jumps between regions of the main cracks were observed.

(d) There may be some tearing away of small bits of materials at areas where crack branching occurred.

Although these observations were made on micro-cracks Derucher[23] revealed that at loads of approximately 75% of the ultimate strength of the concrete, the bridging of the matrix micro-cracks begins and as the compressive stress field is further increased, these cracks continue to widen to macro-cracks and propagate in an unstable manner until failure occurs.

Beeby[24] described cracking in a reinforced concrete structure as a semi-random phenomenon depending both on material properties, loads, accuracy of workmanship, and on the size, shape and disposition of individual pieces of aggregate and the exact position of distribution reinforcement in relation to the section under maximum stress.

A detailed description of fracture mechanics is not intended here, but the above points are to highlight the fact that cracks in plain or reinforced concrete structure are inevitable. In fact it is well documented[18], that micro-cracks occur prior to any application of loads.

Allowable crack widths for the structures covered by the code of practice for retaining water and other aqueous liquids[25] need to be checked for crude oil and other volatile liquids. Moreover Beeby[24] argues that the limited crack widths, recommended in the code are not meant to cover water-tightness. He suggested that research be carried out, to ascertain acceptable crack width for water tightness. Anchor[26] states that cracks of limited width do not allow liquid to flow, or if percolation of liquid does occur initially, it may be subsequently sealed by

autogenous healing. He therefore suggests that for design, a limiting crack width can be specified. Neville[27], observed that autogenous healing is probably due to continued hydration, and may also be aided by carbonation. Application of pressure across the crack also assists healing. In the present investigation therefore attempts will be made to define an allowable crack width for crude oil tightness.

2.2.1 Mathematical formulations

Previous laboratory investigations[28] on air flow through ventilators and gaps around windows and doors found that, the rate of air flow was proportional to the square root of the pressure difference (ΔP) acting across the gap, and arrived at the equation (2.1)

$$\Delta P = 1.4\ Q^2/A^2 \qquad (2.1)$$

where Q = volume flow rate m^3/s

A = cross-sectional area of gap m^2

This equation was later found to deviate in practice because[29]

1. The open area A increases, as the pressure difference ΔP increases due to distortion of the gaps.
2. The numerical constant incorporates a discharge coefficient so any variation in discharge coefficient, introduces a corresponding variation in the constant.
3. The square law approximation is not strictly true for all types of gap, gap geometries and pressure difference.

A further investigation by the British Gas[29], showed that equation (2.1), when written as shown in equation (2.2) would be satisfactory for on-site determination of adventitious open areas.

$$\Delta P = 1.4\ (Q/A)^{1.6} \qquad (2.2)$$

Equations 2.1 and 2.2 may not however be satisfactory for the determination of liquid flow through cracks. This is primarily because

(a) For a practising engineer, an estimation of the depth of liquid in a containing vessel may be less time consuming than a determination of pressure drop across the vessel. Hence an equation involving a total liquid head may be more adequate.

(b) The equation is derived for air flow, which is a lighter fluid than oil or water.

The equations however show that

$$\Delta P \propto (Q/A)^n \tag{2.3}$$

Also $$\Delta P \propto h \tag{2.4}$$

$$\therefore \quad h \propto (Q/A)^m \tag{2.5}$$

i.e. $$h \propto V^m \tag{2.6}$$

$$\therefore \quad h = kV^m \tag{2.7}$$

Where $V = Q/A$ = velocity of liquid (m/s)

h = total pressure head (i.e. height of liquid in the tank), metre head of liquid

k, n and m are constants

Attempts will be made in Chapter 4 to relate h to some function of velocity in the present research. It is envisaged that such empirical relations would be of great value to the design engineer.

Equations 2.1 to 2.7, are however not dimensionally homogeneous, thus they do not obey the fundamental law of fluid mechanics (i.e. Reynolds law of similitude). To attempt a theoretical analysis of the problem, the principle involved in the fluid flow through pipes would be applied to fluid flow through cracks, and appropriate modifications made to allow for crack geometry.

Dimensional analysis can be used to obtain dimensionless

groups which describe the flow through geometrically similar pipes [30-33].

$$\text{For pipe flow } \frac{\Delta P}{\frac{1}{2}\rho V^2} = f\left(\frac{V.D}{\nu}\right) = f(Re) \qquad (2.8)$$

where Re = Reynolds No. $= \frac{VD}{\nu}$

ΔP = pressure difference N/m^2

V = velocity of fluid m/s

ρ = density of fluid kg/m^3

D = diameter of pipe m

ν = kinematic viscosity m^2/s

For the flow through geometrically similar cracks therefore

$$\frac{\Delta P}{\frac{1}{2}\rho V^2} = f\left(\frac{V.d_n}{\nu}\right) = f(Re) \qquad (2.9)\ [29]$$

where d_n = hydraulic diameter of crack m

$$d_n = \frac{4(\text{fluid flow cross-section area})}{\text{wetted circumference}}$$

$$d_n = \frac{4A}{\text{wetted circumference}} \qquad (2.10)$$

A = cross-sectional area m^2

Putting $V = Q/A$, and defining

$$C_D = Q/A\ \sqrt{\rho/2\Delta P} \qquad (2.11)$$

Equation 2.9 becomes

$$\frac{1}{C_D^2} = f(Re) \qquad (2.12)$$

C_D = discharge coefficient (dimensionless)

For crack of length 1, width y

$$d_n = \frac{1.y}{2(1+y)} \qquad (2.13)$$

For crack of length = 150mm, width 0.3 (maximum crack width used)

$1 >>> y$, $\therefore \quad 1 + y \simeq 1$

$$\therefore \quad d_n = 1.y/21 = y/2 \tag{2.14}$$

Also by analogy with pipe flow, the ratio z/d_n, could be a dimensionless parameter

$$\therefore \quad C_D = f(Re, z/d_n) \tag{2.15}$$

where z = crack depth

A theoretical analysis, based on equation (2.15) carried out by Hopkins and Hansford[29] (and later modified by Etheridge[34]) obtained a functional relationship between the dimensionless ratios, as given in equation 2.16.

$$\frac{1}{C_D^2} = C_A \frac{z}{Red_n} + C_1 \tag{2.16}$$

where C_1 is a constant

C_A is an apparent coefficient which depends on aspect ratio z/y, and Reynolds No. Re.

Etheridge modified equation 2.16 to obtain

for laminar flow

$$\frac{1}{C_D^2} = 96 \frac{z}{Red_n} + C_1 \tag{2.17}$$

for turbulent flow

$$\frac{1}{C_D^2} = 96 \frac{z}{Re^{0.25} d_n} + C_2 \tag{2.18}$$

Equation 2.16 appears to be most suitable, since C_A could account for other uncertainties, such as characteristics of the flow surface and fluid properties (e.g. wax content). While deriving equation

2.17, assumptions of ideal fluid flowing on perfectly smooth surface was made. This condition is not applicable to real fluids flowing on rough surfaces.

The investigation therefore intends to find out whether this theory is applicable to oil and water flow through cracks (of varying shapes and dimensions) in concrete. If experimental results hold reasonably well with the theoretical predictions of equations 2.16, it follows therefore that oil and water flow through cracks in concrete can be described adequately by the fundamental law of fluid dynamics (i.e. the Reynolds law of similitude).

2.3 Pore structure of hardened cement paste (HCP), mortar and concrete

2.3.1 Importance of pore structure

The importance of specific surface area (i.e. the surface area of pores per unit weight or volume of the substance) and the total pore volume has been recognized for a long time[35]. It has been established that there is an exponential decrease in the strength of concrete with increasing porosity of HCP[36-39]. This is because the strength is in the solid and not in the pores. This relationship was also observed in other brittle materials in which water leaves pores behind[40, 41, 42]. It is known that drying shrinkage is a volume change associated with the removal of water from the pores of the paste. If a fully saturated specimen is placed in a dry environment, until equilibrium is reached, the core of the specimen will have a higher degree of saturation than the outer part due to loss of moisture from the pores[43]. This differential moisture content sets up stresses which may cause micro-cracking and thereby damage the concrete[44-46]. Reversible and irreversible shrinkage was found to have linear relationship with porosity[47]. Evidence also shows that elastic

modulus varies linearly with porosity.

Pores influence the process of hydration in cement paste. Once the cement paste hardens, its total volume and void volume are determined. Since the specific volume of the hydration product is larger than that of the unhydrated material, as hydration process proceeds, the pores of the paste are slowly filled with the hydration products. In very small pores, hydration stops because there isn't enough room for the hydration products to nucleate and grow into crystals. This limitation could effect the strength development of the paste, but may be useful in preventing damage due to freezing and thawing of water in concrete[50]. It has also been shown that the characteristics of the pore system in cement paste influences to a great extent the permeability of the paste. This will be discussed fully in section 2.4.4

2.3.2 Formation of calcium silicate hydrate (C-S-H)

The nature of formation of C-S-H, is clearly stated by Newman[51]. Immediately after mixing, the unhydrated cement particles in a fresh cement paste are dispersed in an aqueous solution. During the first few minutes, the reaction rate is very rapid and calcium silicate hydrate, usually called cement gel, forms a coating around the cement grains. As hydration continues, hydration products, including calcium hydroxide are precipitated from the saturated solution in the capillary pores. Ishai[52] observed hydration as comprising of an inward process resulting in an increase in the thickness of the amorphous gel coating, and outward process as the calcium silicate ions diffuse through the coating and then crystallize outside it in a layer forming tobermorite. These tobermorites were formed in narrow spaces between adjoining cement particles, thereby resulting in a higher density crystallites. These form solid links between the coated cement particles, so producing a continuous

solid matrix within the hardened cement paste.

It was also observed that in a hardened cement paste (HCP), calcium silicate hydrate (C-S-H), which exhibits various degrees of physical and chemical bonding forces with water within the paste, forms a large proportion of the solid phase of the paste[52].

Available information reveals[53, 54, 55], that for a completely hydrated paste, the hydrated product occupies a little more than twice the volume of the cement from which it was derived. Therefore when the hydration is complete, the gel occupies the space once occupied by the cement grains and some or all of the interstitial space originally filled with water. For water-cement ratio less than 0.38, incomplete hydration is obtained as a result of insufficient space for hydrated products to occupy while for w/c > 0.38, all the capillary spaces are not filled by the hydration product. It was also observed that once the paste is set, the total volume of the paste changes by less than 0.3% during the entire hydration period[55].

2.3.3 General description and classification

Pore space can be defined as that which exists between the matrix of the solid phases, hydrated and unhydrated. To separate the solid phase from the liquid phase therefore requires a thorough knowledge of the structure of particularly the C-S-H gel, hence the present definition of pore structure depends much on the current concepts of the structure of the C-S-H gel. In relation to the present investigation, classification of the pore system should be those based on size, interconnectivity, magnitudes of the fluid-solid interaction forces and the morphology of the pore space.

Dubinin et al[56] proposed an arbitrary but reasonable division of pore size ranges. They suggested that for a hypothetical

cylindrical pore shape model, the pores should be divided according to their radii, into three groups: (a) micropores having radii less than 16A°, (b) intermediate or mesopores with radii between 16 and 1000A°, and (c) macropores with radii greater than 1000A°. Karnoukov [57] in his model described pore morphology as comprising of (a) corpsular pore systems, obtained from the imperfect packing of the solid phases, and (b) spongy systems which are the channels and cavities with the solid phases. He[57] also suggested a globular model in which he described pore sizes in terms of pore throat diameter, and the number of contact points of globules in plane sections through a porous system. This useful information provided a possible way of obtaining pore structure information from electron micrographs. Karnaukov's morphological classification also suggests a two stage pore continuity - corpuscular and spongy pore continuities. This concept may be of great advantage in clarifying pore structure in relation to permeability.

Powers and Brownyard [55], utilized the B.E.T. theory[58] and obtained surface areas which are proportional to the non-evaporable water content of the paste. At vapour pressure of about 45 to 100% saturation, the amount of water absorbed was found to be proportional to the initial w/c ratio. Based on this, Powers divided the hardened cement paste into an aggregation of gel pores and capillary pores. Those occupied by water at vapour pressure < 0.45 were called gel pores while others were capillary pores. Mikhail et al[59] observed that gel pores have radii less than 20A°. Powers model seems to compare favourably with the morphological model of Kernaukov as shown in table 2.1.

The complex nature of the pore system necessitates that a pore shape model should be assumed. Often cylindrical, slit-like or spherical pores are assumed. In the present investigation, a cylindrical pore shape in HCP, mortar and concrete is assumed, for it is simple to apply and in

line with the theory developed for pore structure analysis using mercury intrusion porosimetry.

The three pore classifications described in this section are summarized in table 2.1 below

SIZE[56]	MORPHOLOGY[57]	HARDENED CEMENT PASTE[55]
Macropores Mesopores Micropores	corposcular spongy	capillary pores gel pores/interlayer spaces

TABLE 2.1 CLASSIFICATION OF PORE SYSTEM

2.3.4 Pore structure of hardened cement paste (HCP)

This section is devoted to the structure of hardened cement paste, based on Powers classification and its subsequent modifications. The pore structure of a porous material is defined by the following characteristics:

1. Porosity (ε) (cc/cc or cc/gm)

This is the fraction of the total volume occupied by pores Powers and Brownyard[55] defined the pores in the portland cement paste as the space in the paste that may be occupied by evaporable water. Evaporable water is that which exhibits a vapour pressure greater than about 6×10^{-4} mm of mercury at 23°C. They estimated this water to be equivalent to the water lost when a saturated paste is oven dried to a constant weight at 105°C.

2. Specific surface area (S.) (m^2/gm or m^2/m^3)

This is the total external surface area of solids per bulk volume or weight of solids.

3. Pore size distribution cm^3/gm

This is the fraction of total open pore volume in which the pores are within a stated size range.

4. Pore radius: (r_p) $\overset{0}{A}$

This varies along any given pore in all directions

5. Hydraulic radius (r_h) $\overset{0}{A}$

The ratio of pore volume to the surface area of the bounding solid.

6. Tortuosity (T)

Ratio of actual flow path length of fluid particles to the length of the porous material. This factor allows for the discrepancies between actual pore geometry and the hypothetical straight cylindrical model[58].

These averaging parameters do not necessarily provide all the details of the HCP pore structure, but together, they are useful for describing the flow of liquid through the hardened cement paste.

Applying the BET theory[58], Powers and Brownyard[55] obtained the surface areas of fully hydrated pastes to be of the order of 180-220 m^2/gm of dry pastes at a vapour pressure of 0.5μm of mercury (Hg) at 23°C. Within 10% variation, these values were found to be independent of the type of cement. Based on these observations and others (section 2.3.3), and also evidence from other investigators[59, 60], Powers[61] arrived at these very important deductions.

1. During hydration, some products are being formed and with such high surface areas, most are colloidal particles with at least one dimension between 10^{-9} and 10^{-6} meters.

2. The hydration products have characteristic porosity approximately 26% by volume, characteristic pores (gel pores of order 18-20$\overset{0}{A}$ in diameter) and occupy about twice the volume of the original reactants.

3. Pore space of hardened cement paste consists of gel pores within "cement gel" and capillary spaces originating from the initial water filled spaces. Hydration increases the volume of cement gel and reduces that of capillary pores without much change in the overall

volume of the hardened paste.

4. Capillary space may be rendered discontinuous by the growth of the cement-gel if the initial w/c ratio is less than 0.7.

From these observations, a model of HCP was proposed, and computations of total and capillary porosities based on the model carried out[61-64], using initial w/c ratios, degree of hydration and densities of the hydration products and unhydrated cement.

As other methods of obtaining pore characteristics emerged, this Powers model was modified by various researchers. Braunauer et al[65] investigated the nature of C-S-H obtained by reacting lime (CaO) and silica (SiO_2) in water, using X-ray differaction technique. This showed a layered structure, similar to that found in HCP. These were characteristics of the natural mineral tobermorite, and so Braunauer called the C-S-H gel, "tobermorite gel". On the basis of his work and other water vapour absorption studies, he suggested that cement hydrate consists of about 70% C-S-H gel, 20% calcium hydroxide, 7% ettringite and calcium aluminate monosulphate hydrate and 3% unhydrated clinker residue and other minor constituents.

Based on these new evidences, Powers modified his original ideas and emerged with a new model called "Powers-Braunauer" model and is summarized in ref. (66 and 67). This model saw C-S-H gel as being similar to hydrated product of tricalcium and β-dicalcium silicate, which is a poorly crystallized version of the mineral tobermorite. Since the structure of tobermorite is layered, the model considered C-S-H gel as units of two or three layers with each layer about 9 $\mathring{A}$ thick.

Feldman and others[68-71] suggested a model which saw C-S-H gel as a layer structured material, with layers that are irregular in thickness but approximately parallel. On drying these layers collapse on each other and remove the interlayer spaces. On exposure to increasing relative humidity after drying, permits gradual re-entry of water into

the inter-layer spaces. Due to this re-entry of water, water vapour adsorption isotherms yield surface areas that are too high. This model was applied by Feldman and others[72-75] in explaining the mechanisms of creep, shrinkage. modulus of elasticity and density changes in HCP.

2.3.4.1 Recent advance in models of cement paste

In recent years arguments tend to be centred on the validity of the different models rather than establishing new ones [71, 76-79]. Based on the pore structure results obtained using mercury intrusion porosimetry, Winslow and Diamond[80] suggested some very useful modifications to the Powers original postulations. Powers model interpreted hardened cement paste as a conglomeration of (1) cement gel, (2) calcium hydroxide and a small amount of other coarsely crystalline hydration product (3) residual unhydrated cement grains and (4) capillary pores - the remnant of water-filled space existing between the cement grains at the time of setting. The cement gel was viewed as consisting of a solid part, the finely divided or colloidal hydration products which are mostly calcium silicate hydrate, and a non-solid part, the "gel-pores". The pores were treated as intrinsic part of the gel and were said to occupy 28% of the volume of the gel. The gel pores are initially filled with water, but the water can be removed by evaporation like those in the capillary pores but at different temperatures. Diamond's modifications to this view are as summarized below.

1. The content of pores finer than 82Å, as estimated by the difference between intruded volume and total volume, is significantly less than the volume of gel pores assumed to be present in Power's model.

2. The content of pores between 0.1 and 0.01μm, (i.e. between capillary and gel pore sizes by the current notion) is found to be substantial at all ages.

3. The evidence therefore implies that most of the volume in HCP, is neither capillary nor gel porosity, but consists of spaces left between particulate hydration products found to be present in a scanning electron microscope observations.

These observations are quite important in the concept of permeability and pore size distribution and their relevance is to be sought in the present investigations.

Most of the discussions so far have concentrated on the physical and chemical properties of C-S-H gel. Recently however, to avoid erroneous conclusion derived from simple experimental data, it was suggested[81] that the mechanics of solid should be taken into consideration when describing the real strucutre of HCP. Another aspect under consideration is to formulate a statistically representative characterisation of the multi-phase complex microstructure. This may involve a probabilistic description of materials' properties. With these a computer simulation of the pore system is envisaged. This is however beyond the scope of the present investigation.

Up to the present date, the concept of the structure of HCP as consisting of three major components, vis: solid phase, pores and water are still valid but new models are also developing.

Wittman[82] developed a model known as "The Munich Model". This is based on sorption measurements with some additional informations from direct measurements of Vander-Waals forces at low distances. Thermodynamic calculations and experiments to determine creep, shrinkage and strength as functions of relative humidity also aided the development of the model. The model suggests that the influence of water content on the properties of HCP can be explained by means of two different phenomena. (1) The surface energy of the colloidal particles and (2) the disjoining pressure. In the region below 50% relative humidity (RH), all pore properties are predominantly influenced by the surface energy

of the gel particles. The surface energy changes due to sorption as the hygral equilibrium is changed. At higher R.H., gel particles are separated by thin water films due to the action of spreading pressure of water. In the high humidity region therefore, the xerogel (i.e. the structure of the solid phases), is mechanically less stable than in the dry state. Wittman claimed that his model has proved to be successful in predicting quantitatively, the properties of concrete.

Diamond[83], utilizing the suggestion made by Berger et al[84] classified C-S-H gel into four morphological types:

TYPE I Fibrous particles observed at the early ages of hydration. About 0.5 to 2μm in length, and usually less than 0.2μm across.

TYPE II Reticular network: Elongated particles of roughly the same cross-sectional dimensions as type I particles. Several branched portions diverge at considerable angles to form interconnected reticular network in three dimensions.

TYPE III Equant grain. These are rather common irregular equant or flattened particles.

TYPE IV Inner product: Maintained to an outer shell of other hydration products. This type is possibly filling the space originally occupied by C_3S. Has dimpled appearance with closely packed pores.

This classification however did not cover all the variety of different morphological details. Also many impurities have been detected in xerogel, to the extent that could affect these morphologies[85]. Wittman[81], therefore argues that considering the huge morphological variety in HCP, it may be impossible to relate mechanical and non-mechanical properties directly with these structural details.

The probable effect of w/c ratio on the morphology of the hydration product was studied by Midgley and Pettifer[86]. They found

that for high w/c ratios, both the fibrous and the crumpled foil forms of C-S-H gel were formed. This therefore indicates that porosity of the gel could vary with the w/c ratio.

Later development was in the use of trimethylsilylation in the determination of the degree of polymerization of silican (Si) in hydration product. Based on the earlier work by Lentz[87], Tamas et al[88] utilized the method in 1976. As a result of great successes found in this method recently, its application is spreading and new informations emerging from its usage[89-93] showed that 1. It seems that the structure of hydration products differs markedly from the quasi-crystalline C-S-H such as tobermorite or jennite as earlier believed. 2. There is no reason to believe that there is a layered structure. A new model however is yet to emerge from the latest findings and further test results are required to validate the method,

Another major area of contention in cement science is how to apportion the amounts of water present in hydrated calcium silicate, as interlayer, adsorbed and loosely held pore water, for the development of a correct model for the HCP. While carrying out work on the effect of frost action and ice formation in HCP, various authors[94-96] determined phase transitions of water held in the pore system. Wittman[81], reported the results of these investigations, as summarized by Stockhauser et al, who concluded that different modifcations of adsorbed and capillary condensated water can be distinguished as follows:

1. In capillaries with radius bigger than 100nm (1000A^0), bulk water is observed. These big pores are only filled if the sample is in direct contact with water.

2. Water condensated in capillaries with radius bigger than 10nm (100A^0) has a reduced chemical potential because of the interaction with the solid surfaces. As a result, the freezing point of this second

modification is shifted towards lower temperature. This type of water is taken up by capillary condensation at high vapour pressures, 90% ≤ RH ≤ 100%.

3. In still smaller capillaries, the condensated water is structural. The corresponding capillary radius may range between 3 and 10nm (30 to 100Å). These pores are filled by condensation between 60% to 90% R.H. The water undergoes a phase transition at a temperature of around 143°C.

4. Water adsorbed in layers not thicker than 2.5 monolayers. This type of water does not freeze until at a temperature of at least -160°C. The adsorbed films are firmly held on the surface but water molecules are very mobile within the layer.

These divisions were based on experiments carried out at temperatures below 0°C. However Wittman[81] indicated that the conclusions from the experiments may reasonably apply at room temperature. Very important deduction from the classification is the fact that the behaviour of the water molecule in a particular pore range could be associated with the pore size. This phenomenon may have some effect on the permeability of HCP and should be considered in the later chapters.

Despite these advances towards a more comprehensive understanding of the structure of HCP, it still appears that Powers model still gives the clearest quantitiative explanation of the structure of hardened cement paste.

2.3.5 Method of pore structure determination

The description of pore structure requires the determination of the total pore volume, the pore shape, pore surface and the distributions of the pore sizes. The two most widely employed methods of pore structure analysis are the sorption method by Wheller[97] and the mercury intrusion porosimetry by Ritter and Drake[98].

Evidence from several workers[55, 99-103] show that the adsorption method can only measure some meso and micro pores. In a critical comparison of the two methods Diamond[104] made some observations which could be of great value to a choice of method, when pore-structure is to be linked with permeability. His findings can be summarized as follows:-

1. Neither of the methods appear to be capable of recording all of the pore spaces in a given sample of cement paste.

2. For mercury porosimetry, the missing pores could be accepted to be not in the micropores which could not be intruded by mercury, but could be encapsulated pockets of gel, which cannot at any pressure be intruded by mercury. These encapsulated pockets, can also be difficult to fill by capillary condensation, except perhaps by a slow diffusion mechanism.

3. Measurements of the distribution of pore sizes in hydrated cement pastes differ considerably when using both methods. Mercury intrusion methods indicate that the entire distribution is much coarser than the capillary condensation results suggest. Also mercury porosimetry shows very much less pore space than capillary condensation results in sizes less than 100Å, and particularly less than 50Å in diameter.

4. Evidence available from other techniques such as scanning electron microscopy, x-ray small angle scattering[105] suggests the relative importance in cement pastes for pores with diameters larger than can be measured by capillary condensation and indicates that capillary condensation methods are relatively inadequate in describing the general character of pore sizes present.

5. Reported agreement between mercury porosimetry and capillary condensation results in the region of overlap for some materials other than HCP, and for some condensates indicates the prospective validity of both methods for pores larger than 30Å in diameter and smaller than

the upper limit of sizes measured by the capillary condensation technique. However the use of nitrogen as the condensate and the use of not wholly-appropriate "t" curves with other condensates may have caused the apparent discrepancies observed at the fine pore end of the distributions.

Mikhail et al[76] later argued in support of the adsorption method, as the best method for pore structure analysis of HCP. In a recent paper by Bentur[106], pore structure analysis of β-C_2S, C_3S and cement pastes were each carried out using mercury porosimetry, water adsorption and nitrogen adsorption method. It appears that, this is the only comparison that exist for the same sample in the available literatures. The following findings were made from the test.

1. The gas-adsorption tests were not sensitive to pores bigger than several hundredths of a micrometer in diameter, while the mercury porosimetry test is limited by its pressure capacity and could not detect pores which are smaller than 20Å in diameter (for the type of porosimeter used).

2. All the three test methods are theoretically effective in measuring the mesopore range.

3. Despite the second deduction, even in the limited meso-pore range, consistent conclusions cannot be drawn regarding the effect of the chemical composition of the hydrating product on its pore structure.

4. Interpretation of the water adsorption curves above $P/P_o = 0.40$ assuming only capillary condensation effects, as expected when using Kelvin equation[107], can lead to erroneous high values, which were in line with his water vapour adsorption results of pore volume and surface area.

5. Very little nitrogen penetrated into the micropores.

Another possible area which may be of interest soon is the conversion of intrusion-extrusion curves (i.e. the hysteresis) from

mercury porosimetry to condensation-evaporation isotherms. This method was proposed by Lowell[108] for use in obtaining larger pore size distribution. However its validity is yet to be ascertained.

It is logical to think that only larger pores should play major role in permeability of the porous materials. Also pore structure analysis of crude oil saturated paste reveals that (Chapter 6), most of the smaller pores (pores below 650$\mathring{A}$ in radius) were totally blocked by the probably waxy deposits of the oil. Hence the saturated permeability of the oil through the paste, mortar or concrete can only be achieved via the larger pores. The clugging characteristic was not observed in water saturated specimens, however, Mehta and Manmohan[109] observed that pores, with diameter less than 1320$\mathring{A}$, play insignificant role in water permeability through HCP. It there appears that large pores ($\geq$ 650$\mathring{A}$), should be the most important contributor to permeability. Hence the choice of mercury porosimetry method for the pore structure determination in the present research appears to be reasonable.

A very important observation from the work of Winslow, Diamond and Lowell[80, 110] using mercury porosimetry, is the identification of a"threshold diameter". After carrying out a series of carefully conducted tests, they deduced that

1. Above the threshold diameter, there is comparatively little intrusion into the paste and immediately below it, the greatest portion of the intrusion commences.

2. The threshold diameter decreases steadily with age.

3. A slowing down of the rate of penetration of mercury was observed while making intrusion measurements near the threshold diameter.

4. Fracture surfaces examined under the microscope revealed that, just below the threshold diameter many regions on the surface had little evidence of mercury penetration while just above the threshold

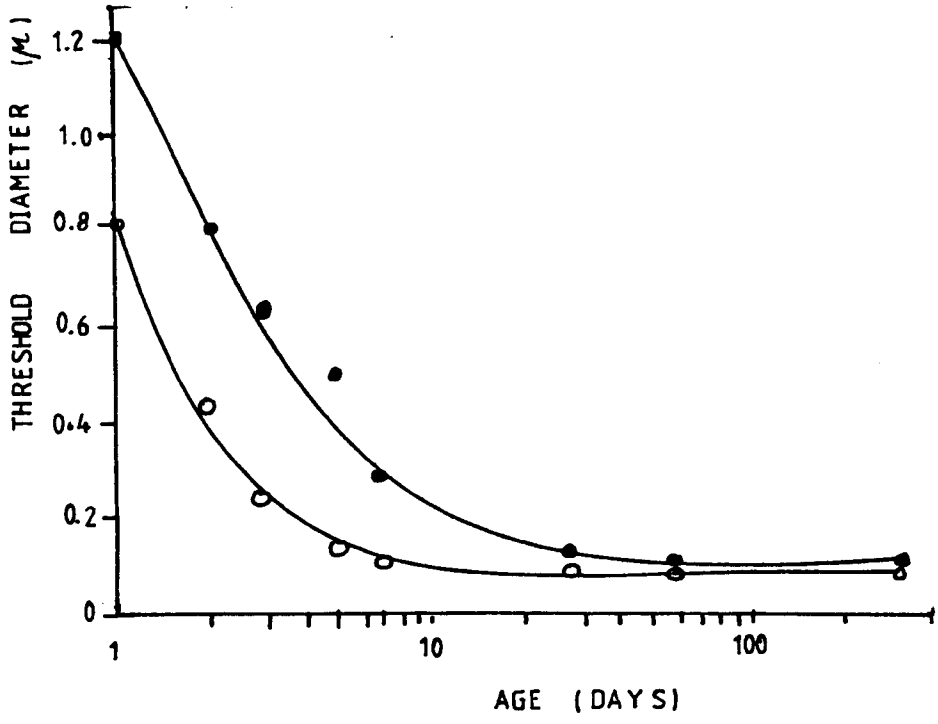

FIG 2.1 THRESHOLD DIAMETER AS A FUNCTION OF AGE FOR HCP[80]

diameter showed droplets of intruded mercury uniformly spaced over all the regions of the fracture surface.

These led to the deduction that threshold diameter represents the minimum diameter of pores which are geometrically continuous through out the regions of the hydrated cement paste. Winslow and Diamond, therefore defined the pore system of HCP as consisting of a geometrical system analogous in some respect to a finely branched river system, with relatively large pores intruded at the threshold diameter corresponding to the major rivers flowing through a geographical region while the rest of the pores correspond to local branch streams. The variation of threshold diameter with age is shown in Fig. 2.1, and obtained from ref (80). This very important pore parameter was also noted and confirmed for HCP, by other investigators[111-114]. Nyame and Illston[111,114] defined a "maximum continuous pore radius" as the pore radius at which dv/dp, from the mercury intrusion curve had a maximum value. This parameter is essentially the same as the Diamond's "threshold" radius. They found that this pore radius was related to water permeability for all the pastes tested. Their studies include pastes of w/c ratios between 0.23 to 1.00 hydrated for up to 20 months.

2.3.5.1 Sorption Method

One theory advanced to explain the adsorption of gases and vapours by solid materials is the multi-molecular adsorption theory or BET theory[58]. This rests on the fact that when a specimen of hardened cement paste or concrete at room temperature is exposed to water vapour or to air containing water vapour, its water content spontaneously changes until equilibrium between the water held in the specimen and the outside water vapour is established. Hence a specimen can remain saturated only when it is in contact with saturated vapour or liquid. The BET theory therefore requires that taking up of a gas or vapour by a solid is as a

result of physical attraction between the molecules of the gas and the surface molecules of the solid.

The amounts of adsorbate lost or gained with changes in relative gas or vapour pressure at constant temperatures can be measured to enable estimates of pore size distributions and surface areas of the solid phases of a porous solid to be carried out[108, 115]. It has been observed[45, 116, 117] that complications could arise when using the method for surface area determination of cement hydrate, because in cement paste, dehydration and rehydration can occur when water is used as the adsorbate.. However evidence obtained[66], using low angle x-ray method, show that the effect of dehydration and rehydration is negligible. Another source of doubt on the use of sorption method for surface area determination was based on theoretical grounds. The BET equation was derived based on layer by layer adsorption, but the micropores are filled by volume mechanism, as such the BET equation cannot give the correct surface area for micropores, hence some of the pore surface areas have been found to be excessively high[118, 119].

The Kelvin equation for condensation in capillaries used for pore parameter determination can be written as

$$\frac{P_r}{P_o} = \frac{-2\gamma\bar{V}\cos\theta}{rRT} \qquad (2.19)$$

where P_o = equilibrium vapour pressure of a liquid over a plane surface

P_r = the corresponding vapour pressure over a surface with radius r

γ = surface tension

$\bar{V}$ = molar volume

θ = contact angle of the liquid

R = gas constant

T = absolute temperature ^{o}K

According to the Kelvin equation, a vapour will condense into pores of radius r when the equality expressed in equation 2.19 is realized. The pore radius given in equation 2.19 is that part of the pore not covered by the adsorbed molecular layers, hence corrections are usually carried out for the thickness of the adsorbed film.

For a complete pore structure analysis of those pores that could be detected by the sorption method, two methods are developed.

1. Analysis of mesopores (i.e. pores in which capillary condensation and evaporation occurs). This is the modelless method which uses the hydraulic radius for analysis[120, 121].

2. Analysis of micro-pores "MP method", used for the determination of the parameters of pores less than 16$\overset{0}{A}$[121-124].

Various adsorbates such as nitrogen, argon or water vapours have been used by various investigators[59, 99, 125, 126] and there are conflicting arguments as to the suitability of each adsorbate[59, 68, 69, 70, 77].

2.3.5.2 Mercury porosimetry

The principle of mercury porosimetry technique, is based on the fact that mercury behaves as a non-wetting liquid (i.e. one forming a contact angle greater than 90^{o}) to most substances. Consequently it does not penetrate into the open pores and cracks in these substances because of surface tension effect (capillary depression). This resistance may be overcome by exerting a certain external pressure. The pressure applied is related to the pore size as shown in equation 2.20[80]

$$P = \frac{-4\gamma \cos \theta}{d} \qquad (2.20)$$

where P = absolute pressure exerted N/m^2

γ = surface tension of fluid MN/m

θ = contact angle between solid surfaces and liquid surface (degrees)
d = diameter of intruded pore A

Winslow and Diamond[80] measured the contact angle using samples obtained using two drying techniques. For P-dried HCP (i.e. drying over a mixture of magnesium perchlorate hydrates), the contact angle was found to be 130°, and for oven-dried pastes, θ = 117°. Contact angle determination however is faced with the problem that the solid surface is not the same as during mercury penetration into the porous body. Most solids have rough surfaces, and it has been stated[127] that roughness of the surface may increase the effective contact angle. It has also been suggested recently that because of the roughness and certain other geometrical properties of non-smooth, non-cylindrical pores, a good choice of contact angle should be around 180°[128]. The commonest reported angles are however between 130° to 140°[128]. Results obtained from contact angle measurements on large variety of samples, averaged to 141.3°, while surface tension measurements gave average value of 480 dynes/cm[129]. These values therefore were utilized in the present investigations. Despite these approximations, the nature of the porous media will remain unchanged throughout the pore range for a given sample. However, a displacement in absolute sense may occur in pressure-radius function of the pores, but the pore radius distribution remains correct in a relative sense. Further description of the method is given in Chapter 6.

2.3.5.3 Other Methods

Other methods that utilize the presence of a meniscus to characterize a pore system includes: suction (i,e, drainage and re-imbibition of a wetting liquid) and capillary condensation method. Also most transport phenomena in porous media, explain the pore characteristics in some way. These transport phenomena include molecular diffusion, viscous flow and heat conductivity.

More direct methods include the use of light microscope, electron microscope and in a limited pore size range, by the scattering of x-rays. These measurement techniques give fundamentally different kinds of information about the pore characteristics of porous media. At times however they lead to similar results, provided an adequate choice of variables is made[127].

Two other techniques worth mentioning are: 1. The quasi-elastic or inelastic neutron scattering method[130, 131], 2. The helium inflow and helium pyenometric technique[114, 117].

Method 1, is used to determine to a good approximation, the free and bound water in HCP. Detailed discussions of this method is available in refs (130, 131). Helium pyenometry employs the gas laws to determine solid volume by displacement principle. With the technique, changes in pore structure can be followed as water is removed from the system or as it re-enters the system [45, 116]. However results obtained from this technique have been questioned[81, 82]. Nyame[114] observed that the results from helium flow determination of total pore volume were very unreliable and preferred the use of weight loss on drying to a constant weight at 105^{o}C. However some researchers find the helium-pyenometry technique quite valuable[69, 132, 133].

2.4 Permeability of HCP, mortar and concrete

2.4.1 Introduction

Permeability is that property of a porous material which characterizes the ease with which a fluid may be made to flow through the material by an applied pressure gradient. It is the fluid conductivity of the porous material. The flow of fluid in a porous system is achieved when the state of equilibrium of fluid in the material is disturbed. This can be brought about by the gradient of the moisture contents, hydrostatic pressure, stress, temperature or concentration of chemicals.

The durability of concrete is adversely affected by its permeability, since permeability largely determines the vulnerability of concrete to external agencies[10], such as frost action. For reinforced concrete, the ingress of moisture and air may result in the corrosion of steel which invariably results in cracking and spalling of concrete cover. Permeability is also of interest in liquid retaining structure (Chapter 1). It affects the thermal insulation properties of concrete and is also of interest in the problems of hydrostatic pressure in the interior of dams[134].

2.4.2 Permeability theories

If the fluid state, that is its density, local velocities and temperature are assumed to be continuous functions of space and time, the equations of continuity and conservation of momentum could be applied to obtain full differential equations describing the motion of the fluid [135, 136]. The solution however requires the specification of the boundary conditions of the fluid and the solid phases of the material. In case of a porous material, especially hydrating cement paste or concrete, which is always in a state of change due to hydration, these boundary conditions are difficult to obtain. Hence empirical laws are often applied to obtain relationships between the gradients and the fluid flow.

2.4.2.1 Darcy's law

This law defines permeability in terms of measurable quantities. It is a semi-empirical law relating hydraulic gradient to the steady state rate of fluid flow in a saturated porous material, and is given as

$$Q = k \quad A \frac{dh}{dl} \qquad (2.21)$$

where dh/dl = hydraulic gradient across the material in the direction of flow

k = coefficient of permeability m/s or c m/s

A = x-sectional area cm^2 or m^2

Q = steady state volume flow rate m^3/s or cm^3/s

As defined in equation (2.21), the coefficient of permeability describes the resistance of the material to fluid flow. The flow is assumed laminar. k depends on the structure of the porous solid and the properties of the flowing fluid, provided that only hydrostatic gradient is responsible for the flow. Attempts, made to modify equation (2.21), to incorporate the fluid properties[137, 138] yield equation 2.22

$$Q = k_o \frac{\rho g}{\mu} A \frac{dh}{dl} \qquad (2.22)$$

where k_o = specific permeability (m^2 or cm^2). This depends on the structure of the porous material alone, and independent of the flowing fluid.

ρ = density of fluid (kg/m^2)

g = acceleration due to gravity (m^2/s)

μ = absolute viscosity Ns/m^2

The viscosity of fluids in porous materials with high surface areas such as HCP, may be higher in smaller pores than in the larger ones because of strong physical forces of attraction emanating from the solid surfaces. Hence viscosity appears to be a function of the size of flow channel[139]. This uncertainty therefore exludes the use of equation (2.22) in the present investigation.

Darcy's equation has reasonable application over varieties of porous media. However certain deviations were observed and discussed extensively by Scheidegger[140]. These include, but are not limited to the following:-

1. At a certain Reynolds number (Re) equivalence of onset of turbulence would be observed. At this number, Darcy's law is no more valid. A great discrepancy in relation to a universal Re above which Darcy's law would no longer be valid is evident, and values varying from 0.1 to 75 have often been quoted[140]. This range however seems unattainable in HCP, mortar and concrete, and therefore has no effect.

2. Effects due to very high forces of attraction between the molecules of the fluid and the surfaces of the solids in small flow channels. The effect could be evident in HCP, but its determination is very difficult because of the clogging action during test.

3. Osmotic effects - this could be obtained due to the differential alkali concentration in HCP[139, 141]. Powers[141] however observed that the effect is negligible in HCP.

2.4.2.2 Model theories

These are obtained by representing the porous media with theoretical models, which when solved mathematically would attempt to relate flow to the microstructure of the media. An extensive discussion of the various models have been carried out[140] and only few are intended for discussion in this work.

2.4.2.2.1 Straight Capillaric Model

This is a linear model which represents a porous medium by a bundle of straight parallel capillaries of uniform diameter d. The flow Q, through a capillary is then given by the Hagen-Poiseuille equation

$$Q = \frac{-\pi d^4}{128\mu} \quad \frac{dp}{dx} \qquad (2.23)$$

where dp/dx = pressure gradient along the capillary.

If there are n such capillaries per unit area of x-section of the model, the flow per unit area q (i.e. the microscopic or filter velocity) is given by

$$q = \frac{-n\pi d^4}{128\mu} \frac{dp}{dx} \tag{2.24}$$

When a porosity factor is introduced, and comparing equations 2.24 and 2.21, equation 2.25 is obtained[140] as

$$k = \frac{\varepsilon \bar{d}^2}{32} \tag{2.25}$$

where ε = porosity

$\bar{d}$ = a form of average diameter of pores.

Scheidegger [140] observed that equation (2.25) does not adequately represent the relationship between the permeability and porosity in the porous medium. A modification factor was introduced to account for the fact that:

1. The part of flow is not a straight line, rather the part length of flow is greater than the length of the sample.

2. Some of the pores are unconnected cavities and even the connected pores have varying diameters along their lengths. This modification is called "tortuosity" factor (T). Also if S is defined as the average specific surface area as earlier mentioned

Then $$S = n\pi d \tag{2.26}$$

and $$k = \frac{\varepsilon^3}{T^2 S^2} \tag{2.27}$$

2.4.2.2.2 Parallel type model

This model was developed in an attempt to put one-third of the capillaries in each of the three special dimensions. The permeability k was obtained as

$$k = \frac{\varepsilon d^2}{96} \tag{2.28}$$

2.4.2.2.3 Serial type model

The two models already discussed assumed that all the pores pass from one face to another with uniform radius throughout the channel. The assumption is however questionable[141]. Scheidegger[140], therefore assumed that capillaries are of varying pore diameter linked in series one after another. He therefore modified equation (2.25) to obtain equation (2.29), by varying the diameter of each capillary along its length according to the pore size distribution

$$k = \frac{1}{96} \frac{\varepsilon d^2}{T^2} \tag{2.29}$$

2.4.2.2.4 Branching type model

The various models neglect the fact that fluid flow path may branch and later join again. In order to account for this, branching models were developed[142, 143]. This may be of importance to Diamond's description of threshold region[80] as obtained by mercury injection technique. However, Scheidegger[140] stated that the application of the model, is with regard to immiscible displacement processes and that no significant effects have been observed with such models, with respect to the physical aspects of single-phase permeability.

2.4.2.2.5 Hydraulic radius theory

This assumes that permeability is proportional to: 1. some hypothetical square length, 2. a dimensionless ratio which is a some function of porosity. With the two basic assumptions, the theory arrived at the basic expression of permeability

$$k = C \frac{\gamma_h^2}{F(\varepsilon)} \tag{2.30}$$

where γ_h^2 = hydraulic radius

$F(\varepsilon)$ = porosity factor

C = some dimensionless constant.

Carman (1941) as reported by Scheidegger[140] observed the following

1. No pores are sealed off
2. Pores are distributed at random
3. Pores are reasonably uniform in size
4. The porosity is not too high
5. Diffusion (slip) phenomenon is absent
6. Fluid motion is occuring like motion through a batch of capillaries.

Nyame and Illston[144] found that the hydraulic radius theory describes the water permeability of HCP, provided that the pore sizes have not reduced to molecular dimensions.

2.4.2.2.6 The Kozeny theory

This appears to be one of the most widely accepted explanation of permeability as influenced by the geometrical properties of the porous medium. A detailed analysis of this theory can be obtained from ref (137, 140). The functional relationship in Kozeny's theory is stated below

$$q = -\frac{C\varepsilon^3}{\mu S^2}\frac{dh}{dl} \qquad (2.31)$$

When compared with Darcy's law, and also introducing the tortuosity factor

$$k = \frac{C\varepsilon^3}{TS^2} \qquad (2.32)$$

where C = Kozeny constant.

For a variety of media, Carman[145] obtained C = 0.2. For

a porous medium dominated by small pores, he observed that the equation gave a very high permeability. Based on this, he concluded that only part of the porosity (called the effective porosity) is effective in liquid transmission. This particular deduction is of great interest in the present investigation. Carman later modified the Kozeny equation, which is now known as Kozeny-Carman equation

$$k = \frac{\varepsilon^3}{5S^2(1-\varepsilon)^2} \qquad (2.33)$$

Powers [146] in his analysis of the bleeding rate of cement pastes, observed that the effective porosity ε_e, should be utilized in equation 2.33. Based on his experimental results, Powers deduced that

$$\varepsilon_e = \varepsilon - \sigma(1 - \varepsilon) \qquad (2.34)$$

where σ = a constant, defined as the amount of immobile fluid per unit volume of solids in the medium

Other theories describing flow with pore parameters were proposed[140]. These include; 1. the drag theory; 2. the Iberall's theory etc. While considering the conflicting arguments as to the suitability of each of the models, Scheidegger observed that a reliable general correlation between porosity and permeability, does not exist for all the porous media. It follows therefore that a reliable method could be a judicious combination of theoretical and experimental relationship, which could help in establishing some form of relations for a particular material.

2.4.2.2.7 The diffusion theories

Fick's law of diffusion are of two differential forms (136, 147)

$$Jx = -Dx \frac{\partial C}{\partial x} \tag{2.35}$$

$$\frac{\partial C}{\partial t} = Dx \frac{\partial^2 C}{\partial x^2} \tag{2.36}$$

where Jx = fluid flux to a direction s, at position x

Dx = diffusion coefficient of position x

$\partial C/\partial x$ = concentration gradient at position x

Equation (2.35), describes the rate of permeability per unit area of any medium in terms of the concentration gradient across the medium. Equation (2.36) refers to the accumulation of matter at a given point in the medium as a function of time.

Equation (2.36) as reproduced in equation (2.39) was applied by Hall[148], in solving problems arising from unsaturated water flow in building materials. Applying the Boltzmann's transformation

$$x = \phi (\theta) \, t^{-\frac{1}{2}} \tag{2.37}$$

and the boundary conditions

$$\theta(0, t) = 1, \; \theta(x, 0) = 0 \tag{2.38}$$

The partial differential equation

$$\frac{\partial \theta}{\partial t} = D_x \frac{\partial^2 \theta}{\partial x^2} \tag{2.39}$$

is transformed to an ordinary differential equation of the form

$$2 \frac{d}{d\phi} \left(D \frac{d\theta}{d\phi} \right) + \phi \frac{d\theta}{d\phi} = 0 \tag{2.40}$$

where θ = water content mm^3

D = water diffusivity mm/min

ϕ = position of centre of mass mm

After a rigorous analysis of equation (2.40), Philip[149, 150]

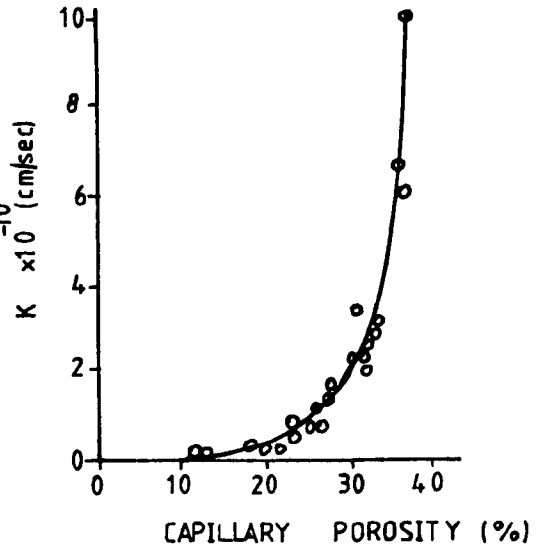

FIG 2.2 RELATIONSHIP BETWEEN PERMEABILITY AND CAPILLARY POROSITY OF HCP[53]

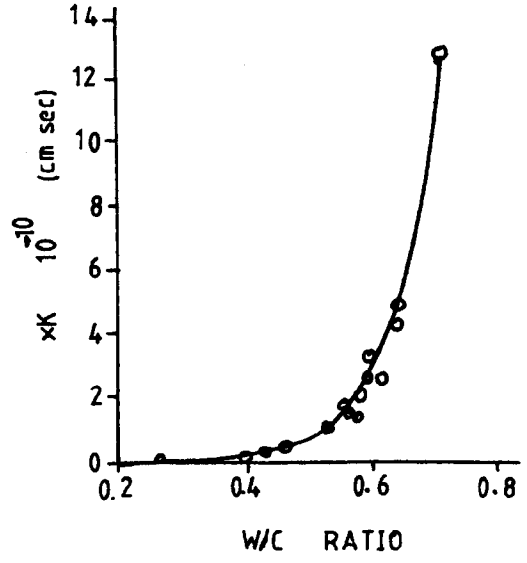

FIG 2·3 RELATIONSHIP BETWEEN PERMEABILITY AND W/C RATIO FOR MATURE HCP 93% HYDRATION[27]

arrived at equations 2.41 and 2.42, shown below

$$i = st^{\frac{1}{2}} \tag{2.41}$$

$$u_o = \tfrac{1}{2}st^{-\frac{1}{2}} \tag{2.42}$$

where i = cumulative absorption/unit area mm^3/mm^2

s = sorptivity (which is a characteristic of the medium) $mm/min^{-\frac{1}{2}}$

u_o = sorption flux mm

t = time min

This predicted $\sqrt{t}$ dependence of water absorption was confirmed by Jansson[151] for bricks. The present work intends to investigate this dependency of water absorption in concrete. Other liquids such as crude oil, diesel and parafin will also be used. If this relationship holds in practice, a possible relationship could exist between sorptivity and saturated permeability, which could be a valuabe indirect method of testing the permeability of HCP, mortar and concrete.

2.4.3 Permeability of HCP and concrete

The original cement minerals in a fresh paste is progressively replaced by cement gel, during the chemical reaction between cement and water. As a result of higher volume generated by the hydration products, the water filled spaces (the capillary pores) are systematically being filled by the gel, with a consequent reduction in permeability[152]. The permeability of gel has been found to be 7×10^{-16} cm/s[54]. It was also observed that the permeability of HCP, is 20 to 100 times higher than the permeability of the gel. This therefore led to the deduction that permeability of HCP is controlled by the capillary porosity[54]. The relationship between permeability and capillary porosity of HCP, is shown in Fig. 2.2. Table 2.2 shows the effect of hydration on k[152].

Age (Days)	Coeff. of Permeability k (cm/sec)
Fresh	2×10^{-4}
5	4×10^{-8}
6	1×10^{-8}
8	4×10^{-9}
13	5×10^{-10}
24	1×10^{-11}
Ultimate	6×10^{-11} (calculated)

TABLE 2.2 Variation in Permeability of cement pastes of w/c ratio 0.7 with progressing hydration (ref. 152).

For the same degree of hydration, k increases with increase in w/c ratio for HCP[27] as shown in Fig. (2.3). A reduction in w/c ratio from 0.7 to 0.3 lowers k a thousandfold and is similarly observed in a paste at say 0.7 w/c ratio, hydrating between the ages of 7 days to one year.

At the same w/c ratio, it is observed[152], that coarse cement produces paste of higher porosity and permeability. Powers[152] however found that the compound composition of the cement affects permeability insofar as it influences the rate of hydration, but not the ultimate porosity and permeability. Permeability increases with decrease in strength. Drying of the paste increases its permeability because drying shrinkage ruptures some of the gel between capillaries, thereby opening new passages to water.

The permeability of the aggregate affects the permeability of concrete. If aggregate of low permeability is used, its presence reduces the effective area over which flow can take place. Addition of aggregate reduces the number of flow channels per unit gross cross-sectional area.

Also since the flow path has to circumvent the aggregate particles, the effective path becomes considerably longer, thereby causing a reduction in permeability[153]. Neville[27] however noted that the influence of the aggregate content in the mix is small. He states that since the aggregate particles are enveloped by the cement paste, in a fully compacted concrete, it is the permeability of the paste that has the greatest effect on the permeability of the concrete. Oyeka[17] observed that concrete has higher crude oil permeability than the cement paste.

It was found that[154-156] moist and steam curing reduce permeability. Steam cured concrete also has a lower permeability than the wet cured.

Air entrainment appears to reduce the permeability[157,158]. This is probably because it improves workability and so permits the use of lower w/c ratio. Neville[27] observed that the effect of air entrainment on permeability is not adverse. Polymer impregnation also reduces permeability significantly. Oyeka[17] reported that super-plasticised concrete is less permeable than ordinary concrete of similar mix proportions. This is again explained in terms of an improved workability when super-plasticisers were added.

Smaller maximum size of aggregate has been found to reduce the permeability[153, 159, 160]. This is probably because smaller aggregates pack more efficiently in the paste matrix with corresponding reduction in the interconnectivity of the pore system. For a w/c ratio of 0.6, Oyeka[17] observed that the optimum fine to total aggregate ratio for reduced permeability is between 40 to 55%. This means that concrete with approximately even distribution of fine and coarse aggregate would result in low permeability. Norton and Pletta[160] observed that permeability increases with an increase in the volume concentration of aggregate, irrespective of the grading of the aggregates.

2.4.4 Pore structure and permeability of HCP, mortar and concrete

This section is aimed at highlighting some empirical correlations between pore parameters and permeability. This is to enable an appreciative study of the effects of changes in pore structure on permeability which is of interest in the present research to be made.

Powers et al[139] applied Stokes law to concentrated suspensions of HCP and deduced a semi-empirical relationship between permeability and pore structure as

$$k_1 = \frac{B}{\mu_o(T)} \frac{\varepsilon^2}{1-\varepsilon} \exp - \left[\left(\frac{\alpha}{T} - \gamma \right) \left(\frac{1-\varepsilon}{\varepsilon} \right) \right] \qquad (2.43)$$

where $$B = \frac{\tau(C)\rho_f g d_s^2}{27} \qquad (2.44)$$

ρ_f = density of fluid

g = gravitational constant

d_s = Stokes diameter

$\tau(C)$ = function of concentration which corresponds to the Kozeny-Carman tortuosity factor

$\mu_o(T)$ = dynamic viscosity of water at temperature T

$\frac{\alpha}{T\left(\frac{(1-\varepsilon)}{\varepsilon}\right)}$ = correction term applied to normal viscosity

$\frac{\gamma}{(1-\varepsilon/\varepsilon)}$ = temperature independent factor

ε = porosity

T = absolute temperature ^{o}K

Values of B, α and γ were obtained from experiment as $B = (1.36 \pm 0.1) \times 10^{-10}$, $\alpha = 1242 \pm 133$ and $\gamma = 0.7 \pm 0.5$. Applying the hydraulic theory, Nyame and Illston[144], were able to relate k to the hydraulic radius and porosity as

$$\log k = 38.45 + 4.08 \log(\varepsilon r_h^2) \qquad (2.45)$$

They confirmed that total porosity is not a unique function of permeability, and suggested that the flow space in HCP is confined to distinct flow channels. Watson and Oyeka[161] deduced empirical relationship between crude oil permeability and total porosity for HCP as

$$k_s = k_2 \exp [D(\varepsilon_m)] \qquad (2.46)$$

When superplasticizers were added, the relationship became linear as given in equation (2.47)

$$k_s = k_3 \varepsilon_m + F \qquad (2.47)$$

where ε_m = meso-pore volume

k_2, k_3, D and F are constants.

The values of k_2 and D were found to vary with the applied oil pressure. The difference in permeability when super-plasticizers were added suggests a possible re-orientation of the pores. This could be as a result of a different mode of hydration or probably the amount of initial pore space before the process of hydration. Applying the Kozeny equation, Watson and Oyeka[161] obtained a semi-empirical relationship between permeability and applied pressure, mesopore volume and hydraulic radius as

$$k_s = T A^{\theta} \varepsilon_m^{\beta} r_h^{\gamma} \qquad (2.48)$$

where T = tortuosity factor

θ, β and r are constants.

For ordinary Portland Cement Paste (OPC)

$T = 2.47$, $\theta = 0.450$, $\beta = 0.938$, $\gamma = 0.382$

For Sulphate Resisting Portland Cement (SRPC)

$T = 8.41$, $\theta = 0.400$, $\beta = 0.816$, $\gamma = 0.067$

Mehta and Manmohan[109], found that the permeability of HCP, can be correlated to the volume of pores greater than 1320$\overset{0}{A}$ diameter as shown

$$k_1 = \exp(3.84V_1 + 0.20V_2 + 0.56 \times 10^{-6}TD + 8.09MTP - 2.53) \quad (2.49)$$

where V_1 = volume of pores greater than 1320$\overset{0}{A}$

V_2 = volume of pores between 290 - 1320$\overset{0}{A}$

TD = threshold diameter

MTP = modified total porosity (which is equal to the total pore volume divided by the degree of hydration)

Mehta and Manmohan, observed that negligible permeability is obtained when the pore sizes in HCP are smaller than 1320$\overset{0}{A}$ in diameter. Further correlations could be obtained from Powers work[162].

A general deduction from these correlations is that, it is apparent that total pore space may not contribute to the flow of fluid through cement paste, mortar or concrete, but that the flow may be linked to probably interconnected flow paths or even possibly cracks. The measurements of effective and ineffective flow pore spaces therefore poses a special problem. Hancox[163] employed the concept of electrical resistivity of fluids in saturated and partially saturated ordinary portland and high alumina cement pastes in determining the effective porosity. He ascertained that the pore space limiting flow is independent of the time of hydration and is related to the porosity of the sample by

$$F = \varepsilon^{3.4} \quad (2.50)$$

where F = fractional cross-sectional area of pastes limiting flow.

The above observations clearly show that permeability description requires more than one pore parameter. It is therefore important that those pore parameters which could significantly affect the

flow of oil through mortar and concrete be sought and analysed.

2.4.5 Methods of measuring permeability of HCP, mortar and concrete

A widely used method is the steady state flow of fluid through the saturated specimen of HCP, mortar or concrete. When a steady state is reached, which is often achieved only after many weeks, depending on the applied pressures, the quantity of water flowing in and out of the specimen in a given time is determined[55, 134, 139, 152]. The long period associated with the test means that the specimens continuously hydrate and alter the pore structure, hence the permeability of the test specimen. Dunagan[164] stated that exact steady state flow cannot be achieved until complete hydration has taken place. For oil flow however, the specimen is first dried and then saturated in oil (Chapter 3), so the problem of continuous hydration in the presence of water may be absent.

Comparison of permeability on a relative basis, can be carried out, by studying the rates at which partially dried cement paste, mortar or concrete absorbs fluids[165-168]. The disadvantage of this method rests on the fact that the rate of absorption depends on the initial moisture contents of the samples. The initial absorption test (ISAT) developed by Lewitt[166] is based on a low pressure method of measuring permeability used by Glanville[169], and is now recognized as a British Standard Test for hardened concrete[170]. It involves the measurement of the amount of water absorbed by the surface of concrete under a fixed hydrostatic head of 200mm, in a specified time of 10 mins and 24 hours. This test therefore indicates the permeability of the surface of concrete and may not be suitable for interpreting the permeability of the whole material. The Building Research Station[9] modified the method used by Pearson[3] while studying the absorption of petrol by coated materials. This method, which is of interest to the present work used hollow prisms

37mm x 37mm x 200mm high with a central hole 18.75mm in diameter and 187.5mm deep partially immersed in the liquid in a closed container. The prisms were reweighed at intervals after removing the surplus liquid from the outer surface, by blotting with filter paper. This method is utilized in the present work to investigate the effect of liquid properties on permeability of concrete (Chapter 5). Oyeka[17] obtained a linear relationship between oil absorbed by concrete dried at 105°C and their permeability coefficients. This linear relationship, therefore justifies the use of an absorption method for a comparative study of the permeability of concrete to petroleum products.

Another widely used technique is the penetration method, for estimating permeability. This depends on the application of Fick's law to the motion of saturated front of the liquid under an applied hydrostatic pressure[156, 158]. Murata[158], using a range of hydrostatic pressure up to 20kgf/cm^2, measured the penetration of water in sealed specimens with time, up to 48 hours. Before being immersed in the liquid, the specimens were dried at room temperature for fixed periods of up to 10 days. Applying Fick's law, Murata obtained a relationship between a diffusion coefficient and a permeability coefficient as

$$D = \frac{kE}{\rho_w} \tag{2.51}$$

where D = diffusion coefficient (cm^2/s)

k = permeability coefficient (cm/s)

E = compressibility of saturated concrete (g/cm^2)

ρ_w = density of water (g/cm^3)

Matti[14] using the penetration method, obtained an empirical relationship between k, penetration period and applied pressure head as

$$k = \frac{A^2 B t^{2B-1}}{h} \tag{2.52}$$

where h = applied pressure head (m)

t = time of test (sec)

A and B are constants.

His result was based on Darcy's equation.

Valenta[171] employed a theoretical approach using Fick's law on the movement of the liquid front, while the driving force is assumed to be due to constant capillary attraction. The relationship between k and effective liquid head was

$$\frac{dx}{dt} = V = k \left(\frac{h+h_o}{h}\right)^n \qquad (2.53)$$

where h = real liquid head (m)

h_o = liquid head representing the capillary elevation (m)

dx/dt = rate of rise of liquid front (m/sec)

Since $h \ll h_o$, h_o could be neglected, and equation (2.53) becomes[171]

$$t = \frac{x^2}{2} \cdot \frac{1}{kh} \qquad (2.54)$$

Equation (2.54), shows that the depth of penetration is proportional to the second root of time, i.e. $x \propto t^{\frac{1}{2}}$. This method requires that suitable uniform moisture content should be maintained through all the test samples. Also the initial moisture content should be the same for all the test samples.

The present investigation employs the steady state permeability coefficient in investigating the permeability of HCP, mortar and concrete to crude oil. The changes in permeability due to hydration, w/c ratio and aggregate inclusions is studied, and an attempt has been made to relate these changes to changes in pore structure. Unsteady state flow, using an absorption method, would be utilized in looking at the effect of various oil properties on permeability of HCP, mortar and concrete.

CHAPTER 3

EXPERIMENTAL PROGRAMME, MATERIALS AND PREPARATION OF SPECIMENS

3.1 Introduction

A detailed description of the experimental programme and apparatus is provided in each chapter dealing with the separate aspects of the investigation. This chapter only summarizes the main areas of study, materials used and the method of preparing the specimens.

3.2 Experimental Programme

Below is a summary of the main areas of study. The investigation is divided into two main sections. Section 1, is contained in chapters 4 and 5 and deals with the flow of crude oil through various crack shapes in concrete (Chapter 4); the relationship between the direction of casting and the permeability of concrete, and the permeability of concrete to various grades of oil (Chapter 5).

The mix proportions for the tests are given in Table 5.1. The hollow concrete cylinder 175mm ext. dia. x 300mm high and 50mm thick (A of plate 3.1) used to investigate the flow of different grades of oil, and the 150mm dia x 50mm thick discs used for investigating the flow of crude oil through different cracks, were cast from concrete with 0.6 w/c ratio. Concrete of w/c ratio varying from 0.40 to 0.80, and slump varying from 5mm to 140mm at 0,4 w/c ratio and applied fluid pressure from 16.60 to 99.60 metre head of oil, were used in investigating the variation of flow with direction of casting. These specimens were initially cured for 28 days in the constant temperature room (fog room) at 21 $\pm$ 1.0°C and 99 $\pm$ 1% R.H., before any test. A permeability apparatus already developed in the department [17] and modified as described in section 4.3, to accommodate larger flows, was used for both flow through cracks and tests to study the effect of the direction of casting. Plastic containers were used to partially immerse the hollow concrete cylindrical

tanks at varying liquid depths of 50mm, 80mm, 100mm and 125mm as shown in B of plate 3.1.

Section 2, describes the investigation of how some basic parameters influence the internal pore structure of HCP, mortar and concrete, and the relationship between pore structure and saturated permeability. The varied parameters were (i) initial w/c ratio (2) period of hydration and (3) fine and coarse aggregate proportion. Since permeability tests were carried out on oil saturated specimens, (section 3.8.2), the probable effect of pre-saturation on pore structure is also investigated.

A summary of the range of variables used in this investigation is given below

Pore structure and permeability studies

Hardened Cement Paste (HCP)

w/c ratio 0.35 - 0.70

Hydration 7 days to 6 months

Mortars: normal fine aggregate (Table 3.3)

Mixes: 1:1, 1:1.5, 1:2, and 1:3 cement/sand ratio

w/c ratio: 0.35 - 0.70

Hydration: 7 days to 6 months

Concrete: Normal fine and coarse aggregate (Table 3.2)

Mix: 1:1½:1½ cement:sand:coarse aggregate

w/c ratio: 0.35 - 0.70

Hydration: 7 days - 6 months

Maximum size of coarse aggregate of 6.30mm.

Some HCP, mortar and concrete specimens were cured in the fog room for up to 6 months, while other similar specimens were cured in the constant temperature room (C.T.R.) at 16 $\pm$ 0.5^{o}C and 50 $\pm$ 1% R.H. for up to 3 months. Pre-saturation and drying were carried out on some specimens of HCP, mortar and concrete after curing for 28 days, using Kuwait crude (KU), North-Sea crude (NS), Diesel (DE) and Parafin (PA), prior to their

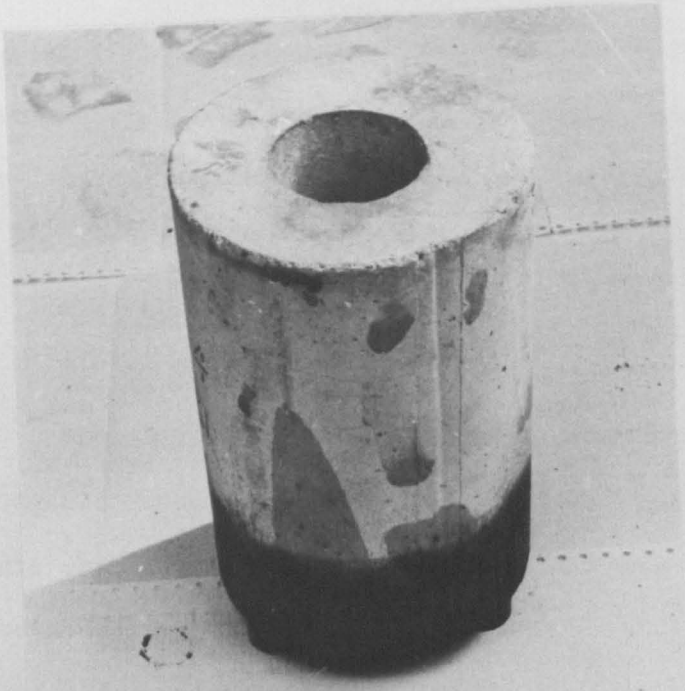

A

MODEL CONCRETE TANK

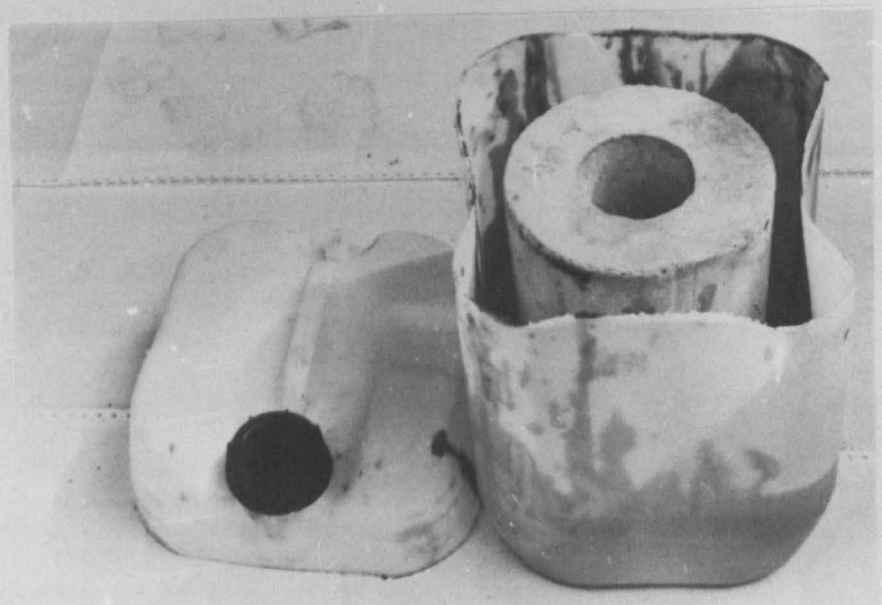

B

PLASTIC CONTAINER

PLATE 3.1

pore structure analysis.

The pore structure analysis was carried out using the mercury porosimeter described in section 6.3, while the permeability tests were carried out in the permeability apparatus (section 4.3).

3.3 Materials

3.3.1 Cement:

Ordinary Portland Cement (OPC), manufactured and marketed by the Blue Circle Group, Hope Cement Works, near Sheffield was used. Its approximate chemical composition is given in Table 3.1 (By the courtesy of the Production Division, Blue Circle Cement).

3.3.2 Aggregate:

Normal river-aggregates were used for the fine and coarse aggregates.

The coarse aggregate was graded irregular shaped gravel obtained from Bradsford river, Derbyshire. 10mm maximum size was used for concrete specimens 50mm thick and above, while 6.30mm maximum size was used for concrete specimens 25mm thick. This is to conform with the standard practice that the maximum aggregate size should not be greater than 1/5 to 1/4 of the minimum dimension of the concrete section[27]. Small sized specimens were used to facilitate saturation and to obtain steady state flow in a relatively short period. The grading and properties of the coarse aggregate as obtained from tests are shown in Table 3.2. The fine aggregate, also obtained from Bradsford river, Derbyshire, was a quartzite sand graded to zone 3, of BS 882:1965. The properties and sizes are shown in Table 3.3. Tables 3.2 and 3.3 are plotted in the grading envelopes of Figs. 3.1 and 3.2 respectively.

Grading, loose bulk density, water absorption and specific gravity tests were carried out according to the British Standard (BS812) for both fine and coarse aggregates, while the angularity factor was

COMPOUND COMPOSITION	ABBREVIATION	% BY WEIGHT
Tricalcium Silicate	C_3S	59.0
Dicalcium Silicate	C_2S	12.8
Tricalcium Aluminate	C_3A	11.2
Tetracalcium Alumonoferite	C_4AF	7.0
Silica	SiO_2	20.0
Insoluble residue		0.3
Alumina	Al_2O_3	5.7
Ferric Oxide	Fe_2O_3	2.3
Lime	CaO	65.5
Magnesium Oxide	MgO	1.0
Sulphur Trioxide	SO_3	2.8
Alkalis	Na_2O	0.2
	k_2O	0.6
Loss on Ignition	LOI	1.0
Specific surface area		$332m^2/kg$
Initial setting time		145 minutes
Final setting time		185 minutes

TABLE 3.1 Chemical Composition of the Cement used in the Investigation

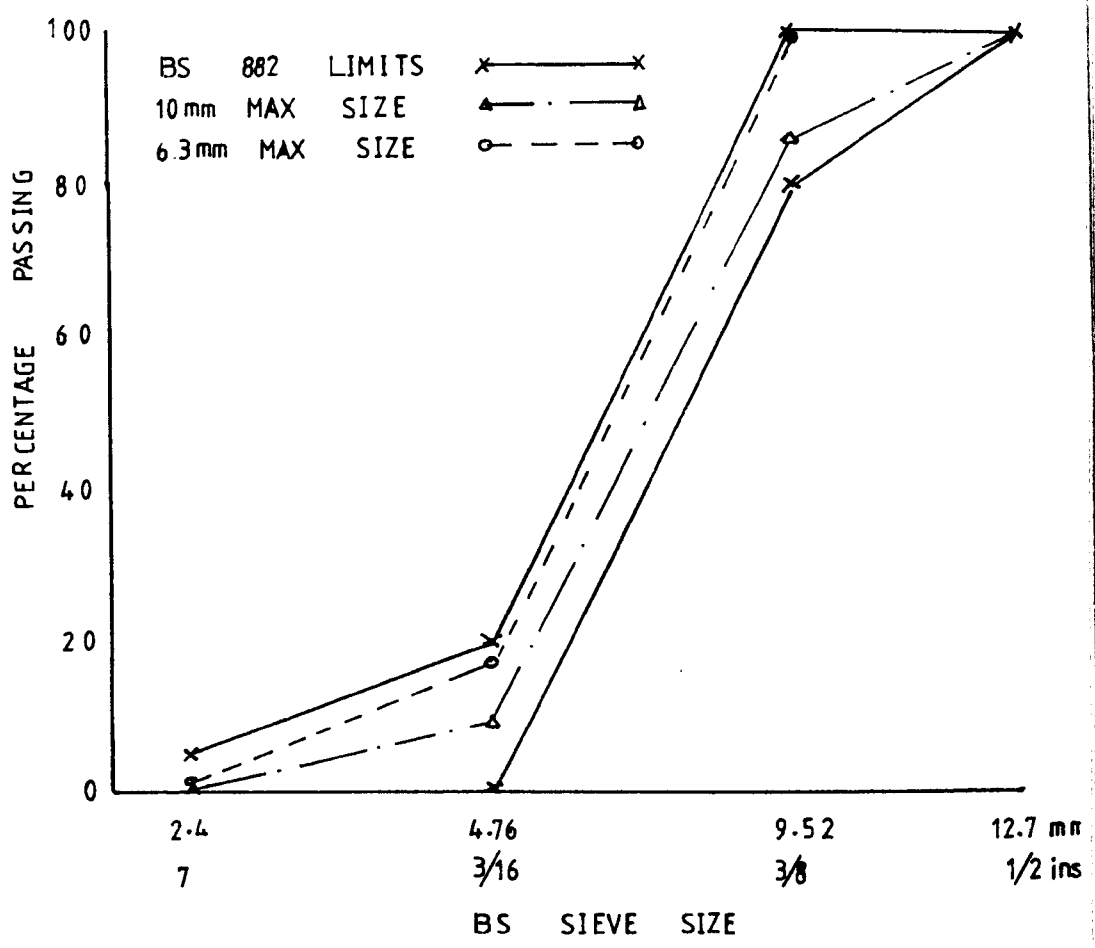

FIG 3.1 GRADING FOR COARSE AGGREGATES OF 10mm AND 6.3mm MAX. SIZE

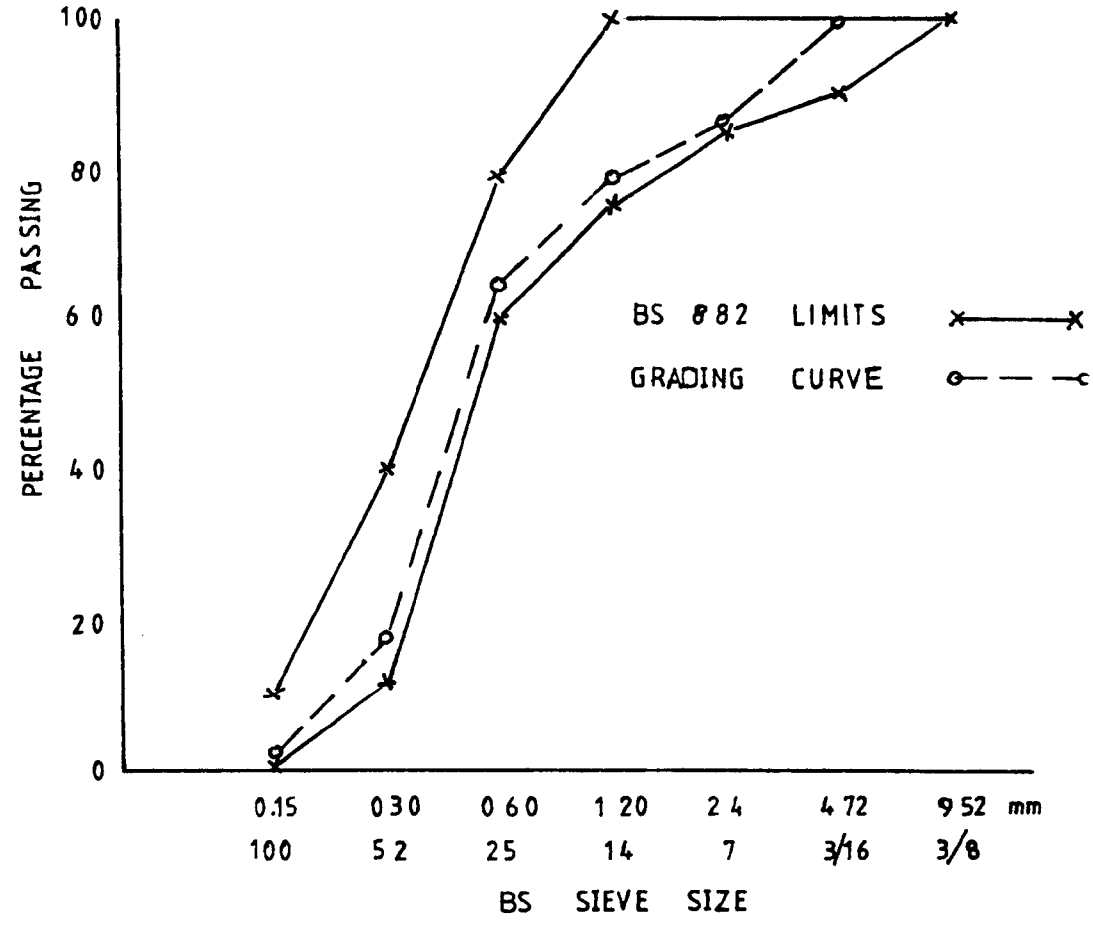

FIG 3.2 GRADING CURVE FOR FINE AGGREGATE (ZONE 3)

Coarse Aggregate Properties

Natural and irregular river gravel
Water absorption 1.78%
Specific gravity 2.60
Angularity factor 1.02

Grading:

10mm (⅜") max size Loose bulk density 1550 kg/m^3		B.S. Requirements	6.30mm (¼") max size Loose bulk density 1620kg/m^3	
Sieve size (mm)	%age passing		Sieve size (mm)	%age passing
12.7 (½")	100	100	12.7 (½")	100
9.52 (⅜")	86	85-100	9.52 (⅜")	100
4.76 (3/16")	9.2	0.20	4.76 (3/16")	17.5
2.40 (No7)	0.1	0-5	2.40 (No7)	1.0

TABLE 3.2 Physical specifications of coarse aggregate

Fine Aggregate properties

Washed and dried river sand

Zone 3 gravel

Water absorption 0.98%

Specific gravity 2.62

Angularity factor 1.10

Grading:

Sieve size		% passing	BS requirement
in	mm		
⅜	9.52	100	100
3/16	4.72	99.6	90-100
No.7	2.40	86.4	85-100
14	1.20	79	75-100
25	0.60	64.6	60-79
52	0.30	17.9	12-40
100	0.15	1.6	0-10
200	0.075	0	0

TABLE 3.3 Physical specifications of fine aggregate

PLATE 3.2 HOBART BENCH MIXER

determined as recommended in ref. (172).

3.3.3 Liquids

Most of the tests were carried out using North Sea crude oil. However for comparative studies, other liquids such as tap water, Kuwait crude oil, Diesel and Parafin were used. An analysis of each type of oil was carried out in the Chemistry Department of Sheffield University to identify some of their physical and chemical properties and the results are shown in Tables 3.4 to 3.7. Table 3.8 shows some of the properties of water which are relevant to this present investigation. Table 3.9, shows

Properties of water		
Density at 15°C	1×10^3 kg/m^3	ref.30
kinematic viscosity at 15°C	1.14×10^{-6} m^2/s	
surface tension at 15°C	73 MN/m	
molecular size	3Å (174)	

Table 3.8 Some properties of water at atmospheric pressure

the analysis of North Sea crude oil after being in contact with concrete for a period of 2½ years. A comparison of table 3.4 and 3.9 shows that no noticeable change has occurred on the physical and chemical properties of the oil. Hence within this time, there was no reaction between concrete and oil which had any adverse effect on the physical and chemical properties of the crude oil. This finding was also established by a previous investigator[14], after a storage period of 3 years.

3.4 Preparation and Casting of HCP Samples

3.4.1 Cement Pastes:

Samples were prepared from ordinary portland cement with the composition given in Table 3.1. Mixing was done in a Hobart-bench mixer, plate 3.2. The required amounts of cement and water were weighted to an

1. Distillation up to 300°C (cumulative % of total volume)

Temperature °C	% Volume (Cumul.)
40 - 80	4.70
80 - 90	9.12
90 - 110	10.22
110 - 120	11.88
120 - 145	14.64
145 - 159	18.51
159 - 165	20.72
165 - 181	34.26
181 - 190	43.10
190 - 200	47.24
200 - 218	59.12
218 - 235	66.03
235 - 255	75.70
255 - 280	85.37
280 - 290	88.96
290 - 295	92.27
295 - 300	100.00

2.	Sulphur Content	2.07 - 2.09%
3.	Moisture content (as H_2O)	1.15%
4.	Calcium content	non detected
5.	Specific gravity (at 16°C)	0.890 - 0.891
6.	Viscosity at 15°C	22.43 centistokes
	30°C	20.45 centistokes
	60°C	18.47 centistokes
7.	Wax content	5.7% by wt.
8.	Surface tension at 16°C	32.17 dynes/cm
9.	Moleculate sizes	highly variable, ranges 1 to 18 Å, high occurence of between 5 and 7 Å

TABLE 3.4 Analysis of Kuwait crude oil (Ref. 17)

1. Distillation up to 320°C

Temperature °C	% Volume
40 - 60	1.50
60 - 70	1.85
70 - 80	0.75
80 - 90	1.65
90 - 105	2.10
105 - 110	2.00
110 - 130	2.95
130 - 145	1.95
145 - 160	2.50
160 - 185	4.20
185 - 215	4.10
215 - 250	5.90
250 - 270	4.00
270 - 290	2.90
290 - 320	7.05

2.	Sulphur	0.52 - 0.53%
3.	Moisture	1.28%
4.	Calcium content	0.004%
5.	S.G. (16°C)	0.8610 - 0.8615
6.	Viscosity at 15°	20.32 centistokes
	30°	17.90 cenitstokes
	60°	15.71 centistokes
7.	Wax content	3.12% (by weight)
8.	Moleculare sizes	1 to 15 Å with high occurence at 3.5 to 8.5 Å

TABLE 3.5 Analysis of North Sea crude oil

1. Distillation up to 360°C

Temperature °C	% Volume
40 - 150	Nil
150 - 160	1.00
160 - 164	0.50
165 - 180	Nil
180 - 185	1.00
185 - 190	0.50
191 - 200	1.00
200 - 215	1.00
215 - 220	7.00
220 - 225	2.00
225 - 235	5.00
235 - 245	5.00
245 - 250	4.00
250 - 260	4.50
260 - 270	1.20
270 - 280	8.50
280 - 295	4.10
295 - 300	9.00
300 - 320	11.50
320 - 335	10.00
335 - 345	10.7
345 - 360	12.50

Distillation recovery 200°C	5%
Distillation recovery 357°C	93%
Relative density (15°C)	0.8550
Kinematic viscosity at 15°C	10.9cs
30°C	6.1cs
Water % (volume)	0.05
Sulphur	1.02%
Calcium	not detectable
Carbon residue	0.08
Molecular sizes	1 to 8 Å with high occurrence at 4 to 6.5 Å

TABLE 3.6 Analysis of Diesel oil

Distillation Range

Temperature ^{o}C	% Volume
40 - 80	1.00
80 - 100	1.00
100 - 110	1.00
110 - 120	1.00
120 - 140	1.50
140 - 145	1.50
150 - 160	0.50
160 - 165	2.00
165 - 170	2.00
170 - 1 80	2.00
180 - 185	5.00
185 - 190	7.00
191 - 200	7.00
200 - 215	10.50
215 - 220	24.00
220 - 225	9.50
225 - 235	14.00
235 - 245	4.00
245	Nil

Distillation range	91.50%
Distillation recovery to $200^{o}C$	33.00%
Relative density ($15^{o}C$)	0.7900
Kinematic viscosity ($15^{o}C$)	9.7cs
($30^{o}C$)	5.0cs
Water % (volume)	0.10
Sulphur	0.60%
Calcium	Nil detected
Ash	0.007%
Carbon residue	0.02%
Molecular sizes	1 to 7 A^{0} with high occurence 4 to 5 A^{0}

TABLE 3.7 Analysis of Parafin

Distillation up to 300°C

Temperature °C	% volume
40 - 80	2.75
80 - 90	2.05
90 - 112	4.00
112 - 120	3.00
120 - 134	2.00
135 - 140	2.00
140 - 145	2.00
145 - 152	3.00
152 - 160	1.00
160 - 164	1.00
164 - 171	1.00
171 - 180	0.50
180 - 185	0.50
185 - 190	3.00
191 - 200	4.50
200- 215	0.50
215 - 220	2.00
220 - 225	3.00
225 - 235	4.00
235 - 245	1.00
245 - 252	2.50
252 - 260	1.00
260 - 270	1.00
270 - 280	2.00
280 - 295	2.80
295 - 300	4.30

Sulphur	0.48 - 0.49%
Moisture	0.60%
Calcium	0.07% as Ca
Relative density API	0.8590 - 0.8594
Kinematic viscosity 15°C	21.7 centistokes
30°C	16.9 centistokes
Wax content (by weight)	3.70%
Petrol Grade (to 149°C)	20.8%
Kerosene Grade (149 - 232°C)	21.0%
Gas oil Grade (232-300°C)	14.6%
Residue (above 300°C)	43.6%
Molecular sizes	1 to 15 Å with high occurrence at 3.5 - 8.5 Å

TABLE 3.9 Analysis of North Sea crude oil after Storage in Concrete

accuracy of 0.5gms. The standard procedure adopted for each batch was to mix for 3 minutes, rest for 5 minutes and mix again for 3 minutes. The mixture was covered with damp cloth and polythene sheet in the CTR during the rest period, to minimise evaporation losses. The double mixing procedure was adopted to prevent false set. After mixing, the pastes were poured into their moulds, plate 3.3, in two layers each layer being vibrated for about 2½ minutes. It was found necessary to vibrate the samples with w/c ratio greater than 0.5 for less than 1 minute. Immediately after vibration, the specimens were transfered to a constant temperature room (CTR), 16 $\pm$ 0.5°C and 50 $\pm$ 1% R.H., covered with polythene sheets and allowed to set for about 2 to 3 hours. The tops were then trowelled flat and the top plate of the mould tightly screwed on, (marked B in plate 3.3.). The moulds were then inverted and covered with polythene sheets for about 24 hours. The specimens were later demoulded and stored in a fog room at a constant temperature of 21 $\pm$ 1°C and R.H. of 99 $\pm$ 1% for up to 6 months. To facilitate easy demoulding, the inner surfaces of the moulds were lightly oiled prior to casting each batch of the samples. This method of mixing and casting was adopted to minimise bleeding of the paste and also to allow comparisons to be made with results from previous investigation[17].

3.4.1.1 Sizes and shapes of the HCP specimens

To facilitate saturation with crude oil the specimens were made as small as possible as given below

1. compressive strength - 50mm cubes
2. pore structure analysis - 50mm cubes
3. permeability tests 100mm dia. x 25mm thick discs

3.5 Preparation and Casting of Cement Mortars

Mortar specimens were prepared in a similar manner as that described above. However vibration of mortar with w/c ratio greater than 0.5 was between 2 minutes to 3 minutes per layer depending on the fine

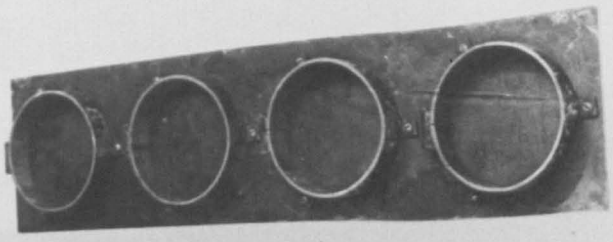

A

B

PLATE 3.3 MOULDS FOR CASTING THE HCP MORTAR AND CONCRETE FOR PORE STRUCTURE ANALYSES

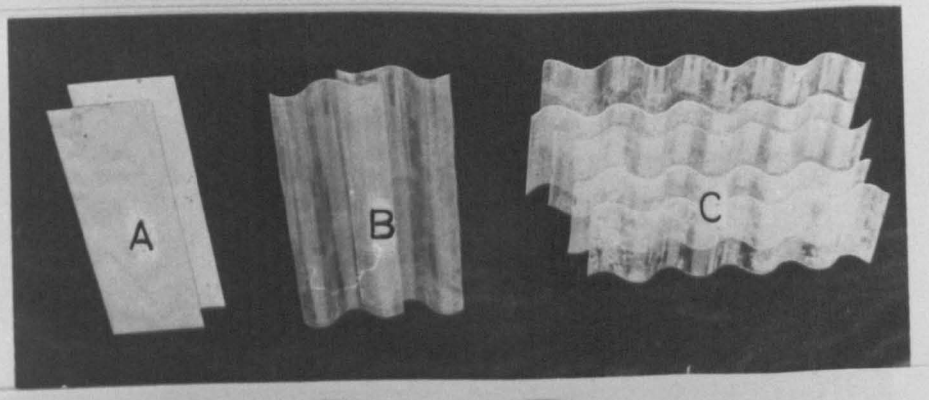

D

A FORMER FOR STRAIGHT THROUGH CRACKS

B " " CRACKS SINUSOIDAL ACROSS THE THICKNESS

C FORMER FOR CRACKS SINUSOIDAL ALONG THE DIAMETER

D MOULD

PLATE 3 4 CRACK FORMERS AND MOULD FOR CRACK SPECIMENS

aggregate proportion. For a cement/sand Ratio of 1:3, and for a w/c ratio lower than 0.5, compaction could not be achieved, and mortar of this mix, but with w/c below 0.5 were not used.

3.6 Preparation and Casting of Concrete Specimens

3.6.1 Concrete specimens for investigating the effects of coarse aggregate inclusions on pore structure and permeability

The method of casting the concrete specimens were the same as for HCP (section 3.4). The vibration period for each layer was 2½ minutes for all the w/c ratios. A mix proportion of 1:1½:1½; cement:sand:coarse aggregate ratio was used. Details of this mix, and those of mortar and HCP mixes are given in Table 6.1.

3.6.2 Mixes for crack specimens, horizontally and vertically cast specimens and model concrete tanks

The w/c ratio was considered to be the principal factor governing the mix design for these tests. Mix design charts of Teychenne et al[173], were used as a guide for obtaining the mix proportions for both trial and final mixes. The mixes are given in Tables 3.10 and 5.1.

3.6.2.1 Mixing of the ingredients

The coarse aggregate was generally dried in the laboratory at a room temperature of about 20 $\pm$ 2°C while the fine aggregate was dried in a mechanical drier at 105°C and allowed to cool to the laboratory room temperature of 20 $\pm$ 2°C for at least 24 hours before use. Having determined the moisture content and absorption by drying three samples of gravel and sand at 105°C for 24 hours, and finding the reduction in weight, the weight of the mixing water was adjusted to bring the aggregates to approximately saturated surface dry (SSD) condition prior to mixing. Batching was by weight to the nearest 1gm. Mixing was done in a $1m^3$ horizontal pan mixer with the aggregate and cement mixed alone for 1 minute before the

Mix Design	w/c ratio	Aggreg to cement	Cement content (kg/m^3)	Proportion by weight		
				Cement	Sand	Gravel
VHS1	0.40	5.02	375	1	1.61	3.42
VHS2		3.19	512	1	1.15	2.04
VHS3		2.91	545	1	1.10	1.80
VHS4		2.67	576	1	1.07	1.60
VHS5		2.47	612	1	1.04	1.43
VH50	0.50	5.09	360	1	1.84	3.26
VH60†	0.60	5.30	340	1	1.96	3.34
VH70	0.70	6.32	293	1	2.47	3.86
VH80	0.80	7.38	256	1	2.95	4.43

† Used for casting the crack specimens and the model concrete tanks

TABLE 3.10 Details of concrete mixes for vertically and horizontally cast specimens

water was added. Mixing was then continued for another 1½ minutes and the slump taken immediately after.

3.6.2.2 Casting of the specimens

3.6.2.2.1 Preformed crack specimens:

Before pouring the mixed concrete, the inner surfaces of the mould and the two sides of the crack former, were lightly oiled to facilitate easy demoulding and separation at the two halves of the specimens. The crack formers were made of flat brass plates 50mm x 150mm x 0.2mm thick (Fig. 3.3) marked in plate 3.4, for straight through cracks, and corrugated plastic sheets 40mm crest to crest, cut in such a way as to form two different patterns shown, marked B and C in plate 3.4 and also shown in Fig. 3.3. The projected dimensions of these sheets are 150mm x 50mm x 1mm thick. The crack formers are stiff enough to withstand vibration without any noticeable change in shape. They were placed in position as shown in D of plate 3.4 before pouring the concrete. The mixed concrete was then poured into the moulds in two layers, each layer being table vibrated until no more air bubbles were seen to emerge, but not long enough to cause segregation. This takes between 1½ to 2 minutes. The crack formers were held firmly against the bottom of the moulds during vibration. The mould and its contents were immediately transfered to the CTR after vibration, and covered with polythene sheets for about 2 to 3 hours. The faces were then trowelled flat and covered again with polythene sheets. They were normally demoulded after 20-24 hours.

3.6.2.2.2 Vertically and horizontally cast specimens

A special mould was designed for the vertically cast specimens, marked "A" in plate 3.5. It consists of a plywood sheet with 150mm dia x 50mm thick circular hole cut through its centre. This was then cut into half, and a hole made for pouring in the concrete. Two steel plates, 6mm thick, were clamped to the sides of the plywood and steel studs used to

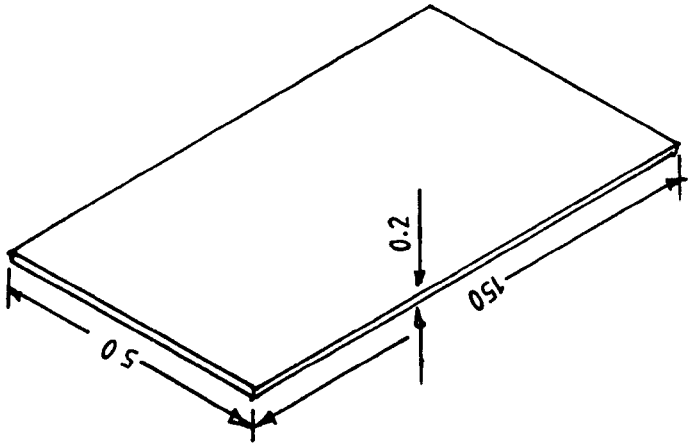

FLAT BRASS PLATE FOR STRAIGHT THROUGH CRACKS

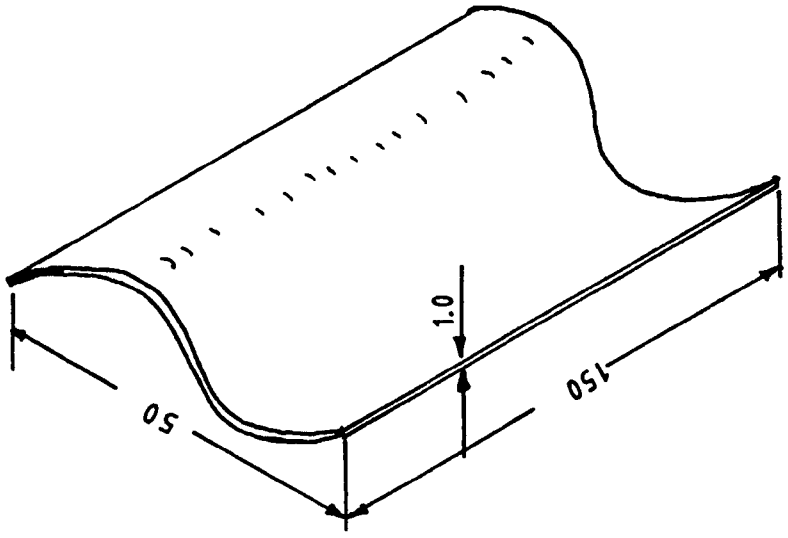

CORRUGATED PLASTIC SHEETS FOR CRACKS SINUSOIDAL ACROSS THE THICKNESS

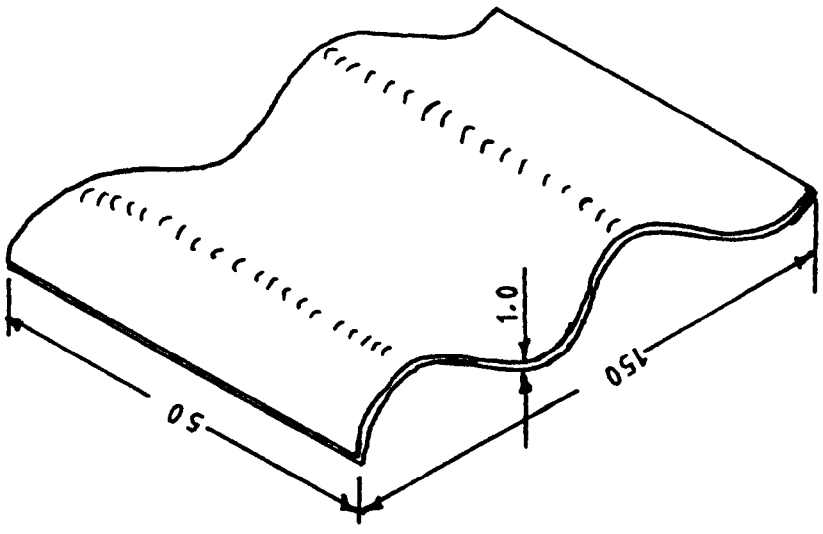

CORRUGATED PLASTIC SHEETS FOR CRACKS SINUSOIDAL ALONG THE DIAMETER

FIG 3.3 CRACK FORMERS FOR VARIOUS CRACK PATTERNS

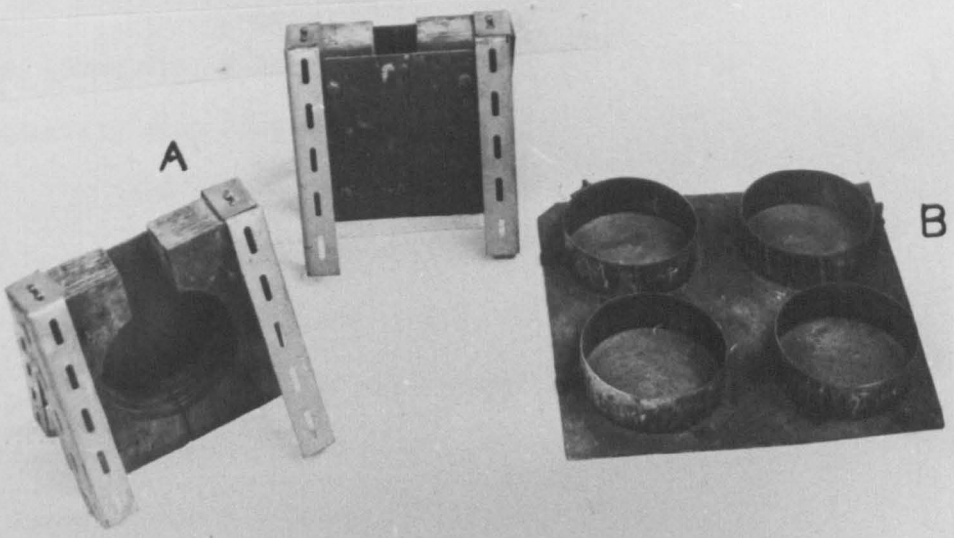

A FOR VERTICALLY CAST SPECIMENS

B FOR HORIZONTALLY CAST SPECIMENS

PLATE 3.5 MOULDS

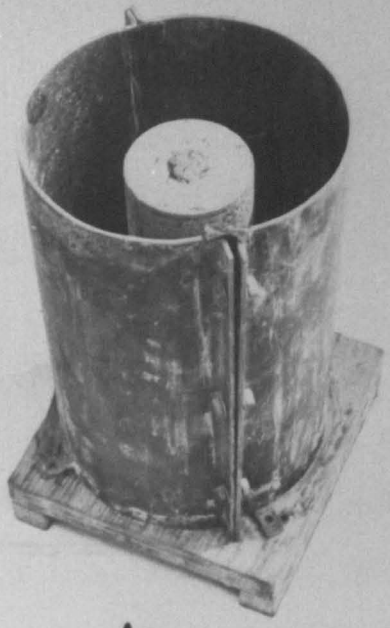

A

MOULD FOR MODEL CONCRETE TANK

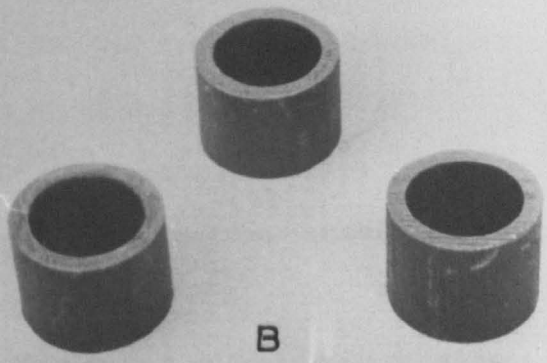

HOLLOW STEEL SPACERS

PLATE 3.6

keep the mould vertical during casting and vibration. A normal steel mould, 150mm dia. x 50mm thick, marked B in plate 3.5, was used for the horizontally cast specimens.

The mixed concrete was poured into the moulds in two layers, each layer being table-vibrated as described in section 3.6.2.2.1. The vibration goes on for about 1 to 3 minutes depending on the w/c ratio, with less time for higher w/c ratios. Table vibration was found to be unsatisfactory when, used alone for compacting the vertically cast specimens, hence a tamping rod was also used. Other treatments carried out on the specimens after compaction are as described in section 3.6.2.2.1.

3.6.2.2.3 Model concrete tanks

The mould for these tanks is shown in plate 3.6 and consists of a wooden base plate and two semi-circular steel plates 8mm thick. The semi-circular steel plates were bolted together and finally screwed to the wooden base plate. The central cavity was created by screwing in a central circular core, as shown in the plate. The core is made of wood and covered with polystyrene sheets to facilitate the removal of the core. During demoulding, the core is removed by dissolving the polystyrene sheets with acetone. The core was made so as to give a 50mm gap with the sides of the steel plates (forming the wall), and 50mm lower than the top of the steel plates to form the tank floor.

The mixed concrete was poured into the moulds in 3 layers. Each of the first two layers was table vibrated for about 1½ minutes. The final layer was then vibrated until no more air bubbles were seen to appear, but not long enough to cause segregation. This also takes about 1½ to 2 minutes. Other treatments after vibration were as described in section 3.6.2.2.1.

3.6.3 Shapes and sizes of concrete specimens

The specimens used for the various investigations were

1. To study the effect of coarse aggregate inclusion on permeability - 100mm dia. x 25mm thick concrete discs. The maximum size of the coarse aggregate was 6.30 mm with grading as shown in Table 3.2. This dimension was chosen to conform with the dimensions of the HCP and mortar specimens for comparative purposes.

2. To study the effect of direction of casting on permeability - 150mm dia. by 50mm thick concrete discs were used, with 10mm maximum size of coarse aggregate.

3. To study the flow of various liquids into concrete (model tanks) - 300mm high x 170mm external diameter cylinders closed at one end were used as the tank. The thickness of the wall and floor was 50mm. Coarse aggregates of 10mm maximum size was used.

3.7 Curing

After demoulding, the specimens were stored in the constant temperature room (fog room) at 22 $\pm$ 1°C and 99 $\pm$ 1% R.H., to hydrate for up to 6 months depending on the testing time. In order to study the effects of curing on pore structure and permeability, some specimens were stored in the CTR immediately after demoulding for up to 3 months.

3.8 Treatments Given to the Specimens after Curing

3.8.1 Crack specimens

Concrete specimens used for testing the flow of liquid through preformed cracks were cured for 28 days. They were then dried at a temperature of 55 $\pm$ 1°C in a mechanically ventilated oven to a constant weight or until the weight loss was about 1gm/day. This took 10-15 days. The oven temperature was raised or lowered at a rate not greater than 8°C/hour to avoid thermal cracking of the specimens. The specimens were allowed to cool to room temperature after drying. The samples for use to investigate the oil flow through cracks were then put in a

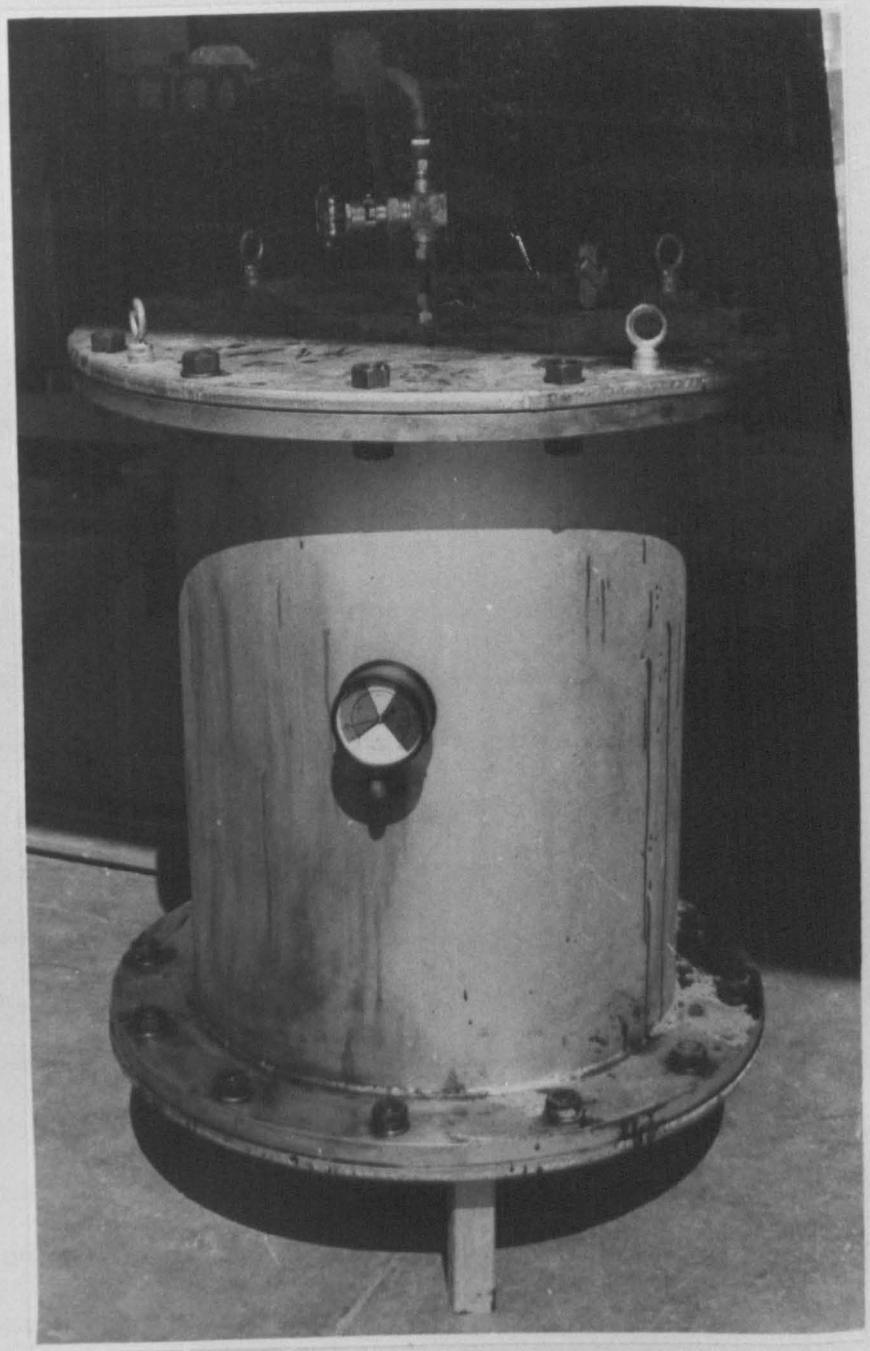

PLATE 3.7 CRUDE OIL PRESSURE VESSEL

pressure vessel filled with crude oil - plate 3.7 and pressurized using nitrogen for 3 months. Those to investigate water flow through cracks were completely sealed in polythene bags and kept in the CTR. An oil pressure of about 0.345 N/mm^2 (50 PSI) was used for saturating the specimens. After the first 3 months of soaking in crude oil, the specimens were stored in a shallow tank of oil at atmospheric pressure prior to test. The specimens for the water flow test were later soaked in a water tank in the CTR for 24 hours prior to test.

3.8.2 Pore structure and permeability specimens

HCP, mortar and concrete specimens for permeability studies were dried at a temperature of 105 $\pm$ 1°C in the mechanically ventilated oven until the weight loss was about 1gm/day. The oven temperature was again controlled as in section 3.8.1. Drying normally took 5-6 days. Specimens for pore structure analysis were dried at this temperature to extract all the evaporable water and leave water free pores for mercury penetration (section 6.3). Specimens for the permeability tests were treated similarly so that the results could be related to the pore parameters, and to enable saturation by crude oil prior to the permeability tests. HCP samples were initially wrapped completely with aluminium foil to ensure a more uniform temperature in the specimen before any water was allowed to dry out. When the specimens reached the required temperature of 105°C, usually in about 25 hours, they were quickly unwrapped inside the oven and left to dry out to a constant weight usually within another 48 hours. This procedure was found to minimise cracking. After drying, the specimens for crude oil permeability tests, were saturated in crude oil in a pressure vessel as described in section 3.8.1.

Specimens for pore structure analysis were stored immediately after drying in a dessicator prior to test in the mercury porosimeter. The specimens used for studying the effect of pre-saturation on pore structure were soaked in the various oil types (Kuwait crude oil, North

Sea crude oil, diesel and parafin) for 3 months, dried after soaking (as in section 3.8.1) and then stored in a dessicator prior to test. Storing in a dessicator was found to minimize any further hydration.

3.8.3 Model concrete tanks

The model concrete tanks were cured for 28 days in the fog room. They were then air dried for 2 months at 22 $\pm$ 1°C and 45 $\pm$ 1% R.H. in a temperature controlled room prior to test.

CHAPTER 4

FLOW THROUGH CRACKS

4.1 Introduction

The flow of liquid through a crack in concrete is governed by the length, width and the meandering nature of the crack. It also depends on the properties of the liquid such as viscosity, density and molecular sizes, and also on the pressure differential across the wall of the containing vessel. Another possible influence on the flow could be the surface texture of the sides of the crack, e.g. flow through a crack in a purely concrete matrix may differ from flow through a crack at the concrete and steel reinforcement interface. The type and shape of aggregate and the fine/coarse aggregate proprtions will also govern this surface texture.

4.2 Scope of the Investigation

This investigation studies the crude oil and water flow through cracks in concrete cast using OPC. The mix proportion used is given in Table 5.1. Flow through various crack patterns was investigated. These patterns are

1. Circular cracks (CIRC) with cores at the centre made of steel, marked "A" in plate 4.1. This crack pattern was obtained by coring through the disc specimens, 150 dia. x 50mm thick, with a 6.3mm dia, diamond tipped drill core. Various steel diameters were obtained to give all-round crack widths of 0.05, 0.1, 0.15, 0.2, 0.25, 0.3mm between the concrete and steel.

2. Preformed cracks - these include (see plate 4.1)

(i) Straight through cracks (STRA) marked B

(ii) Sinusoidal cracks formed across the thickness of the specimen (SINUTH) marked C.

(iii) Sinusoidal cracks formed along the diameter of the specimens

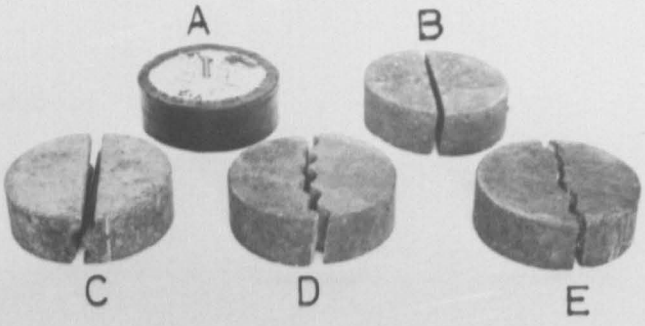

A. CIRCULAR CRACK
B. STRAIGHT THROUGH CRACK ACROSS THE THICKNESS
C. CRACK SINUSOIDAL
D. CRACK SINUSOIDAL ALONG THE DIAMETER
E. NATURAL CRACK

PLATE 4.1 CRACK PATTERNS

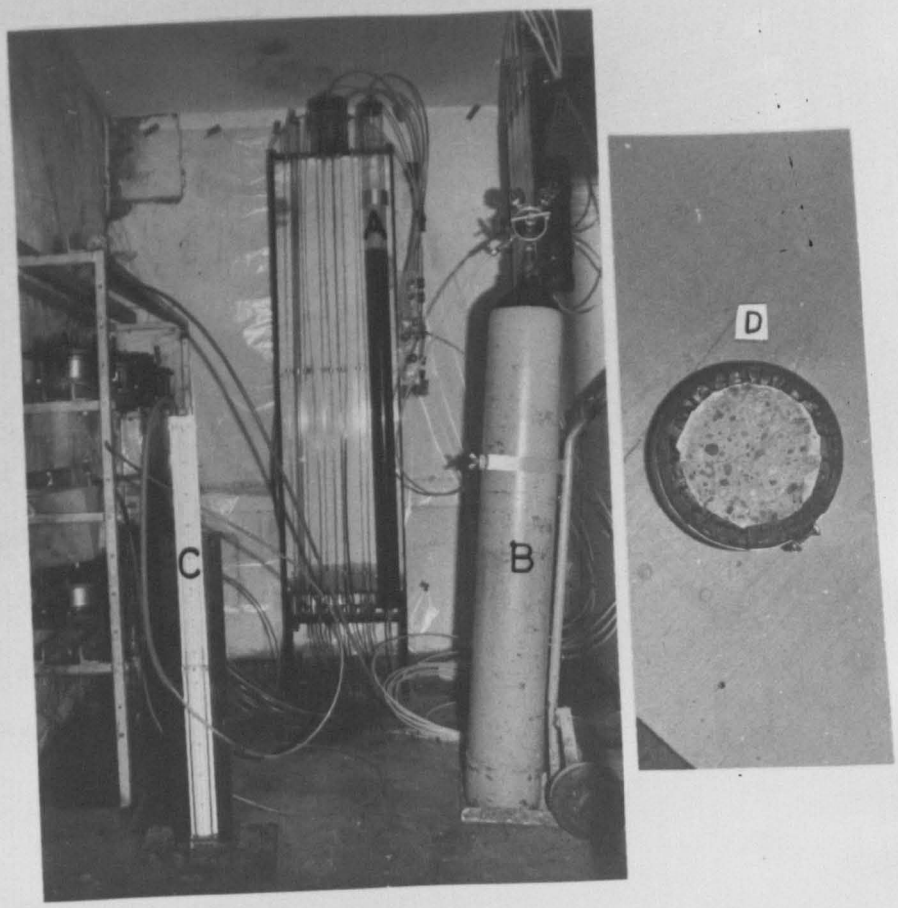

A 78mm INTERNAL DIAMETER PERSPEX TUBE
B NITROGEN PRESSURE BOTTLE
C MERCURY MANOMETER
D CLAMPED SPECIMEN

PLATE 4.2 MODIFIED PERMEABILITY APPARATUS

(SINUDIA) marked D.

These were formed in 150mm dia. x 50mm thick specimens during casting as described in section 3.6.2.2.1.

3. Natural cracks (NATU) These are cracks also formed in 150mm dia. x 50mm thick specimens. After 28 days hydration, the crack was formed in the specimen by loading it along a diameter in the cube testing machine until the concrete split.

The crack widths used for all the preformed and natural cracks were 0.05, 0.10, 0.15, 0.20, 0.25 and 0.30 mm. This was to cover the range of the crack widths found in design codes. Specimens were normally 150mm dia. x 50mm thick, but to investigate the effect of crack depth, specimen thickness of 50, 75, 100 and 125 mm were used for those specimens with natural and circular cracks.

4.3 Apparatus, Specimen Preparation and Testing Procedure

4.3.1 Apparatus

The apparatus used is similar to the permeability apparatus described by Oyeka[17], and full details are given in section 5.2.1.1. The perspex tubes used to measure the oil flow into the specimen, was modified from 4mm internal diameter to 78mm internal diameter, shown marked A in plate 4.2, to accommodate larger flows. The base plate connectors of the permeability cell were subsequently modified.

4.3.2 Specimen Preparation

The following surface treatment was given to the samples, before placing them in the permeability cell, to eliminate surface effects[134], and to obtain specimens of exactly equal thickness. The two surfaces were smoothed using a surface grinder, until the cement laitance was removed and the aggregate particles exposed. To form the cracks of the required thickness, spacer brass plates, of width 5mm, length equal to the specimen

thickness, and of thickness equivalent to the required crack width were inserted at the edges and at the centre of the specimen along its diameter. The two halves of the specimen were then clamped together using G-clamps. The sides of the clamped specimens were thoroughly cleaned with dry fine sand and paper towel, and sealed with two coats of epoxy resin, Feboweld No. 2, at interval of 6 to 8 hours. After a further 15 hours, all the specimens were given 8 to 10 coats of liquid natural rubber around the sides at 30 minutes intervals. After partial drying, the G-clamps were removed and sealing touched up where necessary. Two rubber membranes of 125mm dia. were pulled over the sides and tightly held with tough adhesive tape. To avoid any form of leakage or bursting of the specimens at the side where the two halves were joined, the specimens were finally clamped with steel plates and tightly bolted using 2 to 3 bolts, as shown marked D in plate 4.2. The crack width was again checked using a graduated travelling microscope of up to 40 times magnification before placing them in the permeameter.

4.3.3 Testing Procedures

Specimens for measuring oil flow were first saturated with oil using the technique described in section 3.8.1, before being treated as described in section 4.3.2 and later inserted in the permeameter. The flow test was carried out at ten oil pressures: 0.690, 0.621, 0.552, 0.483, 0.414, 0.345, 0.276, 0.207, 0.138 and 0.069 N/mm^2 corresponding to oil depths of 83.0, 74.70, 66.40, 58.10, 49.80, 41.50, 33.20, 24.90, 16.60 and 8.30 metres respectively. The inlet pressures for water flow were adjusted to give water heads equal to the oil heads, for easy comparisons. The water pressures were 0.814, 0.733, 0.651, 0.570, 0.488, 0.407, 0.325, 0.244, 0.163 and 0.081 N/mm^2 corresponding to water heads of 83.0, 74.70, 66.40, 58.10, 49.80, 41.50, 33.20, 24.90, 16.60 and 8.30 metres respectively. Measurements of liquid flow-rates were begun after the specimen had been in the permeameter for four hours under the minimum pressure of

0.081 N/mm^2, and was then repeated 2 hours later to confirm the validity of the first result. The flow was parallel to the direction of casting for all specimens.

The amount of oil or water flowing into the crack was found by measuring the difference in levels of the liquid in the 78mm perspex tubes held against graduated scales. The outflow was measured by collecting the outflow liquid in a graduated cylinder within a specified time equal to the period used to measure the inflow. This time period depended upon the crack width, type and applied pressure and varied between 1 minute to up to 2 hours. Liquid pressure was held constant with nitrogen gas regulating valves graduated in PSI, to control the pressure from a compressed nitrogen bottle of 13.790 N/mm^2 (2,000 PSI) capacity, marked B in plate 4.2. The inlet pressure, is therefore the pressure as indicated by the controlling valve, while the outlet pressure was measured using mercury manometer, marked C in plate 4.2, connected via a vacuum creating device. An increase in the outflow, produced a corresponding increase in the vacuum pressure created at one end of the manometer, hence the mercury is drawn further up the tube. The change in height of the mercury is read directly on a scale already calibrated in KN/m^2. Recalibration was carried out at intervals for a check.

Measurements were taken at various pressures, mentioned earlier, during a cycle of increasing pressure and repeated during decreasing pressure cycle. The pressure was generally adjusted in steps of 0.081 N/mm^2 (10 PSI). The average of the two values generally agreed to within $95 \pm 4\%$. One exception to this was the oil flow through 0.05mm crack width, in natural crack, where the values were between 10 to 100% apart. Reported results, were the average values obtained from two samples tested, which agreed to within $90 \pm 5\%$. When the two values differed by more than $90 \pm 5\%$, a third sample is tested and the closest averaged.

4.4 Analytical Technique

The equipment for the experimental work is fully described in section 5.2.11, the modifications made on the equipment are described in section 4.3.1. The area of the crack associated with the flow as in equation 2.11, is obtained by multiplying the appropriate crack width by the value of d as shown in the diagram below

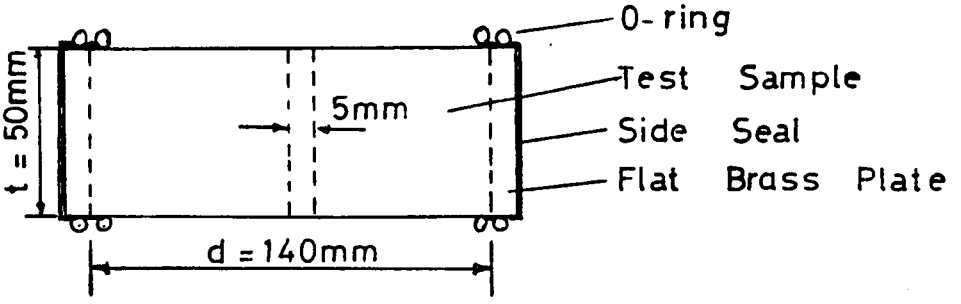

Not to scale

For the cracks, sinusoidal along the diameter, marked "D" in plate 4.1, d = 165mm, and for cracks, sinusoidal across the depth, marked "C" in plate 4.1, t = 55mm. The volume outflow was generally found to be approximately 97 $\pm$ 3% of the volume inflow and the values of V were determined using the volume inflow values.

4.5 Experimental and other Factors affecting the Flow of Oil and Water Through Cracks

4.5.1 Oil and Water Flow

In chapter 2, it was stated that one of the main aims of this research was to ascertain whether the impermeability requirements of water retaining structures, could be applied to oil retaining structures. Results as shown in Table 4.1 and Fig s 4.1 to 4.5 reveal that

1. The flow of water through cracks in concrete is generally greater than the flow of oil through same type of cracks in concrete for any applied pressure. This is observed for all crack patterns and dimensions.

2. The difference between oil and water flow is not unique but varies

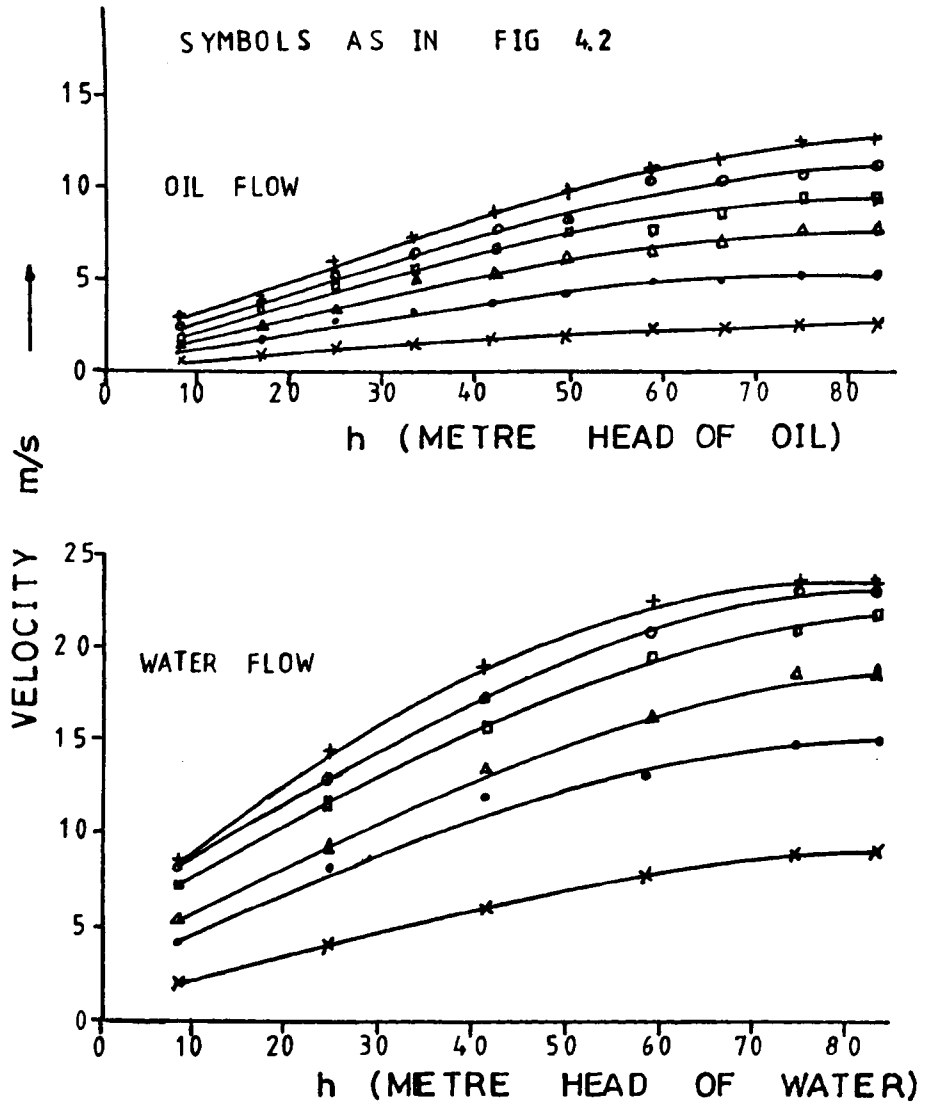

FIG 4.1 FOR CIRCULAR CRACKS

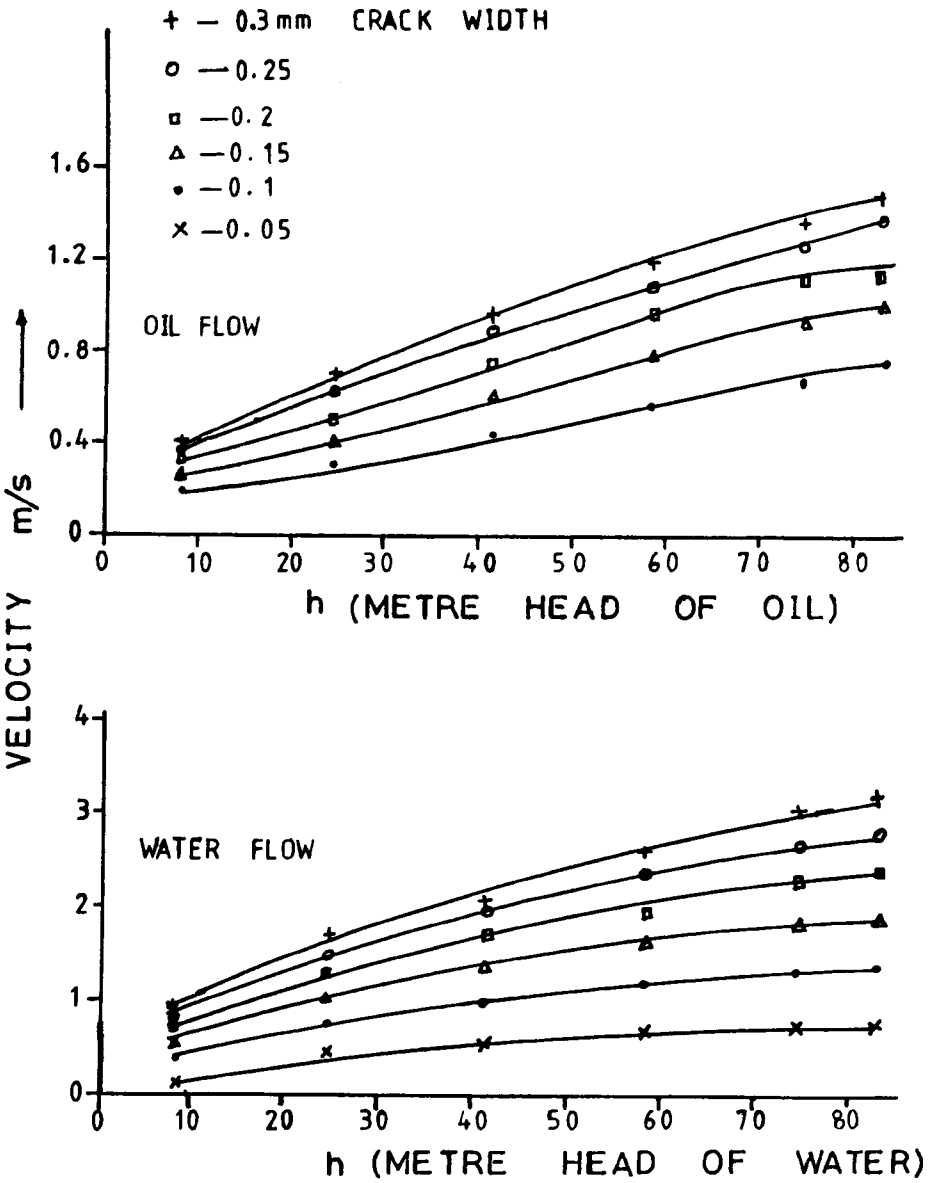

FIG 4.2 FOR NATURAL CRACKS

FIG 4.1 & 42 GRAPH OF VELOCITY VS APPLIED PRESSURE IN METRES HEAD OF LIQUID

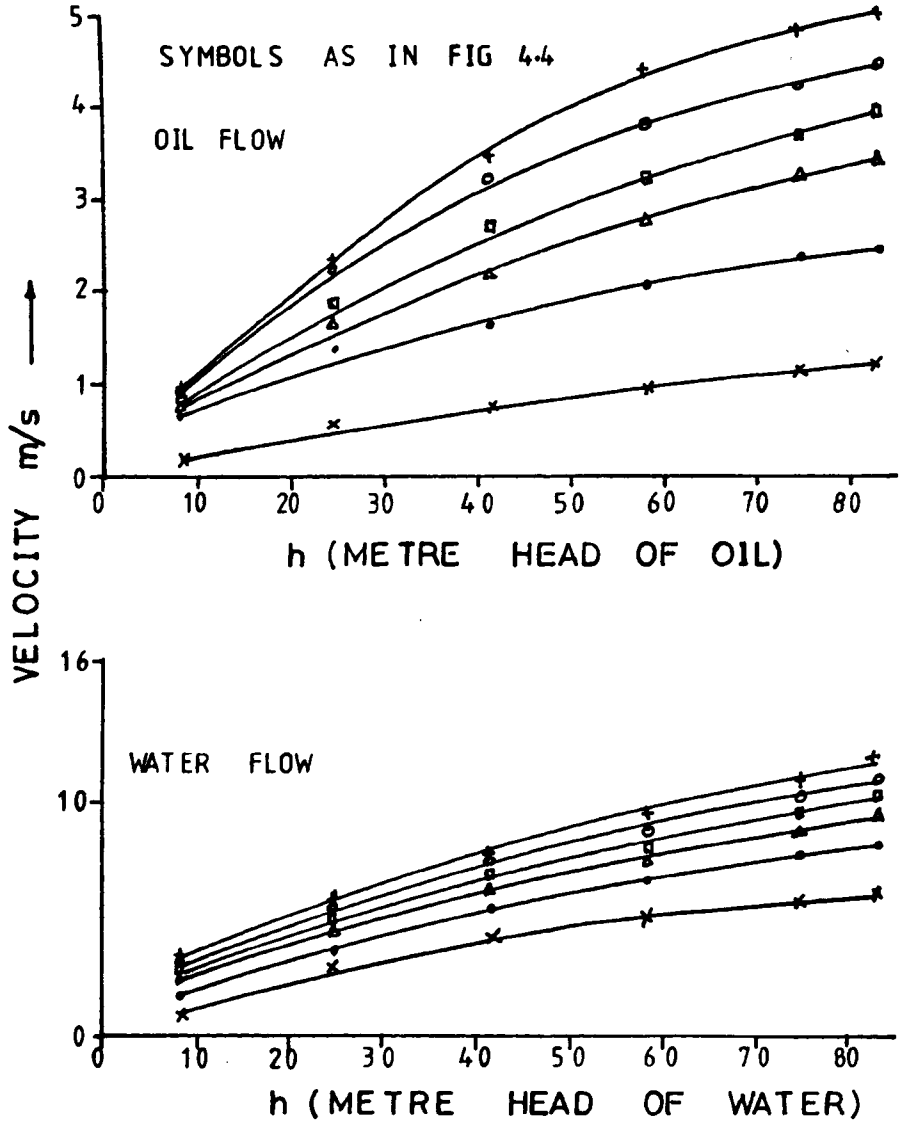

FIG 4.3 FOR STRAIGHT THROUGH CRACKS

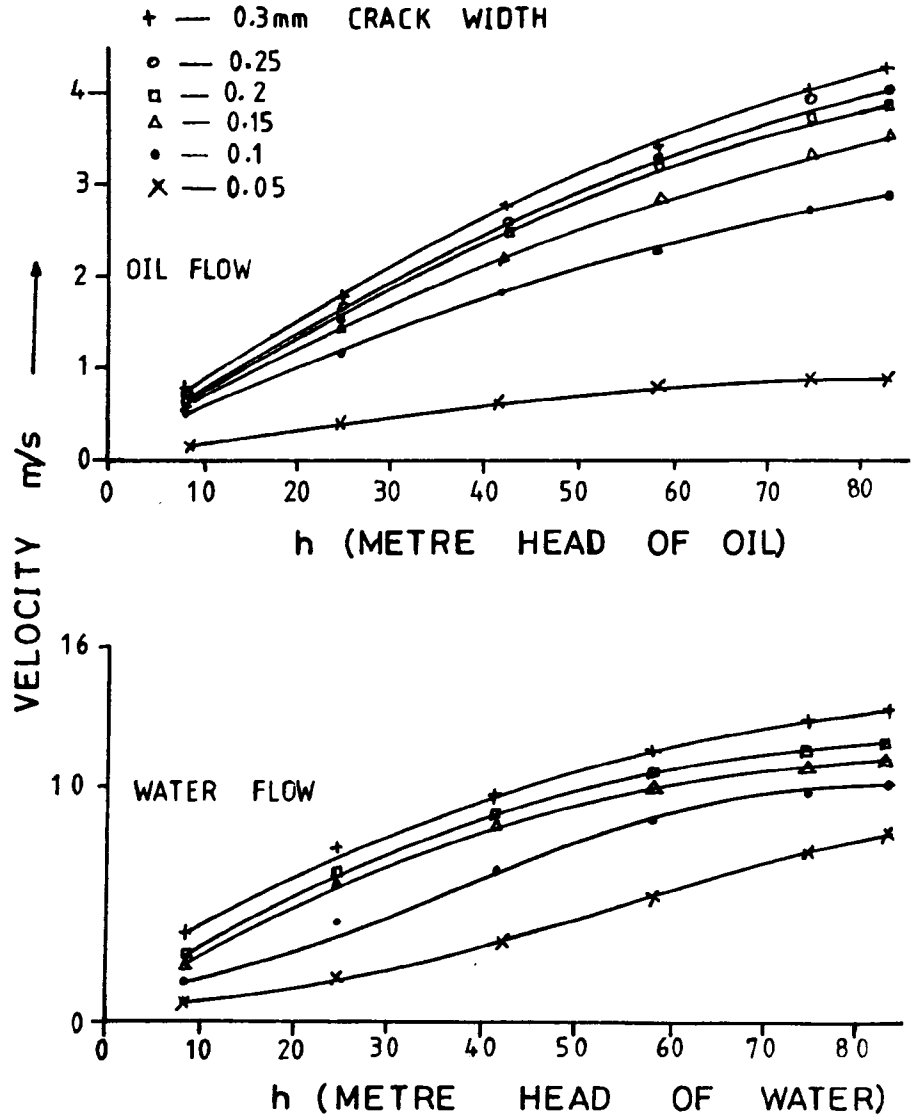

FIG 4.4 FOR CRACKS SINUSOIDAL ALONG THE DIAMETER.

FIG 4.3 & 4.4 GRAPH OF VELOCITY VS APPLIED PRESSURE IN METRES OF THE LIQUID

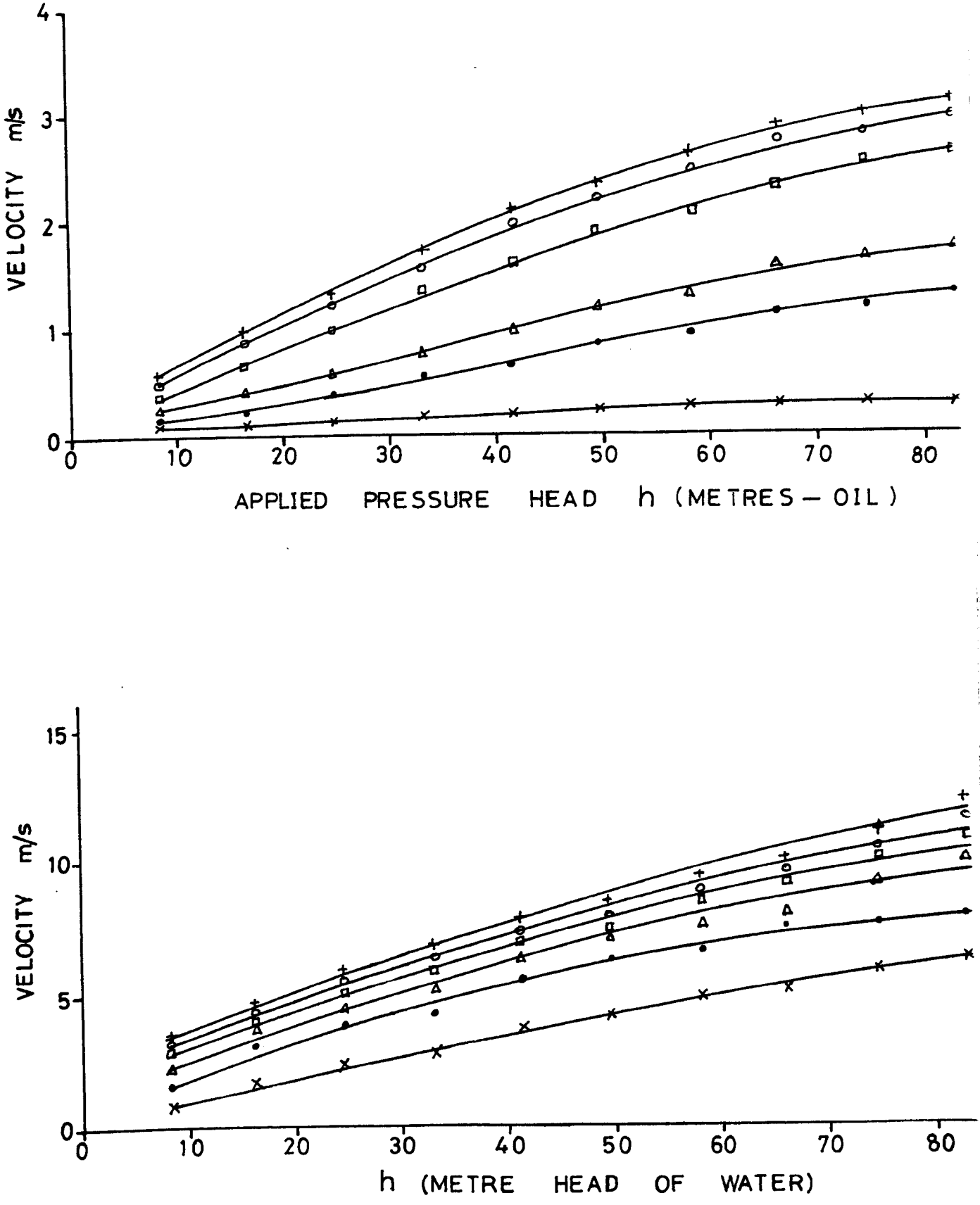

FIG 4.5 GRAPH OF VELOCITY VS APPLIED PRESSURE HEAD OF THE LIOUID FOR CRACKS SINUSOIDAL ACROSS THE THICKNESS

CIRCULAR CRACKS

PRESSURE (m) \ CRACK WIDTH (mm)	OIL FLOW 0.05	0.10	0.15	0.20	0.25	0.30	WATER FLOW 0.05	0.10	0.15	0.20	0.25	0.30
8,30	0.53	1.09	1.55	1.95	2.72	2.88	1.91	4.09	5.50	7.26	8.17	8.19
16.60	0.79	1.32	2.68	3.22	3.45	4.20	2.92	6.48	7.28	10.89	11.39	13.40
24.90	0.91	2.50	3.30	4.52	5.16	5.78	3.92	8.06	10.74	11.50	12.75	14.25
33.20	1.21	3.20	5.50	5.60	6.48	6.90	4.74	9.48	10.80	12.69	13.64	14.74
41.50	1.24	3.76	5.54	6.51	7.89	8.74	5.92	11.92	13.15	15.30	17.00	18.87
49.80	1.64	4.10	6.19	7.65	8.17	9.79	6.56	12.28	14.41	17.09	19.51	21.11
58.10	2.10	4.77	6.39	7.67	10.47	11.06	7.76	12.96	16.03	19.28	20.74	22.51
66.40	2.11	4.98	6.82	8.45	10.49	11.26	8.43	13.22	17.03	20.00	22.30	22.67
74.70	2.21	5.01	7.51	9.45	10.70	12.41	8.98	14.65	18.52	20.83	23.00	23.51
83.0	2.50	5.31	7.75	9.51	11.26	12.56	9.49	14.93	18.70	21.65	23.14	23.56

NATURAL CRACKS

	OIL FLOW						WATER FLOW					
8.30	+0.016	0.19	0.275	0.34	0.375	0.40	0.11	0.475	0.62	0.82	0.91	1.00
16.60	0.033	0.235	0.33	0.42	0.49	0.58	0.27	0.66	0.91	1.02	1.25	1.40
24.90	0.079	0.305	0.415	0.50	0.62	0.70	0.47	0.75	1.01	1.30	1.48	1.70
33.20	0.091	0.35	0.50	0.60	0.74	0.825	0.51	0.84	1.26	1.44	1.56	1.82
41.50	0.068	0.425	0.60	0.75	0.90	0.975	0.54	0.98	1.35	1.72	1.98	2.08
49.80		0.50	0.67	0.82	0.95	1.10	0.61	1.04	1.45	1.81	2.11	2.40
58.10		0.58	0.79	0.98	1.085	1.185	0.70	1.18	1.62	1.95	2.36	2.60
66.40		0.63	0.855	1.125	1.19	1.30	0.72	1.24	1.67	2.20	2.60	3.01
74.70		0.66	0.93	1.21	1.27	1.36	0.75	1.31	1.84	2.31	2.66	3.02
83.0		0.75	1.01	1.31	1.38	1.47	0.76	1.40	1.93	2.42	2.82	3.20

CRACKS SINUSOIDAL ACROSS THE THICKNESS

	OIL FLOW						WATER FLOW					
8.30	0.09	0.16	0.25	0.39	0.50	0.59	0.81	1.55	2.25	2.85	3.15	3.45
16.60	0.10	0.23	0.41	0.63	0.86	0.98	1.60	3.0	3.65	4.00	4.35	4.65
24.90	0.13	0.40	0.57	0.98	1.22	1.32	2.40	3.81	4.50	5.00	5.50	5.81
33.20	0.16	0.55	0.76	1.35	1.56	1.70	2.66	4.10	5.05	5.80	6.31	6.65
41.50	0.20	0.64	0.96	1.60	1.96	2.10	3.70	5.55	6.20	6.90	7.05	7.65
49.80	0.23	0.83	1.20	1.90	2.20	2.32	4.10	6.25	7.00	7.20	7.65	8.25
58.10	0.26	0.94	1.30	2.05	2.48	2.60	4.80	6.55	7.50	8.40	8.75	9.35
66.40	0.27	1.18	1.55	2.32	2.74	2.86	5.10	7.40	7.85	9.01	9.41	9.85
74.70	0.29	1.20	1.66	2.55	2.80	2.96	5.90	7.50	9.20	10.15	10.35	11.00
83.0	0.30	1.31	1.75	2.64	2.92	3.12	6.25	7.85	10.01	11.00	11.70	12.25

CRACKS SINUSOIDAL ALONG THE DIAMETER

	OIL FLOW						WATER FLOW					
8.30	0.16	0.55	0.65	0.70	0.75	0.78	0.90	1.65	2.50	2.85	2.40	3.70
16.60	0.25	0.88	1.05	1.20	1.25	1.33	1.30	2.55	4.60	4.85	3.90	5.80
24.90	0.40	1.15	1.46	1.63	1.66	1.78	2.00	4.35	6.10	6.30	5.25	7.40
33.20	0.55	1.50	1.90	2.10	2.20	2.31	2.50	5.0	7.00	8.00	6.30	8.45
41.50	0.65	1.80	2.20	2.45	2.60	2.75	3.70	6.75	8.40	8.60	7.20	9.90
49.80	0.73	2.10	2.55	2.78	3.05	3.18	4.60	8.01	9.40	9.60	7.85	10.60
58.10	0.82	2.28	2.88	3.20	3.28	3.42	5.50	8.41	10.0	10.35	8.80	11.55
66.40	0.84	2.60	3.05	3.45	3.65	3.80	6.10	9.0	10.50	10.70	9.80	12.15
74.70	0.90	2.75	3.35	3.75	3.95	4.08	7.05	9.60	10.90	11.40	10.30	12.80
83.0	0.92	2.88	3.55	3.91	4.05	4.28	8.10	10.01	11.10	11.80	10.50	13.25

STRAIGHT THROUGH CRACKS

	OIL FLOW						WATER FLOW					
8.30	0.2	0.65	0.76	0.79	0.80	0.88	0.95	1.98	2.50	2.85	3.15	3.25
16.60	0.31	1.02	1.16	1.275	1.375	1.40	1.74	3.04	3.50	3.78	4.72	5.01
24.90	0.55	1.40	1.67	1.90	2.30	2.34	3.05	4.62	5.0	5.20	5.58	5.92
33.20	0.65	1.56	1.97	2.20	2.80	2.96	3.73	4.96	5.56	6.12	6.40	6.75
41.50	0.76	1.60	2.18	2.70	3.20	3.46	4.30	5.50	6.36	6.92	7.51	7.62
49.80	0.84	1.80	2.376	3.00	3.40	4.00	4.50	5.78	6.96	7.25	7.86	8.50
58.10	0.90	2.05	2.72	3.20	3.80	4.40	5.00	6.60	7.40	8.01	8.66	9.40
66.4	0.98	2.22	3.00	3.50	4.00	4.69	5.15	6.94	7.94	8.56	9.28	9.60
74.70	1.12	2.36	3.25	3.70	4.22	4.82	5.68	7.75	8.68	9.40	10.0	10.60
83.0	1.20	2.43	3.44	3.94	4.46	4.98	6.01	8.10	9.45	10.22	10.98	11.8

+ Clogging of the pores by larger particles of the oil very apparent

TABLE 4.1 Velocity of flow (m/s) for different crack width, patterns and applied pressure

from one crack pattern to another. The water flow varies from being about 1.88 times greater than the oil flow in a circular crack, 0.3mm wide with 83.0 metre equivalent head of liquid, to 6.88 times the oil flow in a natural crack 0.05mm wide and 8.30 metre equivalent head of liquid, with intermediate values for other crack patterns, widths and applied pressure heads.

3. For a given crack pattern, the difference in the velocity of flow between the water and oil is not unique but varies with crack width and liquid pressure, Table 4.2. For liquid flow through a natural crack, at 8.30 metre pressure head, water flow varies from 6.88 times greater than the oil flow for a 0.05mm crack width to 2.25 times greater than the oil flow in 0.15mm crack width, with the variation averaging 3.16. It appears roughly, from these results that the smaller the crack width the greater is the difference between the rate of flow of water and oil.

4. For flow through a natural crack of width 0.2mm, the water flow varies from 1.85 times greater than the oil flow at 83.0 metre pressure head, to 3.13 times greater than the oil flow at 24.90 metre pressure head. The variation averages to 2.31 and decreases with increase in pressure head. However this trend is neither clear nor unique.

5. Similar trends are observed in other crack patterns, but the magnitude of the variation differs from one crack pattern to another.

6. Oil flow through a natural crack of width 0.05mm was found to decrease more rapidly with oil pressure after a pressure of 41.50 metre head of oil (Table 4.1). For these low flows therefore, the 78mm diameter perspex tube could not record quite accurately the very small decrease in oil level. Later examination of the surfaces of the crack revealed large quantities of larger oil particles bound to the surface as a waxy deposit. These deposits were thought to have reduced the crack width, leaving only small interconnected flow channels. Such deposits were observed in all crack widths and patterns but were larger in small cracks.

VOLUME FLOW RATE x 10^{-4} m^3/S

CRACK WIDTH / PRESSURE HEAD	0.05	0.10	0.15	0.20	0.25	0.30
	CIRCULAR CRACK (OIL FLOW)					
33.20	0.61	3.20	8.25	11.20	16.20	20.70
49.80	0.82	4.10	9.29	15.30	20.43	29.37
66.40	1.06	4.98	10.23	16.90	26.18	33.78
	CIRCULAR CRACK (WATER FLOW)					
33.20	2.32	9.48	16.20	25.38	34.10	44.22
49.80	3.28	12.28	21.62	34.18	48.78	63.33
66.40	4.22	13.22	25.55	41.66	55.75	68.01
	NATURAL CRACK (OIL FLOW)					
33.20	-	0.35	0.75	1.20	1.85	2.50
49.80	-	0.50	1.01	1.64	2.40	3.30
66.40	-	0.63	1.28	2.25	3.00	3.90
	NATURAL CRACK (WATER FLOW)					
33.20	0.24	0.75	1.52	2.60	3.70	5.10
49.80	0.31	1.04	2.18	3.62	5.28	7.20
66.40	0.36	1.24	2.51	4.40	6.50	9.03

TABLE 4.2 Volume flow rate per metre length of crack

These experimental observations, show that concrete tanks designed to retain water can be expected to adequately satisfy the impermeability requirements of crude oil storage tanks. Care should be taken in extrapolating these results to oil or materials other than those used in the present research, particularly while using oil with smaller molecular sizes than crude oil. This is the subject of discussion in Chapter 5, along with a discussion of the role of the wax content in crude oil.

4.5.2 Effect of Crack Width on Flow

For a given crack length, the crack width is one of the main parameters controlling fluid flow. The graph of velocity vs crack width for these oil and water pressure heads is shown in Figs. 4.6 and 4.7, for two crack patterns. The following observations are made from the plot.

1. The velocity, hence the flow rate per unit area, increases non-linearly, for both oil and water, with an increase in crack width.

2. The rate of increase in velocity decreases with increasing crack width, for the range of crack widths considered and in all the crack patterns, Figs. 4.6 and 4.7. Figs. 4.1 to 4.5 indicate that the rate of increase in velocity with crack width, tends to be much lower between crack widths of 0.1 to 0.3mm than between crack widths of 0.05 and 0.1mm. For example, for oil and water flow through natural cracks at a pressure head of 8.30m, the rates of increse in flow velocity, when the crack width is increased from 0.05 to 0.10, 0.10 to 0.15, 0.15 to 0.20, 0.20 to 0.25 and 0.25 to 0.30 are 11.88, 1.45, 1.24, 1.10 and 1.07 respectively for oil flow, and 4.32, 1.31, 1.32, 1.11 and 1.10 respectively for water flow. This much more regulated rate of increase after a crack width of 0.1mm, indicates that the clogging of the cracks by the waxy deposits of the oil was more effective on crack widths not greater than 0.1mm.

The fact that velocity increased with crack width can be explained from the known behaviour of real fluids as distinct from ideal fluids. An ideal fluid flows with equal velocity at all parts of the cross section,

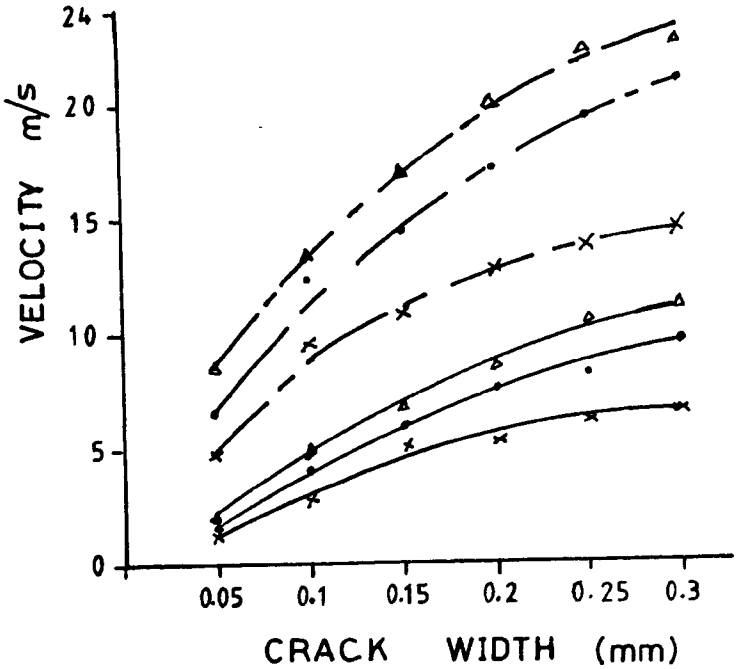

× — 33 2 METRE HEAD OF LIQUID
• — 49.8 " " " "
△ — 66.4 " " " "

——————— OIL FLOW
—— — —— — WATER FLOW

FIG 4.6 GRAPH OF VELOCITY VS CRACK WIDTH FOR CIRCULAR CRACKS

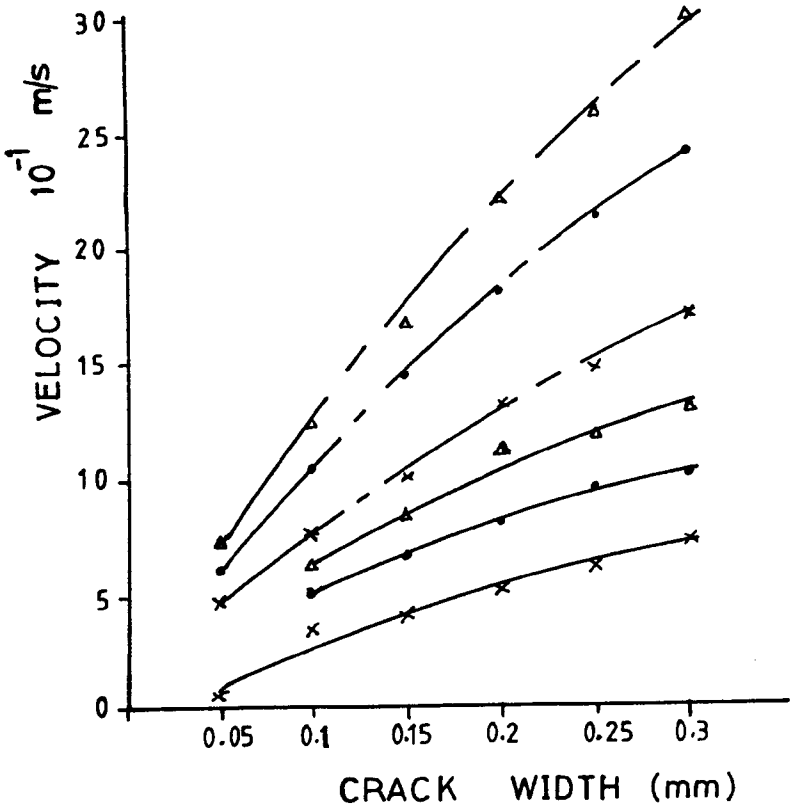

FIG 4.7 GRAPH OF VELOCITY VS CRACK WIDTH FOR NATURAL CRACKS

while a real fluid, as a result of induced viscous shearing, suffers a severe retardation in velocity in the vicinity of a boundary and at the boundary itself the velocity is zero [30]. The layer of fluid adjacent to a boundary where the viscous effects are evident is called the boundary layer. Initially there is a fairly increase in the thickness of the boundary layer, but the rate of increase progressively diminishes with distance along the crack. As the thickness of this boundary layer depends partly on the length of the flow channel, and independent of the width of the crack, the layer may occupy the entire cross-sectional area of the smaller crack width. This would consequently mean greater retardation in velocity. As the crack width increases the magnitude of the retardation in velocity decreases since less proportion of the cross-sectional area of the crack is occupied by this layer, therefore a higher velocity is observed at higher crack width. The boundary layer effect of real fluids may therefore be responsible for the increase in velocity with increased crack width.

3. The rate of increase in volume flow rate (i.e. discharge) increases with increase in crack width as shown in Table 4.2, and Figs. 4.8 and 4.9, for circular and natural cracks respectively. This is because, as the crack width increases, so does the cross-sectional area and hence the volume flow rate i.e. $Q = VA$.

4.5.3 Effect of Applied Pressure

The variation of flow velocity (V), with the applied pressure (h), in metre head of liquid, is illustrated in Figs. 4.1 to 4.5 and in Table 4.1 for all the crack patterns, water and oil flow and for all the crack widths considered. The following observations are made from these results.

1. The flow velocity increases non-linearly with an increase in the applied pressure for all the crack widths and shapes, and for both oil and water flow.

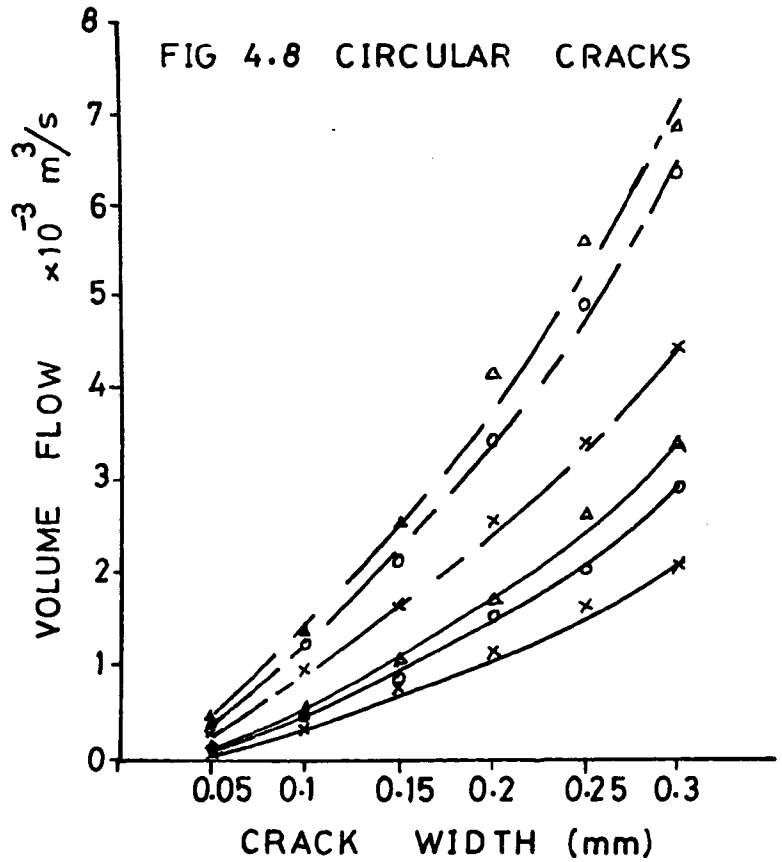

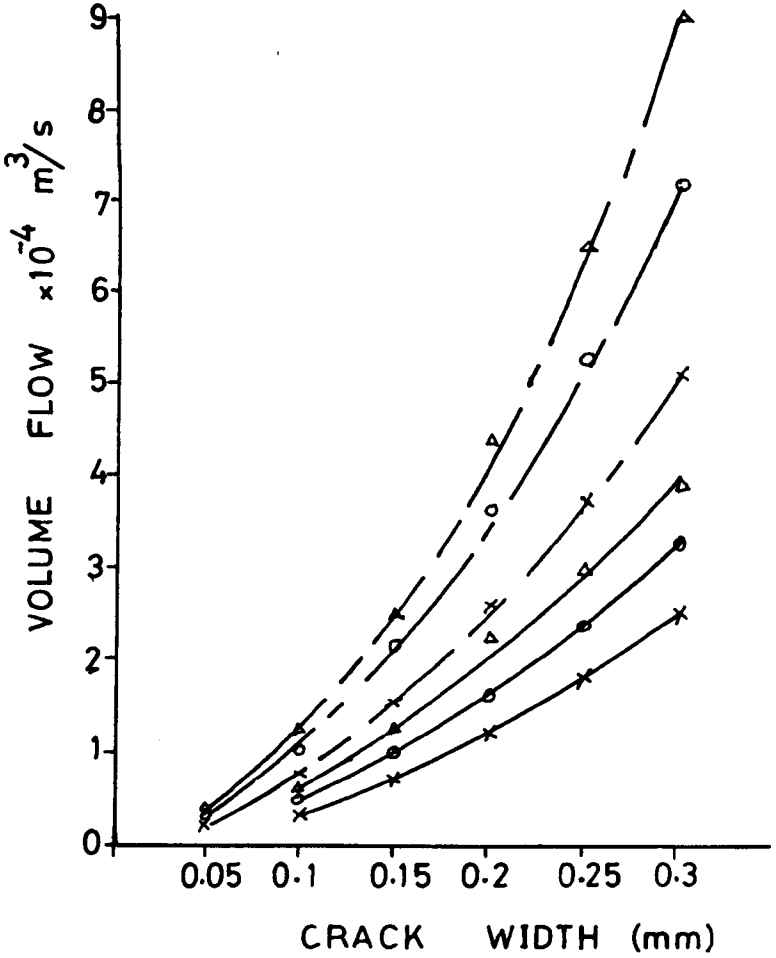

FIG 4.9 NATURAL CRACKS

FIG 4.8 & 4.9 GRAPH OF VOLUME FLOW RATE VS CRACK WIDTH FOR A METRE LENGTH OF CRACK

2. The rate of increase in velocity decreases as the applied pressure increases, within the range of pressures considered in the experiment.

3. The rate of increase in velocity with applied pressure appears to be greater for oil flow than for water flow. For example, if a circular crack is considered, the oil flow at 83.0 metres pressure head of oil is 5.21 times the flow at 8.30 metres pressure head of oil for crack width of 0.3mm. For the same width of crack, the water flow at 83.0 metres pressure head of water is 3.53 times the water flow at 8.30 metres pressure head of water. This trend is observed in most of the tests. However the rate of increase is not constant but varies from one crack width and shape to another.

4. For the flow of oil through the cracks, the relationship between the velocity and applied pressure head can be represented with an empirical equation of the form

$$V = A_o h^{0.75} + V_o \qquad (4.1.)$$

For the flow of water, the empirical relationship is represented as

$$V = A_w h^{0.75} + V_w \qquad (4.2)$$

where A_o, V_o, A_w and V_w are constants, for a given crack width and shape. The values of A_o, V_o for oil flow and A_w, V_w for water flow were determined by regression analysis of the results in table 4.1 and are shown in tables 4.3 and 4.4 respectively, for various crack widths and shapes.

5. Fundamentally V should be zero when h = 0, since flow could only take place under a pressure differential, if only pressure head is responsible for the flow. This is not the case in equation 4.1 and 4.2, where $V = V_o$ or V_w when h = 0. If other factors such as concentration gradient, etc (usually observed in a porous medium) are assumed absent, the flow could be

$V = A_o h^{\alpha} + V_o$ Oil flow $\alpha = 0.75$

	NATURAL CRACK			CIRCULAR CRACK		
CRACK WIDTH	A_o	V_o	r	A_o	V_o	r
0.05	-	-	-	0.090	0.001	0.985
0.10	0.0253	0.031	0.994	0.201	0.180	0.980
0.15	0.0340	0.058	0.995	0.274	0.651	0.974
0.20	0.0451	0.036	0.990	0.342	0.626	0.991
0.25	0.0451	0.132	0.998	0.410	0.692	0.984
0.30	0.0473	0.183	0.998	0.456	0.775	0.992
	SINUSOIDAL ALONG THE DIAMETER			SINUSOIDAL ACROSS THE THICKNESS		
0.05	0.036	0.012	0.985	0.010	0.026	0.990
0.10	0.108	0.012	0.997	0.055	-0.186	0.992
0.15	0.131	0.028	0.998	0.071	-0.166	0.996
0.20	0.146	0.029	0.998	0.105	-0.148	0.997
0.25	0.153	0.038	0.996	0.113	0.004	0.993
0.30	0.159	0.064	0.997	0.116	0.073	0.995
	STRAIGHT THROUGH CRACKS					
0.05	0.043	0.011	0.993			
0.10	0.077	0.400	0.990			
0.15	0.117	0.251	0.997			
0.20	0.140	0.243	0.994			
0.25	0.160	0.311	0.983			
0.30	0.192	0.128	0.985			

TABLE 4.3 Constants of Regression for Equation 4.1 (velocity versus applied pressure load) oil flow

$V = A_w h + V_w$ WATER FLOW

NATURAL CRACK				CIRCULAR CRACK		
CRACK WIDTH	A_w	V_w	r	A_w	V_w	r
0.05	0.0215	0.0977	0.959	0.350	0.102	0.998
0.10	0.0402	0.3019	0.998	0.474	2.73	0.980
0.15	0.0560	0.4115	0.995	0.605	2.91	0.992
0.20	0.0724	0.4644	0.997	0.646	4.64	0.990
0.25	0.0862	0.5033	0.995	0.707	5.11	0.987
0.30	0.0988	0.5393	0.995	0.690	6.59	0.968

	SINUSOIDAL ALONG THE DIAMETER			SINUSOIDAL ACROSS THE THICKNESS		
	b	a	r	b	a	r
0.05	0.328	-1.420	0.988	0.243	-0.411	0.997
0.10	0.393	0.159	0.988	0.282	0.550	0.988
0.15	0.381	1.555	0.980	0.327	0.752	0.995
0.20	0.388	1.833	0.983	0.353	1.018	0.996
0.25	-	-	-	0.357	1.334	0.995
0.30	0.417	2.449	0.989	0.372	1.544	0.997

	STRAIGHT THROUGH CRACKS		
	b	a	r
0.05	0.217	0.309	0.981
0.10	0.258	1.124	0.989
0.15	0.294	1.321	0.995
0.20	0.315	1.455	0.996
0.25	0.326	1.850	0.997
0.30	0.351	1.856	0.996

TABLE 4.4 Constants of Regression for Equation 4.2 (Velocity versus applied pressure water flow)

said to be purely due to pressure differential. V_o and V_w therefore could be due to seepage through the pores of the concrete when the pressure is applied. Apart from some minor deviations in the results from cracks which were sinusoidal across the thickness (SINUTH), generally V_o and V_w increases with an increase in the crack width. This behaviour suggests that other factors, apart from seepage (since seepage should be independent of crack width) did contribute to the emergence of V_o and V_w. These other factors could not be accounted for, however the behaviour shows that increase in the crack width, would mean greater loss of liquid even at very low liquid head.

6. The values of A_o and V_o are generally lower than the values of A_w and V_w respectively for a given crack width and shape. The negative values obtained for some values of V_o and V_w, are attributed to experimental errors.

7. Typical plots of equations 4.1 and 4.2 are shown in Fig. 4.10 for oil and water flow through circular cracks.

The non-linear nature of V versus h plots of Figs.4 .1 to 4.5, could be explained from the behaviour of real fluids. Since real fluids exhibit turbulent flow phenomenon[30], pressure losses are experienced along the crack depth, due to friction. It has been pointed out[30], that these losses increase with an increase in velocity and so a greater reduction in pressure (ΔP) producing the flow is expected at higher velocities. This consequently results in a lower rate of velocity increase with pressure.

The higher rate of increase in oil flow with pressure, than in water flow (point 3), suggests a possible clogging of the flow area by the waxy deposits in the oil at low pressures. At higher pressures, the higher velocities generated, flushes off some of the debris, therefore creating a larger flow area, hence a greater rate of increase than water, which does not have such deposits.

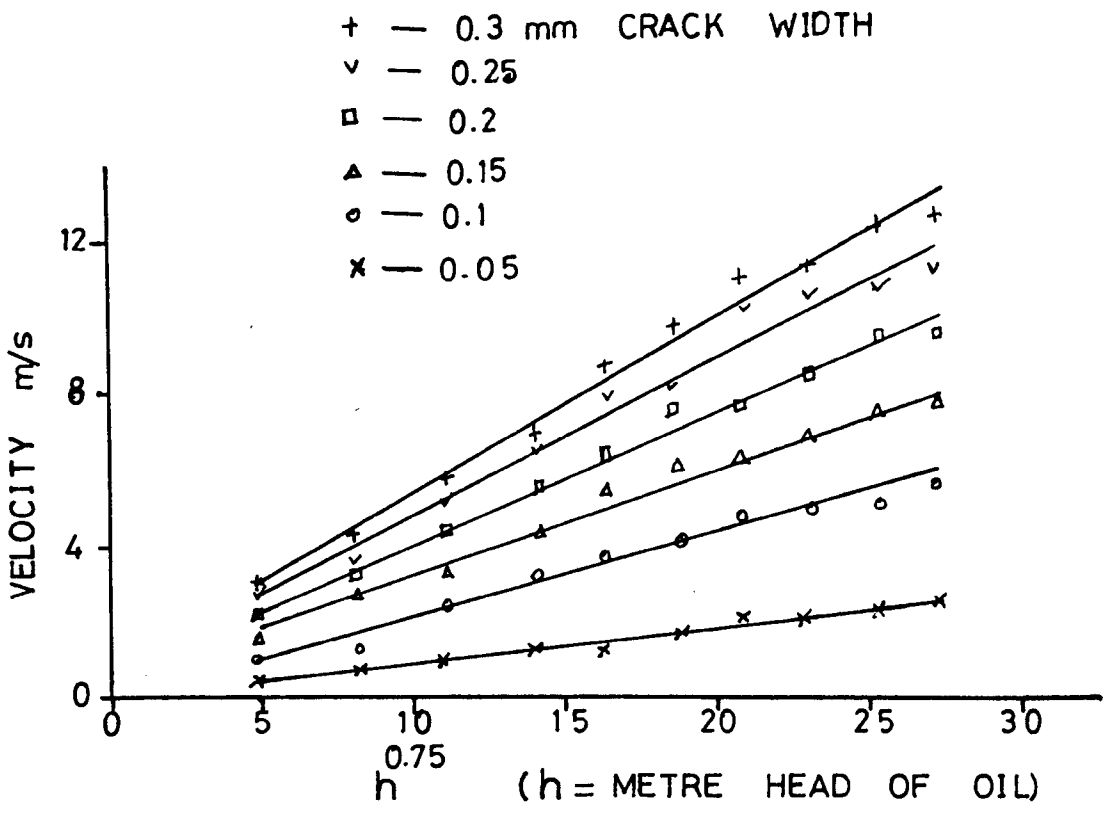

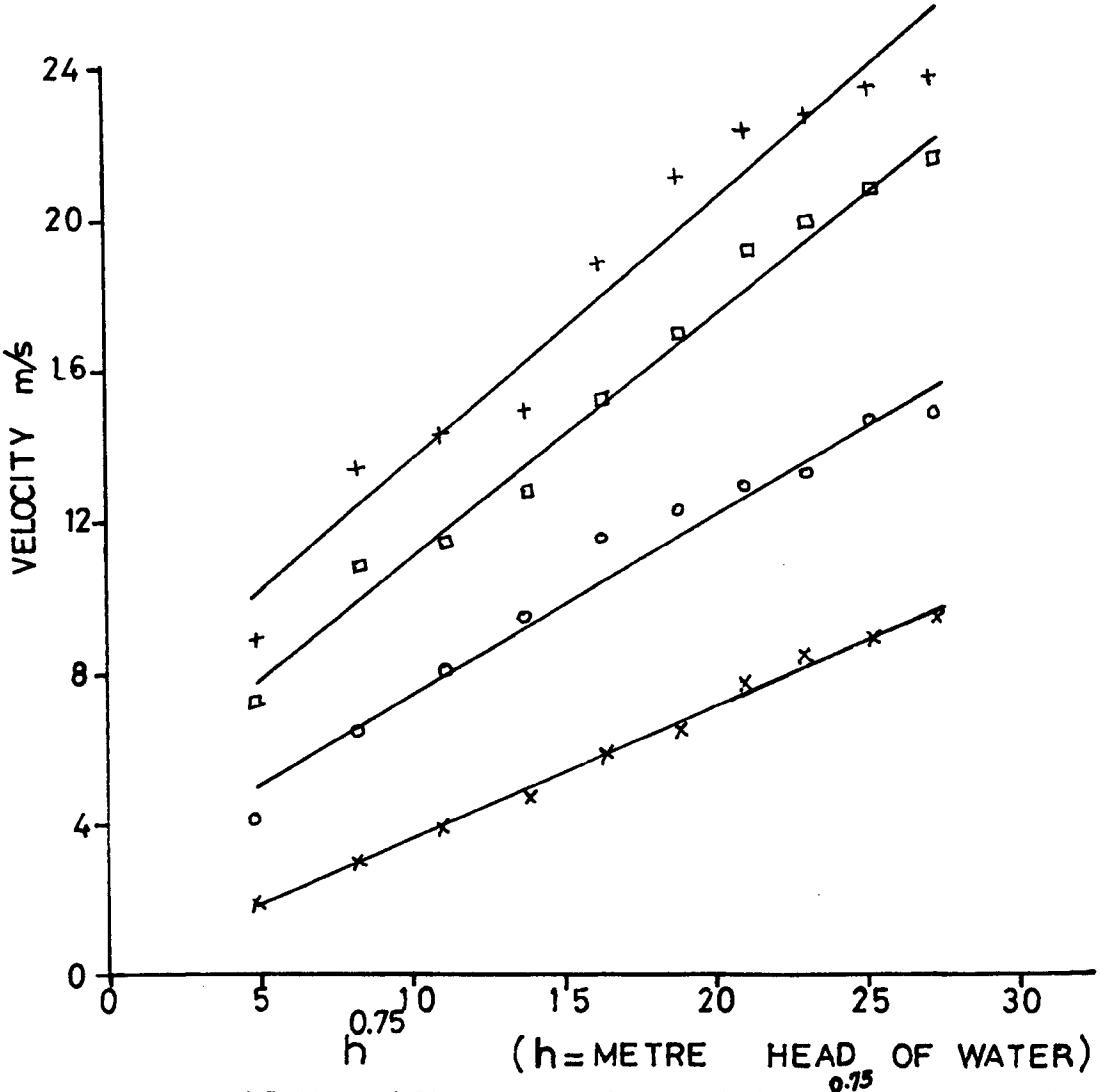

FIG 4.10 GRAPH OF VELOCITY VS $h^{0.75}$ FOR OIL & WATER FLOW THROUGH CIRCULAR CRACKS

Equations 4.1 and 4.2 enable the flow velocity from a liquid retaining structure to be estimated if the tank height is known. This estimate is likely to be more reliable for the initial flow because further hydration may heal the cracks under water flow, and wax and larger oil molecules may be deposited with time for oil flow. In addition the equations are derived for tests using a crack depth of 50mm, with uniform crack widths. In practice, crack widths are not uniform, and the equation can be expected to give only an average value for flow.

4.5.4 Effect of Crack Patterns

The variation of velocity with applied pressure for all the crack patterns is shown in Figs. 4.1 to 4.5. Also the results are tabulated in Table 4.1. The following observations are made.

1. The flow velocities are greater for circular cracks, for any given crack width and for both oil and water flow.

2. Natural cracks tend to show the lowest flow velocities for any given crack width and for both oil and water flow.

3. Cracks sinusoidal along the diameter show slightly higher flow velocities than for cracks sinusoidal across the thickness, for both oil and water flow and for all the crack widths, especially at higher flows. The differences however are quite small.

4. Straight through cracks show slightly lower flow velocities than do the sinusoidal cracks at larger flows, however the flow velocities of these three crack patterns (ie straight through cracks (STRA), cracks sinusoidal along the diameter (SINUDIA) and cracks sinusoidal across the thickness (SINUTH) tend to vary such that there is not a consistent relationship between them (Table 4.5). For example the flow velocity for STRA cracks at 16.60m, pressure head, with a 0.10mm crack width is higher than that for SINUDIA cracks, but at 33.20m pressure head, for the same crack width, the reverse is the case, as could be seen from Table 4.5. This

CRACK WIDTH	0.10			0.20			0.30		
PRESSURE HEAD / CRACK PATTERN (m)	METRE HEAD OF WATER								
	16.60	33.20	66.40	16.60	33.20	66.40	16.60	33.20	66.40
STRA	3.04	4.96	6.94	3.78	6.12	8.56	5.01	6.75	9.60
SINUDIA	2.55	5.00	9.0	4.85	8.00	10.70	5.80	8.45	12.15
SINUTH	3.00	4.10	7.40	4.00	5.80	9.01	4.65	6.65	9.85

TABLE 4.5 Flow Velocities for Three Types of Crack

These very close results obtained for the three crack shapes (i.e. STRA, SINUDIA and SINUTH) do suggest that their flow surfaces are similar. In every case, preformed cracks were obtained by placing spacer plates between the separately cast halves of the specimens. This means therefore that the surface of the crack has a mortar coating formed during vibration. Hence the variation in frictional resistance and roughness, between the three crack types would be minim al.

5. Water flow through circular cracks varies between 9.38 to 18.27 times the water flow through natural cracks, and between 1.43 to 2.54 times the water flow through other crack patterns. Oil flow through circular cracks varies between 7.88 to 16.18 times the oil flow through natural cracks, and between 2.78 to 9.63 times the oil flow through other crack patterns.

6. The circular cracks were formed as described in section 4.2, and used to simulate flow between concrete and steel reinforcement. Because the crack surfaces are smooth, it is expected that the flow obtained would be higher than that likely to be observed in the field. It is however logical to suppose that flow through the interface between concrete and reinforcement would be higher than flow through cracks in the concrete

matrix alone. This flow will be reduced if corrosion of the steel reinforcement takes place. If the flow through a crack becomes so large, then scouring may occur and fine particles of hydration products could be washed away at higher pressure heads.

7. The straight through cracks and sinusoidal cracks were meant to simulate flow through joints in concretes especially in liquid retaining structures. The joints could be of different patterns. Results obtained however suggest, that the pattern of the joint may not play a major role on the flow characteristics of the fluid. Rather the flow could depend more on the physical characteristics of the flow surface such as its frictional resistance and roughness, and on the properties of the flowing liquid (see Chapter 5). Healing of these joint spaces may not be achieved as the hydration products which contribute to the healing process may not be readily available.

8. The natural cracks formed using the splitting process were meant to simulate the most common type of cracks found in concrete structures. Test results show that flow through these cracks is the least for all the crack types likely to be encountered in practice. The maximum water velocity is 3.20 m/s, for a crack width of 0.3mm. Therefore for a crack length of a metre, assumed to have a uniform crack width 0.3mm, across the thickness, for a water tank of 83 metres high a loss of about 9.6×10^{-4} m^3/sec (ie 0.96 litre/sec or 0.211 gallon/sec) may be obtained. This is assuming that the crack is just at the bottom. The amount is quite enormous and probably unacceptable. However in practice, the crack width is not uniform, and infact may not pass right through the thickness of the tank. Autogenous healing of natural cracks is also more likely than the other crack patterns, used in this investigation. A closer look at the results of the natural cracks, however suggests that for oil tanks, and for crack widths less than 0.15, liquid loss through the crack may not be a

primary problem, while for water retaining structures, a lower value of 0.10 may be reasonable. With autogenous healing and for non-uniform crack widths, the code requirements[25] may be adequate for water retaining structure, and infact more than adequate for the crude oil retaining structure, providing the crude oil is of approximately the same properties as the one used in the present research. If the corrosion of the steel reinforcement is to be avoided, then a tighter crack control may be necessary.

4.5.5 Effect of Depth of Crack

This investigation was carried out using natural cracks of width 0.1, 0.2 and 0.3mm and depths of 50mm, 75mm or 100mm for both oil and water flow and using circular cracks of width 0.1, 0.15 or 0.20mm, and depths of 50, 75, 100 or 125mm as shown in Table 4.6. For the natural cracks enough results were not obtained to enable reasonable deductions to be made. This is because leaks were detected at larger crack depths, around the sides of the specimen and also distortion of the crack width was suspected though not detected. For the circular cracks, only water was used and the plot of flow velocity versus crack depth is shown in Fig. 4.11.

The results show that the flow velocity is inversely proportional to the crack depth. The relationship could be explained from the result of a pressure drop on velocity. As the liquid traverses a longer path, pressure losses are greater because of friction. This effect and also because of the liquid penetration into the pores in the concrete, the velocity decreases. The seepage into the pores again increases with crack depth. However, the losses through the pores are considered to be negligible when comparing the permeability coefficient of 10^{-13} m/s for flow through concrete (Table 5.2), with the velocity of fluid flow of about 1 m/s through the cracks.

4.6 Theoretical Predictions of the Experimental Results

Equations 4.1 and 4.2, relate pressure head to flow velocity for

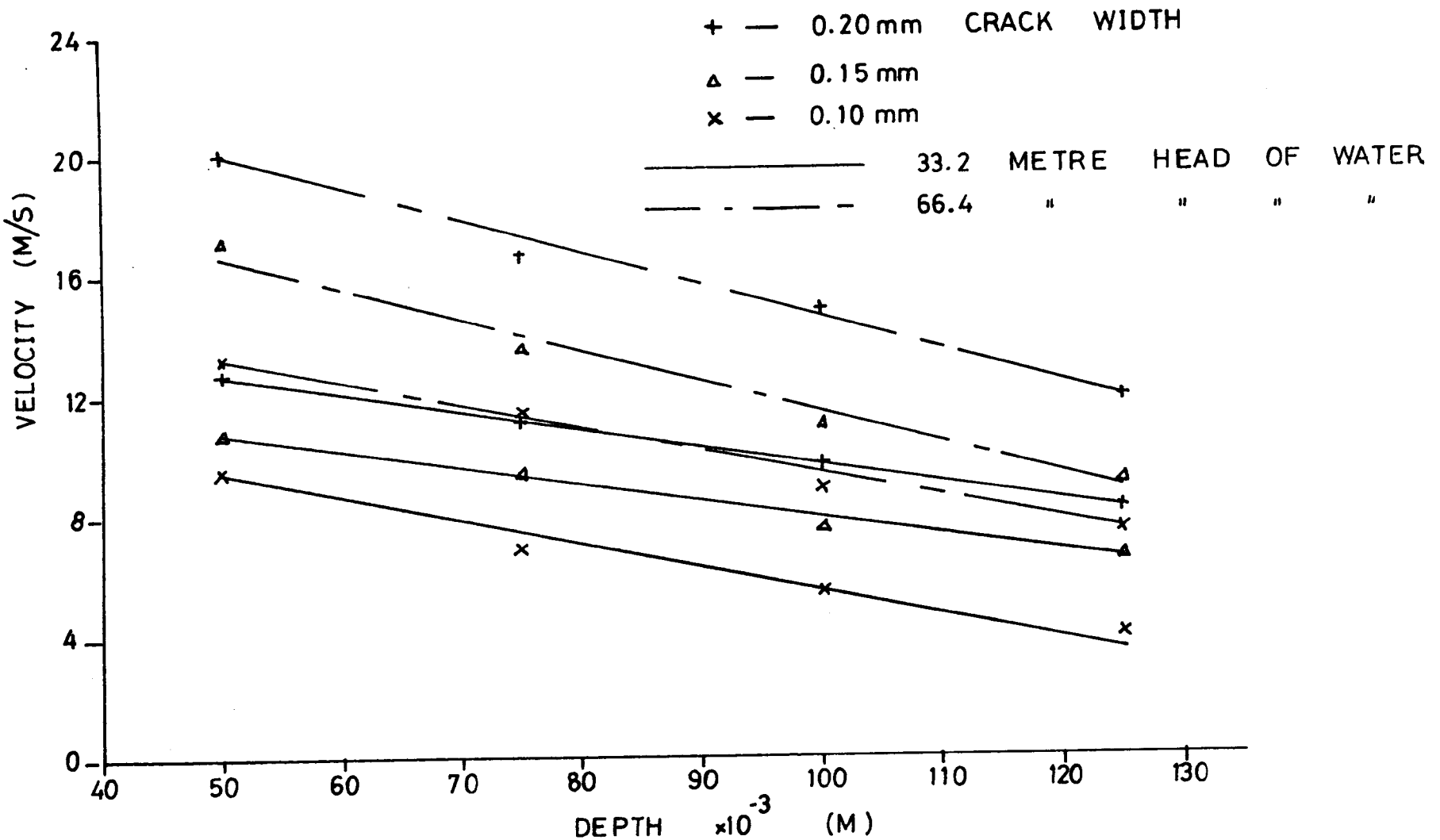

FIG 4.11 GRAPH OF VELOCITY VS DEPTH OF CRACK FOR WATER FLOW THROUGH CIRCULAR CRACKS

	NATURAL CRACK																	
	OIL - Velocity m/s									WATER - Velocity m/s								
crack depth	50mm			75mm			100mm			50mm			75mm			100mm		
crack width / applied pressure (m)	0.1	0.2	0.3	0.1	0.2	0.3	0.1	0.2	0.3	0.1	0.2	0.3	0.1	0.2	0.3	0.1	0.2	0.3
8.30	0.19	0.34	0.40	0.17	0.27	0.38	0.14	0.23	0.30	0.48	0.82	1.00	0.42	0.76	0.91	0.35	0.65	0.83
16.60	0.24	0.42	0.58	0.20	0.38	0.56	0.18	0.31	0.48	0.66	1.02	1.40	0.58	0.94	1.38	0.53	0.71	1.12
24.90	0.31	0.50	0.70	0.25	0.60	0.68	0.20	0.50	0.58	0.75	1.30	1.70	0.70	1.28	1.45	0.60	0.98	1.25
33.20	0.35	0.60	0.83	0.30	0.66	0.80	0.24	0.66	0.67	0.84	1.44	1.82	0.75	1.40	1.76	0.66	1.08	1.48
41.50	0.43	0.75	0.98	0.34	0.82	0.86	0.28	0.72	0.74	0.98	1.72	2.08	0.88	1.71	1.96	0.76	1.29	1.58
49.80	0.50	0.82	1.10	0.42	0.90	0.96	0.35	0.76	0.81	1.04	1.81	2.40	0.90	1.93	2.10	0.79	1.47	1.85
58.10	0.58	0.98	1.19	0.48	0.94	1.10	0.40	0.78	0.96	1.18	1.95	2.60	0.95	2.06	2.28	0.87	1.52	1.98
66.40	0.63	1.13	1.30	0.55	1.00	1.20	0.48	0.88	1.03	1.24	2.20	3.01	1.08	2.13	2.38	0.91	1.63	2.19
74.70	0.66	1.21	1.36	0.57	1.03	1.22	0.49	0.94	1.06	1.31	2.31	3.02	1.23	2.18	2.44	0.97	1.88	2.22
83.00	0.75	1.31	1.47	0.63	1.08	1.29	0.55	0.96	1.12	1.40	2.42	3.20	1.28	2.30	2.57	1.03	1.96	2.33

	CIRCULAR CRACKS WATER FLOW ONLY											
	50mm			75mm			100mm			125mm		
crack width / pressure	0.10	0.15	0.20	0.10	0.15	0.20	0.10	0.15	0.20	0.10	0.15	0.20
8.30	4.09	5.50	7.26	3.11	4.18	6.85	2.54	3.44	5.96	2.04	3.03	5.42
16.60	6.48	7.28	10.89	4.79	6.25	8.77	3.69	4.86	6.87	2.72	4.23	5.98
33.20	9.48	10.80	12.69	6.90	9.48	11.20	5.48	7.58	9.76	4.00	6.60	8.22
49.80	12.28	14.41	17.09	8.91	11.66	13.17	6.99	9.86	11.45	5.51	8.99	10.64
66.40	13.22	17.03	20.00	11.53	13.47	16.68	8.98	10.97	14.96	6.20	9.10	11.95
83.00	14.93	18.70	21.65	12.92	14.45	17.24	10.98	12.16	15.88	8.98	10.89	13.57

TABLE 4.6 Effect of Depth of Crack on Velocity

varying crack patterns, width and liquid types. The equations are purely empirical, based entirely on the test results. The equations therefore lack generality and are not dimensionally homogeneous. However the equations give an estimate of fluid loss to the engineer designing liquid storage tanks, providing the conditions are roughly the same as in these tests.

In the following sections, attempts are made to apply the test results to theoretical equations based on fundamental laws of fluid mechanics, eg the Reynolds law of similitude (equations 2.9 to 2.18).

4.6.1 Water Flow

This section deals with water flow through the different crack patterns. Three crack patterns chosen for the discussions vis (i) the circular crack (CIRC) (ii) the cracks sinusoidal across the thickness (SINUTH) and (iii) the natural cracks (NATU). SINUTH, was chosen to represent also the behaviour of SINUDIA and STRA, since they do exhibit similar characteristics (section 4.5.4). The values of pressure loss ΔP and velocity for the three crack patterns are presented in Table 4.7.

A regression analysis was used to determine the values of C_A and C_l in equation 2.17. Equation 2.18, was found to be inappropriate for the test results and was abandoned. Although it is not clear why equation 2.18 could not fit the results of the experiment, it is not considered that the flows were all laminar. Reynold numbers obtained were typically between 10 at low flow velocity to about 10^4 at high velocities, thereby showing that both laminar and turbulent flows were involved. (Laminar flow obtained at Re <2000 and turbulent flow at Re > 4000[30]). The values of C_A, C_l and r are shown in Table 4.8. Typical plots of $1/C_D^2$ versus $\frac{z}{Re.dn}$ for the three crack shapes are shown in Figs. 4.12, 4.13 and 4.14 respectively and the following observations are made.

1. The fit of equation 2.17 to the test results, shows that the test results, can be predicted using the theoretical equation. This means that flow characteristics in cracks in concrete obey the fundamental law of

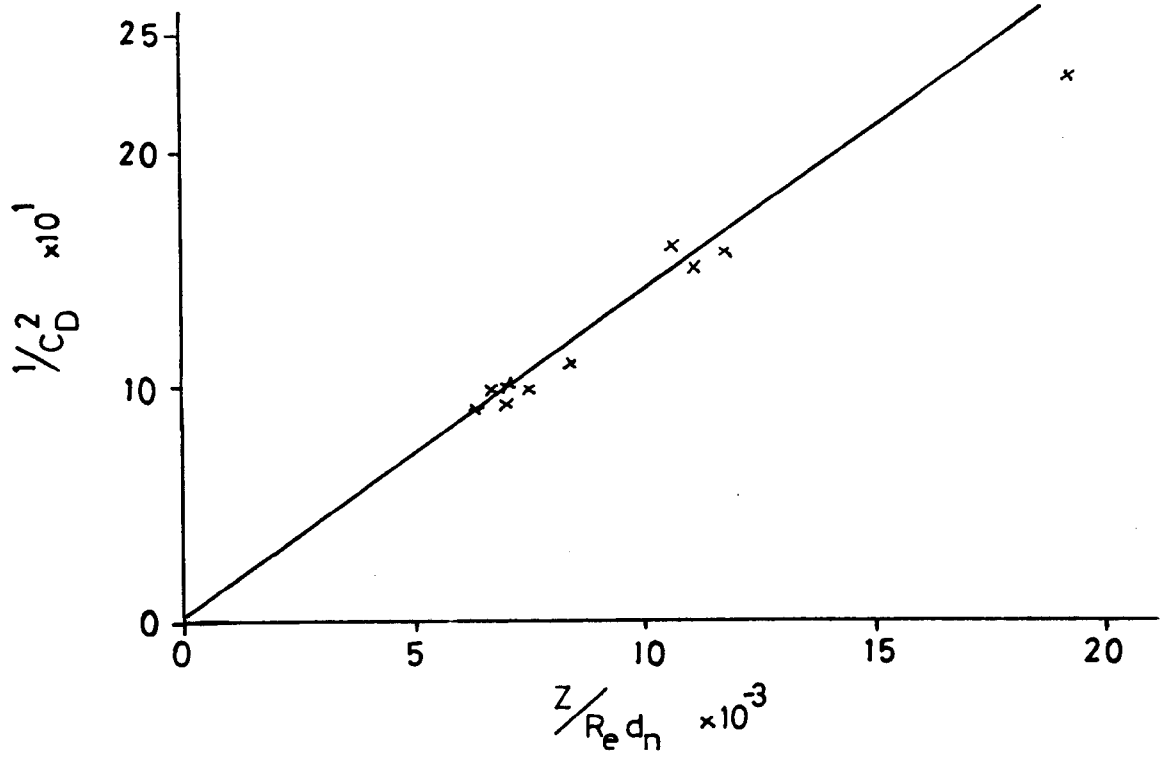

FIG 4.12 FOR CIRCULAR CRACK OF WIDTH 0.3mm

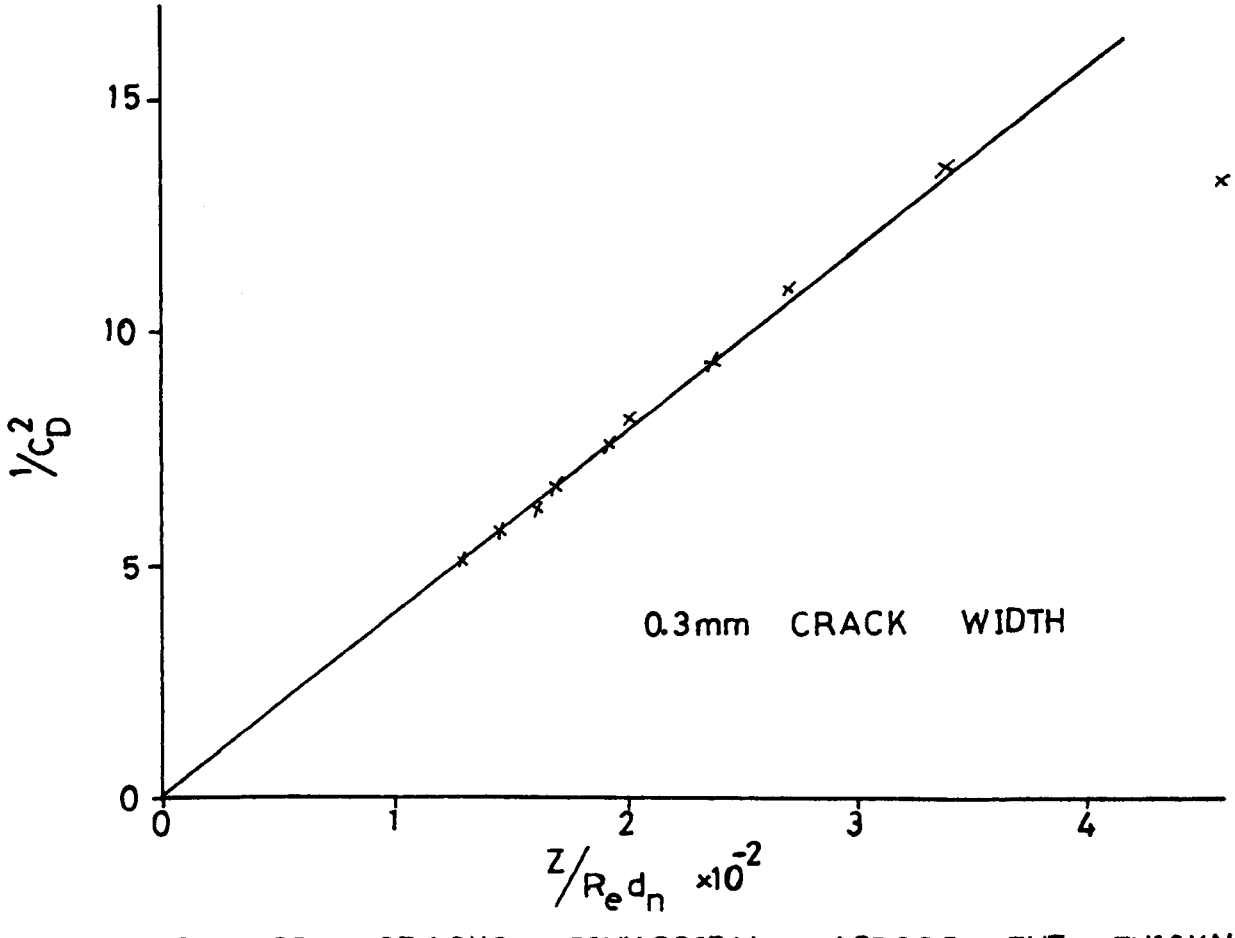

FIG 4.13 FOR CRACKS SINUSOIDAL ACROSS THE THICKNESS

FIG 4.12 & 4.13 GRAPH OF EQ. 2.16 FOR WATER FLOW

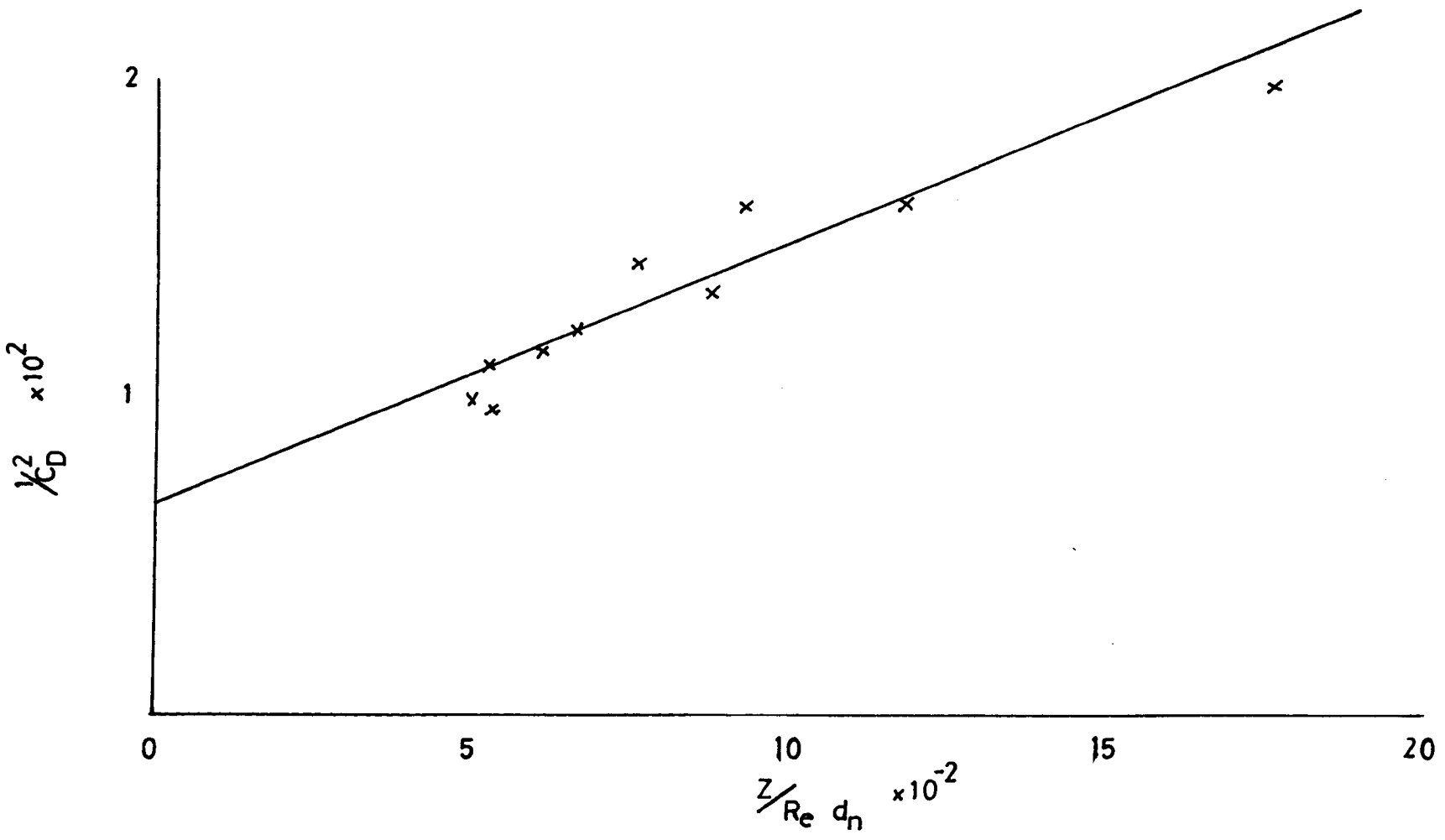

FIG 4.14 PLOT OF EQUATION 2.16 FOR WATER FLOW THROUGH NATURAL CRACK OF WIDTH 0.3mm

N/m^2 $x10^4$ ΔP	m/s V	Δ P	V	Δ P	V	ΔP	V	ΔP	V	ΔP	V
					NATURAL CRACKS (WATER FLOW)						
8.07	0.11	8.07	0.38	8.00	0.52	7.95	0.72	7.92	0.81	7.90	0.90
16.14	0.27	16.14	0.66	16.00	0.91	15.96	1.02	15.91	1.25	15.90	1.40
24.23	0.47	24.20	0.75	23.80	1.01	23.60	1.30	23.43	1.48	23.38	1.70
32.41	0.51	32.40	0.84	32.00	1.26	31.24	1.44	27.31	1.56	26.76	1.82
40.37	0.54	40.27	0.98	39.00	1.35	38.01	1.72	34.39	1.98	31.08	2.08
48.44	0.61	47.45	1.04	42.02	1.45	39.30	1.81	37.36	2.11	35.25	2.40
56.51	0.70	55.38	1.18	48.94	1.62	43.30	1.95	42.14	2.36	39.02	2.60
64.58	0.72	56.13	1.24	49.52	1.67	47.60	2.20	45.65	2.60	44.30	3.01
72.63	0.75	60.35	1.31	54.34	1.84	50.11	2.31	46.90	2.66	44.59	3.02
80.71	0.76	64.50	1.40	57.00	1.93	52.50	2.42	49.40	2.82	47.04	3.20
					SINUSOIDAL CRACKS ACROSS THE THICKNESS (WATER FLOW)						
8.06	0.81	8.02	1.55	7.98	2.25	7.95	2.85	7.92	3.15	7.90	3.45
16.13	1.60	16.10	3.00	16.03	3.65	16.00	4.00	15.21	4.35	14.68	4.65
24.06	2.40	24.00	3.81	23.56	4.50	20.15	5.00	20.01	5.50	18.41	5.81
32.22	2.66	32.13	4.10	26.45	5.05	23.36	5.80	21.51	6.31	20.55	6.65
40.08	3.70	40.00	5.55	32.46	6.20	27.84	6.90	24.49	7.05	23.88	7.65
48.16	4.10	48.58	6.25	36.64	7.00	29.01	7.20	26.47	7.65	25.88	8.25
56.22	4.80	51.03	6.55	40.26	7.50	34.80	8.40	29.39	8.75	29.01	9.35
63.82	5.10	58.00	7.40	41.49	7.85	36.39	9.01	32.78	9.41	30.95	9.85
72.34	5.90	58.80	7.50	48.26	9.20	40.88	10.15	35.94	10.35	34.49	11.00
80.42	6.25	61.52	7.85	52.40	10.01	40.30	11.00	40.63	11.70	38.40	12.25
					CIRCULAR CRACKS (WATER FLOW)						
8.04	1.91	8.02	4.09	8.00	5.50	7.98	7.26	7.88	8.17	7.78	8.19
16.06	2.92	15.98	6.48	15.00	7.28	14.60	10.89	14.40	11.39	14.02	13.40
24.11	3.92	23.96	8.06	22.96	10.74	19.43	11.50	16.82	12.75	15.27	14.25
30.00	4.74	29.88	9.48	25.29	10.80	21.42	12.69	18.59	13.64	17.34	14.74
39.85	5.94	38.57	11.94	31.94	13.15	25.02	15.35	21.26	17.00	19.46	18.87
40.86	6.56	39.25	12.28	37.20	14.41	29.04	17.09	24.39	19.51	22.25	21.11
48.21	7.76	42.01	12.96	40.40	16.03	31.24	19.28	26.06	20.74	23.42	22.51
52.82	8.43	42.90	13.22	41.36	17.03	32.84	20.00	27.18	22.30	25.60	22.67
55.83	8.98	48.00	14.65	44.60	18.52	34.15	20.83	28.03	23.00	25.99	23.51
58.90	9.49	50.96	14.93	47.01	18.70	36.53	21.65	30.07	23.14	27.49	23.56

TABLE 4.7 Test Results

	WATER FLOW								
	CIRCULAR CRACK (CIRC)			SINUSOIDAL (SINUTH)			NATURAL (NATU)		
	C_A	C_1	r	C_A	C_1	r	C_A	C_1	r
0.05	13.74	7.34	0.963	33.32	10.19	0.997	246.01	176.52	0.984
0.10	20.48	2.92	0.965	61.43	10.28	0.983	133.70	599.53	0.824
0.15	36.75	1.74	0.918	97.28	6.33	0.963	278.54	252.88	0.911
0.20	50.20	0.89	0.895	149.13	3.75	0.935	372.39	158.31	0.814
0.25	82.57	0.36	0.937	213.83	2.65	0.940	588.53	98.24	0.870
0.30	113.12	0.20	0.986	279.85	2.19	0.945	822.83	66.94	0.910
	OIL FLOW								
	CIRCULAR CRACK (CIRC)			SINUSOIDAL (SINUTH)			NATURAL (NATU)		
	C_A	C_1	r	C_A	C_1	r	C_A	C_1	r
0.05	2.66	166.18	0.853	13.33	13277.8	0.692	98.82	52578.9	0.955
0.10	6.62	11.80	0.929	43.87	104.20	0.974	24.75	2485.43	0.749
0.15	8.25	8.53	0.983	57.65	144.83	0.985	37.27	1333.14	0.702
0.20	11.32	6.17	0.993	65.44	43.94	0.990	60.97	769.62	0.691
0.25	14.02	4.51	0.922	74.44	50.58	0.995	61.12	693.43	0.751
0.30	17.91	3.33	0.970	86.48	58.44	0.988	71.27	582.51	0.832

r = correlation coefficient

TABLE 4.8 Constants of Regression equation 2.17

fluid flow i.e. the Reynolds law of similitude.

2. The value of C_A however was found to vary with the aspect ratio (Fig. 4.15) i.e. crack depth to crack width (Z/Y), and with the crack patterns. In the three crack patterns, CIRC, SINUTH, and NATU, C_A did not take the value of 96 as found by Etheridge[34], but supports Hopkins and Hereford[29], who predicted that C_A depends on the aspect ratio and Reynolds No. The present results indicate that C_A is a complex parameter which depends not only on the aspect ratio and Re, but also on the nature of the flow surface, such as the frictional resistance and the roughness. It will also depend on the fluid properties, not catered for by Re, such as the molecular size and wax content. Typical plot of C_A vs the aspect ratio is shown in Fig. 4.15. The shape of the curve is very different from that reported in ref. 29, where C_A is seen to increase with an increase in the aspect ratio, but in Fig. 4.15, C_A decreased with an increase in the aspect ratio. The difference in behaviour may be as a result of difference in fluid type, since Hopkins used air while the present research uses water and oil.

3. The value of C_A obtained from the test results are much higher than 96 (Fig. 4.15), obtained from theoretical results and tend to increase with an increase in crack width, for all the crack patterns. The very high values of C_A are difficult to explain but some doubts must exist about the theoretical value of 96, since it was derived for an ideal fluid flowing between smooth surfaces. For a real fluid and rough cracks, C_A could be a more complex function which can only be determined accurately when the variables such as (a) density, viscosity, molecular size and wax content of the flowing fluid are known (Chapter 5), and (b) when the flow surface roughness and frictional resistance of the surface can be accurately determined. This is beyond the scope of the present research. The differences between C_A for various crack widths and for oil and water flow as shown in Figs. 4.16 and 4.21, indicate the importance of the variables

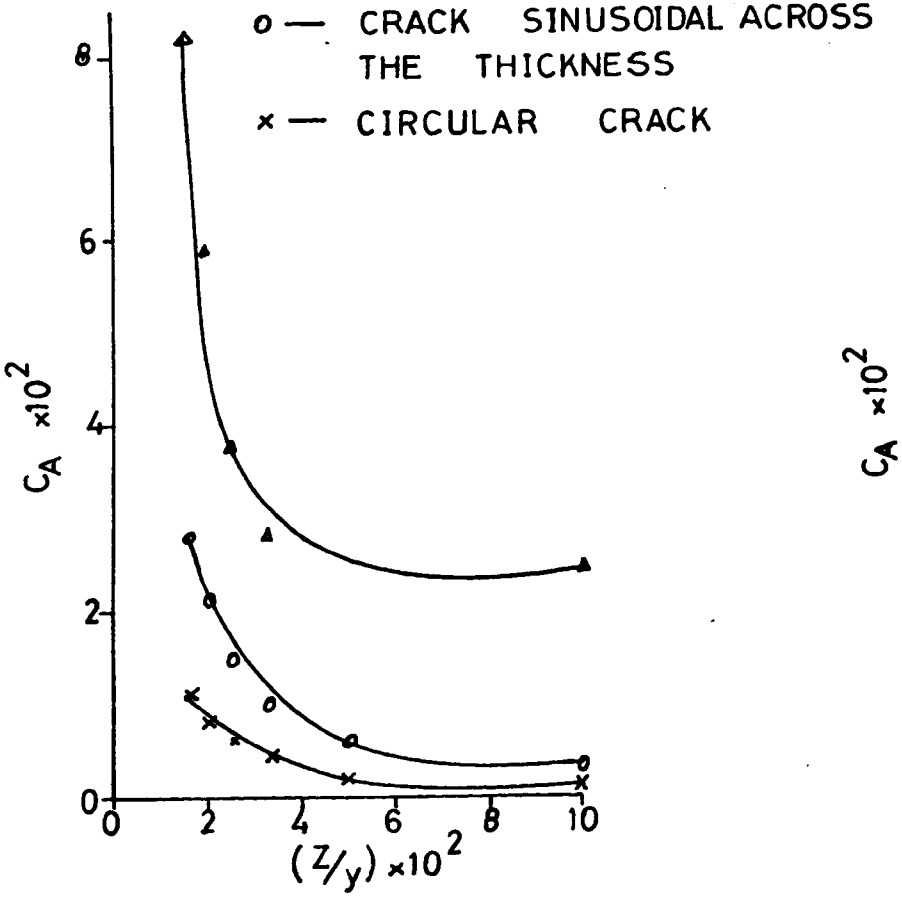

FIG 4.15 GRAPH OF C_A VS ASPECT RATIO Z/y, FOR WATER FLOW

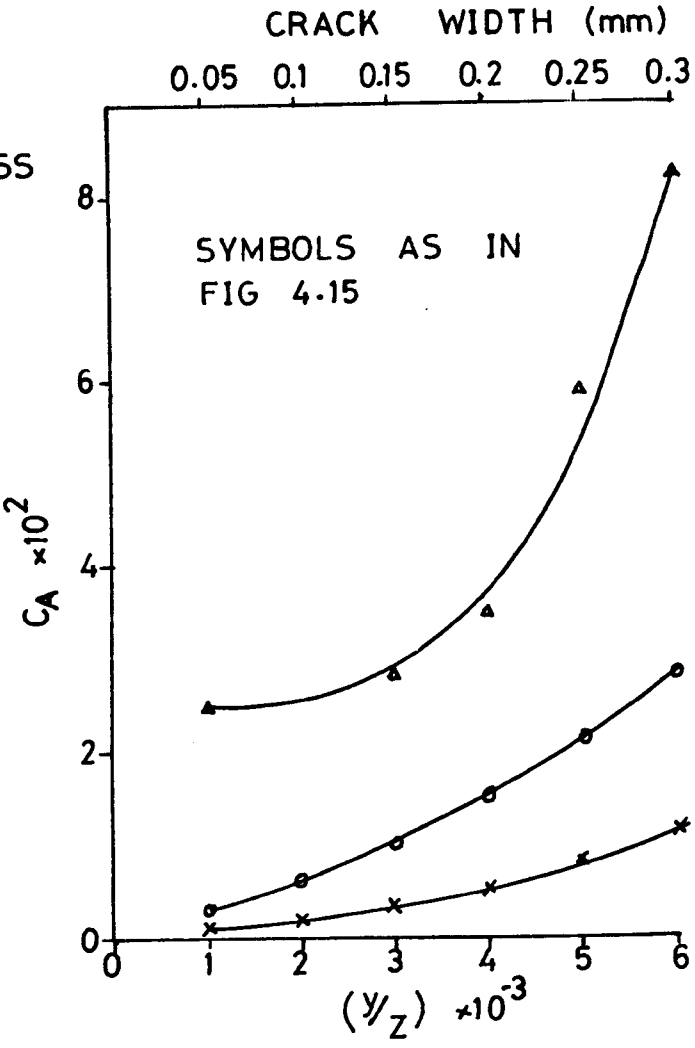

FIG 4.16 GRAPH OF C_A VS y/Z & CRACK WIDTH FOR WATER FLOW.

mentioned in (a) and (b) above.

The accuracy of the values of C_A obtained in the present research is however in some doubt because of the uncertain pressure losses at the connectors and at the exit of flow from the cracks. The connectors provide an abrupt contraction, while the output end of the crack is an abrupt enlargement. Pressure losses are expected at these two sections and could affect the values of ΔP. Modifications of the equipment should reduce these losses and obtain some more reliable values of ΔP.

4. The plot of ln C_A against crack width is shown in Fig. 4.17. The plot shows a linear relationship for the three types of crack (CIRC, SINUTH and NATU) and the slope of the plots is the same for all the crack patterns. An empirical relationship which enables C_A to be expressed as a function of the crack width was obtained as

For a circular crack $$C_A = e^{(7.87w + 2.42)} \quad (4.3)$$

For a crack sinusoidal across the thickness

$$C_A = e^{(7.87w+3.78)} \quad (4.4)$$

For a natural crack $$C_A = e^{(7.87w+4.45)} \quad (4.5)$$

where w = crack width in mm.

If the nature of a flow surface is known, then equations 4.3 to 4.5, could be employed in equation (2.17) to determine the flow of water through cracks of various widths.

5. Apart from some minor variations, C_1 decreased with an increase in the crack width. The value of C_1 is the constant of integration and its significance is not understood.

4.6.2 Oil Flow

Test results for oil flow through the three crack patterns are shown in Table 4.9. Figures 4.18. 4.19 and 4.20 show typical plots of $1/C_D^2$ versus z/Rey·dn for circular, natural and cracks sinusoidal across the thickness respectively. The plots show that

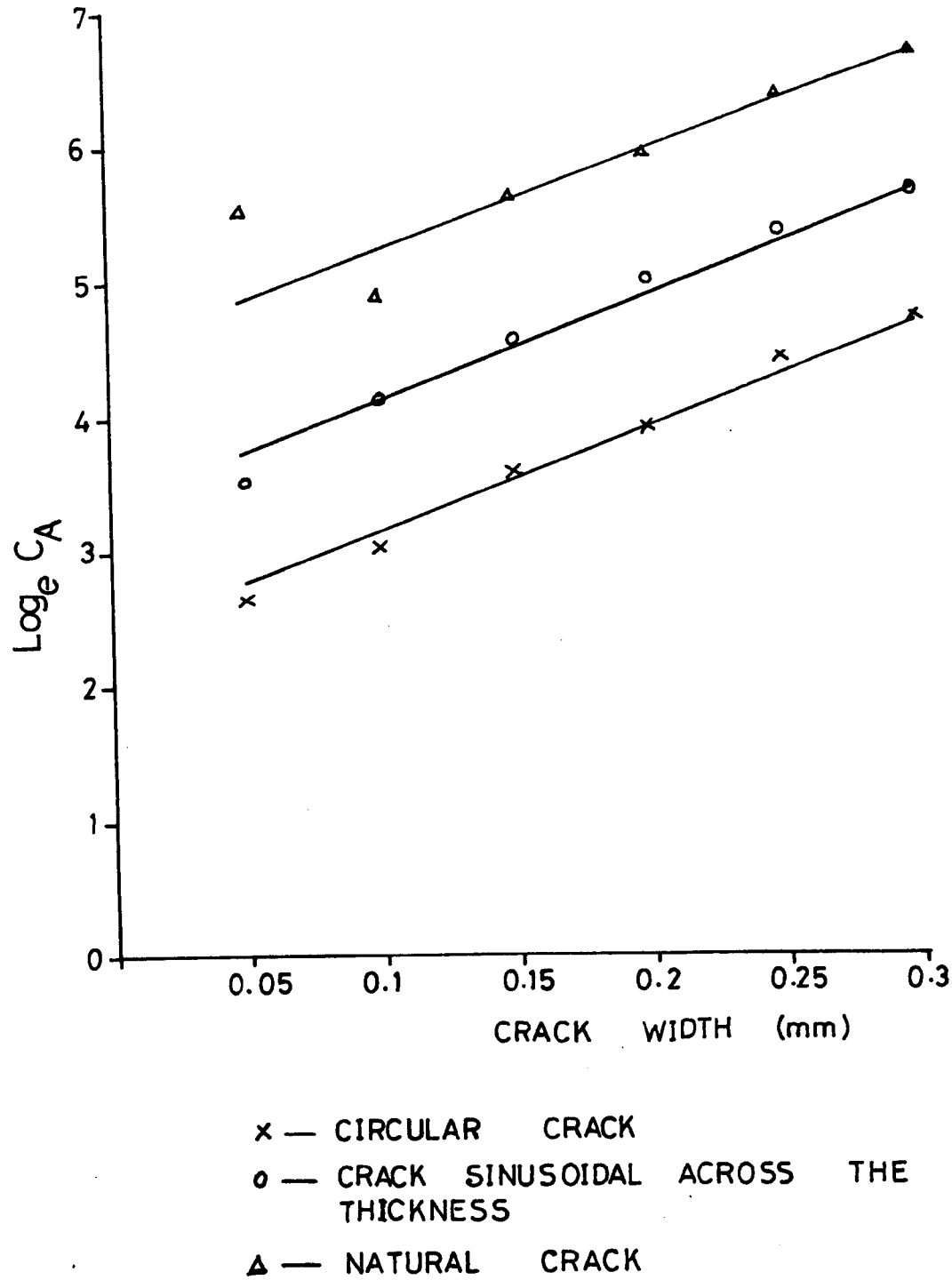

FIG 4.17 GRAPH OF $Log_e C_A$ VS CRACK WIDTH (WATER FLOW)

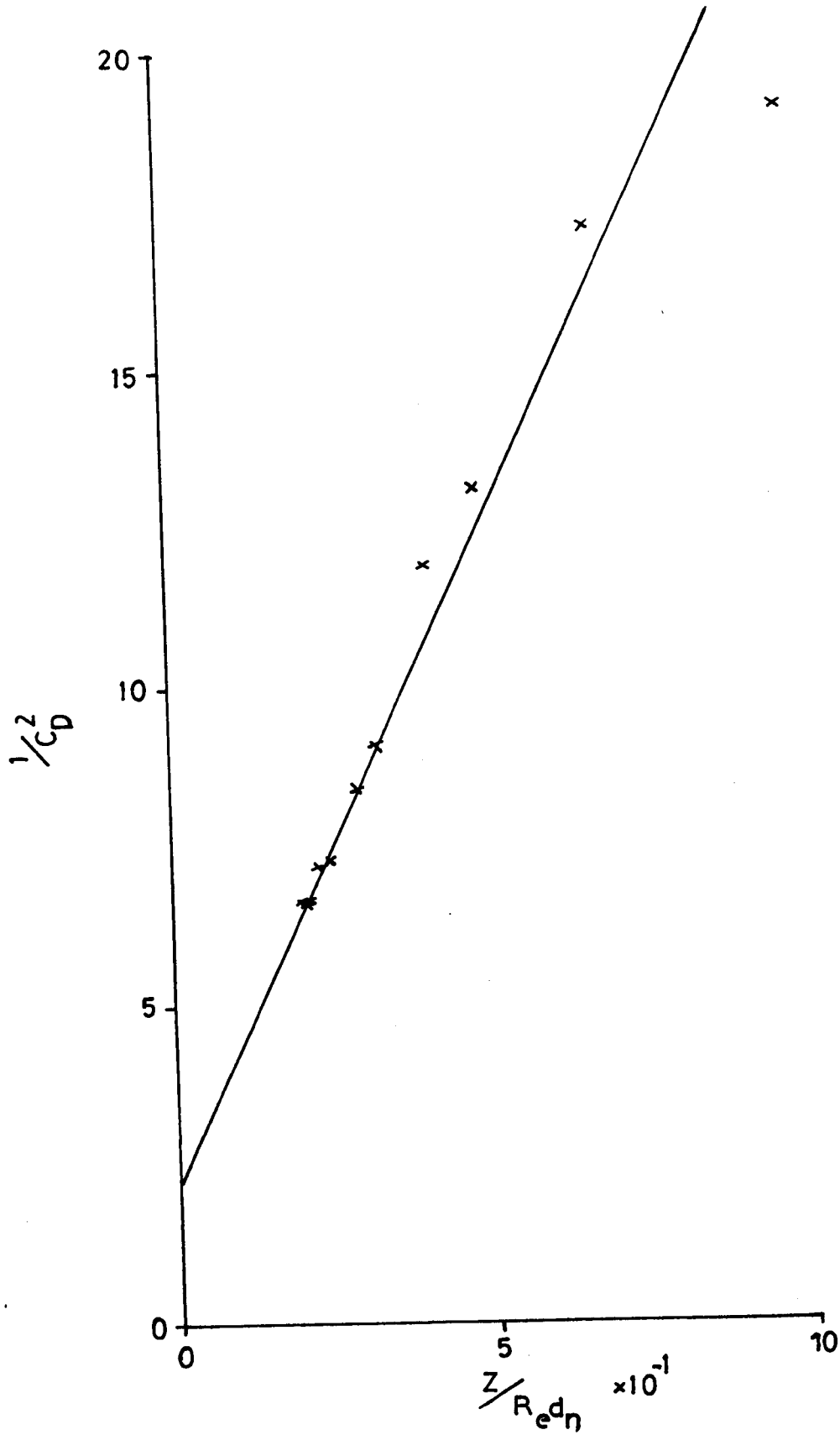

FIG 4.18 GRAPH OF EQ. 2.16 FOR OIL FLOW THROUGH CIRCULAR CRACK OF WIDTH 0.3mm

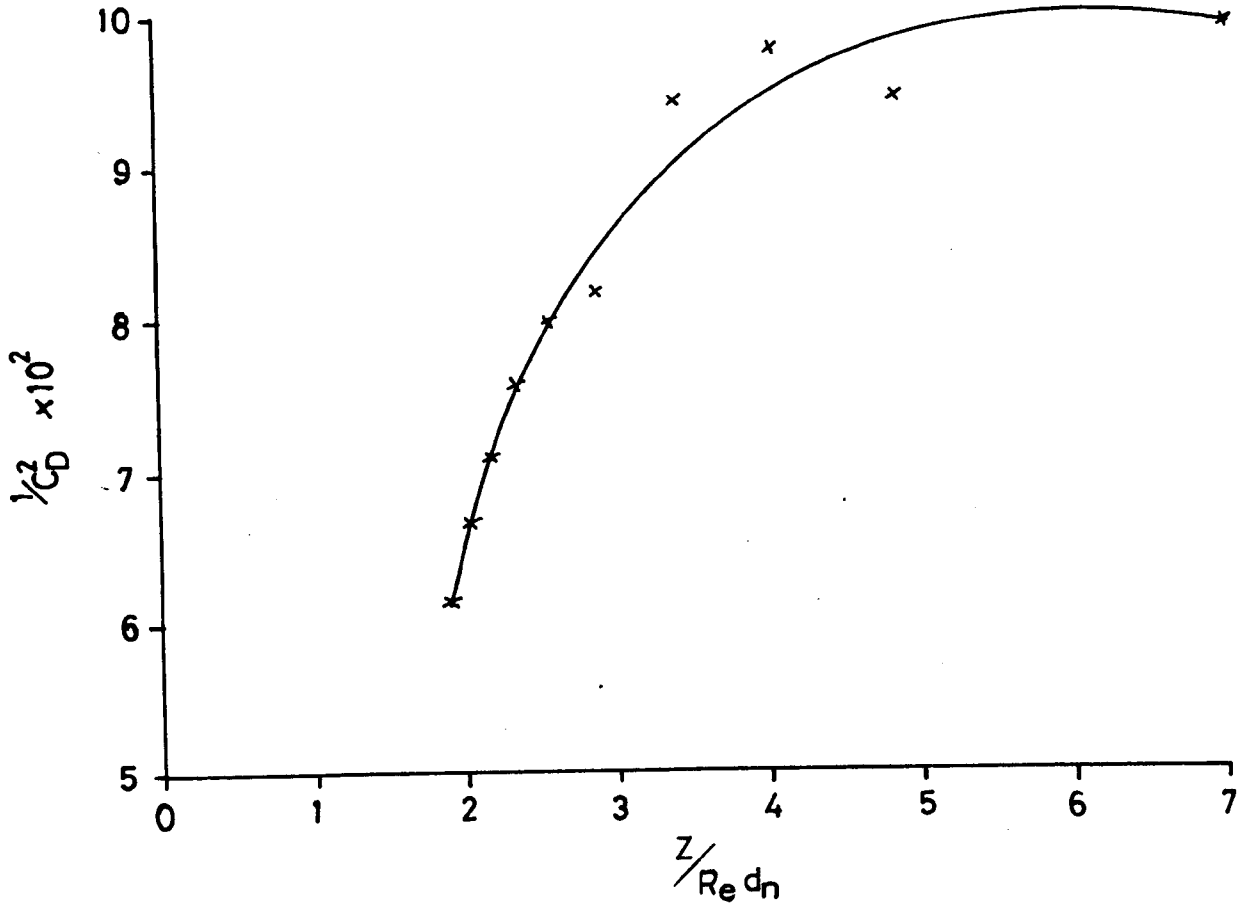

FIG 4.19 PLOT OF EQ. 2.16 FOR OIL FLOW THROUGH NATURAL CRACK OF WITH 0.3 mm

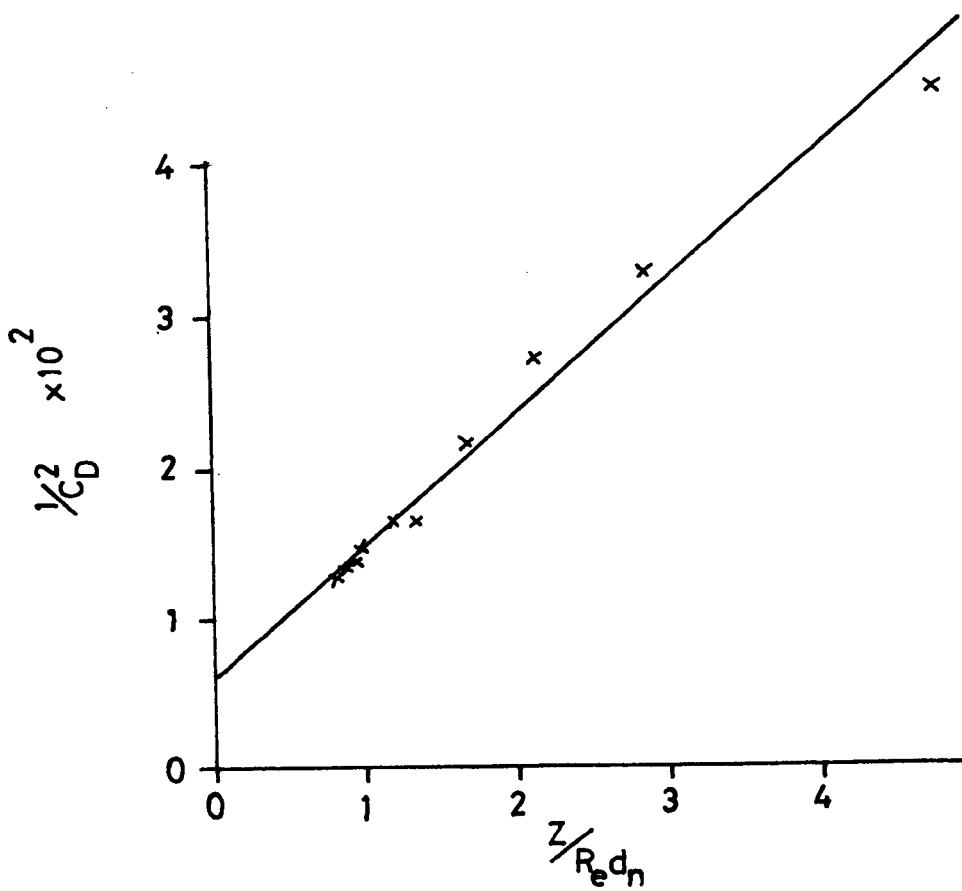

FIG 4,20 PLOT OF EO. 2.16 FOR OIL FLOW THROUGH CRACKS SINUSOIDAL ACROSS THE THICKNESS, OF CRACK WIDTH 0.3mm

NATURAL CRACKS (OIL FLOW)

$N/m^2 \times 10^4$ ΔP	V	ΔP	V	ΔP	V	ΔP	V	ΔP	V	ΔP	V
6.90	0.016	6.90	0.19	6.90	0.28	6.84	0.34	6.82	0.38	6.78	0.40
13.79	0.033	13.79	0.24	13.76	0.33	13.71	0.42	13.68	0.49	13.58	0.58
20.69	0.079	20.69	0.31	20.64	0.42	20.60	0.50	20.54	0.62	20.54	0.70
27.68	0.068	27.67	0.35	27.60	0.50	27.54	0.60	27.46	0.74	27.39	0.83
		34.44	0.43	3.436	0.60	34.32	0.75	34.26	0.90	34.16	0.98
		41.34	0.50	41.26	0.67	41.17	0.82	41.09	0.95	41.05	1.10
		48.34	0.58	48.15	0.79	48.123	0.98	47.94	1.09	47.85	1.19
		55.13	0.63	55.05	0.86	54.97	1.13	54.84	1.19	54.78	1.30
		61.98	0.66	61.89	0.93	61.84	1.21	61.74	1.27	61.66	1.36
		67.88	0.75	66.79	1.01	65.71	1.31	65.54	1.38	65.46	1.47

SINUSOIDAL CRACKS ACROSS THE THICKNESS (OIL FLOW)

6.89	0.02	6.88	0.16	6.86	0.25	6.81	0.39	6.78	0.50	6.70	0.59
13.78	0.10	13.78	0.23	13.62	0.41	13.54	0.68	13.50	0.86	13.46	0.98
20.67	0.13	20.62	0.40	20.61	0.57	20.55	0.98	20.40	1.22	20.19	1.32
27.58	0.16	27.60	0.55	27.55	0.76	27.27	1.35	27.22	1.56	26.95	1.70
34.12	0.20	33.10	0.64	32.76	0.96	32.32	1.60	31.98	1.96	31.68	2.10
41.10	0.23	39.48	0.83	39.13	1.20	38.99	1.90	38.49	2.20	37.95	2.32
47.79	0.26	46.70	0.94	45.48	1.30	45.13	2.05	44.51	2.48	42.11	2.60
54.72	0.27	52.98	1.18	51.03	1.55	49.22	2.32	48.18	2.74	47.32	2.86
61.15	0.29	57.93	1.20	54.48	1.66	52.51	2.55	50.26	2.80	49.73	2.96
66.98	0.30	63.15	1.31	58.48	1.75	53.36	2.64	52.41	2.92	50.53	3.12

CIRCULAR CRACKS (OIL FLOW)

6.89	0.53	6.87	1.09	6.84	1.55	6.82	1.95	6.76	2.72	6.78	2.88
13.60	0.79	13.45	1.32	13.42	2.68	13.21	3.22	13.01	3.45	12.96	4.20
20.35	0.91	20.01	2.50	19.98	3.30	19.43	4.52	19.01	5.16	18.78	5.78
27.49	1.21	27.09	3.20	26.86	5.50	26.45	5.60	25.99	6.48	25.02	6.90
33.81	1.24	33.41	3.76	33.14	5.50	32.94	6.51	31.64	7.89	29.89	8.74
39.67	1.64	38.71	4.10	38.05	6.19	36.91	7.65	35.77	8.17	34.98	9.79
45.97	2.10	45.03	4.77	43.78	6.39	42.68	7.67	41.68	10.47	38.40	11.06
48.19	2.11	47.01	4.98	44.68	6.82	43.76	8.45	41.98	10.47	39.48	11.26
49.38	2.21	48.30	5.01	47.99	7.51	47.42	9.45	44.01	10.70	43.96	12.41
58.73	2.50	52.17	5.31	49.52	7.75	48.12	9.51	45.16	11.26	44.98	12.56

TABLE 4.9 Test Results

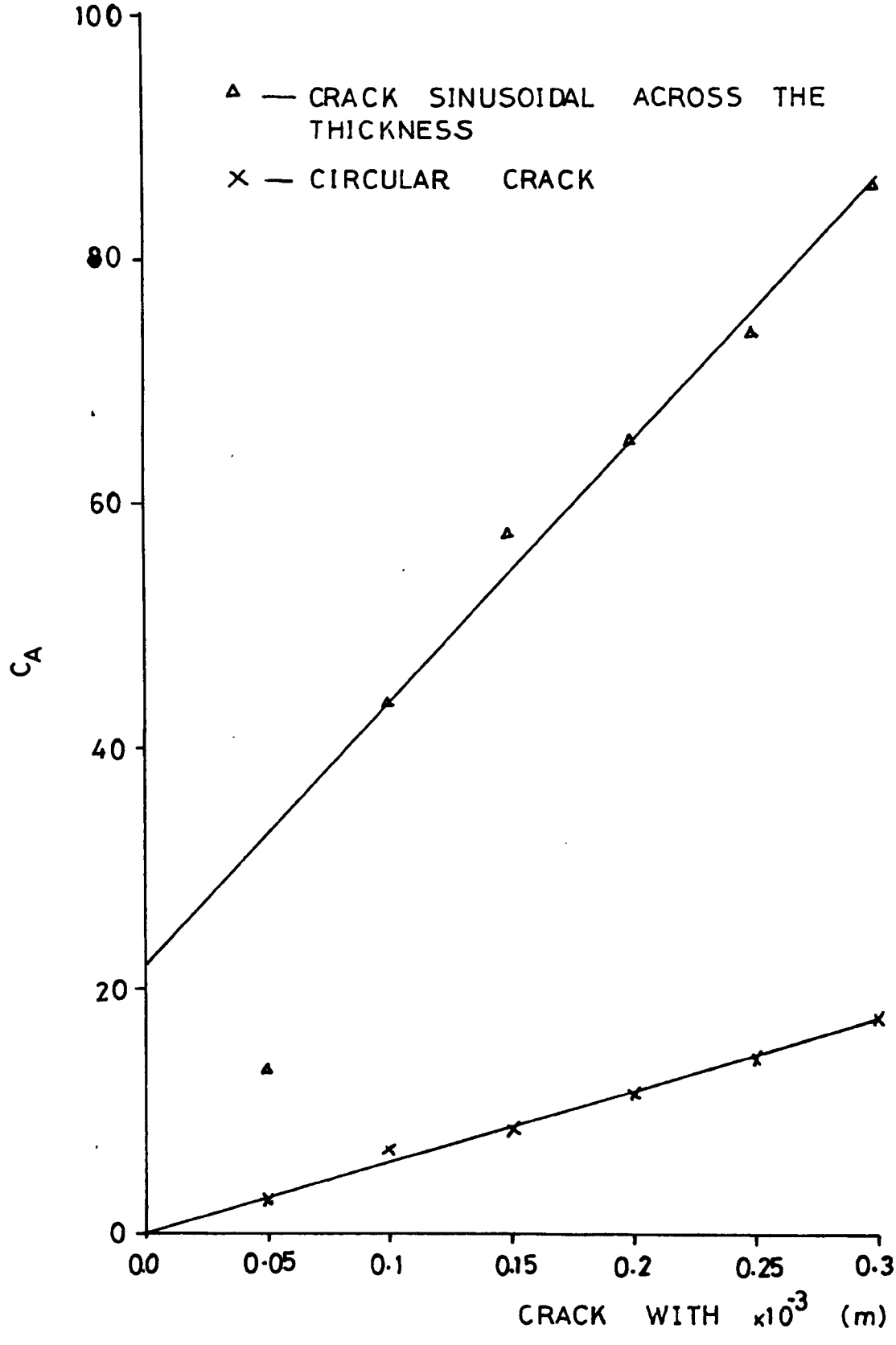

FIG 4.21 GRAPH OF C_A VS CRACK WIDTH (OIL FLOW)

1. The flow of oil through circular cracks and cracks sinusoidal across the thickness can be described by equation 2.17, and hence obey the Reynolds law of similitude. A non-linear relationship between $1/C_D^2$ and z/Re dn was obtained with natural cracks hence it is hard to see if the law applied to oil flow through natural cracks. The scatter could be explained by the very high surface roughness of the natural cracks, and the waxy deposits in the oil which build up quickly and alters the original dimensions of the crack. The build up is also observed in other crack patterns at very low velocities, but as the velocity increases, the deposits are flushed out, hence the original dimension is restored.

2. The value of C_A increases with an increase in the crack width for all the crack patterns. For CIRC and SINUTH cracks, linear relationships are obtained (Fig. 4.21) and are given below

$$\text{CIRC:} \qquad C_A = 60.0w \qquad (4.6)$$

$$\text{SINUTH:} \qquad C_A = 215w + 22 \qquad (4.7)$$

where w = crack width in mm.

3. The different characteristics exhibited by C_A for water and oil flow, emphasises the dependency of this parameter on the fluid properties, while the relationships (Figs. 4.1 - 4.5), show that the crack width is also a critical factor. With values of C_A for each crack width, however, only the fluid properties and the flow surface characteristics are required for a complete description of the liquid flow through cracks in concrete.

Equation 2.17, undoubtedly is a simplified representation of a complex flow situation. Bearing in mind the wide variety of crack types likely to be met in practice it seems that some degree of simplification is inevitable, for example, it is unlikely to find a crack type and dimension that would be everywhere constant, which is one of the assumptions of the equation.

The advantages of equation 2.17 is that (1) it is dimensionally homogeneous, so that the value of the constants do not vary with the particular systems of units used and (2) it takes into account, the effects of Reynolds number (ie the scale effect), which as a result, where an open area can be obtained by direct measurement, the value can be used directly in the equation. These two advantages make a wider use of equation 2.17 than equation 2.1 possible. Etheridge[34] has found favour in using equation 2.17 in determining open areas in doors and windows by applying it in air flow through gaps. Other uses made by him were in prediction of ventilation rates and in model tests in wind tunnels.

4.7 Summary of the Liquid Flow Through Cracks in Concrete

Results presented on the flow of oil and water through cracks in concrete can be summarized as follows

1. The flow velocity increases with an increase in both applied pressure and crack width for all crack types and for both oil and water flow.
2. The flow of water through cracks in concrete is generally greater than the flow of crude oil through the same type of cracks in concrete, for any crack width, pattern or applied pressure. Hence an adequate crack width for water impermeability is likely to be adequate for crude oil.
3. Oil or water flow through a crack at an interface between concrete and reinforcement is likely to be greater than flow through crack in cement matrix alone. Also flow through joints in concrete with the rich mortar surface may be higher than flow through natural cracks.
4. The flow velocities obtained in the tests (Table 4.1) appear to have exagerated the flow velocities likely to be encountered in the field, primarily because of the assumptions made, such as that the crack width and type are everywhere constant. However, the results are quite adequate for use in relative description of oil or water flow through cracks of

different shapes and sizes.

5. Oil and water flow through most of the crack widths and patterns investigated here, obey the Reynolds law of similitude. Hence the dimensionless ratio of equation 2.17, applies to most. An exception however is oil flow through natural cracks, which appeared to exhibit nonlinear relationship when equation 2.17 is applied. This deviation was attributed to a more likelihood of the flow surface being blocked by the waxy deposits of the oil.

6. The flow velocity was found to be inversely proportional to the depth of crack i.e. an increase in crack depth reduces the flow velocity. For example, increasing the depth of crack from 50mm to 125mm, for a circular crack of width 0.10mm, the water flow velocity decreases from 4.09 m/s to 2.04 m/s at a pressure head of 8.30 metres.

7. For the flow of oil or water through concrete to be fully understood, the fluid properties, such as density, molecular size, viscosity, and wax content, and the surface characteristics, such as the surface roughness and frictional resistance should be known.

CHAPTER 5

FLOW CHARACTERISTICS ASSOCIATED WITH TANK SURFACES AND PROPERTIES OF THE FLOWING LIQUID (SORPTIVITY/PERMEABILITY)

5.1 Introduction

This chapter is intended to look at some parameters that could influence the performance of concrete oil storage tanks in service. Chapter 4, revealed that tanks designed to hold water can adequately hold crude oil. This investigation is to be extended in this chapter to include some lighter oil fractions.

A further objective of this chapter is to predict the differences in flow through the tank floor and the tank wall. Two directions of flow were therefore investigated; (i) The flow of oil parallel to the direction of casting (vertical flow) and (ii) The flow perpendicular to the direction of casting (horizontal flow).

The absorption properties of HCP, mortar and concrete are also investigated and attempts made to relate absorption to saturated permeability.

5.2 Experimental Programme, Apparatus and Testing Procedure

5.2.1 Direction of Casting

The horizontally and vertically cast specimens have the same mix proportions shown in table 5.1. VHS1 to VHS5 are for various slumps at 0.4 w/c ratio, while VH50 to VH70 are for varying w/c ratio at medium slump of 50 - 100 mm [27]. The moulds used for casting the specimens and the casting procedures are illustrated in section 3.6.

5.2.1.1 Apparatus

Saturated permeability tests were carried out for both directions of casting. The permeability apparatus used for these tests is similar to that described by Oyeka[17] and is as shown in plate 5.1 and fig. 5.1. Ten permeability cells, using perspex tubes of internal diameter 4 mm, were set up in two groups, one of four and the other of six. Any cell could be

1. INLET VALVE
2. OUTLET VALVE
3. BLEEDING VALVE
4. OUTER SEALING O-RING FOR CONCRETE SPECIMENS
5. INNER " " " HCP "
6. TOP FLANG
7. BOTTOM FLANG
8. EIGHT BOLTS 12mm DIA.
9. SUPPORTING FRAME
10. INLET PIPE 4mm INT. DIA.
11. OUTLET PIPE
12. PRESSURE REGULATING GUAGE
13. BOARD FITTED WITH SCALE IN mm
14. OIL FEEDING VALVE
15. PRESSURE REGULATING GAUGES
16. COMPRESSED NITROGEN CYLINDER (2000 psi)
17. OIL RESERVOIR

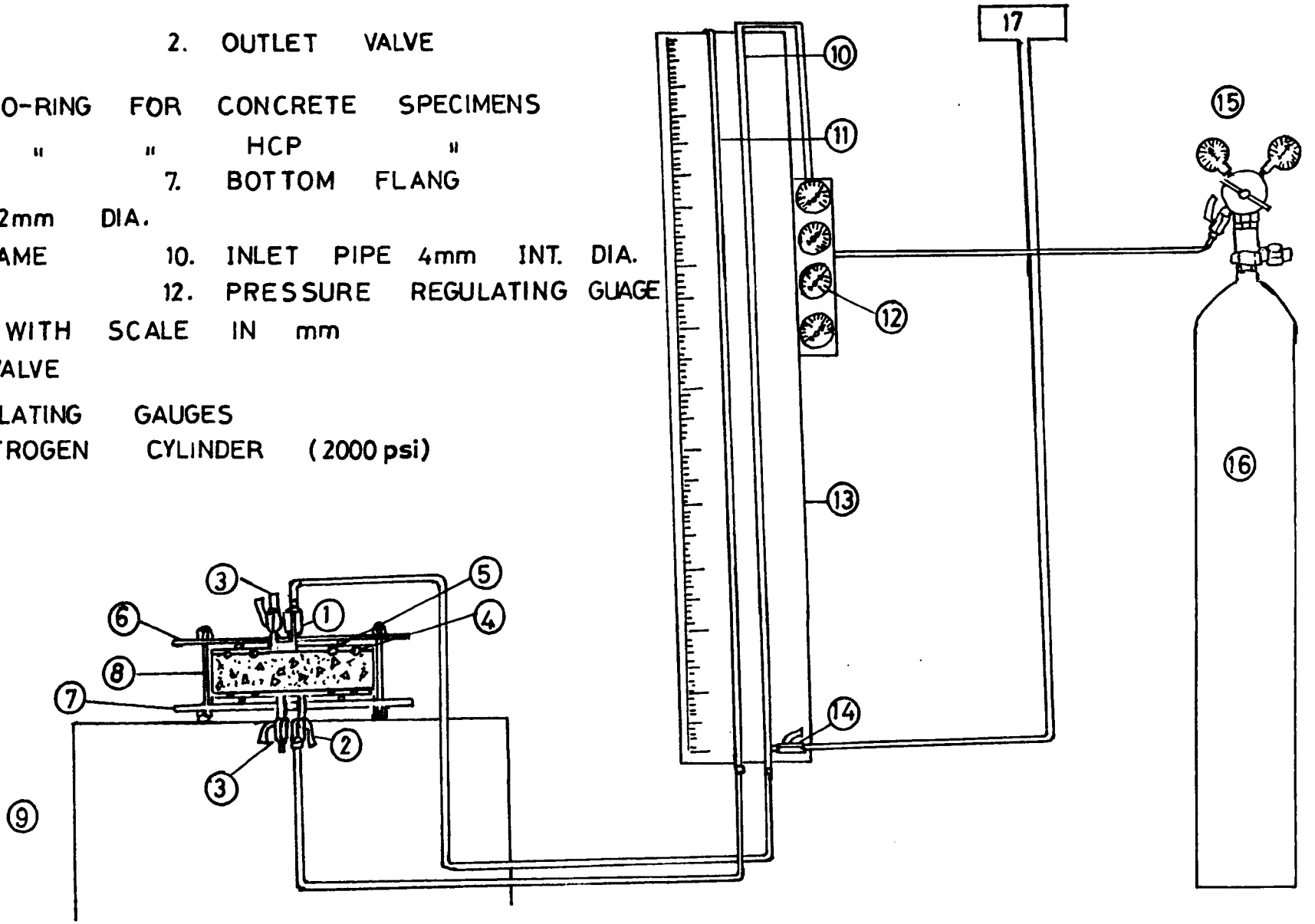

FIG 5.1 SCHEMATIC DRAWING OF THE PERMEABILITY APPARATUS SHOWING A CELL

CONCRETE DESIGNATION	SLUMP mm	CEMENT CONTENT kg/m^3	TOTAL AGG. CONTENT kg/m^3	FINE AGG. FRACTION	w/c RATIO
VHS1	5	375	1885	0.32	0.4
VHS2	40	512	1635	0.36	0.4
VHS3	60	545	1584	0.38	0.4
VHS4	110	576	1538	0.40	0.4
VHS5	140	612	1514	0.42	0.4
VH50	MEDIUM	360	1835	0.36	0.50
VH60$^+$	(50-100)	340	1805	0.37	0.60
VH70		293	1852	0.39	0.70
VH80		256	1890	0.40	0.80

$^+$ Used for casting the crack specimens and the model concrete tanks.

TABLE 5.1: Mix proportions for the vertically and horizontally cast specimens.

disconnected from its group at any time without interferring with the operation of the others. The base plates of the cell were modified to hold samples of 100 mm and 150 mm diameter and thickness varying from 10 to 200 mm. The inlet pressure was held constant by compressed nitrogen cylinders at 13.8 N/mm^2 (2000 PSI), through regulating valves. The amount of oil flowing into or out of the test specimens can be measured by reading the change in the levels of oil in the perspex tubes held against a graduated scale. 7 mm diameter O-rings were used to provide a seal for oil pressures up to 0.84N/mm^2 equivalent to 99.6 metre head of oil.

5.2.1.2 Preparation of specimens and testing

Before placing specimens, in the permeability cell, the concrete specimens were surface ground using a surface grinder until the cement laitance was removed and the aggregate particles exposed. The sides of the specimens were then cleaned thoroughly with dry fine sand and sealed with two coats of epoxy resin (Fabweld) with the second coat applied after 6 to 8 hrs. After partial drying, the sides were then coated with 4 to 6 layers of liquid rubber. The layers being applied at intervals of 20 mins. After applying the last coat, the liquid rubber was allowed to set properly, usually between 15 to 20 hrs. The coating was later tightly held with tough adhesive tapes, prior to the permeability tests. The horizontally cast specimens were tested in the direction of casting, while the vertically cast specimens were tested at right angles to the direction of casting. The tests were carried out in the CTR at 16±0.5^{o}C and 50±1% RH.

The results given in table 5.2, are the averages for two samples. A third sample is tested when the two samples do not agree to within 90% of each other, and the average of the closest two results is taken. All the samples used in the tests were fully saturated in oil, as described in section 3.8, before the permeability tests were carried out.

5.2.2 Sorptivity Tests

The sorptivity tests were carried out on cores obtained from

horizontally and vertically cast concrete specimens, with mixes VHS3, VH50, VH60, VH70 and VH80 of table 5.1. Sorptivity results were also obtained for HCP, mortar and concrete specimens with w/c ratios of 0.4, 0.5, 0.6 and 0.7 and for five different liquids (Kuwait crude oil (KU), North Sea crude oil (NS), Diesel oil (DE), Parafine oil (PA) and water (H_2O)). The mix proportions for these test specimens are given in table 6.1. To condition the specimens before the tests, the 25 mm dia. x20 mm thick (approx.) cores were first dried in the oven at 105°C to a constant weight and then allowed to cool with the oven to room temperature as described in section 3.8. The specimens were then kept in the CTR for about 4 to 6 hrs. to reach the temperature of 16°C. The specimens were then weighed to an accuracy of 1×10^{-4} gm and the initial weight noted, before the sorptivity test began.

5.2.2.1 Apparatus and testing Procedure

The sorptivity test apparatus consists essentially of a tray containing the liquid to a sufficient depth to cover a wire mesh (used to support the specimen), to a depth of about 5 mm as shown in fig. 5.2. The specimen was placed on the mesh and the amount of liquid absorbed after specific time intervals was determined. This was achieved by removing the specimen from the tray, drying off excess liquid from the surface and determining the increase in weight. To minimize loss of liquid by evaporation, the tray was covered with a loose fitting lid, whenever the specimen was in the liquid. This shields the test material from air movement. The increase in weight in a given time was noted and the sorptivity determined using equation 2.4 1. The liquid level in the tray was maintained constant throughout the test.

5.2.3 Model Concrete Tank Tests

The model concrete tanks were cast using mix VH60, of table 5.1. The tanks are hollow cylinders of external diameter 300 mm, height 175 mm and with 50 mm wall thickness. They are closed at one end with a 50 mm floor, marked A in plate 3.1. The specimens were cured in the fog room for

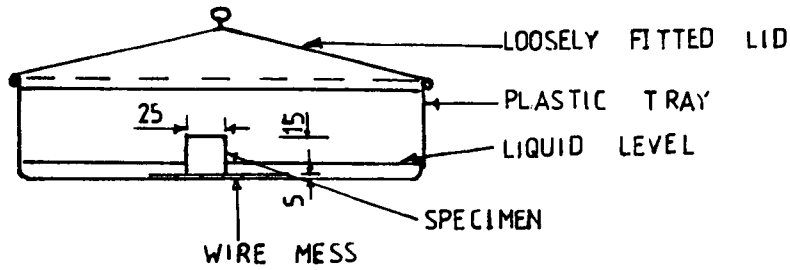

FIG 5.2 SORPTIVITY APPARATUS

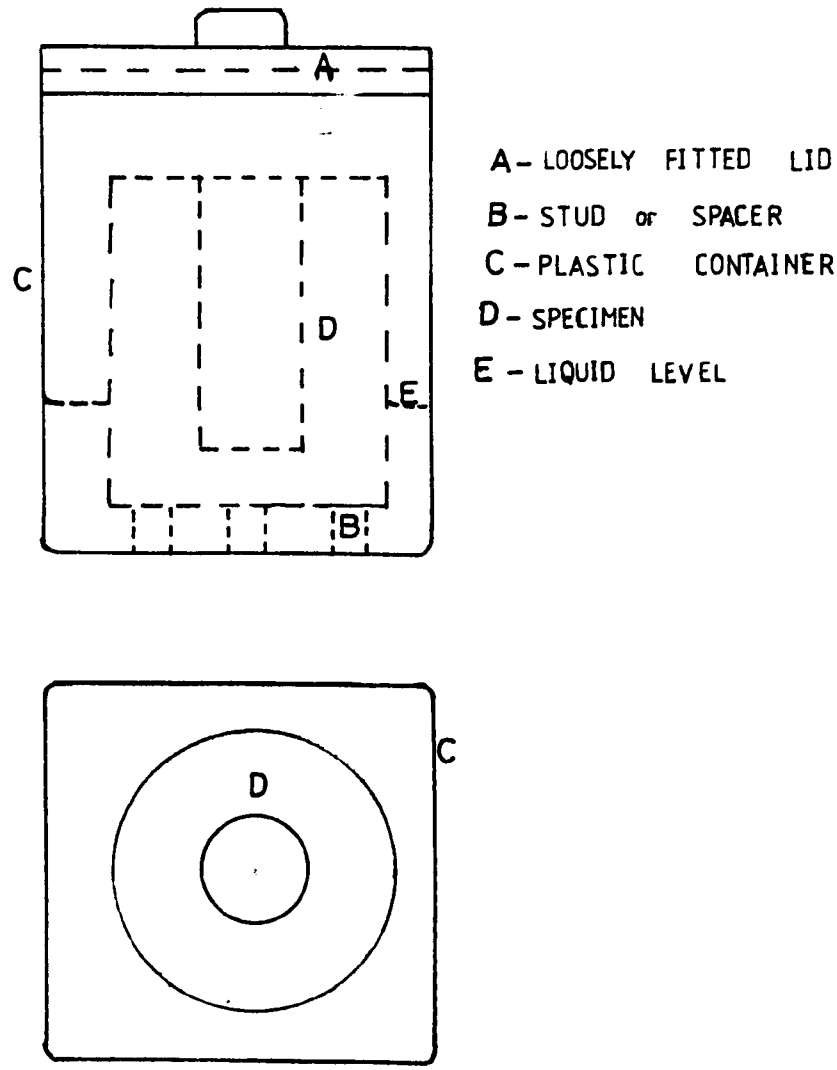

FIG 5.3 MODEL CONCRETE TANK TEST APPARATUS

28 days and air dried in a constant temperature room at 21±1°C and 50±1% RH, for two months prior to test. These specimens were each partially immersed in the five different liquids (Ku, NS, PA, DE and H_2O) in a loosely closed plastic container with hollow steel spacers at the bottom of the container shown in fig. 5.3 and marked B in plate 3.6. For each liquid, 4 different liquid depths were used (50, 80, 100 and 125 mm). The cylinders were re-weighed at intervals after removing surplus liquid from the outer surface by blotting with filter paper. The gain in weight was then recorded for a given time interval.

5.3 Analytical Techniques

The apparatus and testing procedures have been fully described in section 5.2. The coefficient of permeability K(m/s), for vertically and horizontally cast specimens was calculated using Darcy's law of equation 2.21. The value of d used in the equation was 140 mm and h = 50 mm as shown below. The rate of flow of oil into the specimen decreased continuously with

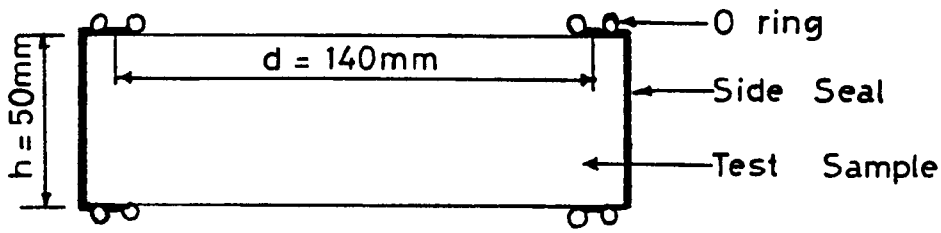

time-over about 120 hrs., after which the rate was approximately constant (section 7.2.1.1 and figs. 7.1 and 7.2). The quantity of oil flowing in the specimens was generally greater than the quantity flowing out. The outflow was between 50 to 95% of the inflow and depends on the inlet pressures with the higher percentage outflow at the higher oil pressures. The values of K were calculated using the inflow values at 120 hrs.

In the sorptivity test, the weight of liquid absorbed per unit area was converted to the volume of liquid absorbed per unit area using appropriate densities given in tables 3.4 to 3.10 for various liquids. The

total weight of liquid absorbed by the model concrete tank was also converted to the equivalent volume of liquid.

5.4 Direction of Casting/Permeability of Concrete

5.4.1 Scope of Study

The primary aim of this work was to establish the influence of vertically and horizontally cast specimen on the oil flow through concrete. The effect of mix variables on permeability of HCP, mortar and concrete is considered in chapter 7, and this section considers only the difference in permeability for the two directions of casting. For each direction of casting, five workability regimes (slump) at 0.4 w/c ratio (achieved by varying the cement/aggregate ratio), five w/c ratios (0.4, 0.5, 0.6, 0.7 and 0.8) and five oil pressures were used. The pressures were 0.827, 0.690, 0.552 0.414 and 0.277 N/mm^2, corresponding to crude oil pressure heads of 99.6, 83.0, 66.4, 49.8 and 33.2 metres. Only North Sea crude oil is used for this test.

5.4.2 Direction of Casting

The values of the coefficient of permeability (K), for vertically and horizontally cast specimens are shown in table 5.2, disregarding variables other than the direction of flow relative to the direction of casting.

1. The coefficient of permeability, (K_V) for flow perpendicular to the direction of casting is observed to be generally higher than K value (K_H) for flow parallel to the direction of casting.

2. The difference in the value is not unique. K_V (ie flow perpendicular to cast direction) was found to be between 1.06 to 1.81 times K_H (ie flow parallel to cast direction) with an arithmetic mean of 1.38 and a standard deviation of 1.26.

3. A plot of K_V versus K_H is shown in fig. 5.4. The relationship between K_V and K_H can be represented with a linear equation, for a line drawn through fig. 5.4, as

$$K_V = 1.718K_H - 5.99 \qquad (5.1)$$

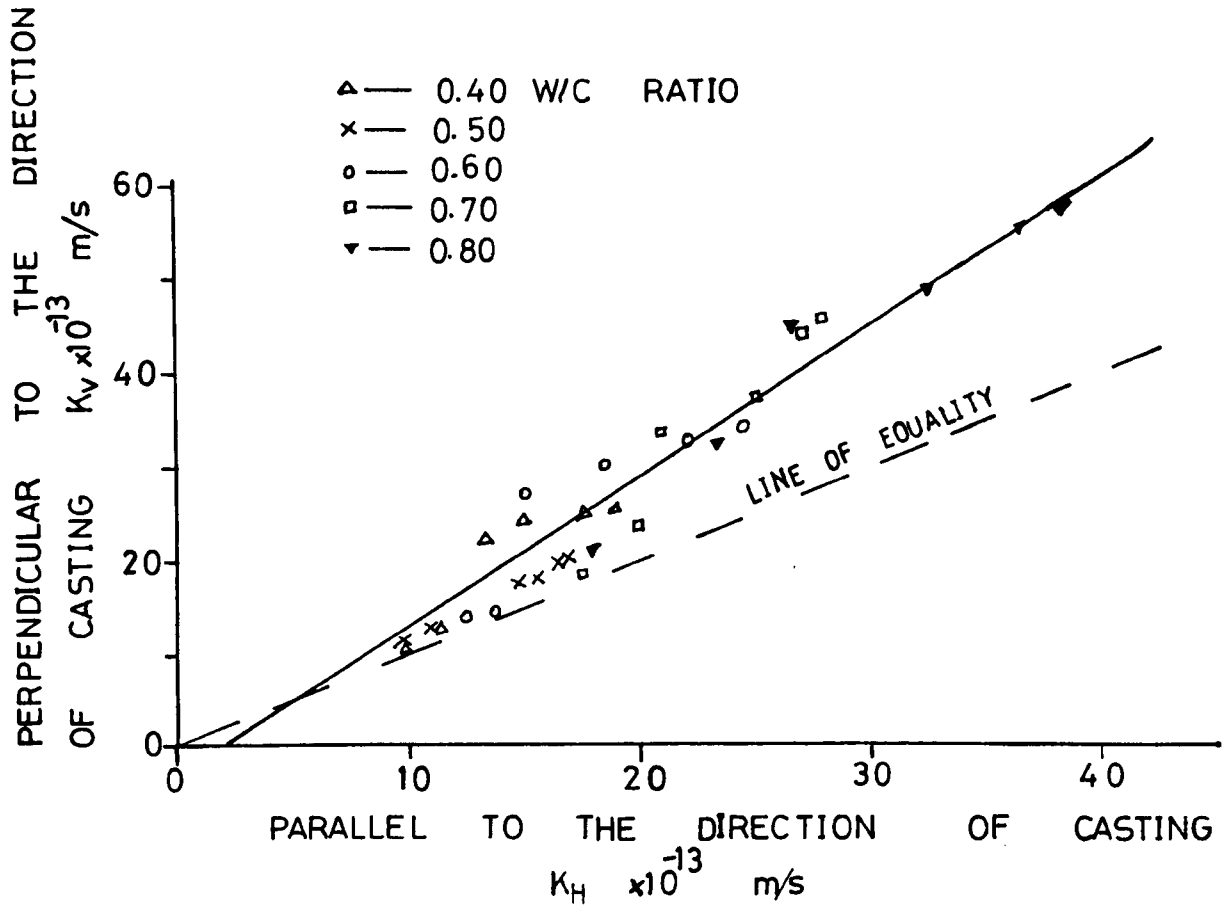

FIG 5.4 EFFECT ~~OF~~ OF DIRECTION OF CASTING ON CRUDE OIL PERMEABILITY OF CONCRETE

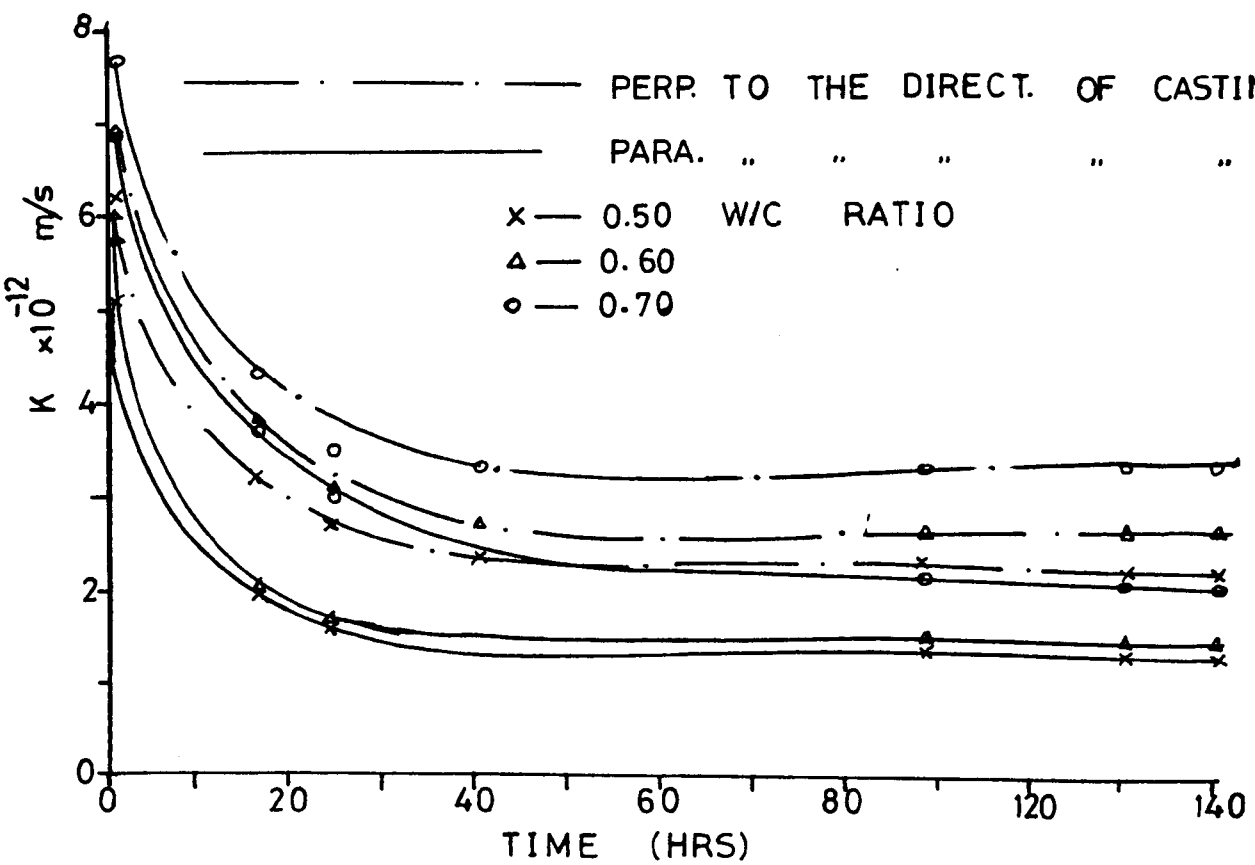

FIG 5.5 GRAPH OF K VS TIME OF TEST AT 49.8 METRE HEAD OF OIL

SATURATED PERMEABILITY K x 10^{-13} M/S													
MIX	W/C RATIO	PARALLEL TO THE DIRECTION OF CASTING							PERPENDICULAR TO THE DIRECTION OF CASTING					
		APPLIED PRESSURE M HEAD OF OIL / SLUMP (MM)	16.60	33.20	49.80	66.40	83.00	99.60	16.60	33.20	49.80	66.40	83.00	99.60
VHS1	0.4	5	14.66	16.93	17.76	20.32	21.46	21.64	17.88	19.46	20.67	23.64	24.55	25.39
VHS2	0.4	40	10.75	12.18	15.00	16.75	17.95	18.35	12.98	14.00	16.01	19.35	20.45	21.25
VHS3	0.4	60	9.80	11.05	14.82	15.62	16.46	16.95	11.37	12.62	17.60	18.00	19.75	20.39
VHS4	0.4	110	10.78	12.25	16.95	17.23	18.22	19.40	12.18	13.49	18.99	19.61	21.14	22.94
VHS5	0.4	140	14.48	15.22	17.05	18.55	20.00	20.25	15.78	16.05	19.02	22.20	23.50	24.95
VHS2	0.4	MEDIUM	9.80	11.05	14.82	15.62	16.46	16.95	11.37	12.62	17.60	18.00	19.75	20.39
VH50	0.5	"	9.90	11.25	13.39	15.00	17.50	19.00	10.70	12.50	22.30	24.20	25.00	25.33
VH60	0.6	"	12.50	13.83	15.00	18.40	22.00	24.50	13.80	14.32	27.10	30.20	32.80	34.22
VH70	0.7	"	17.50	19.84	21.00	25.00	27.00	28.00	18.40	23.80	33.70	37.80	44.00	45.64
VH80	0.8	"	18.00	23.40	26.50	32.50	36.50	38.50	21.00	32.38	44.50	48.50	55.70	57.79
		(50-100)												

TABLE 5.2: Coefficient of Permeability K x 10^{-13} m/s for Vertically and Horizontally Cast Specimen.

where K_V = coefficient of permeability for crude oil flow perpendicular to the direction of casting

K_H = coefficient of permeability for crude oil flow parallel to the direction of casting

From a regression analysis, the correlation coefficient r, was found to be 0.9688.

4. The relationship between K_V and K_H as explained in equation 5.1 appears to hold approximately well for all the applied oil pressure, workability, w/c ratio and mix proportions tested.

5. The difference in K_V and K_H could be explained in two ways: (i) The vertically cast specimens could be seen to stratify into layers during vibration and flow channels may be formed between the strata to increase permeability when turned through 90^o for the flow test; (ii) Bleeding and segregation may produce layers of variable permeability, so that when the specimen is turned through 90^o for the flow test, some of the flow paths are entirely in the higher permeability regions. However, the design of the mix and the casting of the specimen was carefully controlled and the workability is moderate such that segregation is not expected. It appears then that stratification is the more likely cause of higher permeability for vertical cast specimens.

6. Pore structure analysis of the specimens (section 6.6) shows that vertically cast specimen have a greater pore volume intruded by mercury than the horizontally cast specimen (ie 0.170 cc/cc for vertically cast specimens compared with 0.115 cc/cc for horizontally cast specimens). This indicates that the vertically cast specimens have both a more continuous pore system and a greater total pore volume.

5.4.3 Duration of Test

Figure 5.5, illustrates the variation in the coefficient of permeability with time of test, at a pressure head of 49.8 metres of oil , three w/c ratios and for vertically and horizontally cast specimens. The

following observations are made:

1. The coefficient of permeability K, decreased with time during the test period (see also section 7.2.1.1), for both horizontally and vertically-cast specimens.

2. The decrease in K with time is at a decreasing rate and tends to be zero at about 120 hrs. For vertically cast specimen, K_V, after 1 hour of flow was between 2.13 to 2.30 times K_V after 24 hrs., while K_V after 24 hrs. of flow was between 1.06 to 1.20 times K_V after 120 hrs. For horizontally cast specimen, K_H after 1 hour of flow was between 2.28 to 3.53 times K_H after 24 hrs., while K_H after 24 hrs. of flow was between 1.13 to 1.43 times K_H after 120 hrs. The rate of decrease varies with w/c ratio and direction of flow.

The reduction in the rate of permeability could be due to the initial clogging of the pore system by the waxy deposits in the crude oil, or because the specimen was not fully saturated at the start of the test. This may occur because of losses due to evaporation while the surface treatment and sealing of specimen were being carried out. Similar trends were observed for water flow but with smaller decrements[175].

5.4.4 Workability

Though the slump test does not measure the workability of concrete directly, it is very useful in detecting variations in the uniformity of a mix and could be assumed to be an indirect method of workability determination. The slump values were obtained immediately after mixing as mentioned in section 3.6.2.1. The variation of K with slump is given in table 5.2 and fig. 5.6 for both horizontally and vertically cast specimens. The following observations are made from the plot

1. Low slump, below about 30 mm and higher slump above about 110 mm gave more permeable concrete with the least permeable concrete at about medium range slump. This was obtained for only 0.4 w/c ratio, and appears to be independent of the applied pressure. The trend also is observed for

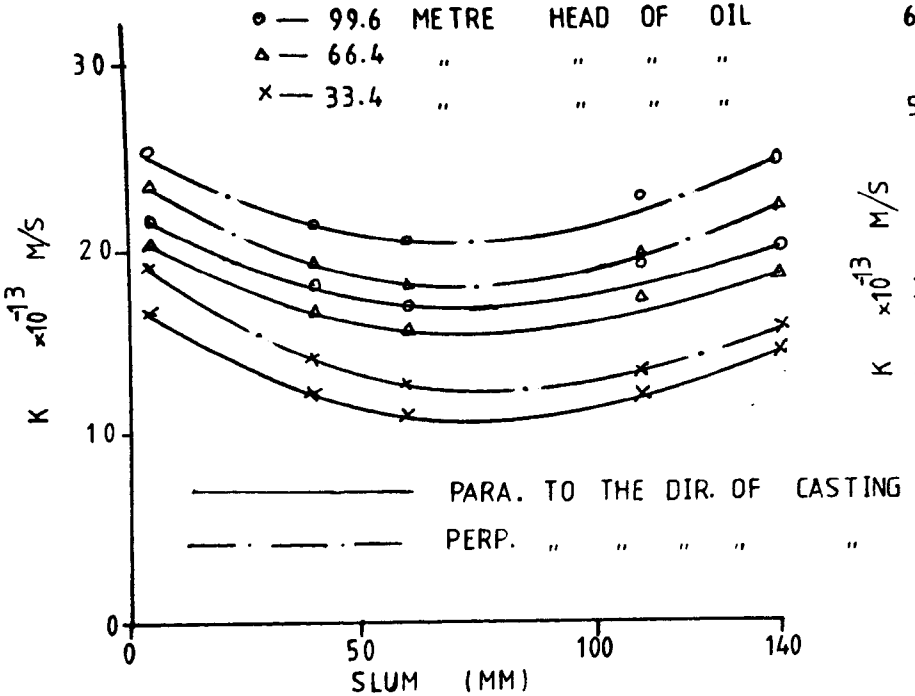

FIG 5.6 VAR. OF K WITH THE CONCRETE WORKABILITY

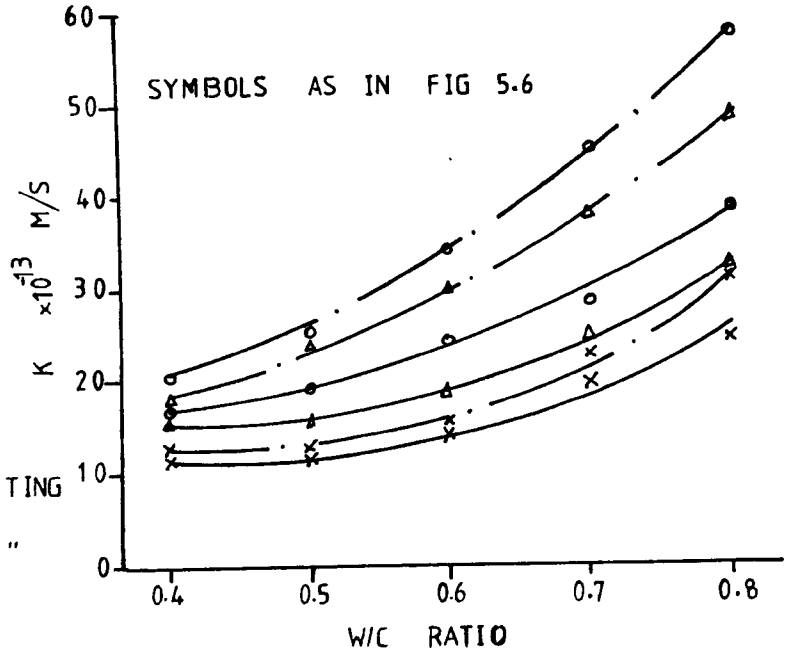

FIG 5.7 VARIATION OF K WITH W/C RATIO

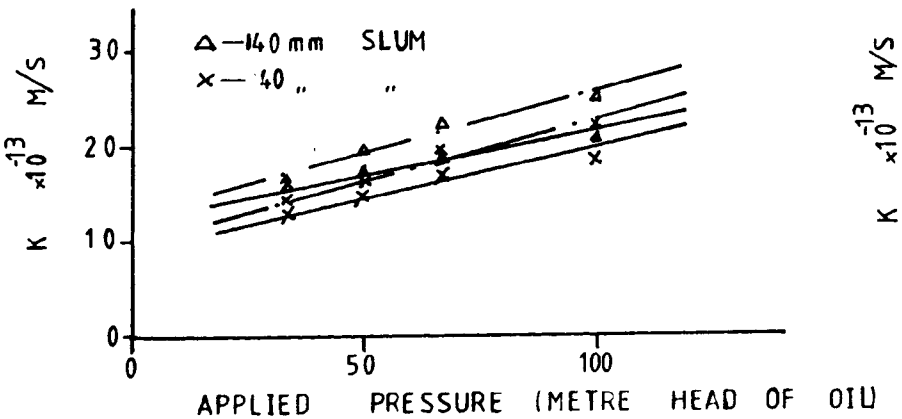

FIG 5.8 VARIATION OF K WITH APPLIED PRESSURE (METRE HEAD OF OIL)

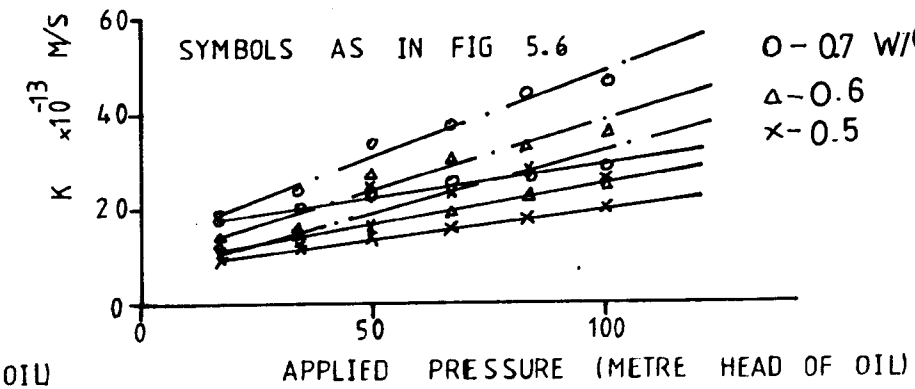

FIG 5.9 VARIATION OF K WITH APPLIED PRESSURE

both horizontally and vertically cast specimens.

These observations could be due to (a) At lower slump, more continuous pore channels are created due to incomplete compactions. Also low slump mixes contain less cement and a lower proportion of fines (table 5.1); (b) High slump mixes tend to bleed, thereby introducing flow channels in the concrete. Points (a) and (b) above would, therefore, tend to increase the K values.

The variation of K with the w/c ratio is given in fig. 5.7 while figs. 5.8 and 5.9 show the variation of K with the applied oil pressure. These variations are for both horizontally and vertically cast specimens. The effect of w/c ratio, applied pressure and other factors on permeability are fully discussed in chapter 7.

5.5 Sorptivity

5.5.1 Introduction and Scope of Study

The penetration of water into a porous solid by capillarity is defined by an advancing profile of water content Θ with distance, as given in equation (5.2)[148].

$$x(\Theta, t) = \phi(\Theta)t^{\frac{1}{2}} \qquad (5.2)$$

This predicts that for absorption which is governed by the extended Darcy equation[148] as shown in eqn. 5.3, the profile advances as $t^{\frac{1}{2}}$, maintaining a constant shape $\phi(\Theta)$

$$U = -K_C \nabla\Phi \qquad (5.3)$$

where U = flow within the porous medium m/s

$\nabla\Phi$ = gradient of the total hydraulic potential

t = time of test sec.

K_C = hydraulic conductivity m/s

x = distance advanced by the liquid into the unsaturated porous solid m

The useful result which follows from eqn. 5.2 and which forms the

basis for this experimental work, is an equation defining the advance of liquid content profile as it is being absorbed into an initially dry porous solid. Unsaturated flow theory therefore provides theoretical support for $t^{\frac{1}{2}}$ laws of liquid absorption and penetration as shown in eqn. 2.41 and reproduced in equation 5.4, with subsidiary equations 5.5 and 5.6.

$$i = St^{\frac{1}{2}} \tag{5.4}$$

$$di/dt = U_o = \tfrac{1}{2}St^{-\frac{1}{2}} \tag{5.5}$$

$$iU_o = \tfrac{1}{2}S^2 = \text{constant} \tag{5.6}$$

where i, S and t are as defined in section 2.3.2.2.7

U_o = the flow velocity at the inflow face where x = O. This represents the maximum rate of absorption of liquid by the porous material.

Equation 5.4, holds for horizontal absorption for any length of time, and for short term vertical movement of the liquid when gravity effect could be neglected[148].

Sorptivity determinations were carried out for both vertically and horizontally cast specimens, using five different liquids, Ku, NS, DE, PA and H_2O. This is to enable a comparative study, to be made of the effect of different liquid properties on flow. However, to establish a relationship between sorptivity and permeability, sorptivity results were obtained for HCP, mortar and concrete whose permeabilities had been determined separately using the method described in section 5.2. Mix properties and permeability results for these specimens are given in chapter 7.

5.5.2 Experimental and Other Factors effecting Sorptivity

5.5.2.1 Direction of casting

Typical graphs of volume of liquid absorbed per unit area (mm^3/mm^2 or mm) versus the square root of time ($min^{\frac{1}{2}}$) for horizontally and vertically cast specimens are illustrated in fig. 5.10 for North Sea crude oil. Other liquid types tested exhibit same behaviour as in fig. 5.10 and therefore are not presented. Sorptivity S($mm/min^{\frac{1}{2}}$), were calculated from the various

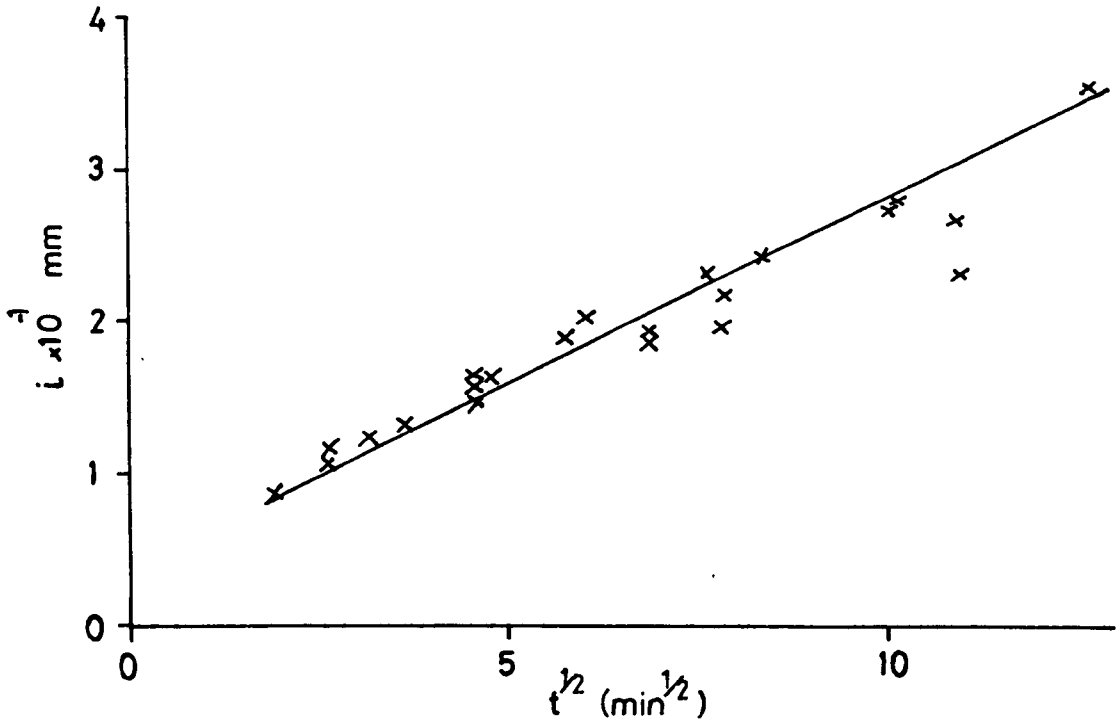

(A) PARALLEL TO THE DIRECTION OF CASTING

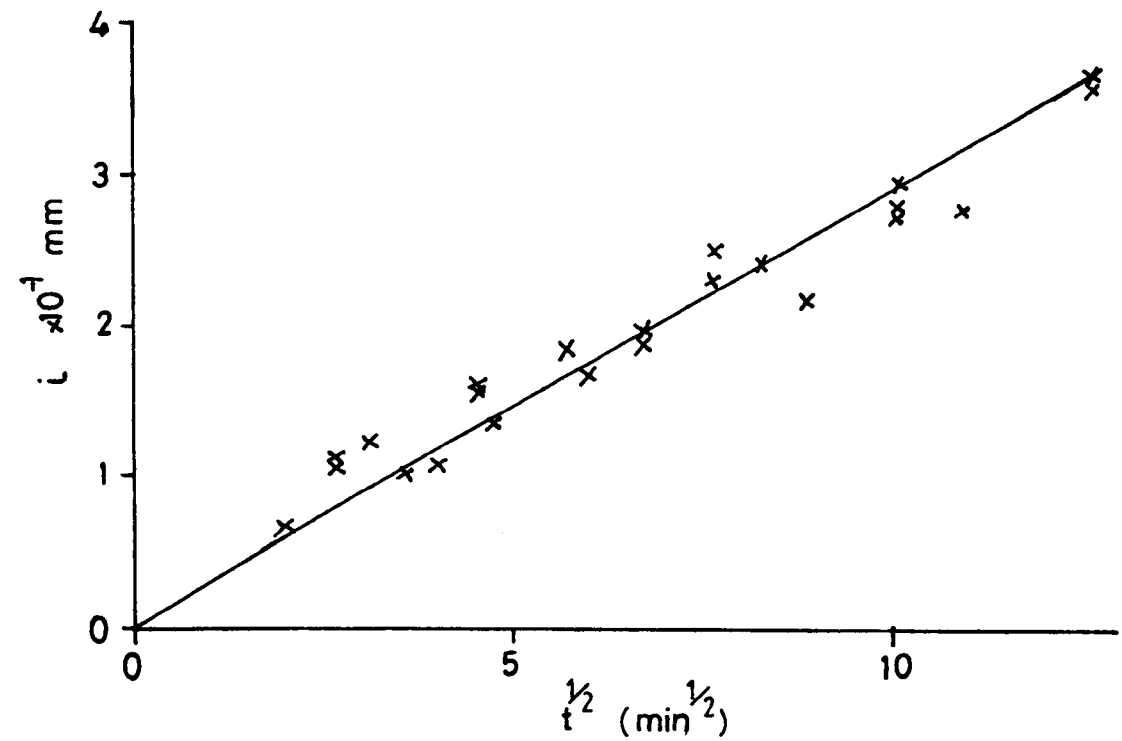

(B) PERPENDICULAR TO THE DIRECTION OF CASTING

FIG 5.10 GRAPH OF NORTH SEA CRUDE OIL ABSORBED PER UNIT AREA VS SQUARE ROOT OF TIME

plots, and are presented in table 5.3 for the five liquid types. Variation of sorptivity for the vertically cast specimens S_V with sorptivity for the horizontally cast specimens S_H for the five liquid types is shown in fig. 5.11. The following observations are made from the results:

1. Absorption of fluid by concrete follows the simple square law which was established using the extended Darcy equation for unsaturated flow. Therefore, the absorption per unit surface area is a linear function of the square root of time, for the five liquid types tested.

2. The sorptivity varies with the liquid type and so is a function of the properties of the individual liquids. See also section (5.5.2.5).

3. The sorptivity value for vertically cast specimen (S_V) is seen to be generally higher than the sorptivity value for horizontally cast specimen (S_H) for all the liquid types (fig. 5.11).

4. The relationship between S_V and S_H is as shown in equation 5.7, for the five liquid types

$$S_V = 1.19S_H + 0.08 \qquad (5.7)$$

where S_V = Sorptivity for absorption perpendicular to the direction of casting (vertically cast specimen)

S_H = Sorptivity for absorption parallel to the direction of casting (horizontally cast specimen).

The equation has a correlation coefficient r of 99%.

These findings are similar to the findings on the effect of direction of casting on permeability. The obvious explanations for the difference in flow value between vertically and horizontally cast specimens are already given in section 5.4.

5.5.2.2 Mix ingredients

Sorptivity tests were carried out on cement paste (HCP), cement mortar (1:1½, cement/sand ratio) and concrete (1:1½:1½ cement:sand:coarse aggregate ratio) all at 0.4, 0.5, 0.6 and 0.7 w/c ratios. Curing and drying procedures for these specimens are given in sections 3.4 and 3.7, while the

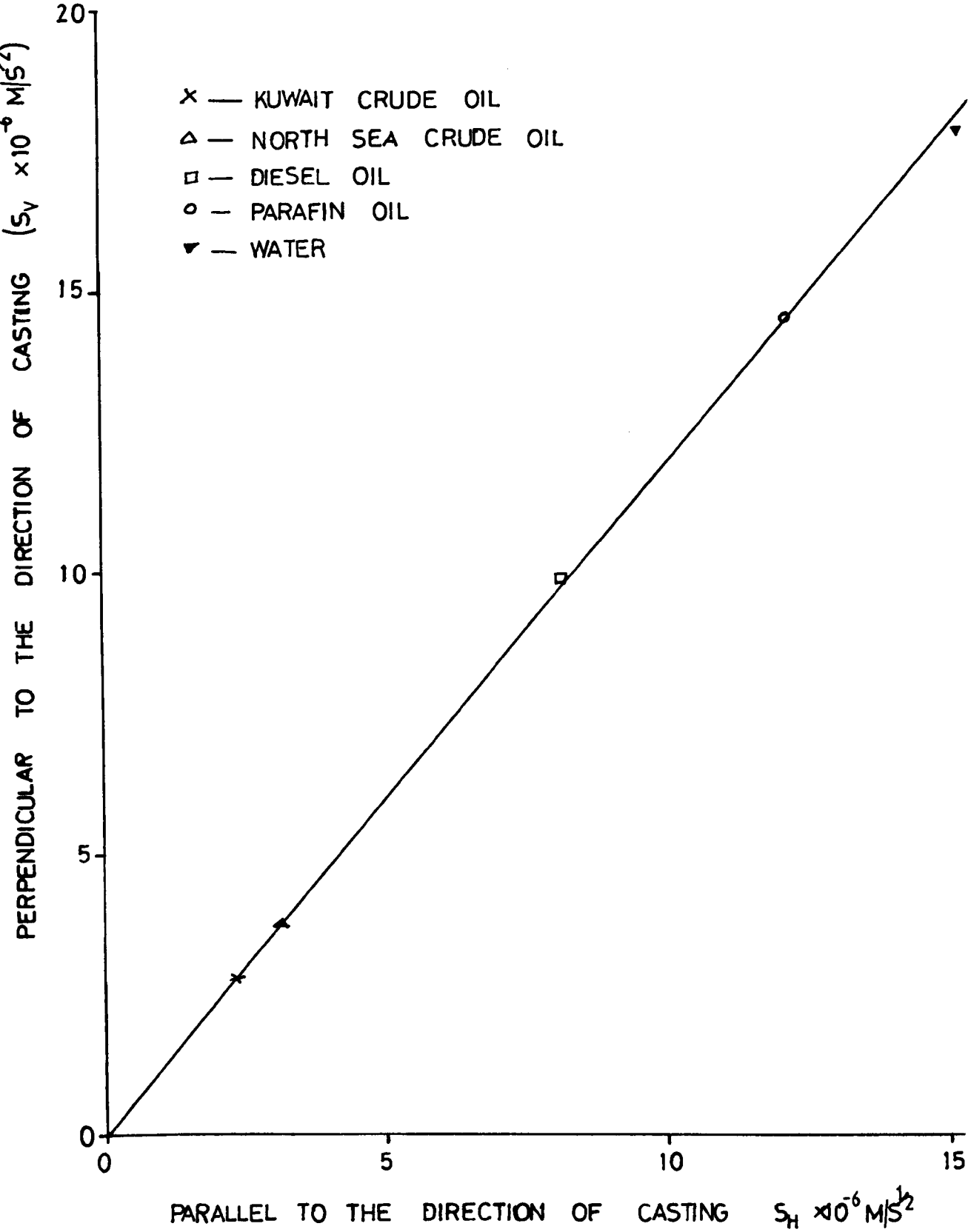

FIG 5.11 GRAPH OF SORPTIVITY S_v FOR THE VERTICALLY CAST CONCRETE VERSUS S_H, FOR THE HORIZONTALLY CAST CONCRETE SPECIMENS

10mm MAX. AGGRE. SIZE.

FLUID TYPE	SORPTIVITY mm/min$^{\frac{1}{2}}$		SORPTIVITY x 10^{-6} m/s$^{\frac{1}{2}}$	
	PARALLEL TO DIRN OF CASTING	PERP. TO DIRN OF CASTING	PARA. TO DRN OF CASTING	PERP. TO DRN OF CASTING
Water	0.1184	0.1385	15.285	17.880
Kuwait crude	0.0182	0.0214	2.350	2.763
North Sea crude	0.0245	0.0289	3.163	3.734
Diesel oil	0.0632	0.0767	8.159	9.902
Parafin oil	0.0940	0.1124	12.140	14.510

TABLE 5.3 Sorptivity of horizontally and vertically cast concrete for different liquid types (Hydrated for 28 days)

	SORPTIVITY x 10^{-6} m/s$^{\frac{1}{2}}$																			
	WATER				NORTH SEA CRUDE OIL				KUWAIT CRUDE OIL				DIESEL OIL				PARAFIN OIL			
SPECIMEN TYPE \ w/c RATIO	0.40	0.50	0.60	0.70	0.40	0.50	0.60	0.70	0.40	0.50	0.60	0.70	0.40	0.50	0.60	0.70	0.40	0.50	0.60	0.70
HCP	33.05	45.57	52.63	64.68	2.69	4.78	5.73	6.30	1.92	2.84	3.74	4.78	11.23	16.01	17.17	18.46	29.70	34.47	45.31	50.61
MORTAR (1:1½)	16.14	18.72	22.59	24.79	2.41	3.11	3.59	4.45	1.65	2.16	2.53	2.93	6.46	7.75	9.06	10.33	15.75	17.43	20.79	22.59
CONCRETE 1:1½:1½	7.49	9.42	11.74	14.59	1.24	1.68	2.34	2.98	1.11	1.56	2.12	2.22	3.83	5.54	6.58	7.00	7.88	7.30	11.88	13.43

TABLE 5.4 Sorptivity results for HCP, mortar and concrete, hydration for 28 days

LIQUID TYPE	WATER			NORTH SEAL CRUDE OIL			KUWAIT CRUDE OIL			DIESEL			PARAFIN		
SPECIMEN	$A_1 x 10^{-6}$	$B_1 x 10^{-6}$	r	$A_1 x 10^{-6}$	$B_1 x 10^{-6}$	r	$A_1 x 10^{-6}$	$B_1 x 10^{-6}$	r	$A_1 x 10^{-6}$	$B_1 x 10^{-6}$	r	$A_1 x 10^{-6}$	$B_1 x 10^{-6}$	r
HCP	101.95	-7.090	0.995	11.78	-1.604	0.959	9.48	-1.894	0.998	22.85	3.150	0.935	73.57	-0.441	0.988
MORTAR	29.82	4.129	0.994	6.60	-0.240	0.994	4.21	0.002	0.997	12.92	1.290	0.998	23.88	6.006	0.990
CONCRETE	23.62	-2.181	0.996	5.88	-1.174	0.996	3.89	-0.387	0.970	10.55	-0.065	0.964	19.23	0.046	0.993

TABLE 5.5 Constants of Regression for equation 4.8 Sorptivity vs w/c ratio

mix proportions are given in table 6.1. Sorptivity tests were carried out on these specimens as described in section 5.2.2, using the five liquid types (Ku, NS, PA, DE and H_2O). The results obtained from the tests are shown in table 5.4. Figures 5.12, 5.13 and 5.14 show the variation of sorptivity with w/c for HCP, mortar and concrete respectively. The following observations are made from the results:

1. Inclusion of fine aggregate reduces the sorptivity and inclusion of coarse aggregate further reduces the sorptivity for all the liquid types tested.

2. The reduction in sorptivity varies from one oil type to another. For 0.4 w/c ratio, water sorptivity of HCP is 2.04 times the water sorptivity of mortar and the water sorptivity of mortar is 2.15 times the water sorptivity of concrete. For the same w/c ratio, Kuwait crude oil sorptivity of HCP is 1.16 times the Kuwait crude oil sorptivity of mortar, which is 1.49 times the Kuwait crude oil sorptivity of concrete.

The higher values of sorptivity of HCP, could be explained by the water/solid (w/s) ratio. Since HCP has the highest w/s ratio, removal of water creates more voids and more capillary channels, hence higher sorptivity. Another explanation could be that the aggregate, which has a very low permeability (about 8.24×10^{-14} m/s)[54] reduces the effective surface area. This reduction however was not taken into consideration in the sorptivity determination.

The coefficient of permeability of these specimens was found to behave in the same manner as the sorptivity (section 7.2.1.2). A probable relation between permeability and sorptivity will be discussed later in this chapter.

5.5.2.3 Water-cement ratio

The variation of sorptivity with w/c ratio for HCP, mortar and concrete is shown in figs. 5.12, 5.13 and 5.14 respectively. and table 5.4. The following observations are made.

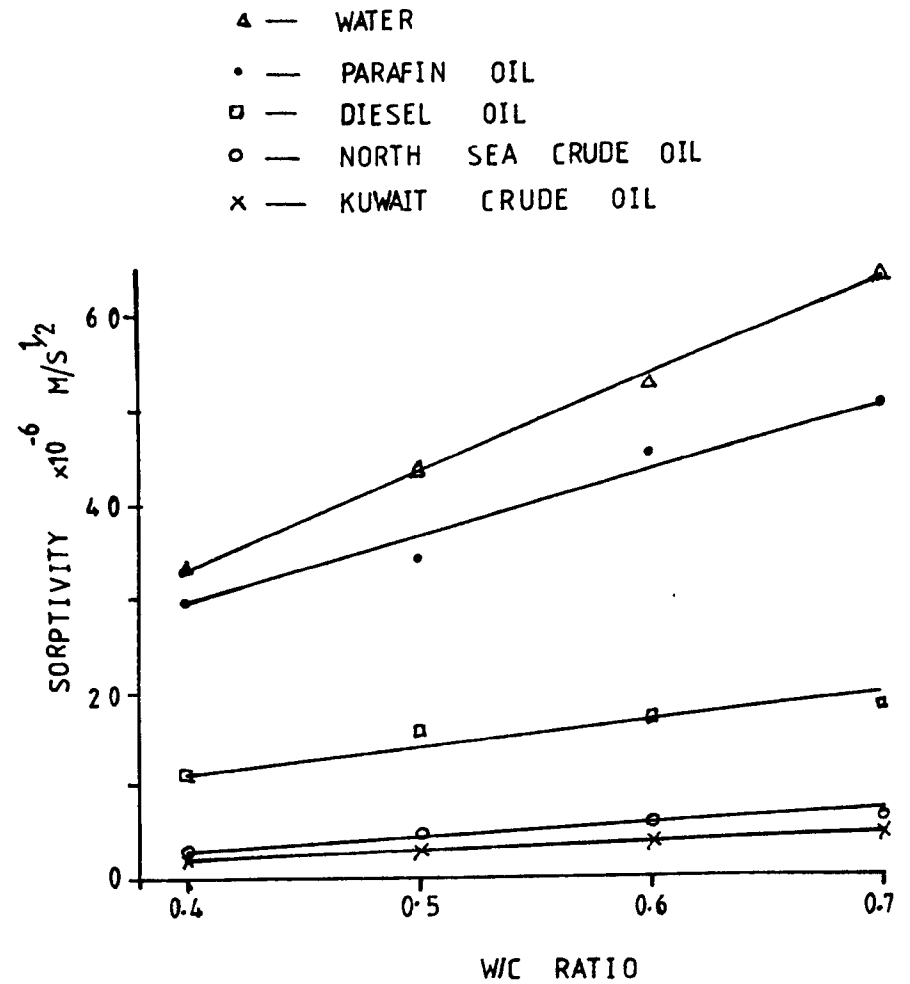

FIG 5.12 VARIATION OF SORPTIVITY WITH W/C RATIO FOR HCP

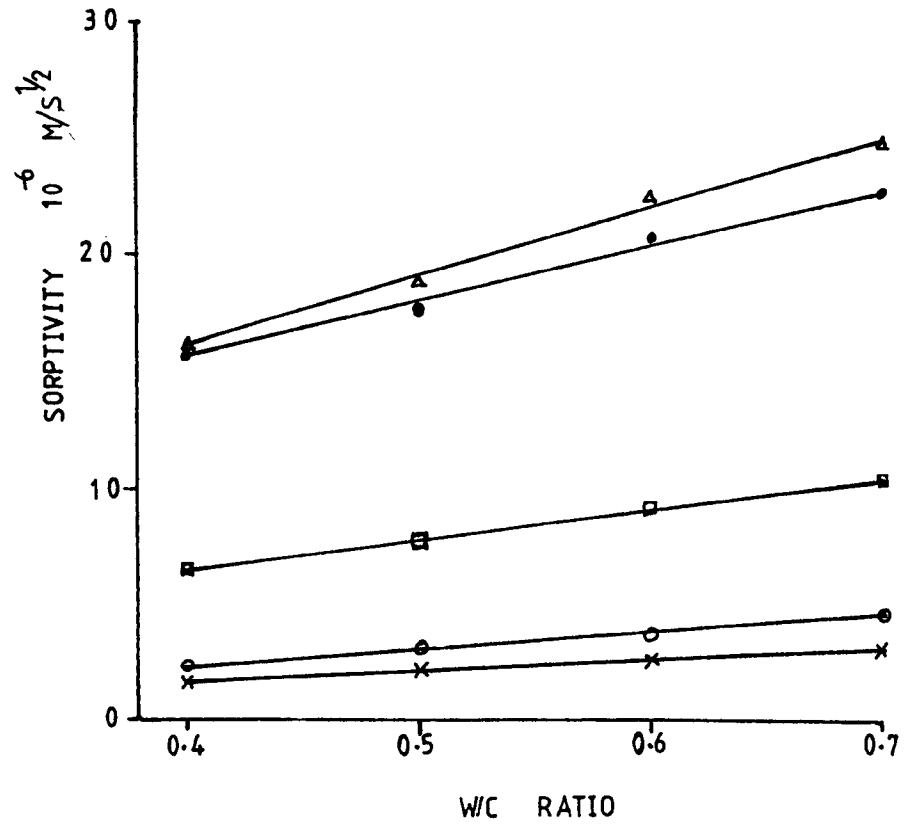

FIG 5.13 VARIATION OF SORPTIVITY WITH W/C RATIO FOR MORTAR

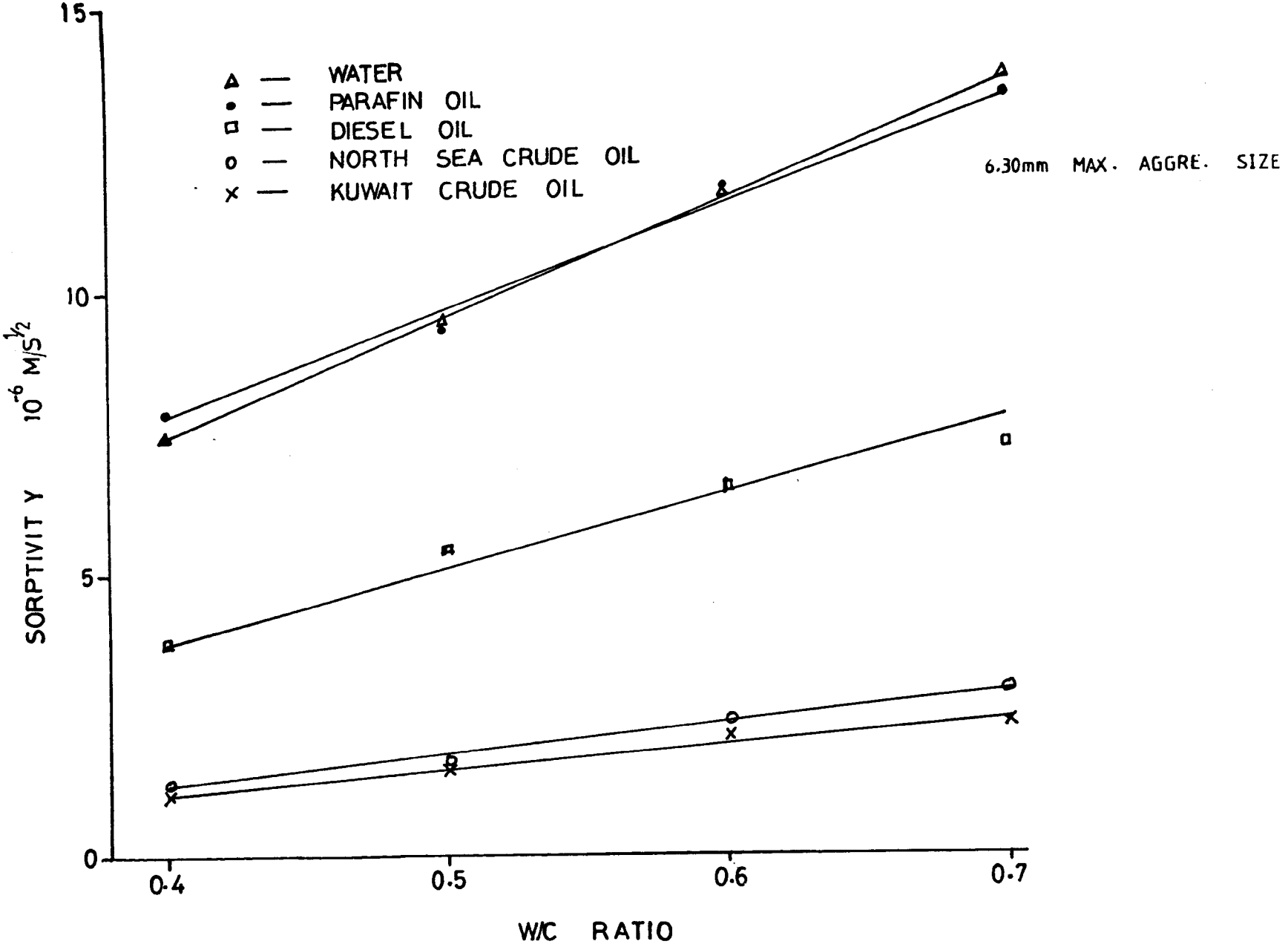

FIG 5.14 VARIATION OF SORPTIVITY WITH W/C RATIO FOR CONCRETE

1. Sorptivity increases linearly with an increase in the w/c ratio, for all the liquid types tested, and for HCP, mortar and concrete.

2. The rate of increase varies from liquid to liquid and from one mix type to another. For HCP, the sorptivity at 0.7 w/c ratio ranges between 1.64 times the sorptivity at 0.4 w/c ratio for diesel oil to 2.49 times the sorptivity at 0.4 w/c ratio for Kuwait crude oil, with intermediate values for other liquids. Also for a particular liquid, say water, the ratio of sorptivity at 0.7 w/c to that at 0.4 w/c ratio is 1.96:1 for HCP, 1.54:1 for mortar and 1.95:1 for concrete.

3. The relationship between sorptivity and w/c is expressed as shown in equation 5.8

$$S = A_1(w/c)+B_1 \qquad (5.8)$$

Where A_1 and B_1 are constants. The values of A_1 and B_1 were determined regressionally and are given in table 5.5 for all the liquid types and for HCP, mortar and concrete.

Tests on the crude oil permeability of these specimens (section 7.2.1.2) also revealed that K increases with an increase in the w/c ratio. The increase however was found to be non-linear and its significance on the possible relationship between sorptivity and permeability is the subject of the next section.

5.5.2.4 Sorptivity and permeability

The total pore volume of HCP, mortar and concrete is often measured as the volume of liquid absorbed at full saturation. The technique is to first dry the specimen to a constant weight, then immerse it in the liquid and measure the increase in weight as a percentage of the dry weight. Neville[70] argues that absorption per unit weight cannot be used as a measure of the quality of concrete, This is because variations in results could occur with different drying temperatures. Drying at say ordinary room temperature, may be ineffective in removing all the water, while drying at high temperatures may remove some of the chemically combined water.

Sorptivity is a measure of absorption per unit area, and does not depend on the weight of the specimen. For an approximately homogeneous solid in which the capillary forces were much larger than the gravitational forces (a condition satisfied by fine-pored materials, e.g., HCP, mortar and concrete, in the first stages of capillary rise), the cumulative absorbed volume per unit area of the inflow surface increases as the square root of time (section 5.5.1). Sorptivity S, as shown in equation 5.4, may therefore be able to describe in a relative sense, the permeability characteristics of porous media provided (a) The porous solid is assumed homogeneous; (b) The test is carried out for a short period, to minimize gravitational attraction; (c) A good representative sample of the specimen is used. Assertion (b) is attained as long as the $\sqrt{t}$ relationship is obtained. Permeability, however, is associated with hydraulic gradient, while sorptivity is not, so while permeability result can only be obtained where there is a pressure differential, sorptivity can be obtained in any unsaturated condition. Therefore, absolute values of the sorptivity cannot be assumed to be permeability values, but could be used in relative terms to describe the liquid flow phenomena in porous solids.

The variations of saturated permeability with sorptivity are shown in figs. 5.15 to 5.18 for water and North Sea crude oil. Sorptivity values are shown in table 5.4, while the permeability values are shown in table 7.2. The following observations are made from the results:

1. The permeability increases with an increase in the sorptivity, for both mortar and concrete with water and North sea oil.

2. For water the increase is found to be non-linear while a linear increase is observed for North Sea crude oil. The reason for the difference in behaviour for the two types of liquid is not clear. It may however be that while the oil is being forced into the pores by a hydraulic head, the flow channels are being clogged and re-orientated by the waxy deposits in the oil. This behaviour which is not obtained in sorptivity thereby affects the permeability results for North Sea oil flow into mortar and concrete,

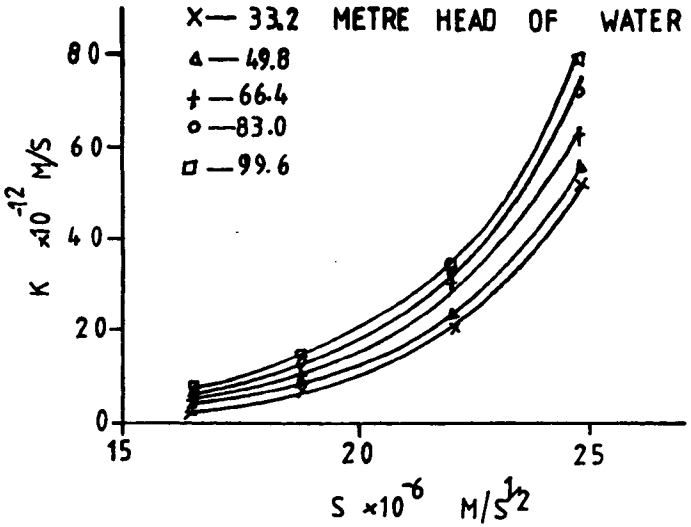

FIG 5.15 GRAPH OF SATURATED PERMEABILITY VS SORPTIVITY FOR MORTAR (WATER FLOW)

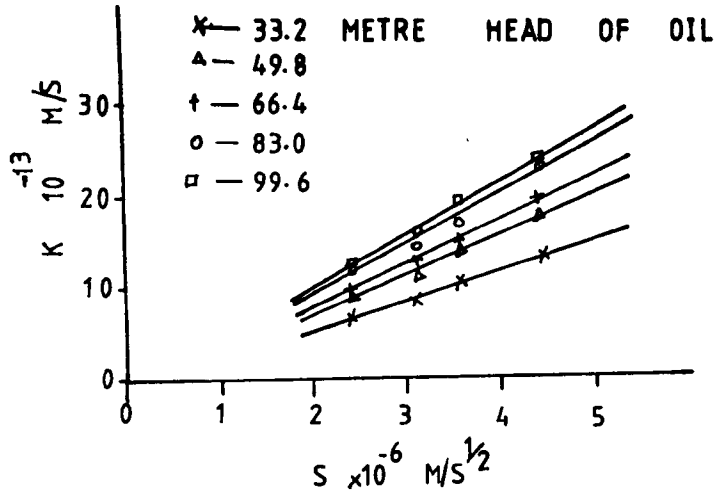

FIG 5.17 GRAPH OF SATURATED PERMEABILITY VS SORPTIVITY FOR MORTAR (NORTH SEA CRUDE OIL FLOW)

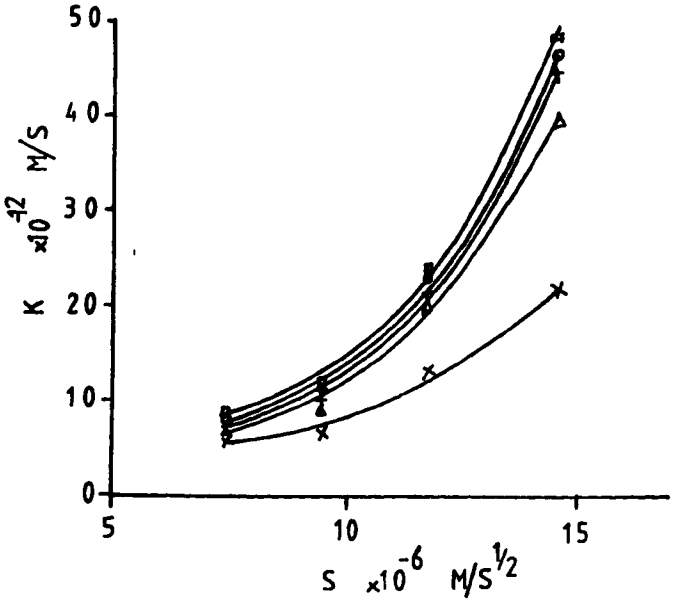

FIG 5.16 GRAPH OF SATURATED PERMEABILITY VS SORPTIVITY FOR CONCRETE (WATER FLOW)

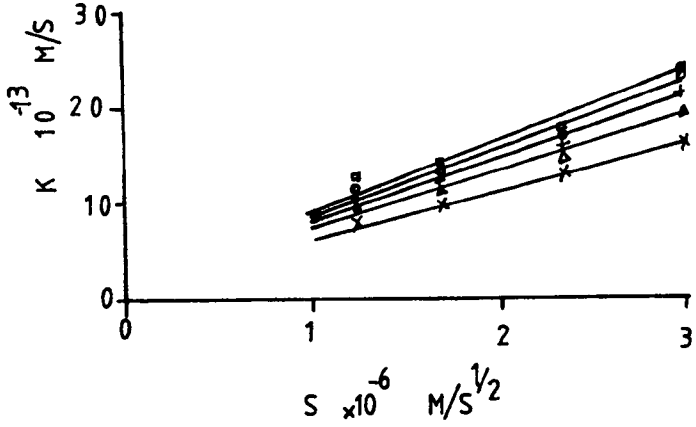

FIG 5.18 GRAPH OF SATURATED PERMEABILITY VS SORPTIVITY FOR CONCRETE (NORTH SEA CRUDE OIL FLOW)

with a consequent effect on its relationship to sorptivity, ie assuming the water flow to be standard.

3. For water flow, the relationship between K and sorptivity can be represented with an exponential equation of the form

$$K = K_o(\exp)^{aS} \qquad (5.9)$$

where K_o is a theoretical coefficient of permeability at zero sorptivity, and a is a constant. K_o and a were determined regressionally for both mortar and concrete and are given in table 5.6, for various pressure heads of water.

4. For North Sea crude oil flow, a linear relationship between K and sorptivity is obtained and represented as

$$K = K_1 S + K_2 \qquad (5.10)$$

where K_1 and K_2 are constants

K = coefficient of permeability m/s

S = sorptivity ($m/s^{\frac{1}{2}}$)

K_1 and K_2 were determined regressionally and are also given in table 5.6, for various oil heads.

The obvious similarities between the coefficient of permeability K, and sorptivity S, manifested all through section 5.5, show that S could be used in relative terms to describe the characteristics of liquid flow through porous solids, and can be employed in the proceeding sections to analyse the flow characteristics of different liquids.

Sorptivity was chosen for this analysis because (a) It is quick to determine, and the results are reliable provided the values are taken while the i vs $\sqrt{t}$ plot remains linear, and (b) It is safer to determine S for liquids, which could be a fire risk.

5.5.2.5 Effect of liquid properties on sorptivity

5.5.2.5.1. Introduction

Sorptivity may be a useful parameter to define the free liquid suction of HCP, mortar and concrete. For a homogeneous material, with

WATER			
APPLIED PRESS. m HEAD OF LIQUID	$K_o \times 10^{-12}$	$a \times 10^{5}$	r
MORTAR			
33.20	0.01285	3.328	0.992
49.80	0.03710	2.990	0.998
66.40	0.04715	2.887	0.998
83.00	0.06890	2.776	0.997
99.60	0.11980	2.570	0.992
CONCRETE			
33.20	1.1490	2.007	0.981
49.80	1.0910	2.441	0.986
66.40	1.1090	2.508	0.989
83.00	1.1860	2.504	0.992
99.60	1.2742	2.476	0.992
NORTH SEA OIL			
M HEAD OF LIQUID APPLIED PRESS	$K_1 \times 10^{-7}$	$K_2 \times 10^{-13}$	r
MORTAR			
33.20	3.078	-1.31	0.981
49.80	4.327	-2.294	0.972
66.40	4.935	-3.053	0.998
83.00	5.368	-1.997	0.967
99.60	5.548	-1.269	0.993

(cont'd...)

CONCRETE			
33.20	4.132	2.188	0.983
49.80	4.886	3.059	0.993
66.40	5.759	2.261	0.988
83.00	5.660	3.505	0.985
99.60	5.736	4.184	0.950

TABLE 5.6: Constants of Regression for equations 5.9 and 5.10. K vs S for water and North Sea oil respectively.

capillary forces much larger than gravitational forces, sorptivity could be used to describe the relative flow behaviours of different liquids in the porous solids. This section deals with the influence of liquid properties on the sorptivity, hence on the flow characteristics of the liquid. All the properties of the liquids under discussion are given in tables 3.4 to 3.8, while the properties required for this section are reproduced in table 5.7 below

LIQUID TYPE	Density $x10^3$ (kg/m^3)	Kinetic Viscosity $x10^{-6}$ (m^2/s)	Average molecular size (A)
WATER	1.00	1.14	3.00
PARAFIN	0.790	9.70	4.40
DIESEL	0.855	10.90	5.10
NORTH SEA CRUDE	0.860	20.32	6.30
KUWAIT CRUDE	0.890	22.43	6.90

TABLE 5.7: Properties of the Liquids.

5.5.2.5.2 Density

The variations of sorptivity with the density of the liquid is illustrated in figs. 5.19, 5.20 and 5.21 for concrete, mortar and HCP respectively. The following observations are made from the results:

1. The influence of density of water on sorptivity (hence on flow of water through porous solids) is quite distinct from the influence of the density of crude oil and its distillates on sorptivity.

2. For crude oil and its distillates, the sorptivity decreases with an increase in fluid density. This is expected since the heavier oil particles should find it more difficult to penetrate through the pores of the specimen.

3. The rate of decrease in the sorptivity is not constant. For a w/c of 0.7, in fig. 5.20, the sorptivity of parafin (density 0.79×10^3

FIG 5.19 GRAPH OF SORPTIVITY OF CONCRETE VS DENSITY

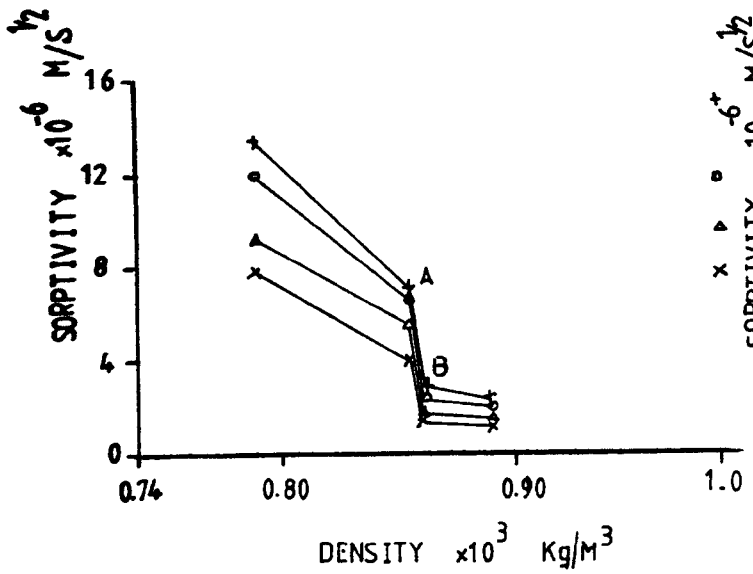

FIG 5.20 GRAPH OF SORPTIVITY OF MORTAR VS DENSITY

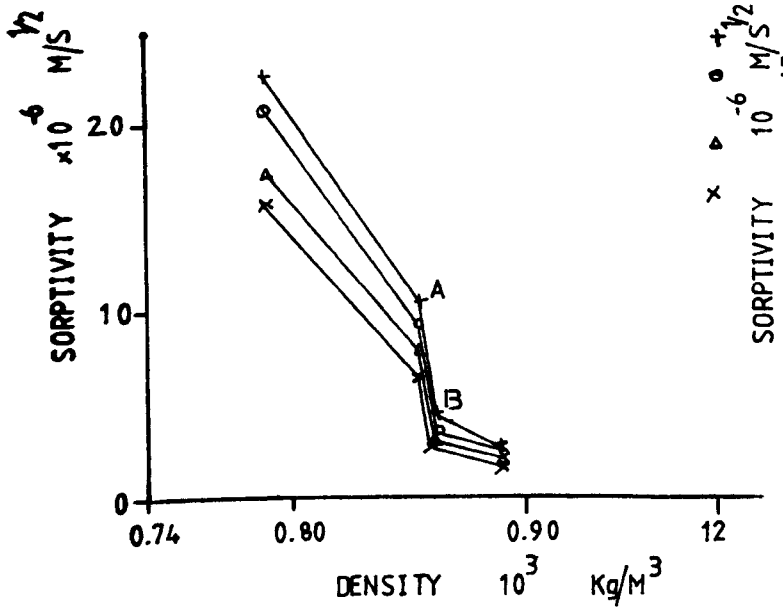

+ — 0.7 W/C RATIO
o — 0.6
Δ — 0.5
× — 0.4

FIG 5.21 GRAPH OF SORPTIVITY OF HCP VS DENSITY

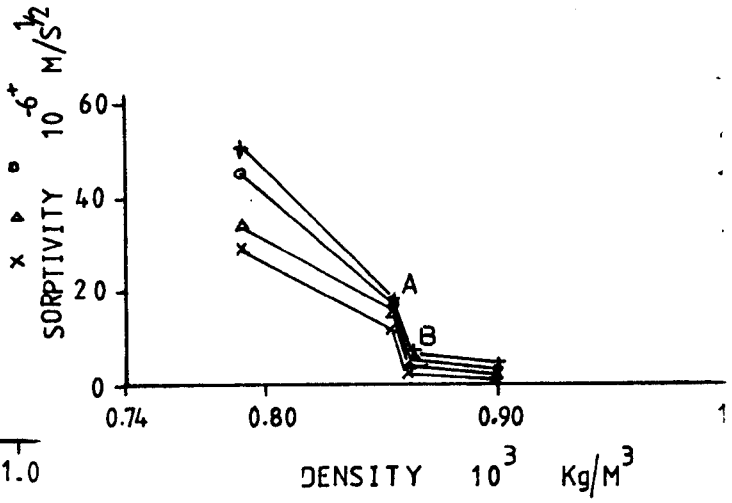

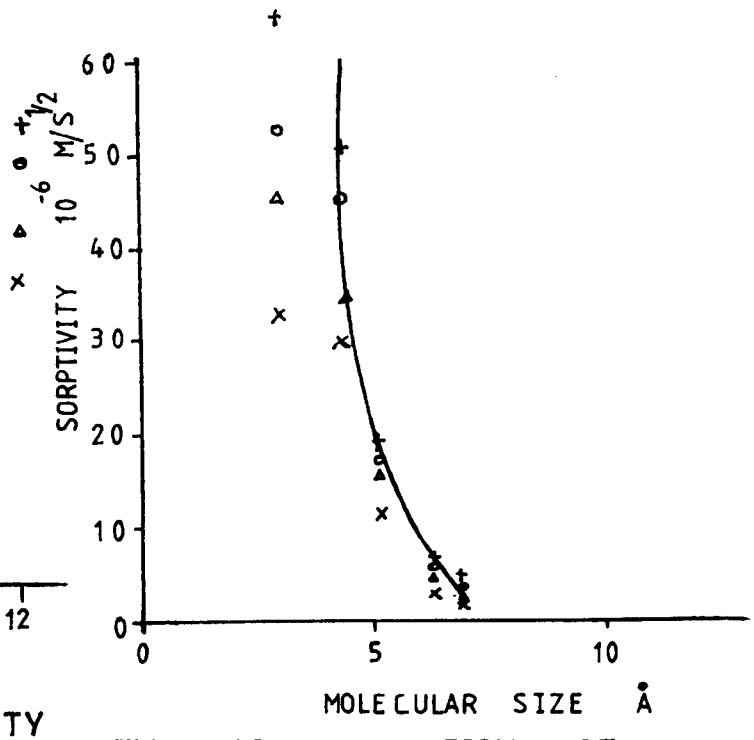

FIG 5.22 VARIATION OF SORPTIVITY OF HCP WITH MOLECULAR SIZE

kg/m^3) is 2.19 times the sorptivity of diesel oil (density 0.855×10^3 kg/m^3), which is 2.32 times the sorptivity of North Sea crude oil (density 0.860×10^3 kg/m^3) which is 1.52 times the sorptivity of Kuwait crude oil (density 0.89×10^3 kg/m^3). Between parafin and diesel, the density increased by 8% and the sorptivity decreased by 54%. Between diesel and North Sea crude, the density increased by only 0.6% while the sorptivity decreased by 57%. Between North Sea crude and Kuwait crude, the density increased by 3.5% while the sorptivity decreased by 34%.

4. A discontinuity is observed between A and B (fig. 19 to 21), where the results for parafin and diesel are above A, and the results for North Sea crude oil and Kuwait crude are below B. The reason for this discontinuity is not understood. A unique property of the crude oils which is not observed in their distillates is the wax content, which probably may have greatly reduced the sorptivity of the crude oils, but has very little effect on their densities.

5. North Sea crude has a wax content of about 3.12% by weight, while Kuwait crude has wax content of about 5.7%. Since the sorptivity of North Sea crude is greater than the sorptivity of Kuwait, it follows that the increase in wax content has coincided with a decrease in the sorptivity. It is likely that a higher wax content impedes the flow of the oil, but more tests are required in order to elucidate this fact.

5.5.2.5.3 Molecular size

The molecular size ranges are given for various types of oil in tables 3.4 to 3.8. The exact distribution is not known. A single representative molecular size was obtained using the procedure illustrated for diesel oil. An arbitrary proportion of the pore size ranges were chosen. 0.50 was assigned to the pore size range with highest occurrences, while the 0.25 was assigned to the two ranges before and after the maximum concentration of the ranges as shown (see also fig. 3.6). 0.25 times average of 1 to 4 Å plus 0.5 times average of 4 to 6.5 Å plus

0.25 times average of 6.5 to 8 Å, given a total of 5.1 Å. The average molecular sizes for various liquids were estimated in this manner and are given in table 5.7.

The variations of sorptivity with molecular sizes are shown in figs. 5.22, 5.23 and 5.24 for HCP, concrete and mortar respectively, and the following observations are made:

1. The molecular size of water influences sorptivity quite differently from that of crude oil and its distillates.

2. For oil, the sorptivity tends to decrease with an increase in the molecular size. The decrease is non-linear, but follows an exponential decay, within the range of the molecular sizes considered.

3. For HCP, mortar and concrete, the relationship between oil sorptivity and molecular size can be represented by an exponential equation of the form

$$S = S_o (\exp)^{a_1 Ms} \qquad (5.11)$$

where S_o is sorptivity of a theoretical oil of infinite molecular size, and a_1 is a constant.

M_s = molecular size (Å)

S = sorptivity $M/s^{\frac{1}{2}}$

S_o and a_1 are determined regressionally for various w/c ratios and are given in table 5.8.

A decrease in flow with an increase in molecular size, would be expected because bigger molecules cannot pass through the smaller pores.

5.5.2.5.4 Viscosity

The viscosity of the various liquids is given in table 3.4 to 3.8. The viscosity of a liquid is said to be a measure of its resistance to flow. The variation of the sorptivity with kinematic viscosity is shown in figs. 5.25, 5.26 and 5.27 for concrete, mortar and HCP respectively. The following observations are made:

1. Sorptivity decreases with an increase in viscosity for all

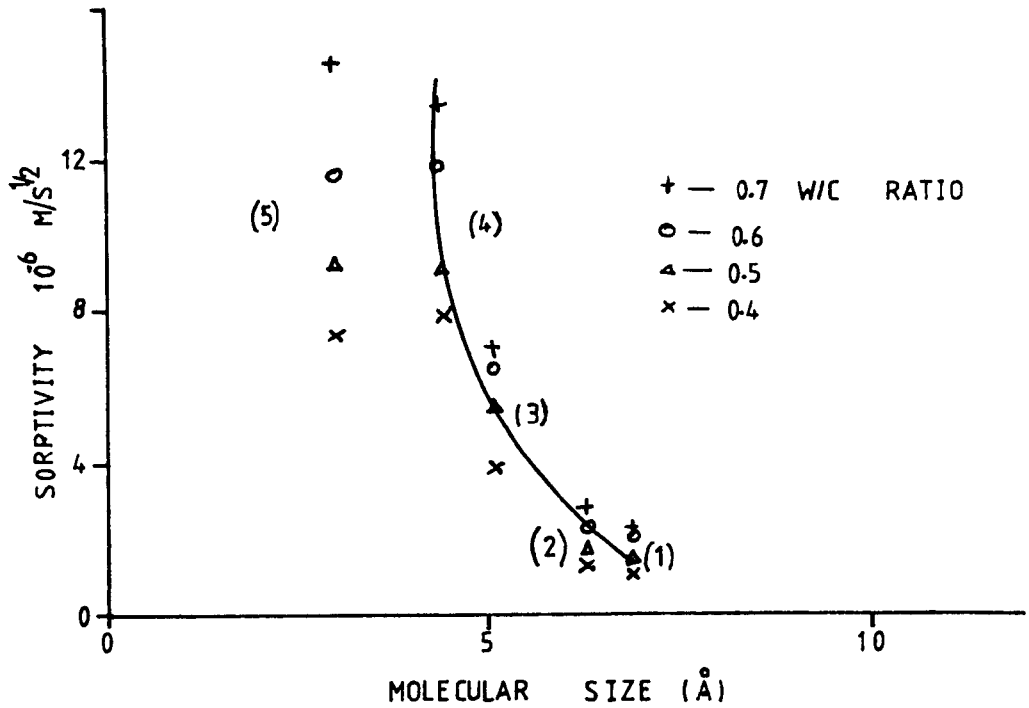

FIG 5.23 VARIATION OF SORPTIVITY OF CONCRETE WITH MOLECULAR SIZE

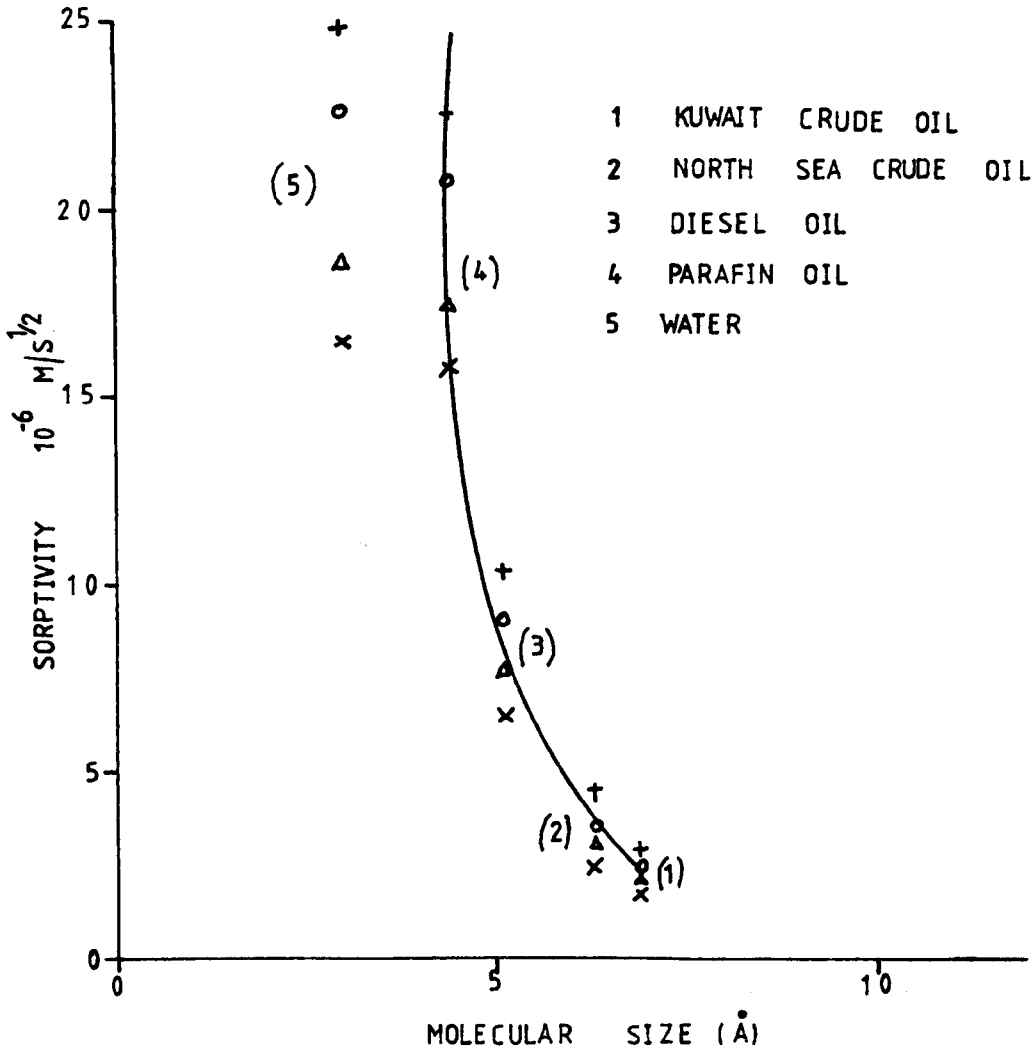

FIG 5.24 VARIATION OF SORPTIVITY OF MORTAR WITH MOLECULAR SIZE

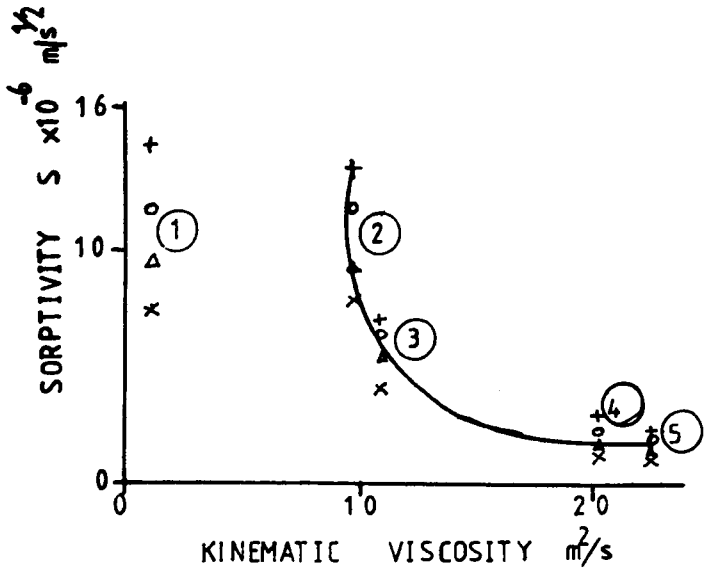

FIG 5.25

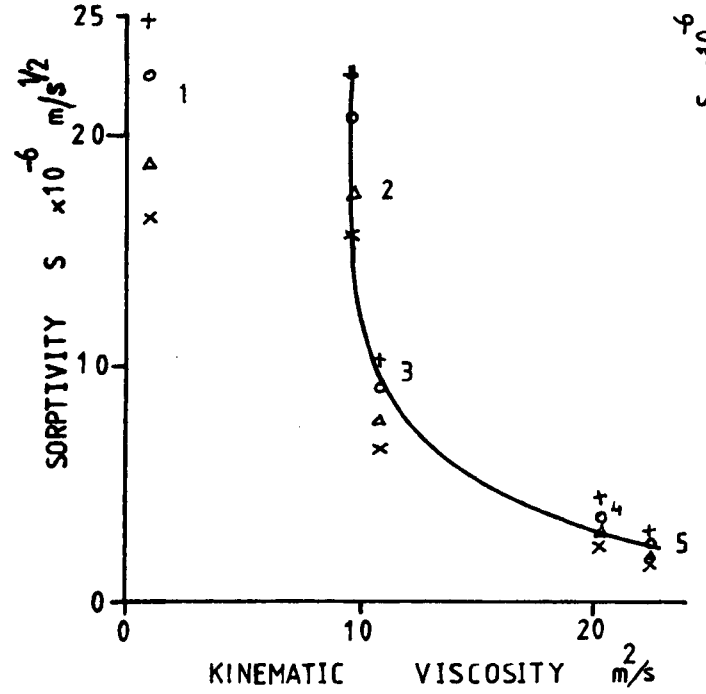

FIG 5.26

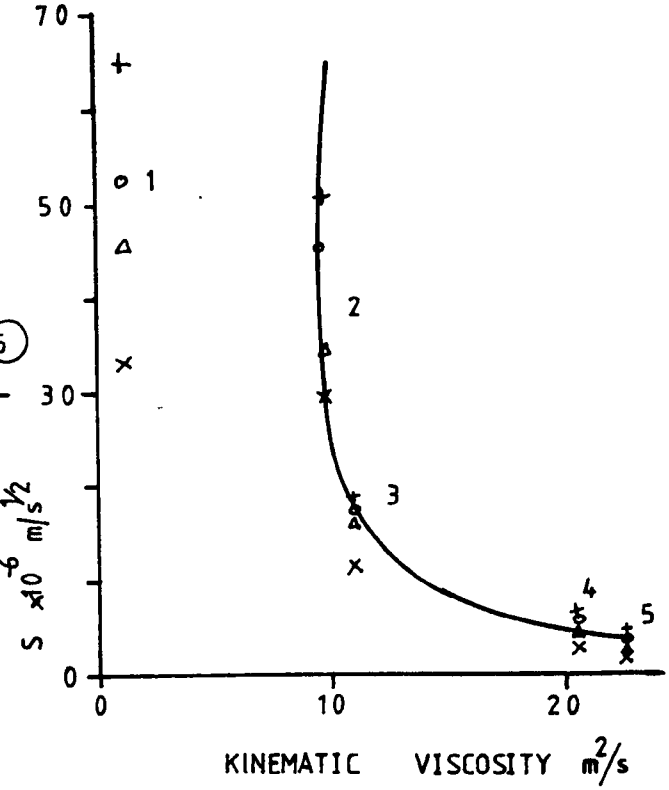

FIG 5.27

1 WATER
2 PARAFIN OIL
3 DIESEL OIL
4 NORTH SEA CRUDE OIL
5 KUWAIT CRUDE OIL

FIG 5.25 VARIATION OF SOPTIVITY OF CONCRETE WITH VISCOSITY

FIG 5.26 VARIATION OF SOPTIVITY OF MORTAR WITH VISCOSITY

FIG 5.27 VARIATION OF SOPTIVITY OF HCP WITH VISCOSITY

w/c RATIO	HARDENED CEMENT PASTE			MORTAR (1:1½)			CONCRETE)1:1½:1½)		
	$S_o \times 10^{-4}$	a_1	r	$S_o \times 10^{-4}$	a_1	r	$S_o \times 10^{-4}$	a_1	r
0.40	36.434	-1.117	-992	7.060	-0.890	-0.992	2.608	-0.820	-0.984
0.50	27.290	-1.001	-998	5.882	-0.824	-0.993	2.678	-0.769	-0.983
0.60	30.434	-0.985	-993	7.216	-0.832	0.992	2.706	-0.724	-0.985
0.70	26.712	-0.939	-985	6.852	-0.797	-0.994	2.976	-0.720	-0.995

TABLE 5.8: Constants of Regression for equation 5.11 Sorptivity vs Molecular size.

w/c RATIO	HARDENED CEMENT PASTE			MORTAR (1:1½)			CONCRETE (1:1½:1½)		
	$S_c \times 10^{-5}$	$b_1 \times 10^{5}$	r	$S_o \times 10^{-5}$	$b_1 \times 10^{5}$	r	$S_o \times 10^{-5}$	$b_1 \times 10^{5}$	r
0.40	13.316	-1.912	-0.971	4.853	-1.504	-0.958	2.500	-1.405	-0.947
0.50	13.674	-1.813	-0.958	4.980	-1.392	-0.959	2.863	-1.344	-0.982
0.60	15.894	-1.666	-0.959	5.960	-1.406	-0.958	3.224	-1.252	-0.973
0.70	15.957	-1.586	-0.950	6.100	-1.375	-0.954	3.350	-1.239	-0.967

TABLE 5.9: Constants of Regression for equation 5.12 Sorptivity vs Viscosity.

w/c RATIO	HARDENED CEMENT PASTE			MORTAR (1:1½)			CONCRETE (1:1½:1½)		
	$S_o \times 10^{-5}$	$c_1 \times 10^{8}$	r	$S_o \times 10^{-5}$	$c_1 \times 10^{8}$	r	$S_o \times 10^{-5}$	$c_1 \times 10^{8}$	r
0.40	4.542	-2.745	-0.972	2.111	-2.177	-0.968	1.055	-2.002	-0.962
0.50	5.430	-2.480	-0.987	2.305	-2.017	-0.969	1.121	-1.904	-0.970
0.60	6.321	-2.412	-0.969	2.736	-2.035	-0.968	1.576	-1.782	-0.966
0.70	6.585	-2.286	-0.956	2.984	-1.955	-0.972	1.759	-1.770	-0.975

TABLE 5.10: Constants of Regression for equations 5.13 and 5.14, Sorptivity vs oil properties.

liquid types.

2. This decrease in sorptivity is seen most clearly for oil and this approximates to an exponential decay pattern.

3. For HCP, mortar and concrete, the relationship between oil sorptivity and kinematic viscosity can be represented with an exponential equation of the form

$$S = S_o(\exp)^{b_1 \nu} \qquad (5.12)$$

where S_o is the sorptivity of a theoretical oil of infinite kinematic viscosity, and b_1 is a constant.

ν = kinematic viscosity m^2/s

S = sorptivity $m/s^{\frac{1}{2}}$

S_o and b_1 are determined regressionally for various w/c ratios and for HCP, mortar and concrete and are given in table 5.9.

Since the viscosity of a liquid is a measure of its resistance to flow, an increase in viscosity means a decrease in flow, which agrees with the findings in this section.

5.5.2.5.5 Summary of the effect of liquid properties on sorptivity

1. Available information shows that the behaviour of water in a porous solid may be quite different from the behaviour of crude oil and its distillates in the same porous solid. Hence the effect of water properties on flow through porous solids may better be studied using water of differing properties such as distilled water, tap water, sea water etc.

2. A critical look at the effect of oil properties on sorptivity shows that one property alone does not uniquely describe the flow of oil through concrete, mortar or HCP. In addition to the properties individually considered, other properties such as volatility of the oil and the wax content may be important. This observation is supported by the fact tnat it takes between 10 hrs. to 4 days for parafin (high volatility and no wax content) to penetrate through the model concrete tank of 50 mm thick, depending on the liquid depth. While the same type of tank (section 5.5.3) is

penetrated by other oil types as follows:

Diesel (medium volatility and no wax content) between 1 day to 7 days.

North Sea crude oil (very low volatility and 3.12% by weight wax content), penetration not achieved after 180 days of test.

Kuwait Crude (very low volatility and 5.7% by weight wax content), penetration not achieved after 180 days of test.

Water (Non-volatility, no wax content) between 10 days to 30 days.

The time of penetration depends on the depth of the liquid in the containing vessel with larger depths penetrating faster.

3. The three outstanding properties of the liquid, namely molecular size (Ms), dynamic viscosity (μ) or kinematic viscosity (ν) and the density (ρ), were combined and the relationship obtained between these and sorptivity is shown below

$$S = S_o(\exp)^{c_1 M_s \nu \rho^2} \qquad (5.13)$$

or

$$S = S_o(\exp)^{c_1 M_s \mu \rho} \qquad (5.14)$$

where S_o represents the sorptivity of a theoretical oil of infinite properties, and c_1 is a constant

M_s = molecular size in M

Other parameters are as defined earlier.

S_o and c_1 were determined regressionally for various w/c ratios and for HCP, mortar and concrete and are given in table 5.10.

4. Equations 2.13 and 2.14, indicate that for a complete understanding of the flow of oil through porous solids, the effect of many oil properties should be considered. It is also felt strongly that the wax content of crude oil has a strong influence on the flow of oil through porous solids but sufficient information is not yet available to clarify this.

5.6 Model Concrete Tank Results

5.6.1 Introduction

The object of this test was to simulate the performance of concrete tanks in service and hence predict the suitability of these tanks for storing crude oil and its distillates. No form of environmental control was introduced. Temperature readings taken during the period of tests reveal that the room temperature varied between $-2^{o}C$ to $20^{o}C$. This range of temperature may be assumed to represent to a good approximation, the weather variation for a year. The tests were carried out as described in section 5.2.3.

5.6.2 Permeability Results

Permeability results were obtained from the absorption curves of the model concrete tanks with various liquids. Figs. 5.28 to 5.31 and table 5.11, show the results of liquid absorbed against time of partial immersion, for four depths of liquid (section 5.6.2.2). The plots reveal the following stages of absorption.

Between 7 days to 28 days, depending on the liquid type and depth, the absorption curve takes the usual form (AB) showing that the rate of absorption decreases with time. This decrease, may be due to increasing resistance to flow with increase in the depth of penetration of the liquid. For water, diesel and parafin, station B is reached earlier with greater depth of fluid, while for North Sea crude and Kuwait crude, station B was reached at 28 days and was independent of the depth of the liquid.

Next, an intermediate period is attained represented in the curve by the portion BC. At this stage, the rate of penetration remains practically constant and station C was attained after 21 to 90 days for water, diesel and parafin absorption, depending on the depth of liquid. North Sea crude and Kuwait crude were within this intermediate stage for the rest of the test. The saturated permeability results recorded in table 5.12 are obtained from the shape of this portion of each curve (cm^3/day), and converted to (m/s) using the appropriate surface area.

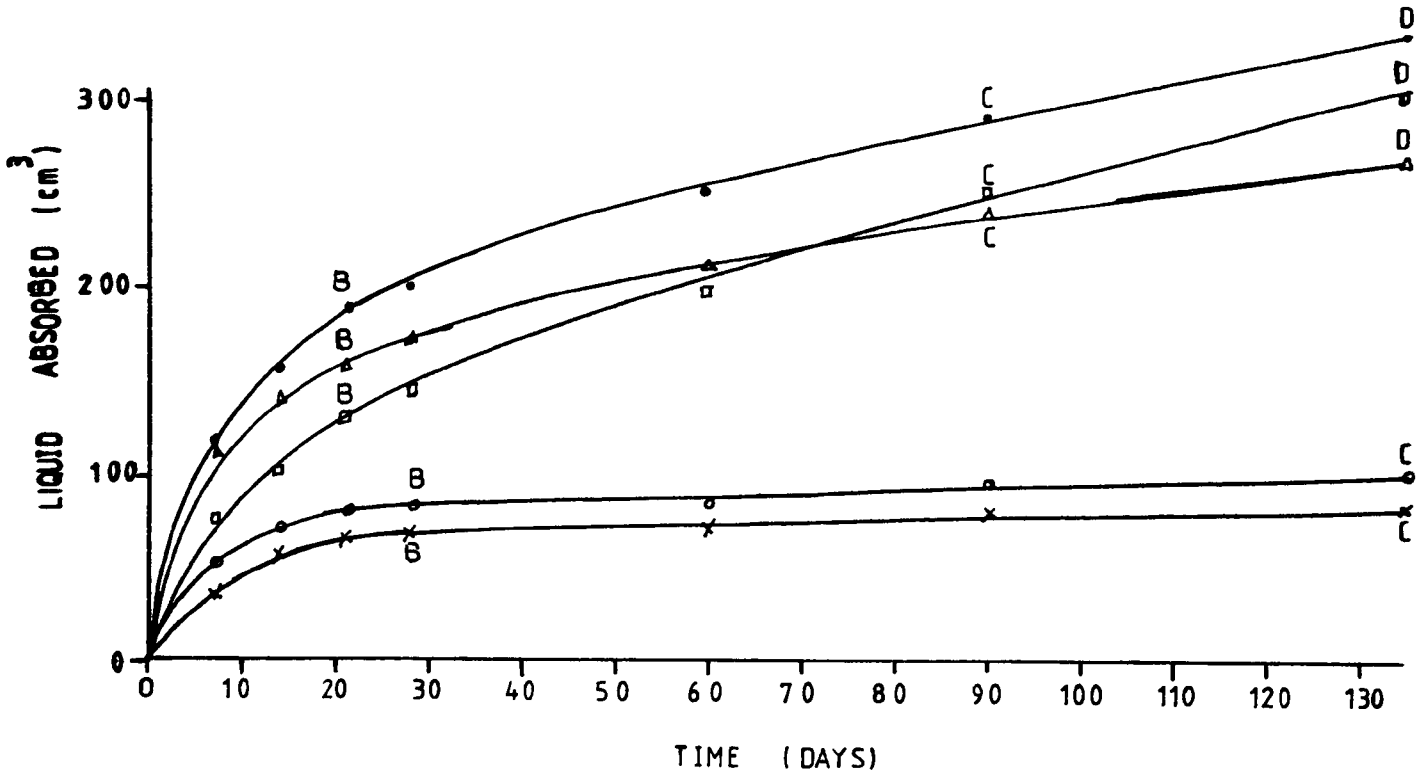

FIG 5.28 VARIATION OF OIL ABSORBED WITH TIME OF PARTIAL IMMERSION FOR 50mm DEPTH OF LIQUID

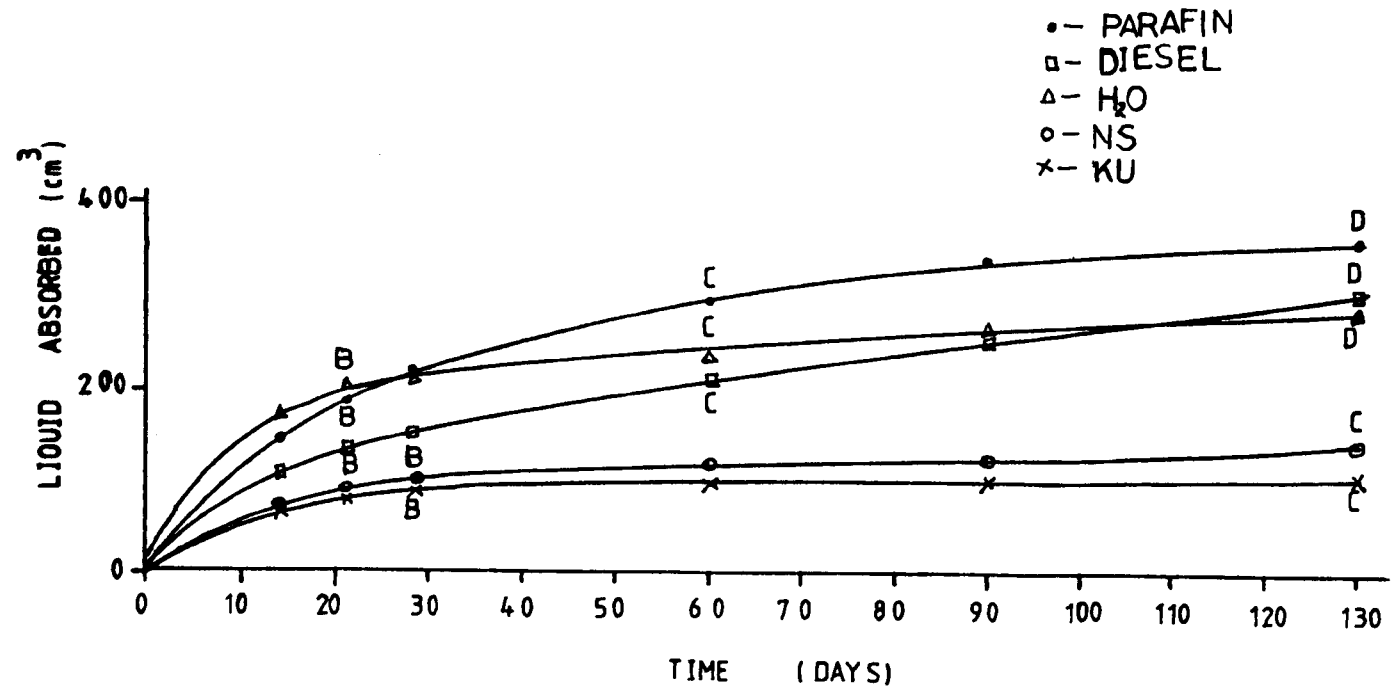

FIG 5.29 VARIATION OF OIL ABSORBED WITH TIME OF PARTIAL IMMERSION IN 80mm DEPTH OF LIQUID

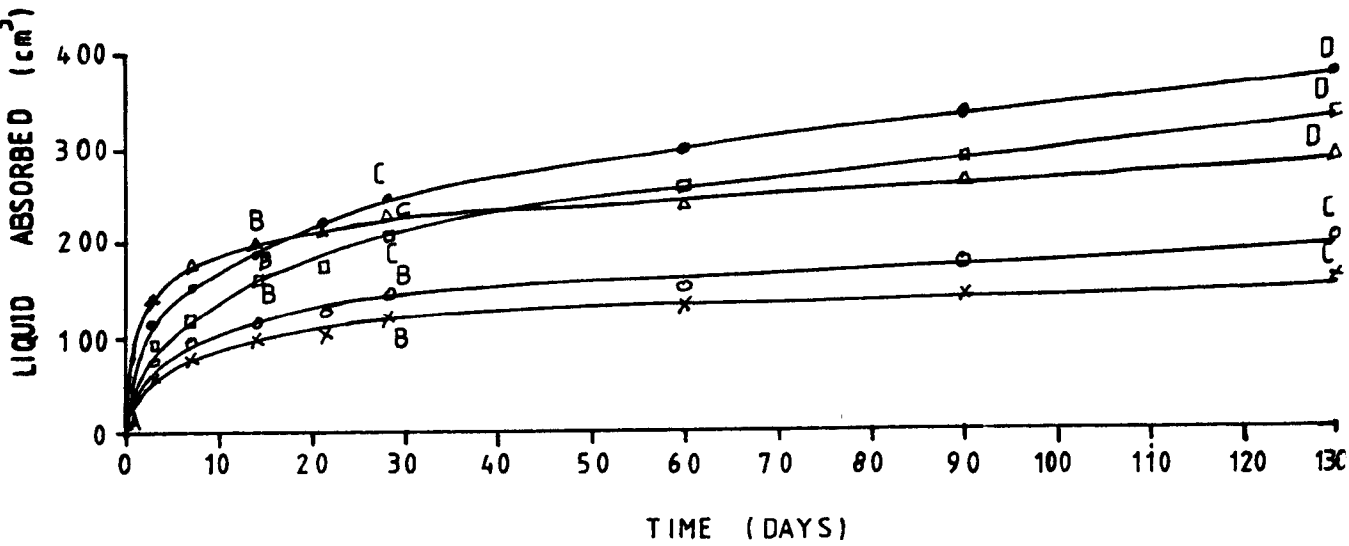

FIG 5.30 VARIATION OF OIL ABSORBED WITH TIME OF PARTIAL IMMERSION FOR 100mm DEPTH OF LIQUID

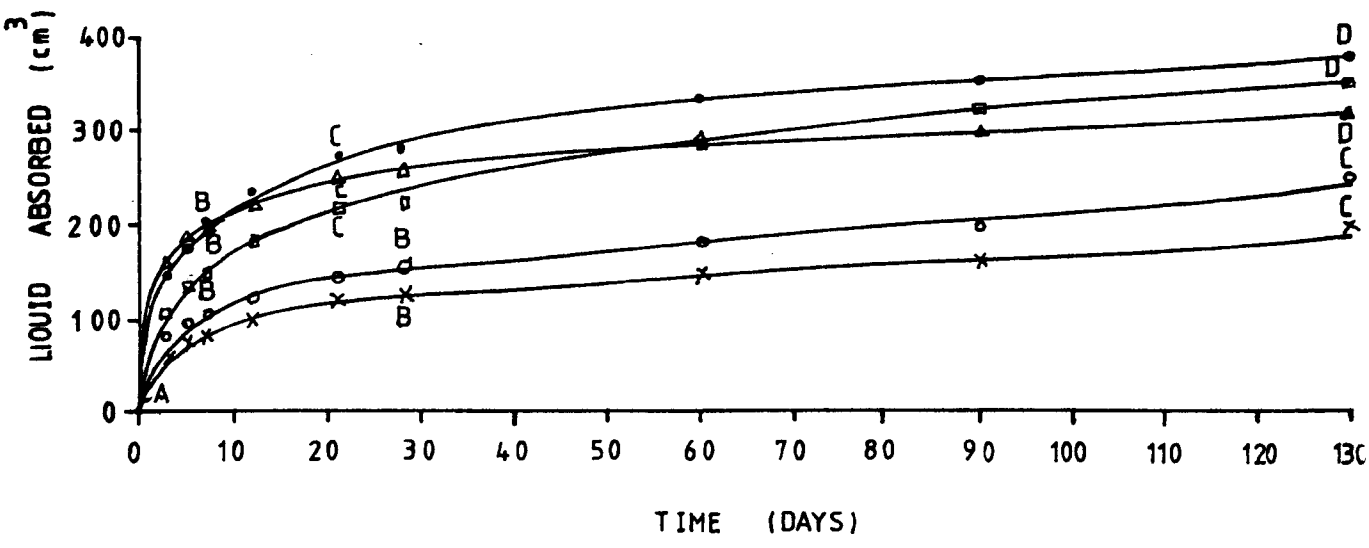

FIG 5.31 VARIATION OF OIL ABSORBED WITH TIME OF PARTIAL IMMERSION FOR 125mm DEPTH OF LIQUID

LIQUID ABSORBED IN CM^3

LIQUID TYPE \ TIME IN DAYS	0	3	5	7	14	21	28	60	90	130
AREA OF FLOOR = 240.0 CM^2, AREA OF WALL = 275 CM^2										
KUWAIT CRUDE	0			37.10	58.40	67.40	69.70	70.80	78.70	80.90
NORTH SEA CRUDE	0			54.65	72.10	80.23	82.56	83.72	95.35	101.16
WATER	0			117.50	143.50	159.50	172.50	210.50	240.50	267.50
DIESEL	0			79.41	103.53	131.76	144.71	194.12	251.46	302.90
PARAFIN	0			120.25	155.70	188.61	200.00	250.18	287.34	334.18
AREA OF FLOOR = 240 CM^2, AREA OF WALL = 440.0 CM^2										
KUWAIT CRUDE	0				67.42	84.23	85.40	91.01	98.88	101.12
NORTH SEA CRUDE	0				77.91	89.53	97.67	117.44	123.26	132.05
WATER	0				173.00	203.00	210.00	231.00	264.00	280.00
DIESEL	0				114.12	137.65	152.94	211.18	252.90	305.30
PARAFIN	0				148.10	186.10	217.72	292.40	339.24	355.70
AREA OF FLOOR = 240.0 CM^2, AREA OF WALL = 549.80 CM^2										
KUWAIT CRUDE	0	57.30		76.40	97.75	100.00	121.35	129.21	143.82	168.54
NORTH SEA CRUDE	0	74.42		103.49	112.78	124.42	143.35	147.67	179.07	209.30
WATER	0	145.00		178.00	199.00	217.00	235.00	244.00	264.00	291.00
DIESEL	0	95.29		124.71	161.18	170.60	210.59	258.82	285.88	335.67
PARAFIN	0	118.99		156.96	191.14	218.99	248.10	297.47	336.71	374.68
AREA OF FLOOR = 240.0 CM^2, AREA OF WALL = 687.22 CM^2										
KUWAIT CRUDE	0	61.80	75.28	77.53	99.26	120.22	125.47	148.31	160.67	195.16
NORTH SEA CRUDE	0	86.05	97.67	109.30	117.40	144.19	151.16	183.72	196.51	250.64
WATER	0	156.00	186.00	198.00	226.00	250.00	252.00	285.00	294.00	317.00
DIESEL	0	108.24	135.29	144.70	182.35	216.47	217.65	288.23	323.53	350.16
PARAFIN	0	148.10	178.48	200.00	239.24	277.22	279.75	337.98	356.96	378.60

TABLE 5.11: Liquid Absorption of Model Concrete Tanks with Time.

SATURATED PERMEABILITY K x 10^{-11} m/s				
FLOOR AREA = 240 cm^2				
LIQUID TYPE / WALL AREA	275.00 cm^2	440.00 cm^2	549.80 cm^2	687.22 cm^2
KUWAIT CRUDE	2.25	2.54	6.17	7.09
NORTH SEA CRUDE	3.73	6.20	8.63	9.13
WATER	22.15	31.50	37.67	46.36
DIESEL	29.77	36.50	50.22	63.99
PARAFIN	28.40	46.41	60.86	68.85

TABLE 5.12: Saturated Permeability calculated from Model Concrete Tanks

Finally, the rate of absorption again decreased with time (portion CD). This portion is attained when the liquid starts to accumulate in the tank. For water, diesel and parafin, portion C to D began from 21 to 90 days, to the end of the test period, depending on the liquid depth as shown in fig. 5.28 to 5.31. For North Sea crude and Kuwait crude point C was never attained.

The outstandingly different times when these three absorption stages were reached for crude oils, compared with the other types of liquid, may be explained by the wax content of the crude oils. The wax binds many molecules together, and thereby impedes the passage of them through relatively smaller pore sizes of the concrete. As a result, the crude could not penetrate through the wall/floor thickness of the tank throughout the test period.

5.6.2.1 Effect of liquid type on permeability

The variation of K for various oil types is shown in fig. 5.32 and table 5.12. The variation of oil properties with sorptivity (hence rate of flow) have been considered in section 5 5, and only a few additional

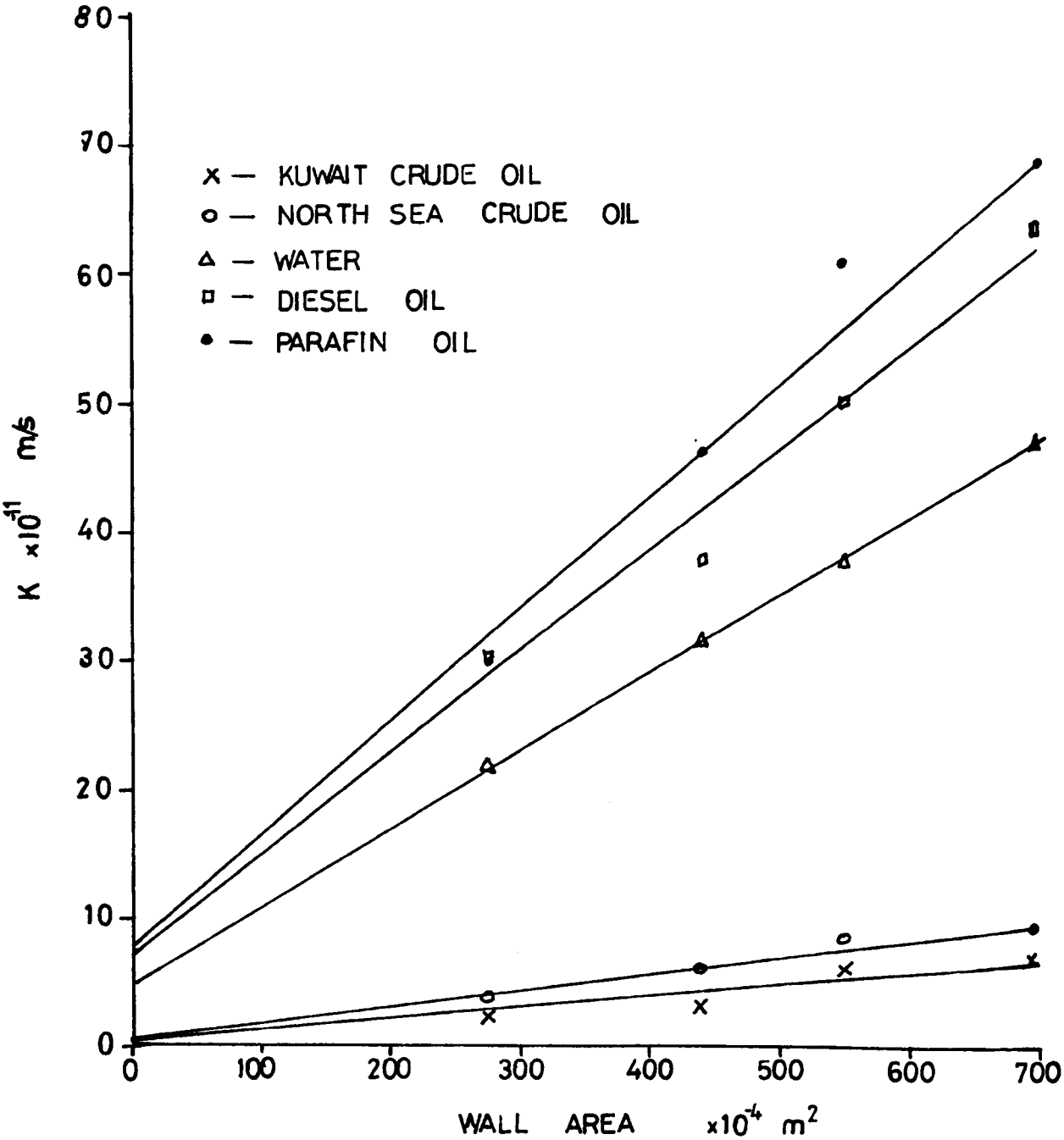

FIG 5.32 PERMEABILITY OBTAINED FROM MODEL CONCRETE TANK VS AREA OF WALL AT CONSTANT FLOOR AREA

observations can be made in this section from the results.

1. The plot shows that K decreased in the following order, Parafin, diesel, water, North Sea crude and Kuwait crude. For a better understanding of this behaviour, only oil properties should be considered. Table 5.7, reveals that the following oil properties (density, kinematic viscosity, average molecular size) increase in the order Parafin, diesel, North Sea curde and Kuwait crude.. This means that the permeability decreased with an increase in the mentioned oil properties. This is in line with the findings on sorptivity, and again suggests that sorptivity could be used to characterize the flow of liquid through porous solids.

Table 5.7, also shows that while water has the lowest molecular size and kinematic viscosity, its density is the highest, and table 5.11, shows that permeability of water is intermediate between the crude oils and their distillates. This anomalous behaviour of water was identified in section 5.5, and it is suggested that the flow characteristic of water should be investigated independently.

The results of the tank tests show that concrete tanks designed to hold water, can adequately hold crude of similar properties to those used in the test. Visual inspection of the tanks showed that water penetrated completely through the walls in 10 to 30 days of partial soaking depending on the water depth, but the crude oils did not penetrate completely throughout the whole test period.

For the crude oil distillates such as diesel and parafin, tanks designed for water retainment, may not be adequate for their retainment. Visual inspection also shows that these oils penetrate the tank walls a lot earlier than water. (section 5.5.2.5.5) Also the effect of capillary rise and evaporation of the liquid particles appear to be adverse in diesel and parafin. Inspection of the tanks soaked in 125 mm depth of liquid, shows that after 60 days, parafin has covered the whole tank surface due to capillary rise and evaporation/condensation in the plastic container, diesel

has risen 130 mm above the liquid level while water was only 10 mm above liquid level. The capillary action of diesel and parafin, coupled with their high volatility[176] (i.e., very low flash points*) make the liquids, fire and environmental hazards. It may, therefore, be more appropriate to have some internal linings in their retaining structures when made of concrete.

* Flash point of a liquid fuel is the temperature at which the oil begins to evolve vapours in sufficient quantity to form an explosive or flammable mixture with air[176].

5.6.2.2 Effect of depth of liquid

Absorption curves, figs. 5.28 to 5.31, show the quantity of liquid absorbed in a given time, while fig. 5.32 shows the permeability calculated from the absorption curves for the various liquid depths. The following observations are made.

1. Absorption increases with an increase in liquid depth for all types of liquid.

2. The rate of increase with depth varies from liquid to liquid. In 60 days, the concrete tank with Kuwait crude oil at 80 mm liquid depth has absorbed 1.285 times the concrete absorption at 50 mm liquid depth. For Parafin the absorption at 80 mm is 1.169 times the absorption at 50 mm.

3. The behaviour of the rate of increase in absorption with depth of fluid is not clear, however, in the region where the absorption remains approximately constant (BC), the rate of increase is approximately constant as shown in fig. 5.32, but varies from liquid to liquid.

4. Variation of K with depth of liquid can be represented with the equation of the form

$$K = K_a D + K_f \qquad (5.15)$$

$$K_w = K_a D \qquad (5.16)$$

where D = depth of liquid m

K = permeability coefficient m/s

K_f and K_a which are constants are determined regressionally and are given in table 5.13.

LIQUID TYPE	$K_a \times 10^{-9}$	$K_f \times 10^{-11}$	r
KUWAIT CRUDE	1.30	1.87	0.920
NORTH SEA CRUDE	1.38	1.78	0.970
WATER	5.85	5.88	0.990
DIESEL	7.69	7.78	0.970
PARAFIN	8.33	8.16	0.980

TABLE 5.13: Constants of regression for equation 5.15 K vs depth of liquid.

K_f may be the contribution to flow through the floor of the tank, which is constant for a particular liquid but depends on the liquid type. K_w may be the contribution from the tank wall to flow, and depends on the depth of the liquid in the tank.

It should be noted that the values of K in this section relate to the conditions of test and neither the effects of pressure nor temperature variation was investigated. The result should be regarded as giving an approximate value for the leakage to be expected under practical conditions in a deep tank.

5.7 Summary of Results on the Effect of Properties of the Liquids on Flow through the Wall and Floor of the Concrete Tank

1. Results reveal that flow through the tank wall is usually greater than the flow through the tank floor.

2. Sorptivity could be used judiciously to characterize the flow of liquids through HCP, mortar or concrete.

3. Studies of the flow behaviour of water should be carried out using water of different properties to avoid mis-interpretation of data when com-

pared with crude oil and its distillates.

4. No specific oil property appears to control the flow of oil through a porous solid, such as HCP, mortar and concrete. The following properties are all important - density, kinematic viscosity, average molecular size and wax content.

5. An increase in the density, kinematic viscosity and average molecular size, decreased the flow of oil through HCP, mortar and concrete.

6. Tanks designed to hold water could be adequate for crude oil containment.

7. Concrete tanks without any form of lining should not be used for the storage of lighter fraction of crude oil distillates such as diesel or parafin.

CHAPTER 6

PORE STRUCTURE ANALYSIS OF HARDENED CEMENT PASTE (HCP), MORTAR AND CONCRETE

6.1. Introduction

The importance of pore structure has been stated in section 2.3.1. The pore structure characteristics of a porous material such as porosity, specific surface area, pore size distribution and pore radius, have been defined in section 2.3.4. This chapter is intended to present the experimental determination of those fundamental pore parameters considered to have significant effects on saturated permeability. The pore parameters of HCP, mortar and concrete are presented. The correlation of these parameters with saturated permeability is the subject of Chapter 8.

6.2 Scope of Investigation and Experimental Technique

As outlined in Chapter 3, the aim of this section is to study three principally different ways of changing the pore structure of the composite, i.e. initial w/c ratio, hydration period and coarse and fine aggregate inclusions and to relate the resulting pore structure to the saturated permeability of crude oil. The mix proportions are given in Table 6.1. In addition to the pore parameters, the dry density, non-evaporable water content and the degree of hydration were also measured.

Pore structure analysis was carried out for the HCP, mortar and concrete mixes of Table 6.1, over four hydration periods, 7 days, 28 days, 3 months and 6 months. The samples were cured in the fog room as described in section 3.7. Some of the 25mm cubes obtained from mixes 2-5, 12-15 and 25-28 were cured in the CTR instead for up to a period of 3 months and tested at 7 days, 28 days and 3 months. All the samples for pore structure analysis were oven dried as described in section 3.8.2 prior to test.

To investigate the effect of different types of oil on the pore structure of the HCP, mortar and concrete, some 25mm cubes from mixes

	SPECIMEN DESIGNATION	w/c RATIO	PROPORTION BY WEIGHT		
			CEMENT	SAND	GRAVEL
1.	OP35	0.35	1.0 HARDENED CEMENT PASTE (HCP)	-	-
2.	OP40	0.40			
3.	OP50	0.50			
4.	OP60	0.60			
5.	OP70	0.70			
	MORTARS				
6.	M35-1	0.35	1.0	1.0	-
7.	M40-1	0.40			
8.	M50-1	0.50			
9.	M60-1	0.60			
10.	M70-1	0.70			
11.	M35-1.5	0.35	1.0	1.5	-
12.	M40-1.5	0.40			
13.	M50-1.5	0.50			
14.	M60-1.5	0.60			
15.	M70-1.5	0.70			
16.	M35-2	0.35	1.0	2.0	-
17.	M40-2	0.40			
18.	M50-2	0.50			
19.	M60-2	0.60			
20.	M70-2	0.70			
21.	M50-3	0.50	1.0	3.0	-
22.	M60-3	0.60			
23.	M70-3	0.70			
	CONCRETE				
24.	C35-1.5	0.35	1.0	1.5	1.5
25.	C40-1.5	0.40			
26.	C50-1.5	0.50			
27.	C60-1.5	0.60			
28.	C70-1.5	0.70			

TABLE 6.1 Mix proportions for the pore structure analysis

2-5. 12-15 and 25-28, were initially cured in fog room for 28 days, then oven dried at 105 $\pm$ 1°C as described in section 3.8.2. After drying and cooling, each cube is cut into approximately five parts, using diamond saw, each part is put in one of the five liquids viz; water, parafin, diesel, North Sea crude oil and Kuwait crude oil and allowed to saturate for a period of 3 months. At the end of 3 months, the specimens were removed from the liquids, dried in the oven again as described in section 3.8.2 and tested for pore parameters.

6.3 Apparatus - The Mercury Porosimeter

The Mercury Porosimeter used in the pore structure determination is the commercial Carlo Erba series 200, with a recorder tracing unit attached. The principle of the porosimeter was outlined in section 2.3.5.2, while the methods of analysing the results are given in section 6.4. A schematic representation of the porosimeter circuit is shown in Fig. 6.1. which contains a mercury level measuring and recording circuit (i.e. the autoclave - to be described later), a pressure multiplication circuit and the pressure measuring and recording circuit. Plate 6.1, shows the porosimeter with the chart recorder on the left (labelled (1)), and a separate filling device (to be described later in the section), on the right (label 3). Full details of the instrument can be obtained from ref. 129.

For the measurement of the pore parameters, a fragment of each specimen is obtained from the inner 1/3 of the sample (25mm cube). This portion was found[114] to represent approximately uniform porosity. The sample usually between 0.5 to 2.5 grams was selected and weighed to an accuracy of $x10^{-4}$ gms, in an electronic balance and placed in a dilatometer, described later in the section. Efforts were made to remove all the coarse aggregates from the concrete specimens prior to weighing. The dilatometer is then mounted on the filling device alreading containing mercury and evacuated for about 45 mins at a vacuum pressure of 1×10^{-3} torr, using a speedivac

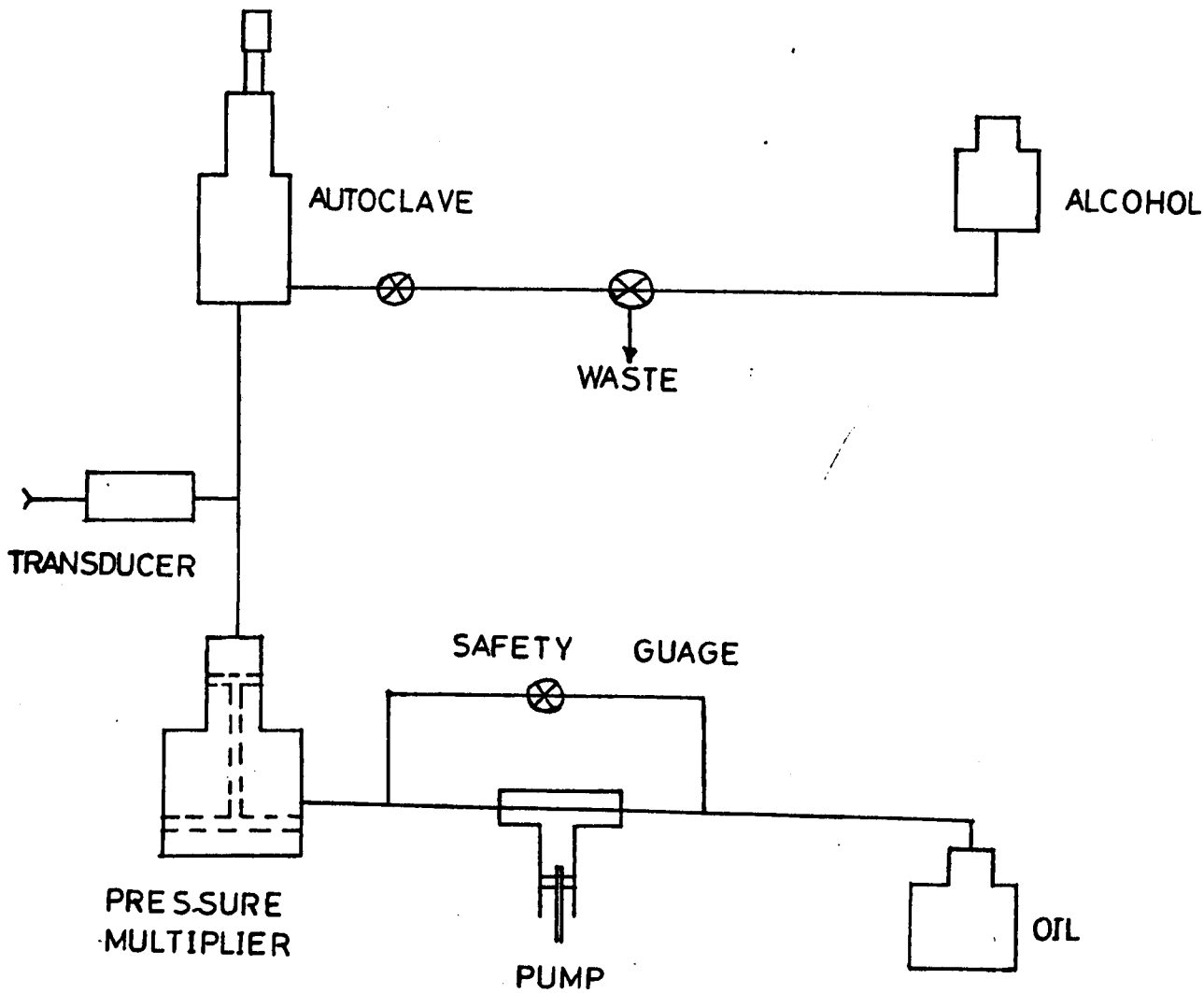

FIG 6.1 SCHEMATIC DIAGRAM OF MERCURY POROSIMETER CIRCUIT

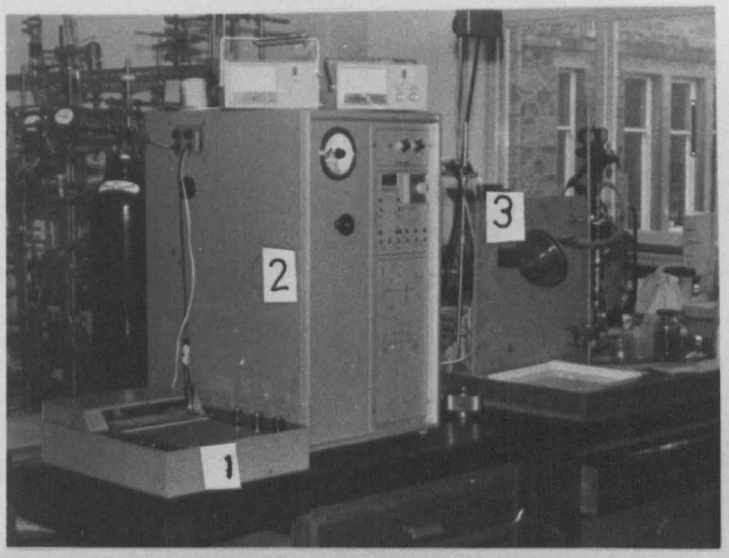

1 CHART RECORDER
2 MERCURY POROSIMETER
3 FILLING DEVICE

PLATE 6.1 MERCURY POROSIMETER UNIT

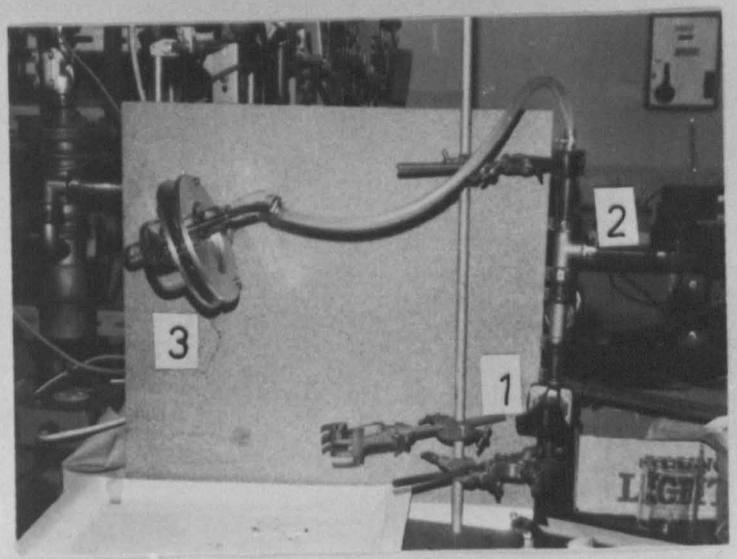

1 SHUT OFF VALVE
2 AIR ADMITTANCE VALVE
3 MERCURY RESERVOIR

PLATE 6.2 THE FILLING DEVICE

high vacuum pump. After evacuation, the dilatometer is filled with mercury while still under this vacuum. It is then placed in the autoclave of the porosimeter, partly assembled, filled with alcohol and then completely sealed before beginning the test. The counter and the chart recorder were zeroed and the recorder calibrated to read the full pressure of 2000kgf/cm^2 ($\simeq$ 2000 bars) before each test.

The autoclave head which forms the closure, contains an axially mounted rod with a micrometer screw fitted at the end with a needle, (the metallic probe, which is electrically connected to the instrument ground) to make contact with the mercury level (Fig. 6.2). The autoclave is filled with ethyl alcohol and when the pump is started, the pressure is transferred to the mercury via the alcohol. The pressure on the alcohol is produced by a small piston of 1:100 pressure intensifier whose large piston is actuated by oil drawn from a reservoir by a low pressure pump. The design of the autoclave ensures that an equal all-round pressure is transmitted by the alcohol to the glass dilatometer, hence enabling pressures of up to 2000 kgf/cm^2 ($\simeq$ 2000 bars) to be reached without breaking the dilatometer. The pressure in the autoclave is measured by a pressure transducer whose output is fed to the chart recorder.

The mercury level is measured electrically whenever an increase in pressure lowers it in the capillary tube of the dilatometer and the rod-mercury electrical contact is interrupted. An advancement motor connected to the rod then turns the micrometer screw till the rod-mercury contact is re-established. Simultaneously, an electronic system starts the recorder chart, which quantitiatively measures the mercury drop. A ten groove cam on the advancement motor shaft operates a micro-switch, giving a pulse to the timer. The counter on the control panel records one pulse, corresponding to 0.1mm of penetration, each time the micro-switch falls into a groove on the cam. The plotting of the pressure-volume data is done automatically and a test takes between 90 to 120 minutes to complete depending on the porosity

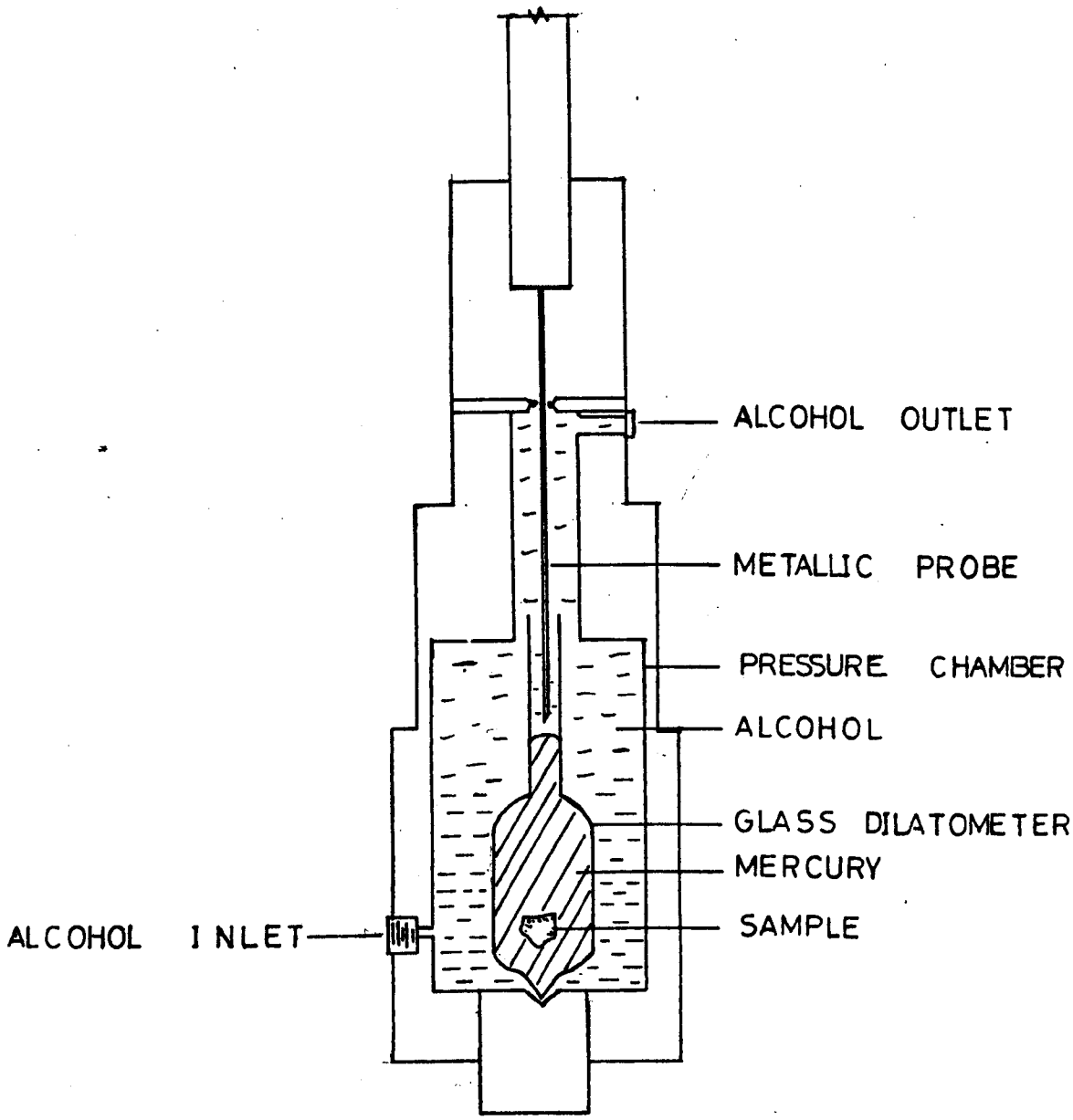

FIG 6.2 DETAILED DIAGRAM OF THE AUTOCLAVE IN THE MERCURY POROSIMETER

of the sample and the delay timer setting.

The glass dilatometer used consists of a sample holder and a stem which has 3mm diameter capillary bore. The constant section capillary tube provides a means of calculating the volume of mercury intruded for any given rod travel.

Degassing of the sample prior to the porosimetry test is achieved using the filling device shown on Plate 6.2. It consists of a shut off valve (1) linked to a vacuum pump, an air admittance valve (2), and a mercury reservoir. The dilatometer stem is sealed to the gasket on the filling device by means of O-ring.

6.4 Analysis of Pore Structures

6.4.1 Introduction

As stated in the literature survey, it was necessary to obtain a simple definition of the threshold diameter found from the pore size distributions by mercury intrusion porosimetry. The total volume of mercury intruded was therefore divided into 40 equal volume intervals and the corresponding pressures determined from the pressure-volume data. This method enables the differential pore size distributions to be found for the pore sizes at which a substantial amount of mercury penetrates into the samples. Typical plots of pressure volume data as obtained from the chart recorder are shown in Figs. 6.3 and 6.4. The vertical axis represents the volume penetrated while the horizontal represents the pressure at which this penetration occurred. To achieve greater accuracy, the recorder has two pressure ranges, from 0 to 200 kgf/cm^2 (i.e. 0-200 bars) on the lower portion and 200-2000 kgf/cm^2 ($\simeq$ 200-2000 bars) on the upper portion of the plot. The threshold region on the plot which corresponds approximately to the region of initial inflection of the pressure-volume function is clearly marked. The point of inflection corresponding to the maximum slope of the pressure-volume curve in the threshold region is used to define the

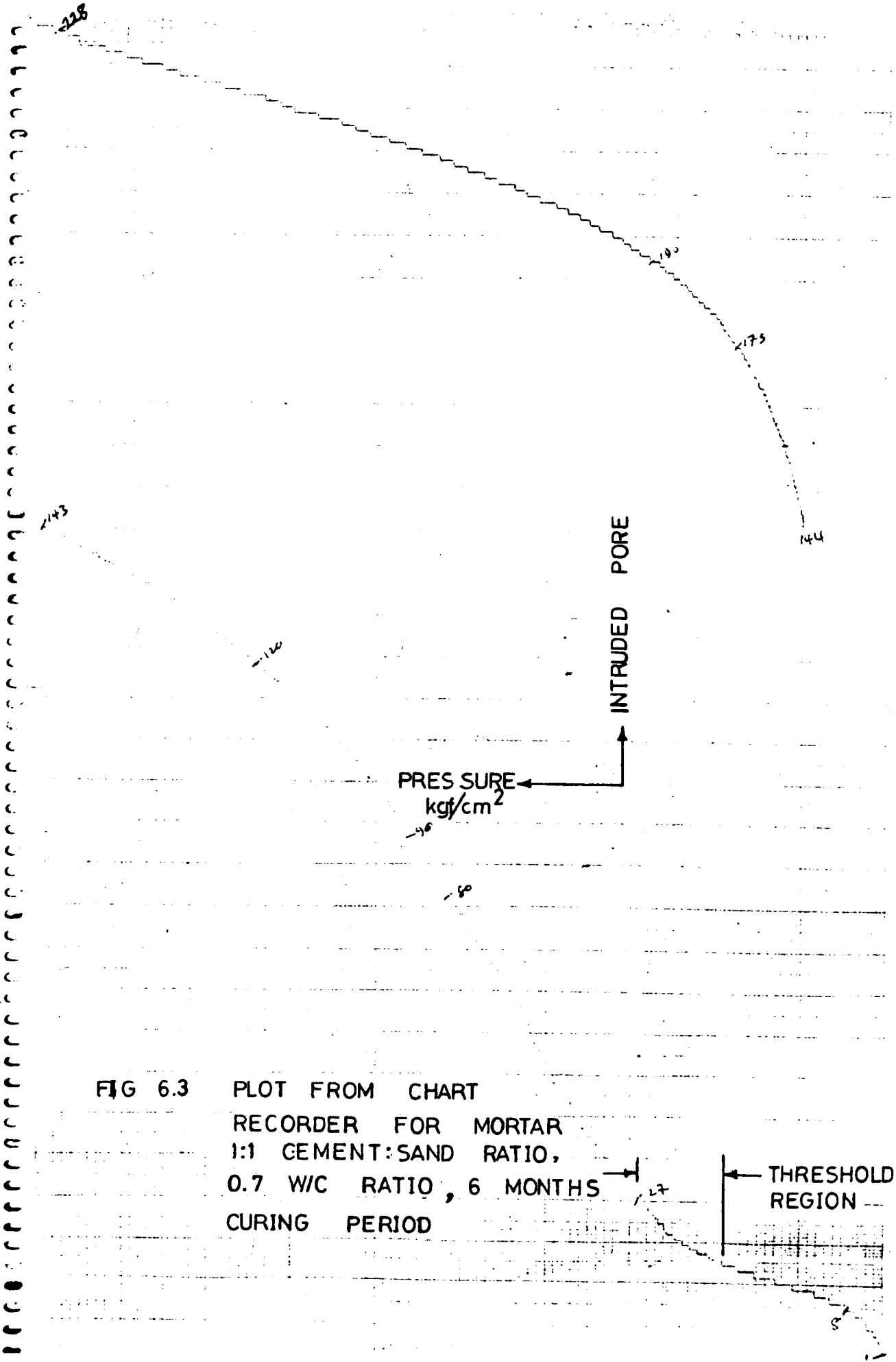

FIG 6.3 PLOT FROM CHART RECORDER FOR MORTAR 1:1 CEMENT:SAND RATIO, 0.7 W/C RATIO, 6 MONTHS CURING PERIOD

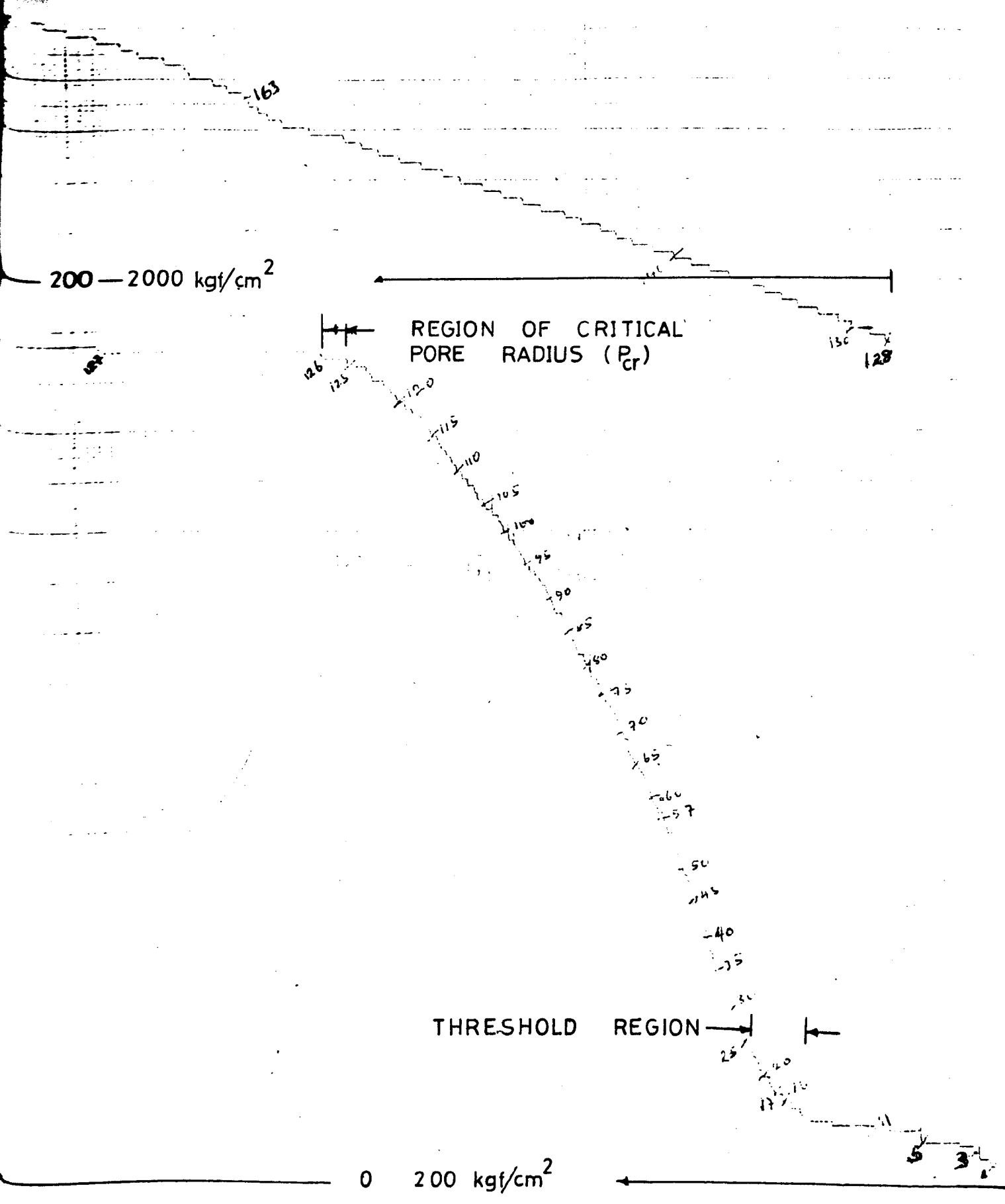

FIG 6-4 PLOT FROM CHART RECORDER FOR HCP SATURATED IN NORTH SEA CRUDE OIL (28 DAYS CURING)

threshold radius as described in section 2.3.5.

6.4.2 Cumulative Pore Size Distribution

The theory of Mercury Porosimetry has been described in section 2.3.5.2. Application of this theory to the present investigation is described here. The relationship between the pore volume V_p, intruded below a given pore radius r_p, and the corresponding pore radius is the cumulative pore volume distribution. By assuming a surface tension for mercury to be 0.48 MN/m (480 dynes/cm) and a contact angle of 140°, the pore radius was calculated from equation 2.20 using the pressure corresponding to equal volume penetration steps. The reasons for the choice of the values of contact angle and surface tension used in the investigation have already been stated in section 2.3.5.2. On substituting these values in equation 2.20 and converting pressure from kgf/cm^2 to N/m^2 by multiplying by 9.81×10^4 gives

$$r_p = 75165/P \qquad (6.1)$$

where P = pressure as recorded in the porosimeter in kgf/cm^2

r_p = Angstrom $\overset{0}{A} = 10^{-10}$ m,

Equation (6.1) is therefore rounded up to

$$r_p = 75000/P \qquad (6.2)$$

Equations 2.20, 6.1 and 6.2 were obtained on the assumptions that all pores are cylindrical. For irregularly shaped pores the ratio between the pore cross-section (relating to the pressure exerted) and the pore perimeter (relating to the surface) is no longer proportional to the radius, but, depending on the pore shape, could give lower ratios of cross-section and perimeter[129]. Also it is not certain whether the contact angle for mercury varies with pressure therefore the numerical values of pore radii can only be regarded as relative rather than absolute.

To correct for the compressibility of mercury, a blank run was carried out without a sample in the 3mm bore dilatometer. These results were deducted from those obtained with the samples in the dilatometer as given in equation 6.3.

$$H'_p = H_p - H_{pHg} \tag{6.3}$$

$$V_p = H'_p \times \frac{A}{w_s} \tag{6.4}$$

where H_p = mercury level drop in (cm) at pressure p, when the sample is in the dilatometer

H_{pHg} = mercury level drop (cm) due only to mercury compressibility at pressure p

H'_p = mercury linear displacement due only to the penetration into the pores as a function of their volume at pressure p

A = cross-sectional area of the dilatometer capillary bore cm^2

V_p = volume of pores intruded by mercury at pressure p cm^3/g

w_s = weight of the sample (gm)

The total intruded pore volume is found at the maximum applied pressure of 2000kgf/cm^2. The cumulative distribution is given by the volume of pores intruded at a given pressure as a function of log r_p as shown in Figs. 6.5 and 6.6, for 0.5 and 0.7 w/c ratios.

6.4.3 Differential Pore Size Distribution

The method suggested by Orr[177] was used in plotting the differential pore size distribution. For a given pore volume dV, residing in pores of radii between r and r+dr, the distribution function is given by

$$dV = f(r)\, dr \tag{6.5}$$

Differentiating equation (2.20), with respect to pressure and pore radius (assuming that the contact angle and surface tension of mercury

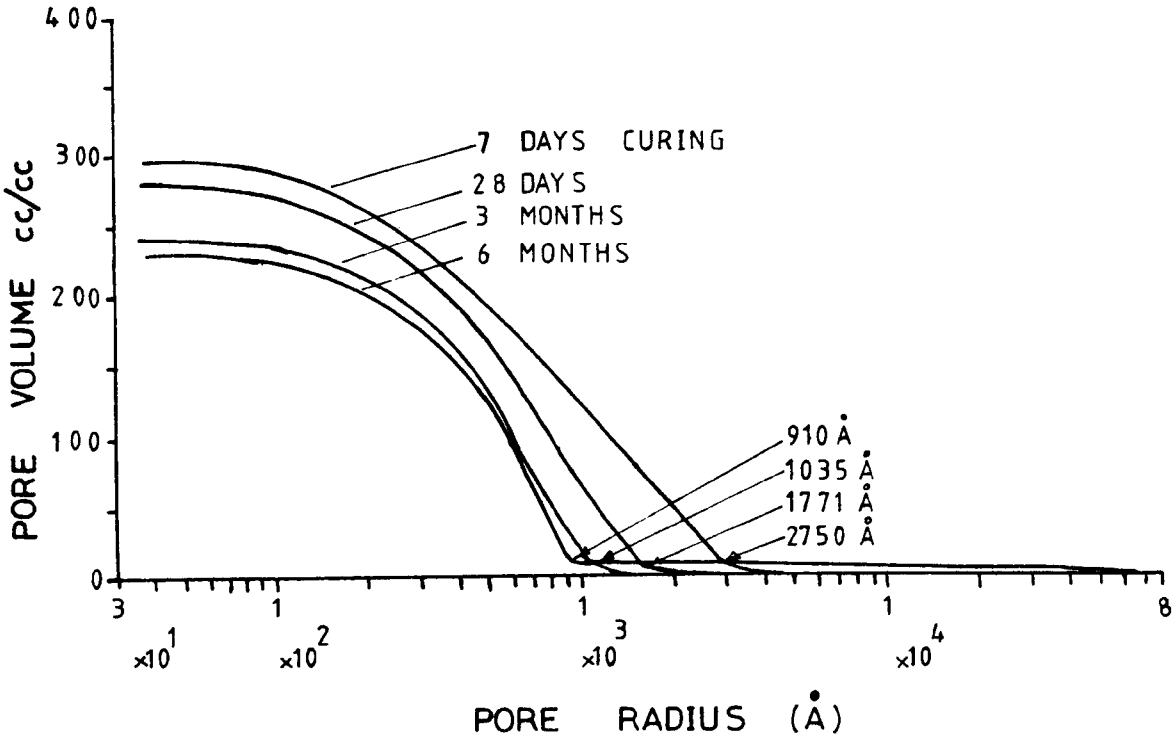

FIG 6.5 EFFECT OF TIME OF HYDRATION ON THE CUMULATIVE PORE SIZE DISTRIBUTIONS OF HCP (0.50 W/C RATIO)

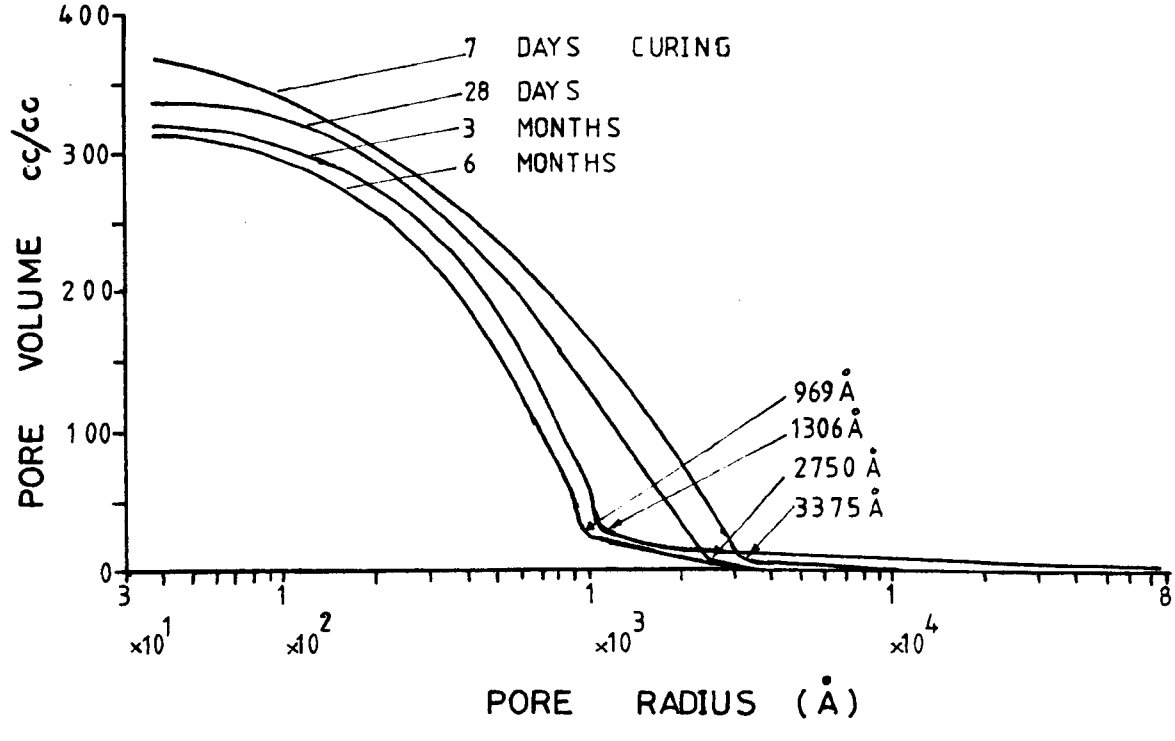

FIG 6.6 EFFECT OF TIME OF HYDRATION ON THE CUMULATIVE PORE SIZE DISTRIBUTIONS OF HCP (0.70 W/C RATIO)

remained constant) gives

$$Pdr + rdP = 0 \qquad (6.6)$$

Combining equatios 6.5 and 6.6 gives

$$f(r) = \frac{P}{r}\frac{dV}{dP} = \frac{dV}{dr} \qquad (6.7)$$

Because of the wide range of pore sizes involved (i.e. between 37Å and 75000 Å) in HCP, mortar and concrete, there is need to plot the distributions on a logarithmic pore radius scale. Therefore the frequency function is transformed from equal radius to equal logarithmic radius, using equation 6.8

$$d\log r = 2.303\frac{dr}{r} \qquad (6.8)$$

dV/dr is transformed to (dV/ dlog r) by multiplying equation 6.7 by r/2.303.

Therefore $f(r)\ r/2.303 = f'(r) = \frac{P}{2.303}\frac{dV}{dP} = \frac{dV}{d\log r}$ (6.9)

where f(r) frequency of occurrence of pores of radius r on an equal radius interval distribution curve

V = pore volume cm^3

r = pore radius Å

P = applied pressure N/mm^2

By taking equal penetrated volume steps and determining the pressure corresponding to each volume increment, it was possible to define the threshold radius[114] as the radius corresponding to the maximum spacing between the links in the crystalline hydration products which also indicates the pore size at which mercury tends to flow into the specimens for small changes in applied pressure [114]. This has been thought to be continuous and its properties as observed by Diamond[80], have been clearly stated in section 2.3.5. Probable relations between these threshold radii and saturated permeability will be discussed in Chapter 8. Typical plots of dV/ dlog r

versus log r are shown in Figs. 6.7 and 6.8 for 0.5 and 0.7 w/c ratios respectively.

6.4.4 Surface Area and Hydraulic Radius

For pores within the instrument range, approximate specific surface area can be calculated. The calculation is once again based on the assumption that all the pores are cylindrical. For cylinder of known volume and radius, the curved surface area is

$$S = \frac{2dV_i}{r_i} \tag{6.10}$$

If it is assumed that there are several such cylindrical pores interconnected within the porous network, then the contributions to the total surface area of the solid phases can be summed for all the volume steps dV_i. Thus the total surface area is given by

$$S_t = \sum_{i=1}^{n} \frac{2dV_i}{r_i} \tag{6.11}$$

The hydraulic radius of the pore system is the ratio of the total intruded pore volume and the total surface area

i.e. $$r_h = \frac{V_{(2000)}}{S_t} \tag{6.12}$$

where S_t = total measurable surface area (m^2/g)

n = number of volume steps used

r_h = hydraulic radius ($\overset{0}{A}$)

$V_{(2000)}$ = total intruded pore volume at 2000 kgf/cm^2

6.4.5 Other Pore Parameters

Other general pore properties were determined as described below.

The evaporable water content (cc/gm or gm/gm), expressed in these tests as gms of water per gm of dry paste, was determined from the measurements of weight loss on drying at 105°C, until a constant weight was reached. The bulk volume (cc/gm) was determined to an accuracy of

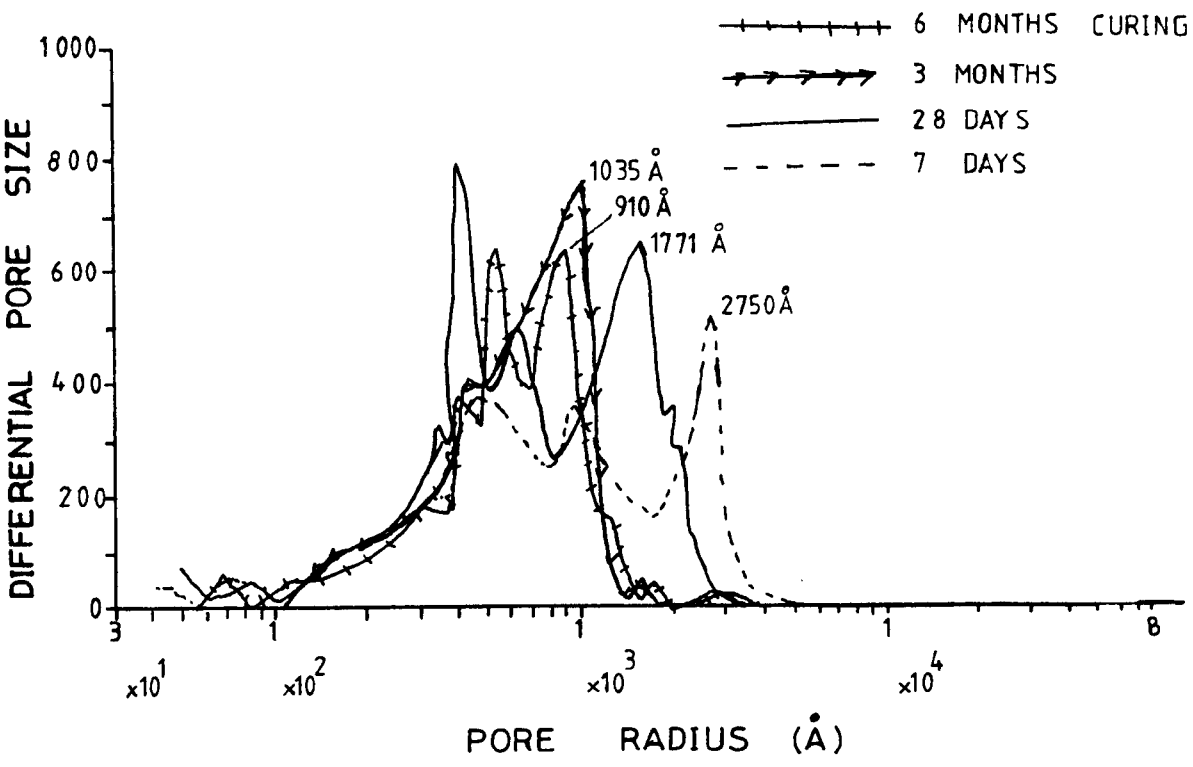

FIG 6.7 DIFFERENTIAL PORE SIZE DISTRIBUTIONS FOR HCP AT VARYING PERIODS OF HYDRATION (0.50 W/C RATIO)

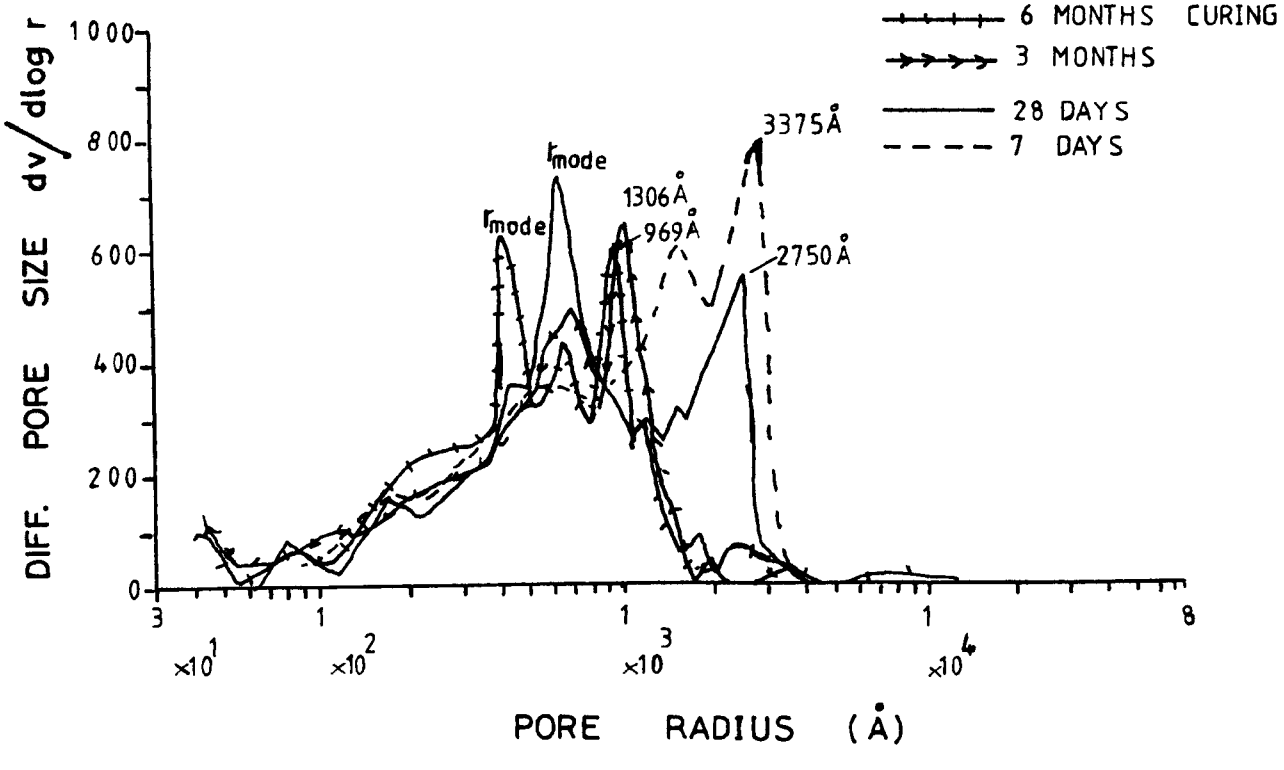

FIG 6.8 DIFFERENTIAL PORE SIZE FOR HCP AT VARYING TIME OF HYDRATION (0.70 W/C RATIO)

0.1cc using a mercury displacement volumeter. The dry density (g/cc) is the reciprocal of the bulk volume. The total porosity (cc/cc) is the evaporable water content in a given volume of sample which also could be expressed as

$$\varepsilon = w_e \rho_s \rho_w \qquad (6.13)$$

where ε = total porosity (cc/cc)

ρ_s = dry density of sample (g/cc)

ρ_w = density of water = 1.0 g/cc

w_e = weight loss at 105°C (gm/gm of dry sample)

Other values determined were

Wt of non-evaporable water $w_n = (w_d - w_i) - I_o C$ (gm) (6.14)

Wt of solids after ignition $C_1 = w_i + I_o C$ (gm (6.15)

Wt of original solid in sample $C = C_1/(1 - I_o)$ (gm) (6.16)

degree of hydration, $m = w_n/w_n^o \times 100\%$ (6.17)

where w_d = wt after drying to a constant weight at 105°C

w_i = wt after ignition at 1000°C

w_n^o = non-evaporable water of fully hydrated HCP

= 0.232 gm/gm[17]

I_o = loss on ignition (gm/gm) = 1.0% (Table 3.1)

The value, $w_n^o = 0.232 \pm 0.005$, was obtained after numerous tests carried out by Oyeka[17]. This was quite comparable with the results obtained by other investigators viz 0.23[27], 0.218[178], 0.235[179], 0.232[180]. The value of 0.232 gm/gm was used in this investigation since the same type of cement as in ref (17) was used.

6.5 Results and Discussions

6.5.1 Introduction

The methods outlined in section 6.4, were used to determine the pore parameters of all the samples tested. The results with discussions

of the pore parameters for HCP, with various time of hydration is presented in section 6.5.2. Section 6.6, discusses the effect of fine and coarse aggregate inclusion on the pore structure of HCP, while section 6.7, looks critically at the effect that various oils may have on the pore structure. In these analyses, the effort is focussed on those pore parameters that might influence the permeability of crude oil through concrete.

6.5.2 Pore Structure of HCP

Some of the properties and porosity of HCP are given in rows 1 to 5 of Tables 6.2, 6.3, 6.4 and 6.5 for 7 days, 28 days, 3 months and 6 months curing periods respectively. Table 6.6 shows the threshold radius. chemically combined water and degree of hydration for the four curing periods. The variations of these parameters with w/c ratio and hydration are the subjects discussed in this section.

6.5.2.1 Total porosty (i,e, total pore volume)

Total porosities for various w/c ratios are shown in column 2 of Tables 6.2 to 6.5. The plot of total porosity versus time of hydration for various w/c ratios is given in Fig. 6.9. Although it is difficult to establish precisely when a sample can be said to be saturated surface dry, (SSD) for the total porosity (total pore volume) to be determined, a consistent procedure was adopted. This involved quick surface drying of the specimens with damp tissue paper, immediately after curing in the fog room and weighing to an accuracy of 0.5gms. After achieving the SSD condition, the specimen was dried to a constant weight in an oven at 105^{o}C as described in section 3.7. It can be seen from Table 7.3, that for the mean value of porosities, this method is reasonably reliable. The following trends are observed from the Tables and Fig. 6.9.

1. The total porosity decreases with an increase in the period of hydration for all the w/c ratios tested. The rate of decrease is greater at the early stages of hydration, but became approximately linear from

	1	2	3	4		5	6	7
	MIX DESIGNATION	TOTAL POROSITY cc/cc	DRY DENSITY cc/cc	TOTAL PORE VOL INTRUDED cc/gm	cc/cc	%AGE OF TOTAL PORE UNINTRUDED %	SPECIFIC SURFACE AREA m^2/g	HYDRAULIC RADIUS ^{0}A
1	OP35	0.380	1.75	0.106	0.186	51.1	12.90	82.2
2	OP40	0.408	1.62	0.156	0.253	38.0	21.9	71.2
3	OP50	0.448	1.46	0.206	0.302	32.6	23.9	86.2
4	OP60	0.464	1.35	0.240	0.334	30.0	33.9	70.8
5	OP70	0.480	1.34	0.274	0.368	23.3	37.1	73.9
6	M35-1	0.212	2.05	0.083	0.170	20.1	4.16	199.52
7	M40-1	0.240	2.00	0.097	0.193	19.4	5.05	192.08
8	M50-1	0.280	1.89	0.119	0.223	20.3	5.53	215.20
9	M60-1	0.328	1.78	0.154	0.273	16.7	7.95	193.71
10	M70-1	0.336	1.73	0.163	0.283	16.1	8.18	199.12
11	M35-1.5	0.192	2.11	0.075	0.157	18.0	3.37	222.55
12	M40-1.5	0.216	2.06	0.084	0.172	20.4	4.37	192.22
13	M50-1.5	0.248	1.98	0.110	0.217	12.6	4.83	227.74
14	M60-1.5	0.288	1.87	0.132	0.246	14.5	5.84	226.03
15	M70-1.5	0.328	1.75	0.162	0.282	14.0	7.10	228.17
16	M35-2	0.164	2.17	0.068	0.148	10.0	3.51	193.70
17	M40-2	0.192	2.11	0.077	0.162	19.0	3.71	207.50
18	M50-2	0.216	2.01	0.091	0.183	15.4	4.37	208.20
19	M60-2	0.256	1.96	0.118	0.231	10.0	5.49	214.94
20	M70-2	0.272	1.90	0.130	0.247	9.6	6.45	201.60
21	M50-3	0.184	2.06	0.072	0.147	20.0	3.36	214.30
22	M60-3	0.212	2.01	0.085	0.167	20.0	3.86	220.21
23	M70-3	0.224	1.97	0.094	0.185	17.0	4.44	211.71
24	C35-1.5	0.150	2.32	0.059	0.136	12.0	2.89	204.15
25	C40-1.5	0.152	2.25	0.058	0.130	15.0	2.37	244.73
26	C50-1.5	0.176	2.16	0.071	0.154	14.0	3.37	228.85
27	C60-1.5	0.184	2.12	0.077	0.164	11.0	3.99	193.00
28	C70-1.5	0.192	2.09	0.084	0.176	8.5	4.39	191.34

TABLE 6.2 Test results for 7 days cured HCP, mortar and concrete

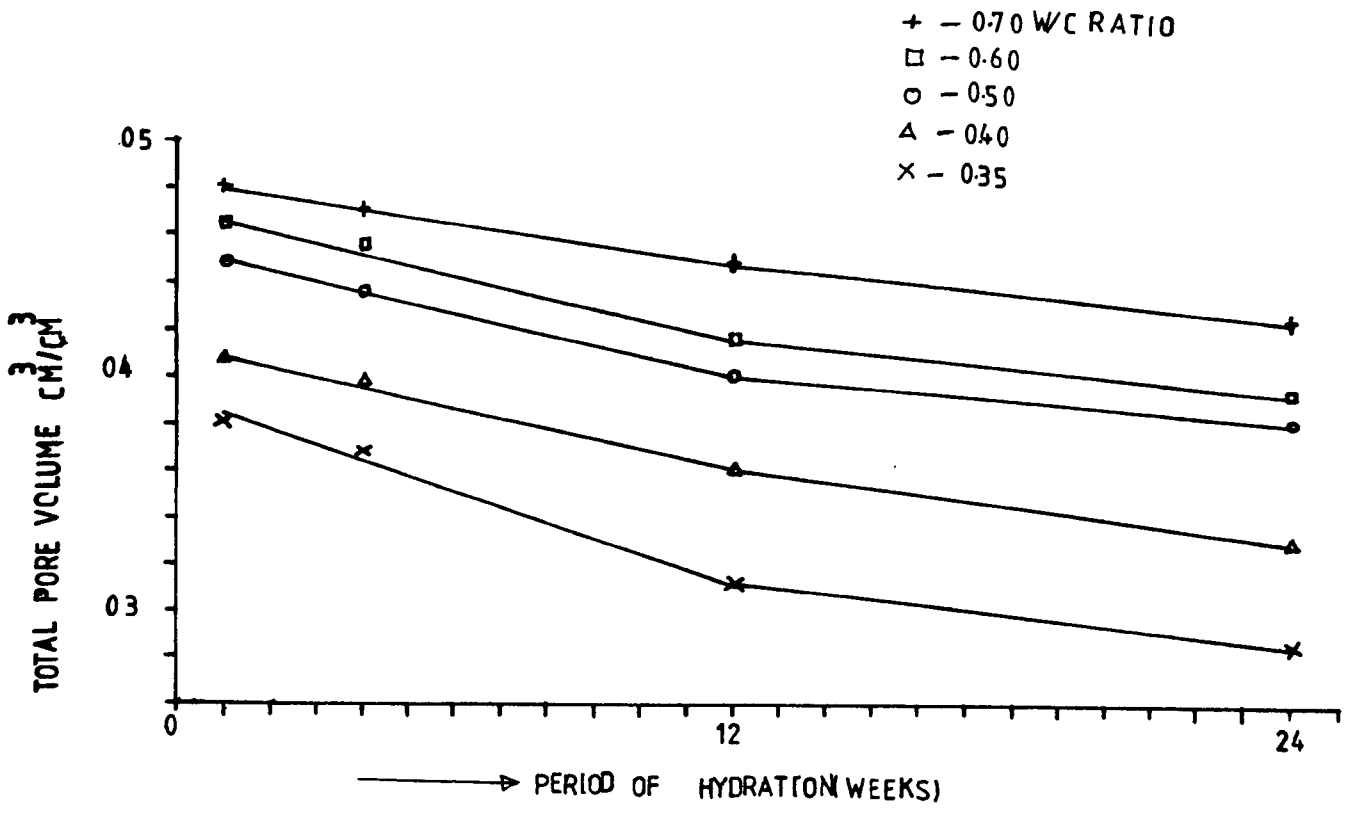

FIG. 6.9 EFFECTS OF W/C AND TIME OF HYDRATION ON THE TOTAL POROSITY OF HCP

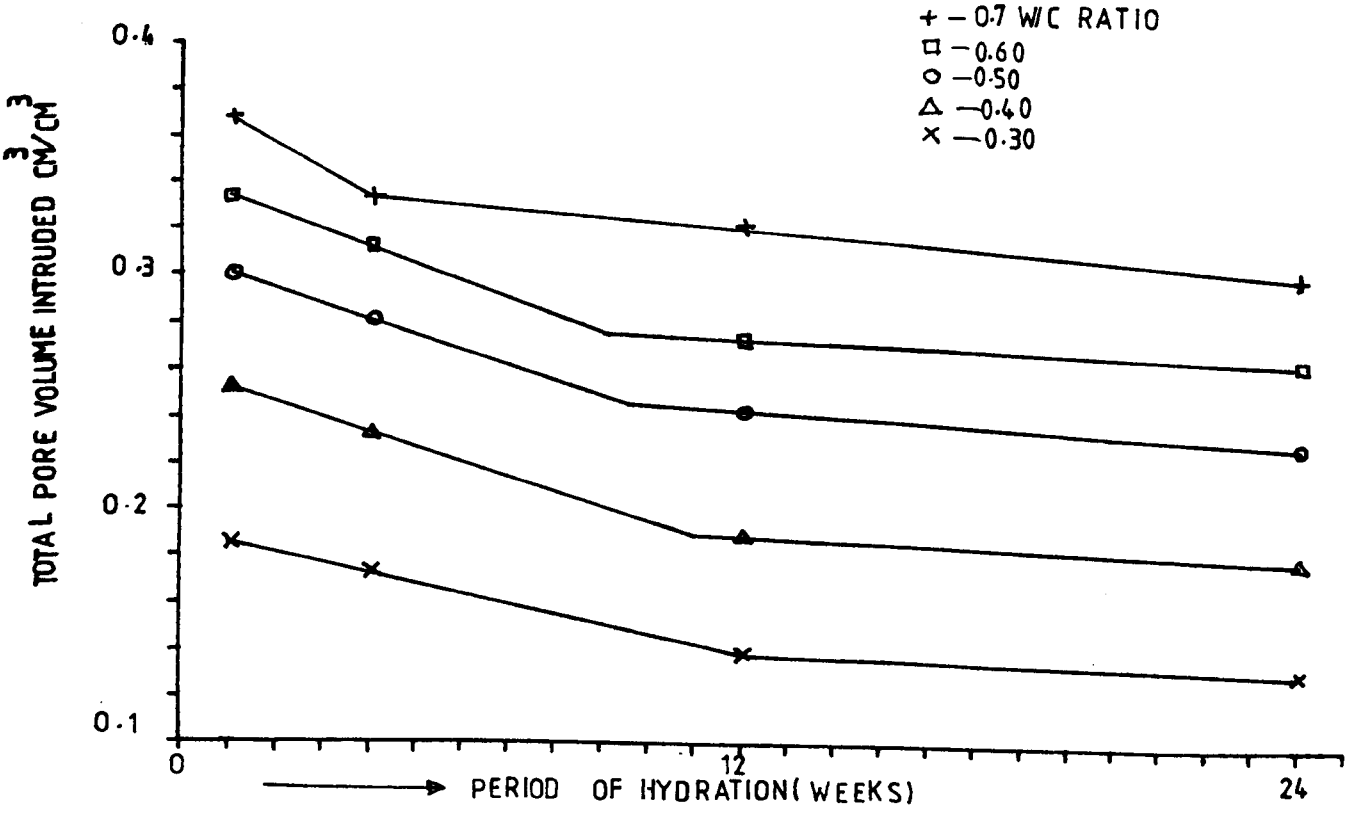

FIG 6.10 EFFECT OF W/C RATIO & TIME OF HYDRATION ON THE TOTAL PORE VOLUME INTRUDED

	1	2	3	4		5	6	7	8
	MIX DESIGNATION	TOTAL POROSITY cc/cc	DRY DENSITY g/cc(105°C)	TOTAL PORE VOL INTRUDED cc/gm	cc/cc	%AGE OF TOTAL PORE UNINTRUDED %	SPECIFIC SURFACE AREA m^2/g	HYDRAULIC RADIUS Å	COMPRESSIVE STRENGTH N/mm^2
1	OP35	0.368	1.78	0.099	0.175	52.5	14.4	68.8	84.9
2	OP40	0.398	1.65	0.143	0.235	40.7	16.1	88.8	72.6
3	OP50	0.436	1.50	0.189	0.283	35.1	21.7	87.1	52.0
4	OP60	0.456	1.41	0.223	0.314	32.2	27.2	81.9	45.4
5	OP70	0.470	1.37	0.246	0.335	28.7	32.5	75.6	40.2
6	M35-1	0.192	2.08	0.075	0.156	19	3.78	198.4	81.4
7	M40-1	0.224	2.02	0.075	0.151	32	4.22	177.8	76.6
8	M50-1	0.272	1.92	0.100	0.191	30	5.30	188.7	56.8
9	M60-1	0.320	1.79	0.130	0.234	27	7.04	184.7	46.1
10	M70-1	0.332	1.75	0.144	0.251	24	7.18	200.7	43.4
11	M35-1.5	0.176	2.14	0.069	0.147	16	3.20	215.6	79.3
12	M40-1.5	0.192	2.08	0.072	0.150	22	3.25	221.5	74.6
13	M50-1.5	0.224	2.00	0.092	0.183	18	4.54	202.6	63.0
14	M60-1.5	0.272	1.94	0.117	0.226	17	5.66	206.7	50.0
15	M70-1.5	0.312	1.87	0.138	0.260	17	6.49	212.6	40.0
16	M35-2	0.160	2.18	0.056	0.121	24	2.76	202.9	81.0
17	M40-2	0.176	2.10	0.066	0.139	20	3.14	210.2	77.2
18	M50-2	0.208	2.03	0.076	0.154	26	3.79	200.9	63.5
19	M60-2	0.248	2.00	0.101	0.199	17	5.31	190.2	50.0
20	M70-2	0.256	1.91	0.123	0.234	8.6	6.27	196.2	40.2
21	M50-3	0.160	2.17	0.061	0.127	22	2.85	214.0	59.5
22	M60-3	0.200	2.02	0.081	0.163	18.5	3.74	216.6	47.5
23	M70-3	0.216	2.00	0.087	0.174	19	4.12	211.2	43.9
24	C35-1.5	0.144	2.39	0.044	0.104	28	2.48	177.4	75.7
25	C40-1.5	0.152	2.26	0.053	0.121	21	2.70	196.3	72.6
26	C50-15	0.168	2.20	0.063	0.140	17	2.86	220.3	61.4
27	C60-1.5	0.176	2.15	0.067	0.144	18	2.94	227.9	50.9
28	C70-1.5	0.192	2.11	0.078	0.165	14	4.02	194.0	36.0

TABLE 6.3 Test results for 28 days cured HCP, mortar and concrete

	1	2	3	4		5	6	7
	MIX DESIGNATION	TOTAL POROSITY cc/cc	DRY DENSITY g/cc ($105^{o}C$)	TOTAL PORE VOL INTRUDED cc/g	cc/cc	%AGE OF TOTAL PORE UNINTRUDED %	SPECIFIC SURFACE AREA m^2/g	HYDRAULIC RADIUS ^{0}A
1	OP35	0.312	1.83	0.076	0.139	55.5	9.84	77.2
2	OP40	0.360	1.74	0.109	0.189	47.0	12.90	84.5
3	OP50	0.400	1.57	0.154	0.243	38.0	21.24	72.5
4	OP60	0.416	1.55	0.176	0.274	33.0	19.54	90.1
5	OP70	0.448	1.49	0.216	0.322	28.0	30.78	70.18
6	M35-1	0.192	2.08	0.065	0.135	30.0	3.66	177.6
7	M40-1	0.220	2.06	0.067	0.139	37.0	3.89	172.2
8	M50-1	0.252	1.91	0.092	0.175	29.0	5.12	179.7
9	M60-1	0.280	1.89	0.109	0.206	26.0	6.01	181.4
10	M70-1	0.308	1.78	0.132	0.235	19.0	7.14	184.9
11	M35-1.5	0.168	2.16	0.062	0.133	21.0	2.82	219.9
12	M40-1.5	0.192	2.09	0.064	0.134	30.0	3.68	173.9
13	M50-1.5	0.224	2.02	0.083	0.168	25.0	4.06	204.4
14	M60-1.5	0.256	1.97	0.102	0.201	22.0	4.82	211.6
15	M70-1.5	0.288	1.88	0.128	0.240	17.0	6.41	199.7
16	M35-2	0.160	2.18	0.053	0.115	28.0	3.02	174.9
17	M40-2	0.168	2.13	0.056	0.123	29.0	2.98	187.9
18	M50-2	0.192	2.08	0.069	0.143	25.0	3.97	173.8
19	M60-2	0.244	2.01	0.098	0.196	20.0	5.16	189.9
20	M70-2	0.256	1.92	0.109	0.210	18.0	5.74	189.9
21	M50-3	0.156	2.10	0.057	0.120	23.0	2.81	202.9
22	M60-3	0.184	2.06	0.071	0.147	20.0	3.14	226.1
23	M70-3	0.208	2.04	0.090	0.184	12.0	3.82	235.6
24	C35-1.5	0.136	2.41	0.041	0.098	28.0	2.40	178.8
25	C40-1.5	0.148	2.29	0.048	0.111	25.0	2.64	181.8
26	C50-1.5	0.156	2.22	0.054	0.120	23.0	2.78	194.2
27	C60-1.5	0.164	2.15	0.066	0.141	14.0	3.45	191.3
28	C70-1.5	0.184	2.12	0.078	0.165	18.0	3.74	209.7

TABLE 6.4 Test results for 3 months cured HCP, mortar and concrete

	1	2	3	4		5	6	7
	MIX DESIGNATION	TOTAL POROSITY cc/cc	DRY DENSITY g/cc (105°C)	TOTAL PORE VOL INTRUDED cc/g	cc/cc	%AGE OF TOTAL PORE UNINTRUDED %	SPECIFIC SURFACE AREA m^2/G	HYDRAULIC RADIUS Å
1.	OP35	0.304	1.85	0.072	0.132	56.5	9.46	76.1
2	OP40	0.328	1.76	0.103	0.181	46.0	15.36	67.1
3	OP50	0.380	1.60	0.143	0.230	40.0	20.12	71.1
4	OP60	0.392	1.58	0.167	0.264	34.0	21.96	76.0
5	OP70	0.422	1.52	0.201	0.307	27.3	29.94	67.1
6	M35-1	0.184	2.09	0.061	0.127	32.0	3.76	162.2
7	M40-1	0.216	2.07	0.064	0.132	39.0	3.94	162.4
8	M50-1	0.248	1.95	0.090	0.176	31.0	4.95	181.8
9	M60-1	0.276	1.90	0.102	0.193	30.0	5.70	179.0
10	M70-1	0.292	1.81	0.129	0.232	20.0	6.82	189.2
11	M35-1.5	0.160	2.19	0.057	0.126	21.0	2.88	197.9
12	M40-1.5	0.182	2.14	0.061	0.130	35.0	3.70	164.9
13	M50-1.5	0.216	2.07	0.074	0.152	30.0	3.83	193.2
14	M60-1.5	0.240	1.97	0.087	0.171	29.0	4.43	196.4
15	M70-1.5	0.280	1.90	0.121	0.231	16.5	6.36	190.3
16	M35-2	0.152	2.18	0.048	0.104	32.0	2.53	189.7
17	M40-2	0.168	2.14	0.051	0.108	34.0	2.71	188.2
18	M50-2	0.192	2.08	0.064	0.133	31.0	3.47	184.4
19	M60-2	0.224	2.04	0.081	0.164	27.0	4.48	180.8
20	M70-2	0.248	1.98	0.096	0.185	24.0	5.29	181.5
21	M50-3	0.152	2.11	0.053	0.111	27.0	3.02	175.5
22	M60-3	0.176	2.08	0.063	0.132	25.0	3.63	173.6
23	M70-3	0.200	2.07	0.083	0.172	14.0	4.42	187.8
24	C35-1.5	0.132	2.41	0.040	0.095	29.0	2.04	196.1
25	C40-1.5	0.144	2.29	0.045	0.102	25.0	2.73	164.8
26	C50-1.5	0.152	2.25	0.051	0.115	24.0	3.02	168.9
27	C60-1.5	0.160	2.20	0.058	0.128	20.0	3.60	161.1
28	C70-1.5	0.182	2.15	0.069	0.149	20.0	3.62	190.6

TABLE 6.5 Test results for 6 months cured HCP, mortar and concrete

about 3 months. This decrease would be explained from the fact that as hydration proceeds, the solid hydration products occupy about twice the original volume of solids in the pastes (section 2.3.2) and since the volume after setting changes by only about 0.3%[55], the hydration products inevitably have to occupy the pore spaces. Also as hydration continues, the amount of unhydrated material decreases and rate of production of hydration products must equally decrease giving rise to a decrease in the rate at which the pore spaces are filled.

2. The total porosity increases with an increase in the w/c ratio for all the hydration periods. This is as expected since the porosity is the original space occupied by the mixing water which is not yet chemically combined. An increase in the w/c ratio would mean an increase in such water held in between the inert and unhydrated particles hence an increase in the porosity

6.5.2.2 Total pore volume intruded by mercury

The total intruded pore volume by mercury is shown in column 4 of Tables 6.2 - 6.5 and Fig 6.10. Assuming that the overall total pore volume is that obtained by drying to 105°C as described in section 6.5.2.1, the percentage of the total pores unintruded is given in column 5 of Tables 6.2 - 6.5. The plot and Tables reveal that

1. The total pore volume intruded by mercury decreases with the period of hydration. The rate of decrease is greater at the early stage of hydration, but becomes approximately constant at a hydration period which depended on the w/c ratio. The constant reduction in the rate begins at 4, 9, 9.8, 11 and 12 weeks for 0.70, 0.60, 0.50, 0.40 and 0.35 w/c ratios respectively, as shown in Fig. 6.10. This trend in the reduction rate is not clear at present and may be linked with the chemical processes of hydration which is beyond the scope of this investigation. The decrease in the intruded pore volume with hydration could be explained from the fact that as hydration proceeds, the hydration products have gel pores far below

37 $\mathring{A}$ [27], which is the minimum pore radius that the mercury porosimeter could detect. Coupled with subdivision of pores by the hydration products [80] some pores previously intrudable became unintrudable, with consequent reduction in the intruded pore volume.

2. The total pore volume intruded increases with an increase in the w/c ratio for all the curing periods. The rate of increase however neither depends on the age nor the w/c ratios. For a 28 day curing period, the intruded volume for 0.5 w/c ratio is 1.32 time the intruded volume for 0.4 w/c, while the intruded volume at 0.7 w/c ratio is 1.10 times the intruded volume at 0.6 w/c ratio, and the intruded volume at 0.6 w/c ratio is 1.18 times that at 0.5 w/c ratio.

The higher total porosity, and greater total intruded pore volume which occur for higher w/c ratio pastes, show that pastes with higher w/c ratios contain not only a greater quantitiy of pore space but coarser pores. This deduction may be of great value in relation to permeability and will be explored further in Chapter 8.

It is also observed that in all cases, the total intruded pore volume is less than the calculated volume of the pore space (section 6.5.2.1). This is not surprising since pores having nominal radii less than 37 $\mathring{A}$ radius and encapsulated pores could not be recorded by the porosimeter. What is significant is that from 0.4 w/c ratio to 0.7 w/c ratio and even at 6 months hydration, with degree of hydration of between 77.2 to 94.3%. up to 60% of the pores were still intrudable by mercury. This shows that these pastes even after almost complete hydration, still contain substantial pores with nominal radii signficantly larger than the size associated with the sorption method of pore structure analysis (i.e. 10 - 100 $\mathring{A}$) [17]. These coarser pore sizes are believed to have greater influence on permeability than the fine pores, thereby justifying the use of the mercury porosimeter, even though pores below 37 $\mathring{A}$ cannot be detected. This view is further amplified in section 6.7.

6.5.2.3 Density of HCP

The density of the paste for each w/c ratio is given in Tables 6.2 - 6.5, for the four hydration periods and also illustrated in Fig. 6.11. The following deductions are made.

1. The density increases with the period of hydration. The increase was more rapid at the initial stages of hydration, up to a period of about 3 months. This behaviour is expected, since an increase in the volume of solid materials within an approximately constant volume (section 2.3.2 or 6.5.2.1.), would mean an increase in density of the bulk material. The lower rate of increase in density after 3 months, must mean that the hydration rate was slowing down. As hydration continued, the remaining volume of unhydrated material continuously decreased, but it probably never completely disappeared because some is shielded from water by the hydration products formed around it. Fig. 6.12, also illustrates this slowing down in the rate of hydration with age.

2. The dry density decreases with an increase in the w/c ratio for all the hydration periods. This is not surprising, since a higher w/c ratio means more pores and less solids for a unit volume (section 6.5.2.1). The rate of decrease however varies greatly. At 7 days curing period, OP35 paste has a density of 1.08 times the density of OP40, while OP40 paste has a density of 1.11 times that of OP50, and OP60 paste has a density of 1.007 times the density of OP70 paste. The rate of decrease in dry density with w/c ratio appears to be constant after 3 months hydration. (Plot 6.11 exhibits approximately parallel lines after 3 months hydration). This may imply that after 3 months hydration, most pastes exhibit approximately the same hydration rate.

6.5.2.4 Pore size distribution

The determination of pore size distributions was carried out using the mercury porosimeter described in section 6.3. 86 results were obtained for HCP, 420 results for mortar (of varying proportions of

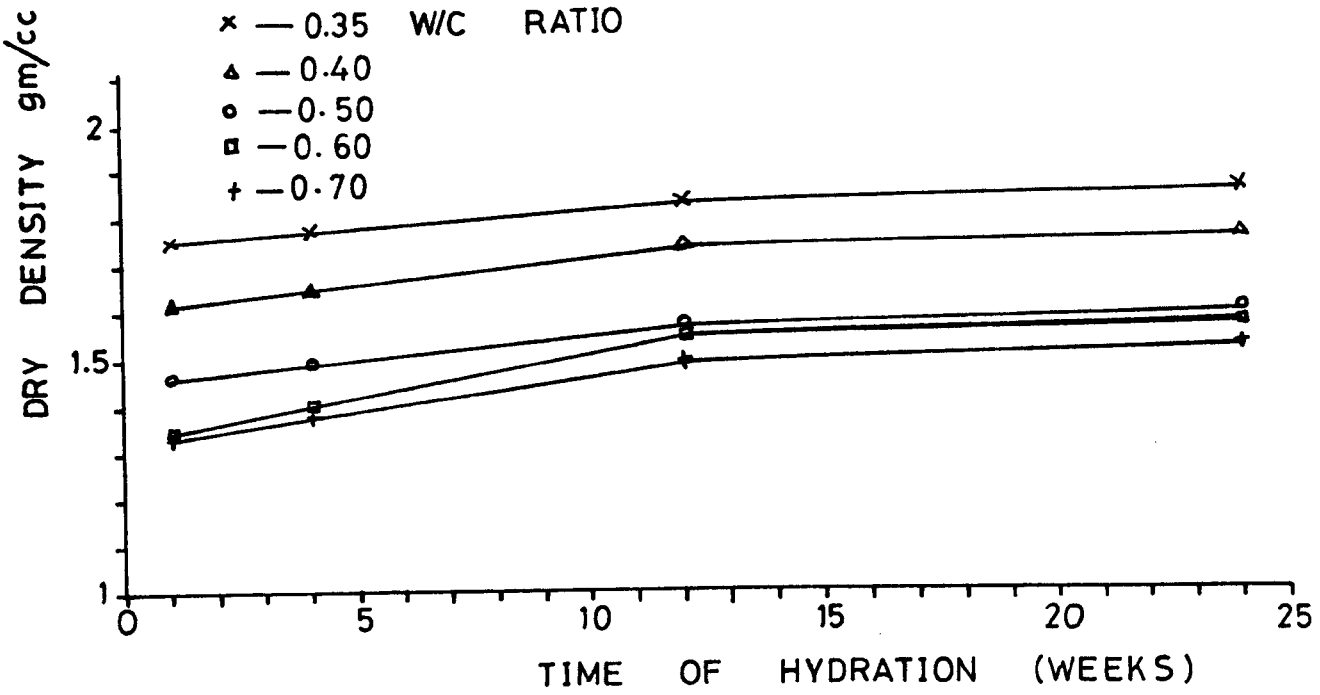

FIG 6.11 GRAPH OF DRY DENSITY VERSUS TIME OF HYDRATION AT VARYING W/C RATIO

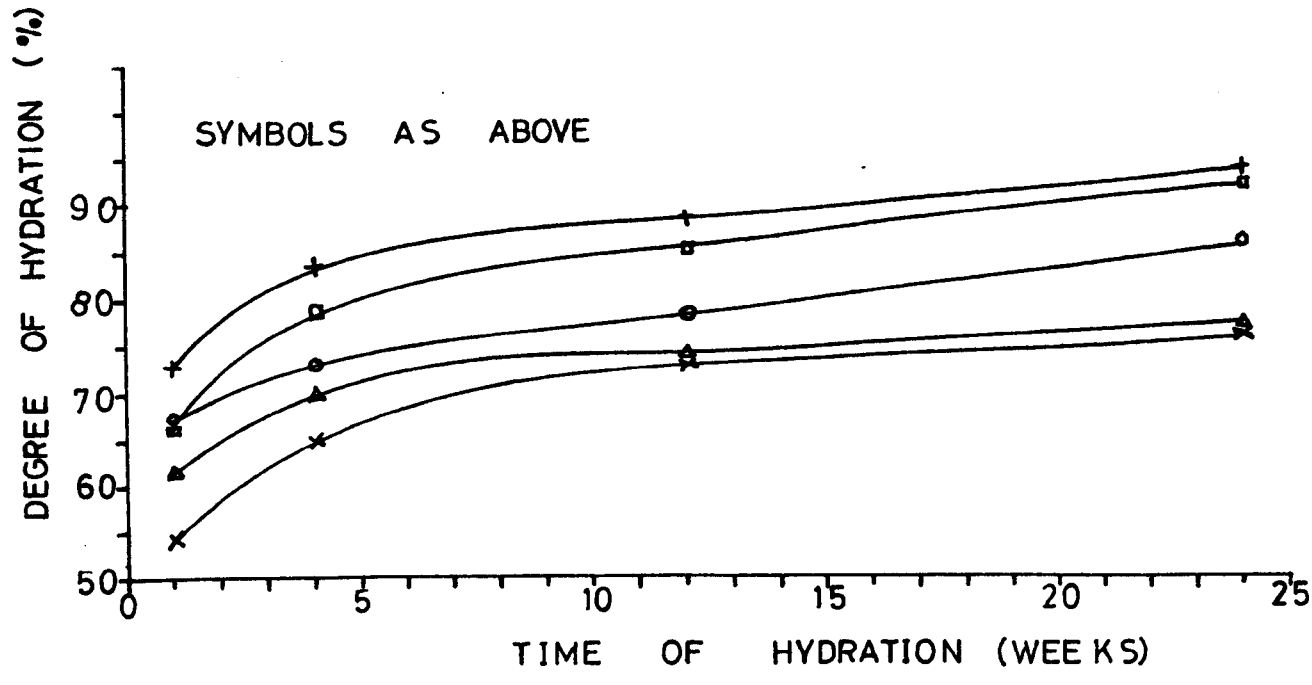

FIG 6.12 GRAPH OF DEGREE OF HYDRATION WITH TIME OF HYDRATION, AT VARYING W/C RATIO

sand and cement) and concrete, (1:1½:1½, cement: sand and coarse aggregate ratio), and 168 results for HCP, mortar (1:1½ cement/sand ratio) amd concrete (1:1½:1½) which had been saturated in various oils. These other results will be discussed later in section 6.7. A computer program was used to analyse these results, and each was examined on a screen in a tektonix 4010 plotter to identify the position of the threshold radius (r_T), discussed in section 6.5.2.5) on the pore size distribution curve. Typical plots of cumulative pore size distributions are illustrated in Figs. 6.5 and 6.6 for OP50 and OP70 pastes respectively at varying hydration periods, and Fig. 6.13 for a 28 day hydration period at varying w/c ratios. Figs. 6.7 and 6.8 illustrate the differential pore size distributions for 0.5 and 0.7 w/c ratios respectively, at varying hydration periods, while Fig. 6.14 shows the differential pore size distribution for 28 days of hydration for varying w/c ratios. The distributions represent the pore volumes per volume of pastes, existing below a given pore size as obtained from the measurements. Typical values of the threshold radius are shown on the curves. The following observations are made from these figures.

1. The total intruded pore volume decreases with time of hydration (section 6.5.2.2).

2. As already stated[81], the general distribution shifts to the left with increasing hydration period, that is the pores become finer with age.

3. The curves reveal an apparent threshold radius below which there is relatively little intrusion and immediately above which, the greatest intrusion commences. This is very important and is discussed in section 6.5.2.5.

4. The pore radii occurring most frequently are defined as mode pure radii, r_{mode} and are shown on Fig. 6.14 for the five w/c ratios. This is obtained at the maximum value of the function dV/ dlog r (section 6.4.3). Apart from the OP35 paste, the r_{mode} does not correspond to the

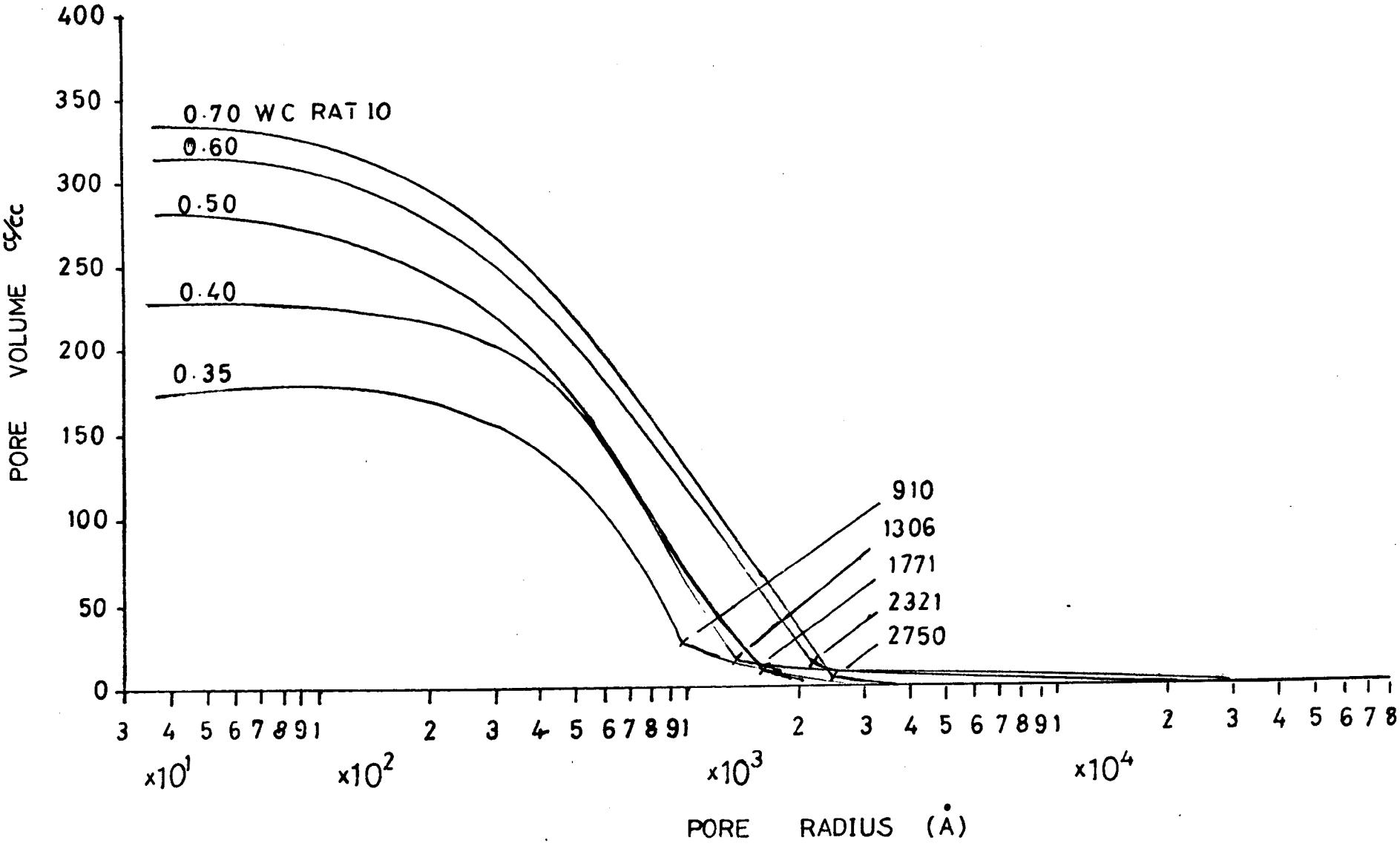

FIG 6.13 EFFECT OF W/C RATIO ON THE CUMMULATIVE PORE SIZE DISTRIBUTION OF HCP HYDRATED FOR 28 DAYS IN THE FOG ROOM

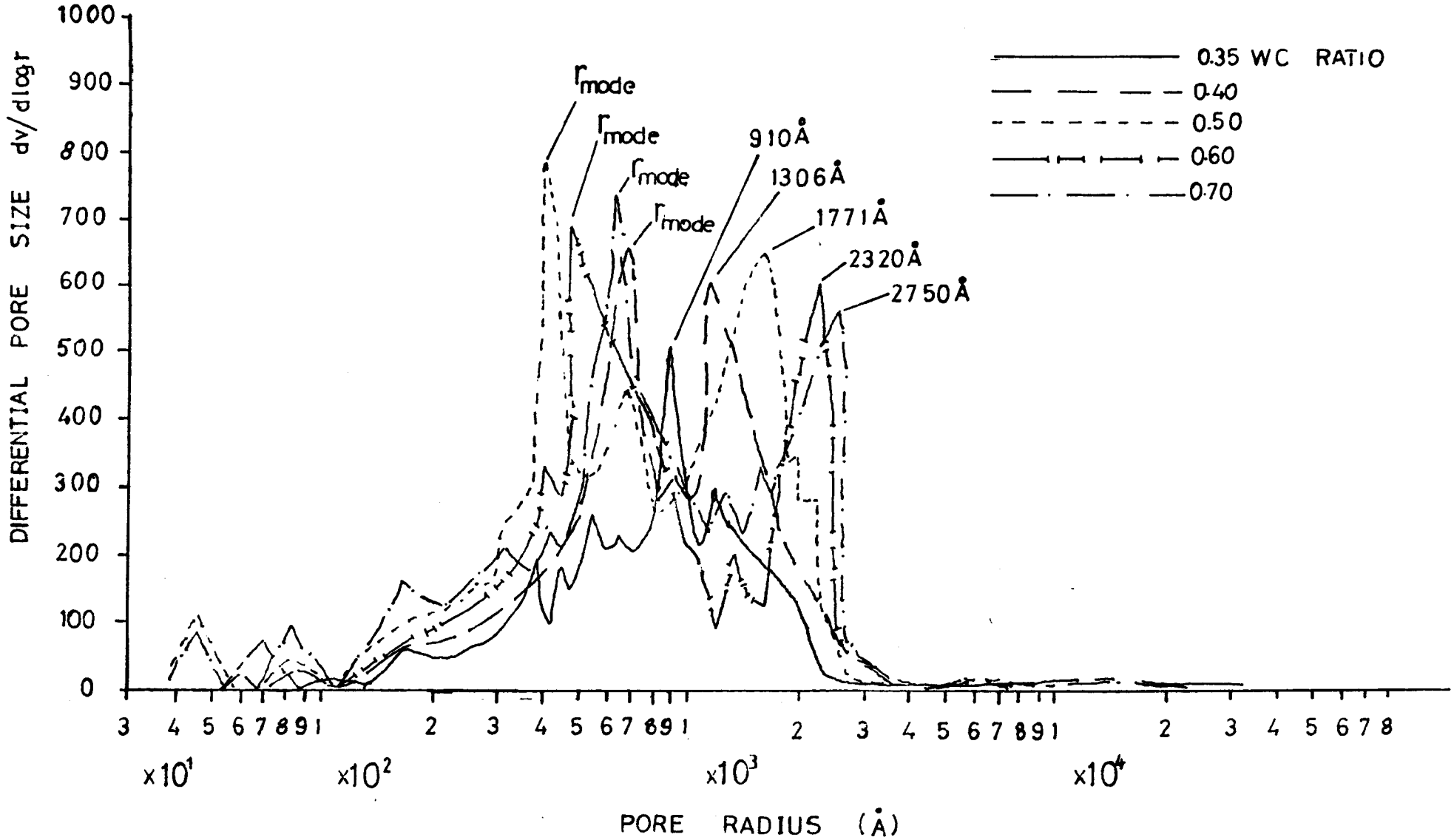

FIG 6.14 DIFFERENTIAL PORE SIZE DISTRIBUTION FOR HCP AT VARYING W/C RATIO (28 DAY CURING)

threshold radius and does not seem to depend on w/c ratio. Since most of the r_{mode} fall below the pores which were closed by the waxy deposits of the crude oil (<650 $\overset{0}{A}$; section 6.7), it is most unlikely to be associated with the saturated permeability of the crude oil, hence further discussion of the parameter is not intended.

6.5.2.5 Threshold radius

The position of the threshold radius was checked with both the shape of the cumulative pore size distribution function and the derivative of the pressure volume data taken at equal volume steps as discussed in section 6.4.1 and 6.4.2 respectively. This parameter corresponds to the region of inflection following an almost horizontal portion of the pore size distribution (Fig. 6.5 and 6.6.) To the right of the inflection, there is little intrusion, while to the left, rapid intrusion starts. This region is also characterized by a steep slope and may suggest that a substantial pore volume exist within this region with a very small range of pore sizes, which suggests that the pore size at this region is continuous to some extent. While carrying out the test, it was also observed that substantial intrusion did occur at very minor increases in pressure in this region. These findings have also been reported by other investigators[80, 114]. The influence of the two variables, i.e. w/c ratio and hydration on this parameter is to be discussed in this section. Discussion on the effect of aggregate inclusions on the threshold radius will be carried out in section 6.6.3, while the significance of the threshold radius on the saturated permeability is to be discussed in Chapter 8.

On the distribution curves of Figs. 6.5, 6.6 and 6.13, and on the differential pore sizes of Figs. 6.7, 6.8 and 6.14 are clearly marked the values of threshold radii for various w/c ratios and periods of hydration. Fig. 6.15, also shows a semi-log plot of the threshold radii and the time of hydration at varying w/c ratio obtained from Table 6.6.

The following observations are made from the plots.

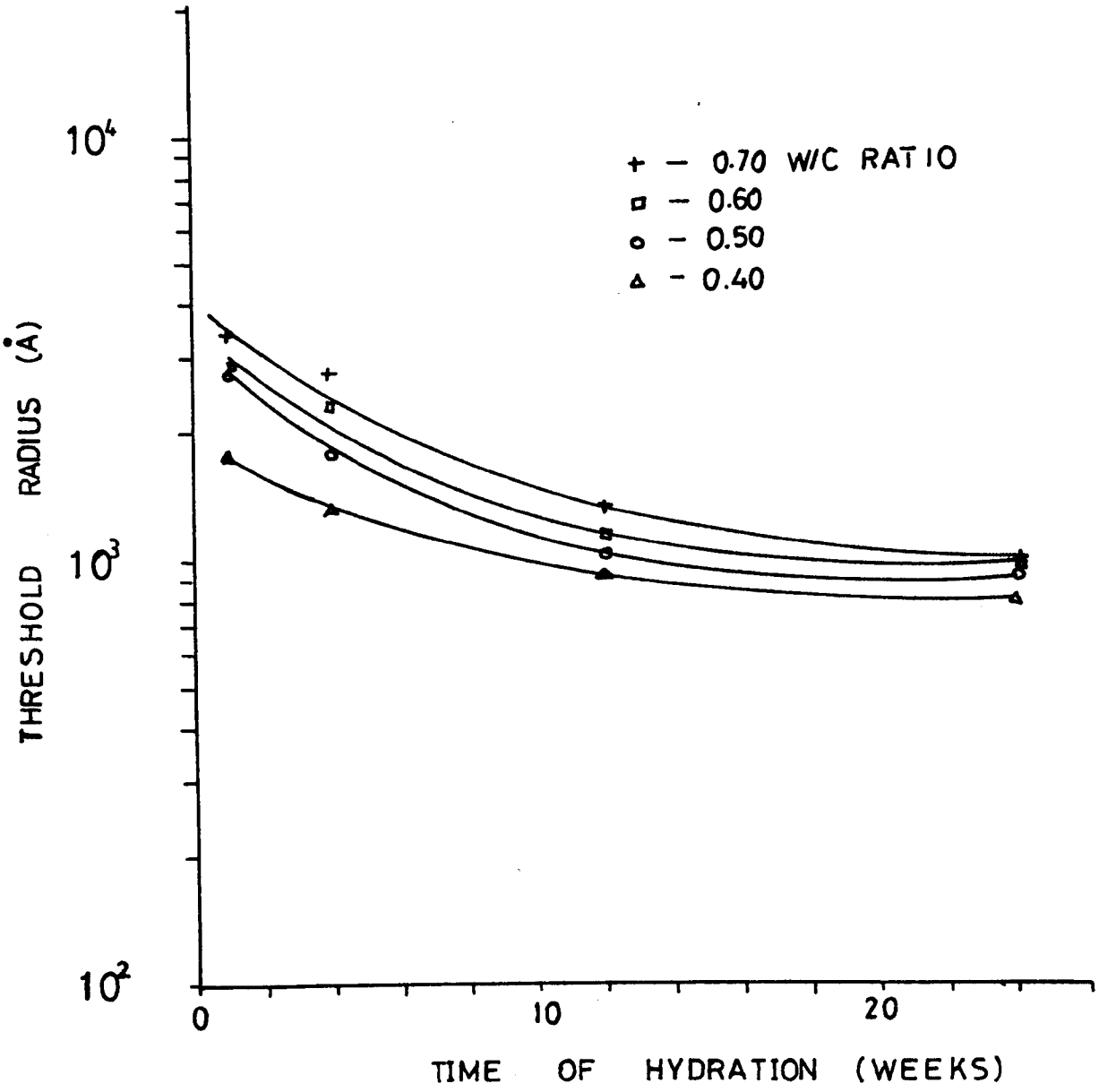

FIG 6.15 THRESHOLD RADIUS AS A FUNCTION OF TIME OF HYDRATION AT VARYING W/C RATIOS FOR HCP

	7 DAYS			28 DAYS			3 MONTHS			6 MONTHS		
1	2	3	4	5	6	7	8	9	10	11	12	13
PASTE DESIGNATION	THRESHOLD RADII	CHEMICALLY COMBINED WATER	DEGREE OF HYDRATION	THRESHOLD RADII	CHEMICALLY COMBINED WATER	DEGREE OF HYDRATION	THRESHOLD RADII	CHEMICALLY COMBINED WATER	DEGREE OF HYDRATION	THRESHOLD RADII	CHEMICALLY COMBINED WATER	DEGREE OF HYDRATION
	(Å)	w_n/C gm/gm	%	Å	w_n/C gm/gm	%	Å	w_n/C gm/gm	%	Å	w_n/C gm/gm	%
OP35	1583	0.126	54.3	910	0.150	64.7	910	0.170	73.2	858	0.177	76.4
OP40	1771	0.143	61.6	1306	0.163	70.4	910	0.172	74.1	792	0.179	77.2
OP50	2750	0.156	67.2	1771	0.170	73.3	1036	0.182	78.4	910	0.200	86.2
OP60	2750	0.154	66.23	2320	0.183	79.0	1112	0.198	85.4	969	0.216	93.0
OP70	3375	0.169	72.8	2750	0.195	83.9	1306	0.204	88.1	969	0.219	94.3

TABLE 6.6 Test results for HCP

	0.50 w/c RATIO					0.70 w/c RATIO				
1	2	3	4	5	6	7	8	9	10	11
CEMENT/ SAND RATIO	AGG VOL CONCEN %	DENSITY gm/cc	POROSITY cc/cc	INTRUD PORE VOL cc/cc	%AGE UNINTR.	AGG VOL CONCEN %	DENSITY gm/cc	POROSITY cc/cc	INTRU PORE VOL cc/cc	%AGE UNINTRU.
HCP	0.0	1.50	0.436	0.283	35.10	0.0	1.37	0.470	0.335	28.70
1:1	36.0	1.92	0.272	0.191	30.0	34.0	1.75	0.332	0.251	24.0
1:1.5	46.0	2.00	0.224	0.183	18.0	44.0	1.87	0.312	0.260	17.0
1:2	53.0	2.03	0.208	0.154	26.0	51.0	1.91	0.256	0.234	8.57
1:3	63.0	2.17	0.160	0.127	22.0	61.0	2.00	0.216	0.174	19.0
CONCRETE SPECIMEN 1:1½:1½ (cement:sand:coarse agg)										
1:1.5:1.5	63.0	2.20	0.168	0.140	17	61.0	2.11	0.192	0.165	14.0
Aggregate	100.0	2.62	0.0247	0.0211	15					

TABLE 6.8 Effect of aggregate inclusions on some pore parameters (28 days curing)

1. The threshold radius decreases with an increase in the hydration period. The decrease is more rapid at the early stages of hydration. For 0.7 w/c ratio, the threshold radius after 7 days hydration is 2.58 times the radius after 3 months which is 1.34 times the radius after 6 months hydration. The obvious explanation for this decrease is that as hydration continued, there seems to be a general subdivision of pores as reported by Winslow [80], with a consequent production of smaller pore sizes.

2. A critical look at Figs. 6.5 and 6.6, reveals that the steep slopes occur at decreasing pore sizes with increased hydration, the total pore volume intruded at that point remained approximately constant and effectively small compared with the intruded total pore volume (about 2% of the total intruded pore volume after 6 months hydration for 0.5 w/c ratio). This tends to suggest that pores larger than the threshold radius, are available but in a small quantity and are easily intruded from the exterior of the specimen. They seem not to be affected by hydration products. They may also be previously encapsulated pores, exposed while preparing the specimen. If this is true, it suggests that the volume of encapsulated pores in the paste depends on the method of preparation and w/c ratio (Fig. 6.13) and is not affected by hydration.

3. The threshold radius increases with w/c ratio. For a 28 day hydration, the threshold radius for 0.7 w/c ratio is 1.18 times the radius for a 0.6 w/c ratio, which is 1.31 times that for a w/c = 0.5, which is 1.36 times that for a 0.4 w/c, which also is 1.44 times the radius at a w/c = 0.35. The rate of increase tends to reduce with w/c ratio for the 28 day hydration period, but this does not seem to be a general pattern for all the hydration periods as could be seen in Table 6.6.

If one adopts the idea that the threshold radius is mainly controlled by the intergranular spacing at the time of set, it will be quite clear that higher w/c ratios generate larger intergranular spacing

and hence larger threshold radius. This intergranular spacing will reduce with hydration, hence lowering the threshold radius with increasing hydration.

6.5.2.6 Surface area from mercury intrusion

A method of estimating the surface area from the pore size distribution data has been outlined in section 6.4.3. The use of the unlikely assumption that all pores are cylindrical, renders surface area determination rather approximate. However the specific surface can give valuable comparative information between different porous materials. Column 6 of Tables 6.2 to 6.5 and Fig. 6.16 gives the variation in surface area with hydration for various w/c ratios.

The specific surface area decreases linearly for OP35 and OP50 and non-linearly for OP40, OP60 and OP70 paste, with the time of hydration. It increases erratically with w/c ratio for all the periods of hydration. After 7 days hydration, the surface area for w/c = 0.70 is 1.09 times greater than that of w/c = 0.60, which is 1.42 times that of w/c = 0.50, which is 1.09 times that of w/c = 0.40 which also is 1.71 times greater than the surface area for w/c = 0.35.

Determination of surface areas by other investigators using mercury porosimetry reveals some agreement with the present investigation (rows 1-5 column 6 of Tables 6.2 to 6.5). Nyame[114] used Type D25 ordinary portland cement paste and maximum pressure of 2000kgf/cm^2 and a contact angle of 141^o, using different casting, curing procedures and conditions. Surface areas ranging from 16 to 27m^2/g for a 0.47 w/c ratio, and from 24 to 42m^2/g for a 0.71 w/c ratio were obtained. Both were tested from 3 days up to 20 months and it was observed that the surface area increased with w/c ratio, but also that for lower w/c ratios, the surface areas decreased with the hydration but at higher w/c ratio it is unaffected by hydration. This later deduction, is not consistent with the present results. Bager and Sellevoid[113] obtained a value of 39m^2/g for

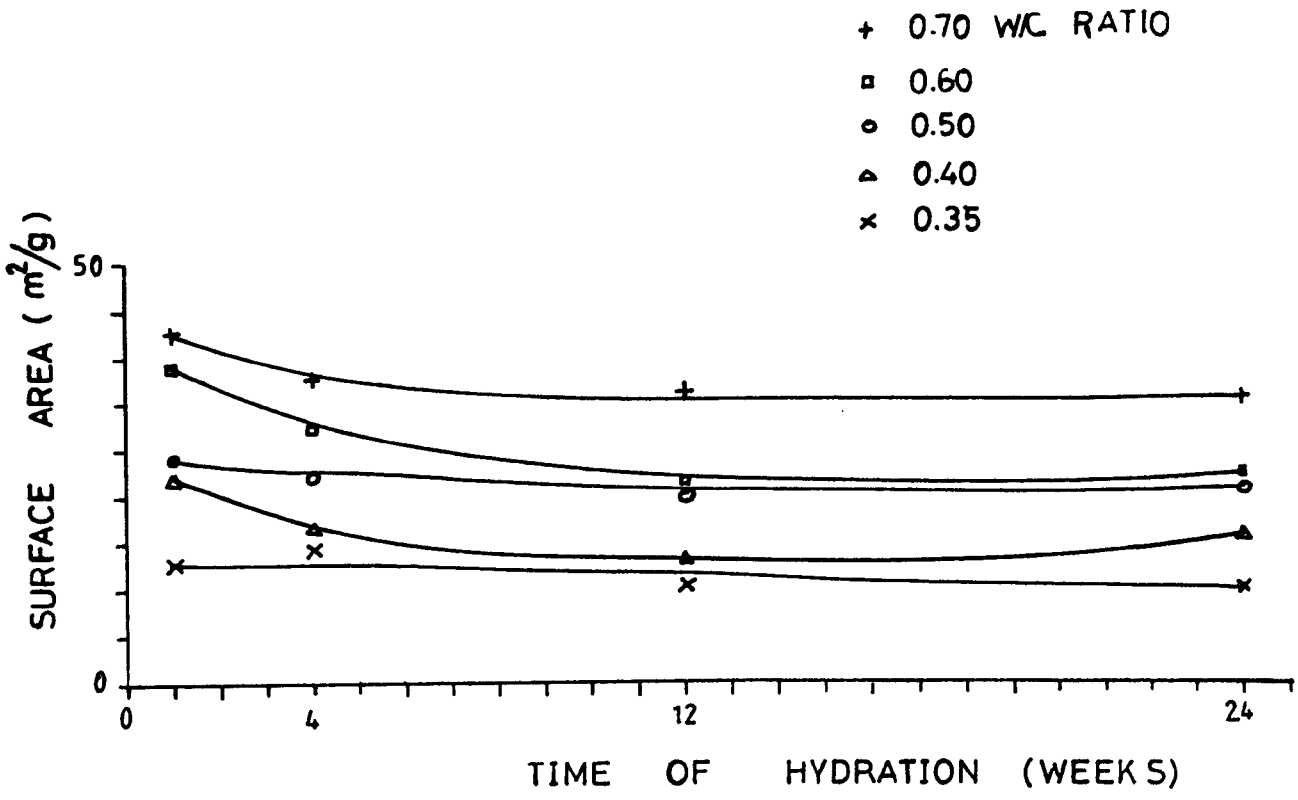

FIG 6.16 VARIATION OF SURFACE AREA OF HCP FROM MERCURY INTRUSION WITH W/C RATIO AND TIME OF HYDRATION

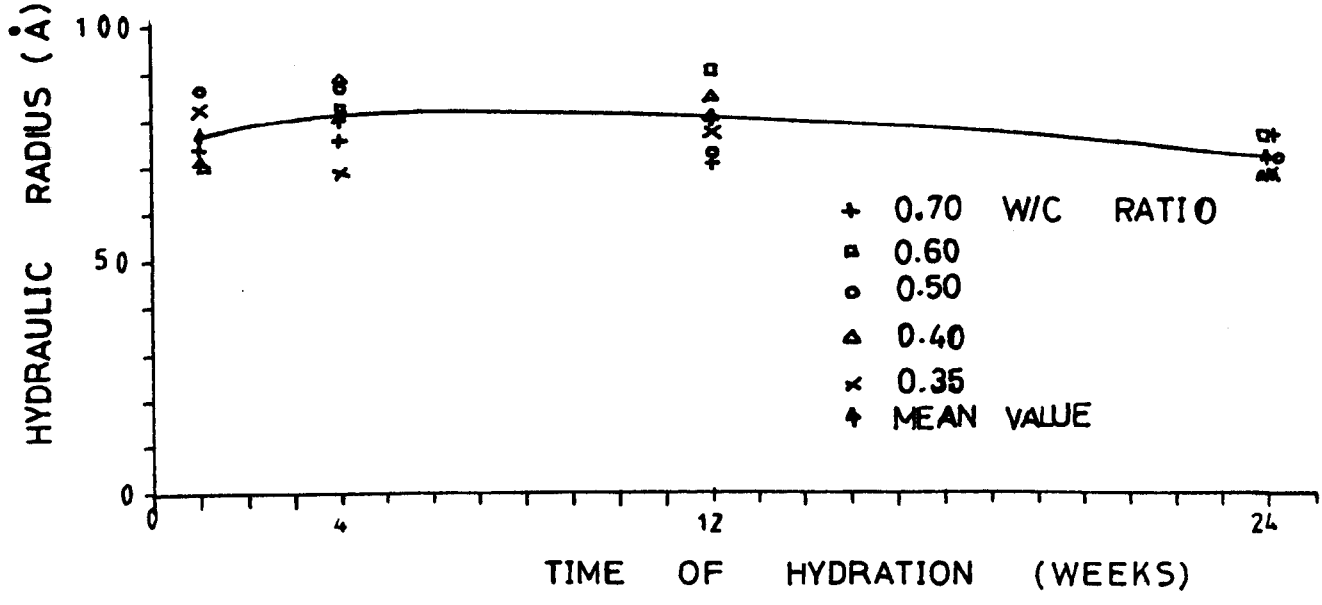

FIG 6.17 VARIATION OF HYDRAULIC RADIUS OF HCP FROM MERCURY INTRUSION DATA WITH W/C RATIO AND TIME OF HYDRATION

0.4/20 months paste of Danish 'Rapid' type cement. The maximum pressure was 3500 kgf/cm^2 and the contact angle was 117^o. Bentur[106], using Type I, ordinary portland cement, with a maximum mercury pressure of 4000 kgf/cm^2 and contact angle of 117^o obtained for 0.4 w/c ratio paste, a surface area ranging from 16 to 28 m^2/gm. The curing conditions and period of hydration were not given. Present test results show a surface area ranging from 9.46 to 37.1 m^2/gm, using OPC as described in Table 3.1. These results indicate lower values than the typical values of 180-220 m^2/gm obtained using water vapour sorption methods, for fully hydrated pastes [53, 55, 61]. The small angle x-ray scattering technique showed equally high values[66]. Typical values < 50m^2/g were recorded using a nitrogen sorption method[106, 181]. The results from the nitrogen absorption method appear to be in agreement with results obtained using mercury porosimetry. A critical look at the elemental values of surface area (ΔS_t), suggest that higher values occur for smaller pore sizes. If this is true, it means that probably a substantial amount of the specific surface was not detected by the porosimeter, hence a lower value was obtained compared with the water-vapour sorption method. The lower surface area obtained using nitrogen adsorption method was attributed to the fact that nitrogen molecules, which are larger than water molecules, could not penetrate between the layers of the cement gel[67].

6.5.2.7 Hydraulic radius of HCP

The hydraulic radius is defined in section 6.4.3. It is also a measure of the average width of the pores. The threshold radius represents a single point measure of distribution, and was able to describe to some extent the changes in the pore system as a result of changes in the w/c ratio and progressive hydration. However, it could not account for the distirubtions of pores below and above itself, or the nature and extent of surfaces of the solid phases formed as a result of hydration. The hydraulic radius, may however account for some of these. Column 7 of Tables 6.2

6.5 and Fig. 6.17 show the variations of the hydraulic radius with w/c ratio and hydration period. The following observations are made.

1. The measured hydraulic radius has a large scatter for all w/c ratios and for all periods of hydratiom, and does not seem to depend on the w/c ratio. The mean value and coefficient of variation for all tests at various hydration periods is shown in Table 6.7.

Hydration period	mean r_h $\overset{0}{A}$	Coeff. of variation %
7 days	76.86	8.1
28 days	80.40	9.2
3 months	78.90	9.4
6 months	71.48	5.6

TABLE 6.7 Mean and coefficient of variation of hydraulic radius

The hydraulic radii obtained by Nyame[104] were found to be very much greater than those in the present research and vary between 63.2 to 188 x 10^2 $\overset{0}{A}$ for curing periods of 7 days to 20 months in water. He also found that the hydraulic radius increases with increasing w/c ratio, which is not the case in the present tests. The reasons for the wide difference is not clear, but may be as a result of differing casting and curing conditions. Bentur[106] found hydraulic radii from 24 to 30 $\overset{0}{A}$ for 0.4 w/c ratio paste. The curing period is not stated. This is below the results obtained in the present tests, but would be accounted for by the type of cement and equipment used as stated in section 6.5.2.6.

2. The hydraulic radius, tended to increase with the time of hydration up to 28 days, and steadily decreased afterwards. The reason for the initial increase is not clear, but the later decrease could be as a result of subdivision and filling of larger pores by the hydration products as explained in section 6.5.2.1.

The insensitivity of the hydraulic radius to w/c ratio compared to the fact that permeability increases with w/c ratio may suggest that hydraulic radius does not influence the flow of liquid through HCP, and the threshold radius may be more important. Very low values of these hydraulic radii as compared with the critical pore radius of 650 $\overset{0}{A}$ (section 6.7) provides further evidence of this.

6.6 Pore Structure of Mortar and Concrete

The study of the changes in the pore structure of HCP with w/c ratio and hydration was carried out in section 6.5. This present section deals with the effect of aggregate inclusion on pore structure. Before carrying out the porosimetry tests on concrete specimens (section 6.3), efforts were made to remove the coarse aggregates from the samples. The pore structure results are presented in rows 6 to 23 of Tables 6.2 to 6.5, for mortars of different cement/sand ratio, w/c ratio and four hydration periods and in rows 24 to 28 for concrete of 1:1½:1½ (cement:sand:gravel) ratio.

6.6.1 Total Porosity and Density

The total porosity and density for varying aggregate volume concentration in mortars and concrete are illustrated in Table 6.8 and Fig. 6.18. The aggregate volume concentration was calculated using equation 6.18[114]

$$Va = \left\{\frac{x}{\rho_a} \Big/ \left[\frac{x}{\rho_a} + \frac{1}{\rho_{hcp}}\right]\right\} \times 100 \qquad (6.18)$$

where x = aggregate/cement ratio by weight

ρ_a = dry density of aggregate gm/cc

ρ_{hcp} = dry density of hardened cement paste gm/cc

Va = aggregate volume concentration %

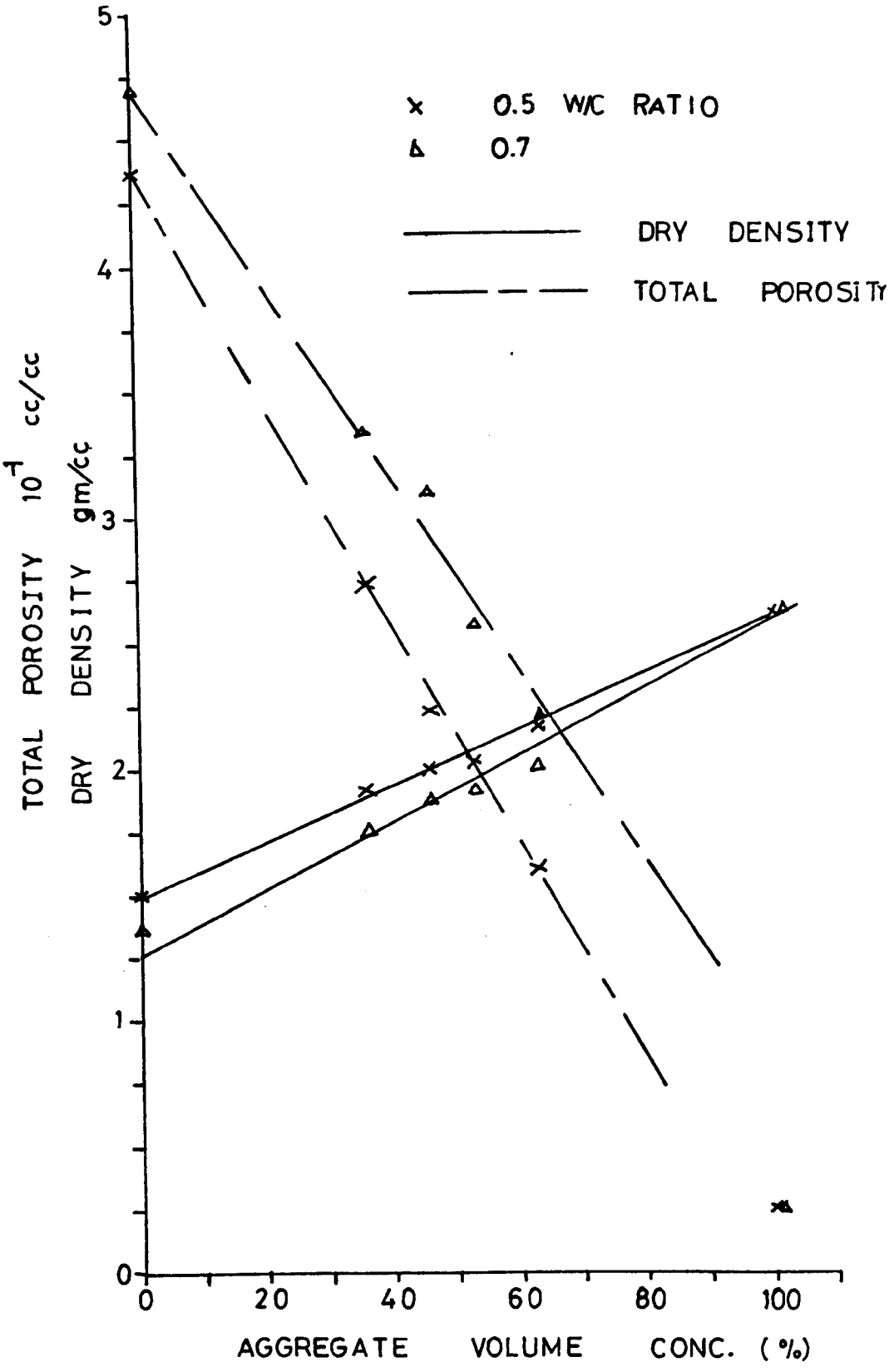

FIG 6.18 EFFECT OF AGGREGATE VOLUME CONCENTRATION ON DENSITIES AND TOTAL POROSITIES OF MORTARS

Aggregate porosity was determined using the absorption method as given by BS812:1967. It was however soaked for 5 days instead of 24 hours to achieve complete saturation. Results obtained reveal the following:

1. Porosity decreased while density increased with an increase in the aggregate volume concentration for the two w/c ratios considered and for all the curing periods. The increase/decrease appears to be linear especially within the range covered by the mortar specimens. As will be shown in Chapter 7, permeability increases with an increase in the aggregate volume and so it appears that a reduction in total porosity does not necessarily mean a reduction in permeability.

The effect of coarse aggregate inclusion on the pore parameters (rows 24-28 of Tables 6.2-6.5) is not apparent, probably because of the maximum aggregate size (6.30mm) which is in the lower limit of coarse aggregate and only just above the size of fine aggregate in normal concrete. There are obviously some inconsistencies in the structure of concrete in relation to mortar, and the discussion will be concentrated not on these inconsistencies but on the pore characteristics of mortar.

6.6.2 Pore Size Distributions

The pore size distributions for mortar of 1:1 cement/sand ratio, after 28 days curing, are shown in Fig. 6.19, and in Fig. 6.20 for 0.5 w/c ratio at varying periods of hydration. Figs. 6.21 and 6.22 illustrate distributions at varying aggregate inclusions for 0.5 and 0.7 w/c ratios respectively. Typical differential pores size distributions are shown in Figs. 6.23 and 6.24. The following observations are made.

1. As deduced for HCP, the total intruded pore volume increases with the w/c, but decreases with the period of hydration (Fig. 6.25) while the percentage pore volume, unintruded by mercury, with only minor exceptions, decreases with an increase in the w/c ratio and increases with the time of hydration (Tables 6.2-6.5). The probable reasons for this behaviour has been explained in section 6.5.

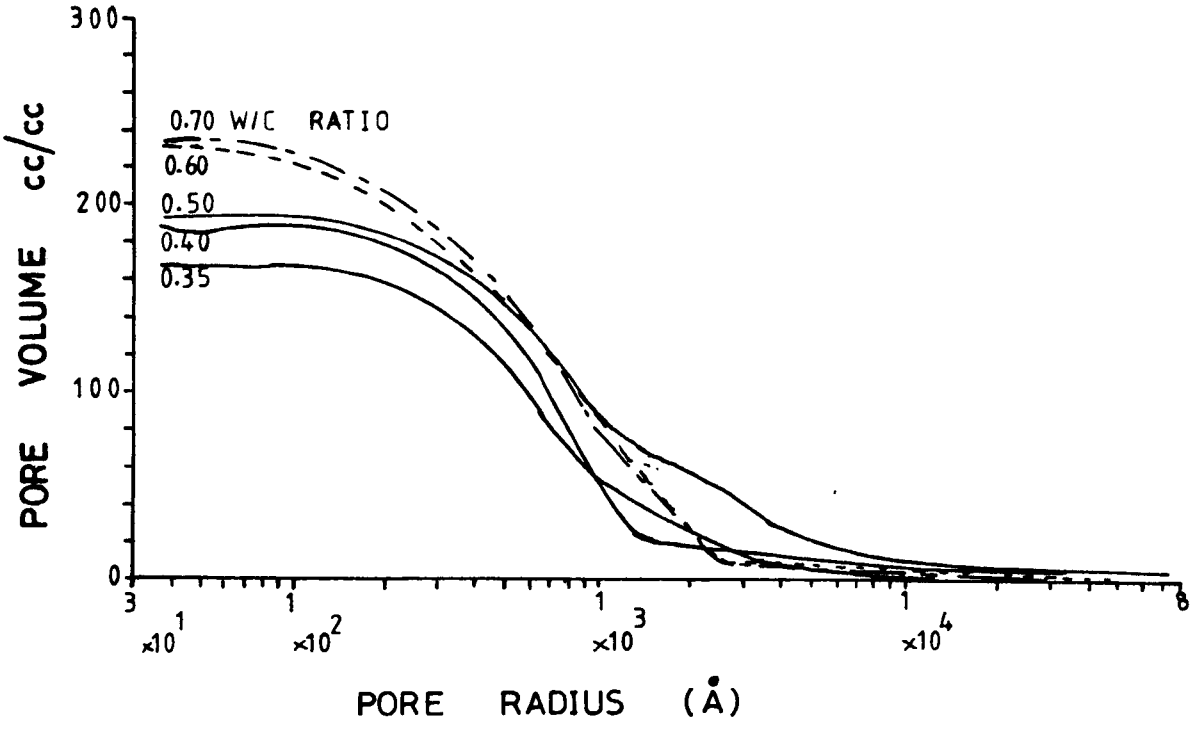

FIG 6.19 PORE SIZE DISTRIBUTIONS FOR MORTAR OF 1:1 CEMENT:SAND RATIO AT VARYING W/C RATIO, 28 DAYS CURING

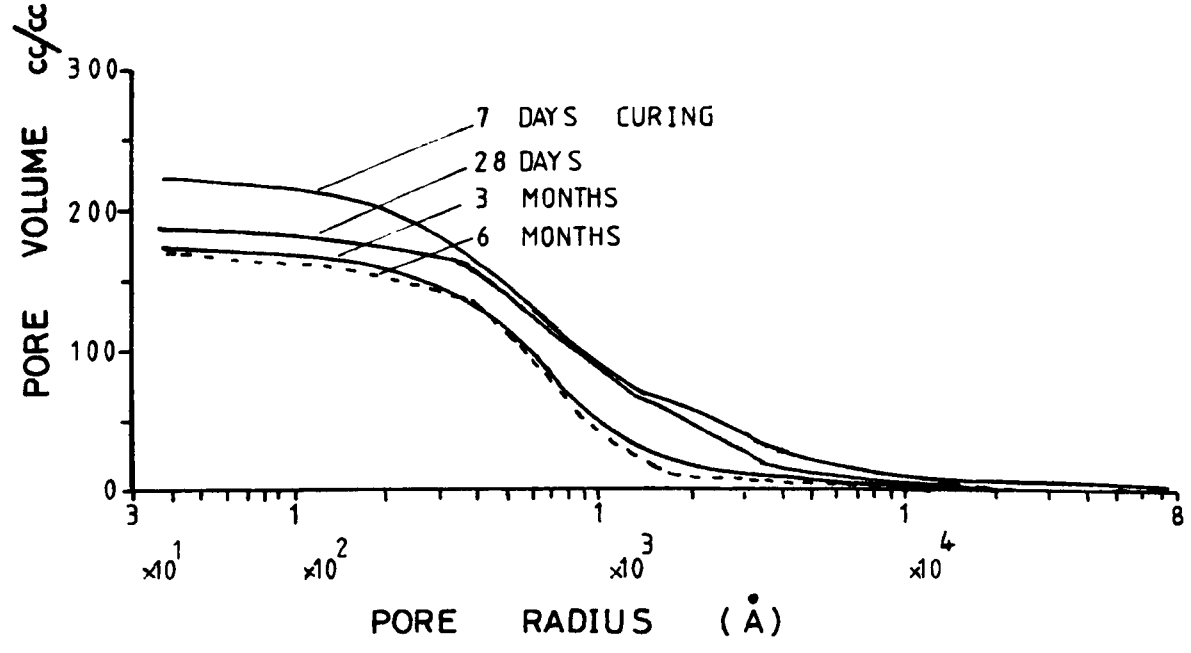

FIG 6.20 PORE SIZE DISTRIBUTIONS FOR MORTAR, 1:1 CEMENT:SAND RATIO AT VARYING PERIOD OF HYDRATION (0.5 W/C RATIO)

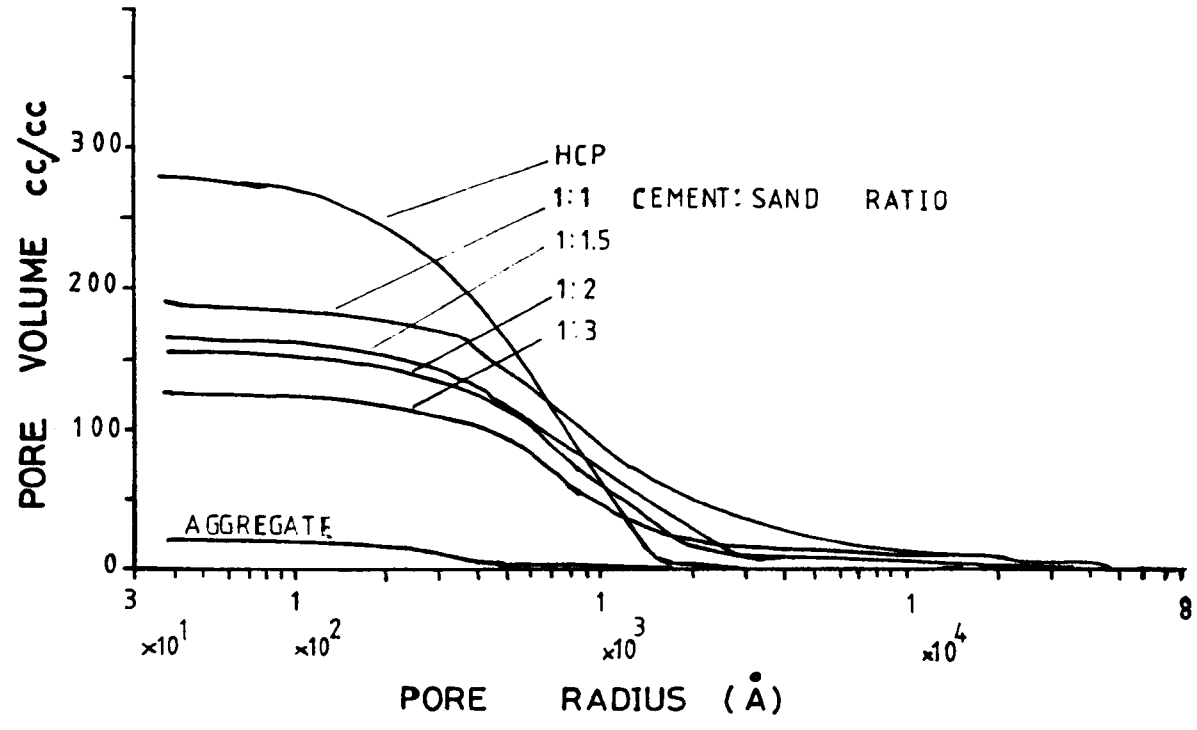

FIG 6.21 EFFECT OF AGGREGATE INCLUSIONS ON PORE SIZE DISTRIBUTIONS
(0.50 W/C RATIO , 28 DAYS CURING)

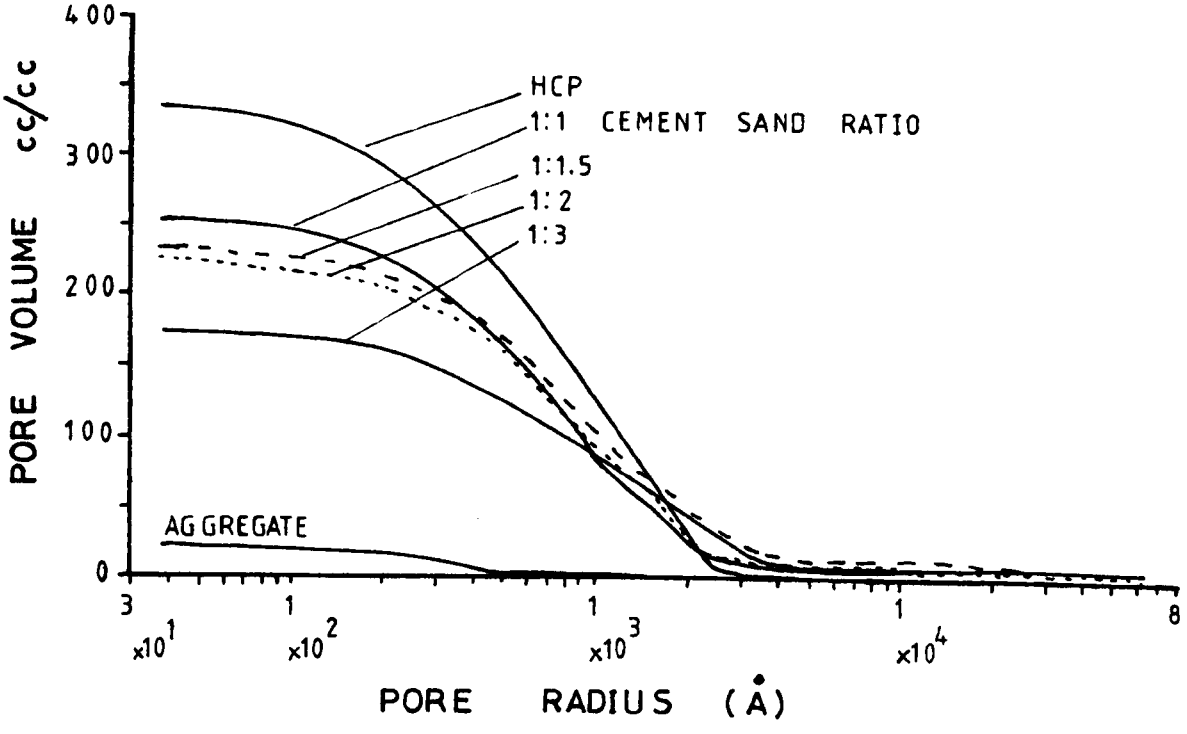

FIG 6.22 EFFECT OF AGGREGATE INCLUSIONS ON PORE SIZE DISTRIBUTIONS
(0.70 W/C RATIO , 28 DAYS CURING)

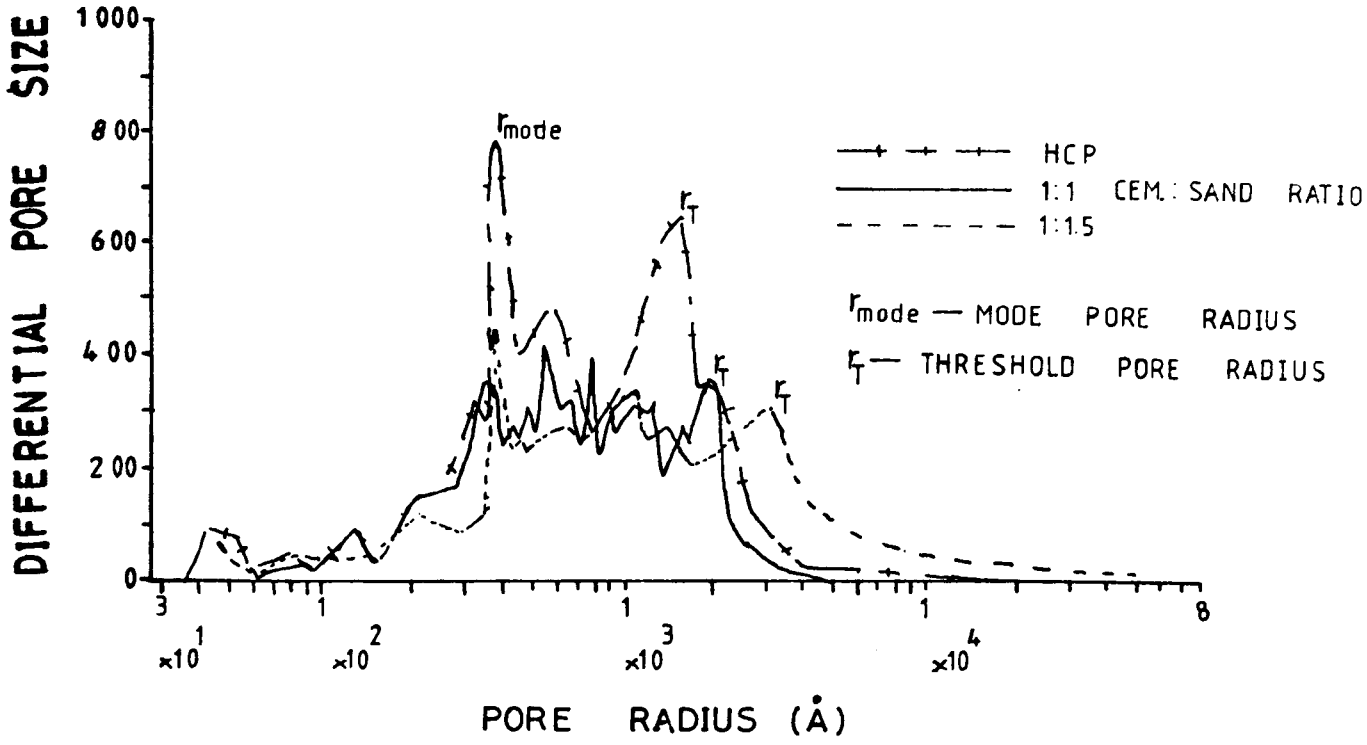

FIG 6 23 TYPICAL PLOT OF DIFFERENTIAL PORE SIZE FOR FOR VARYING AGGREGATE CONTENT, 0.5 W/C RATIO. 28 DAYS CURING

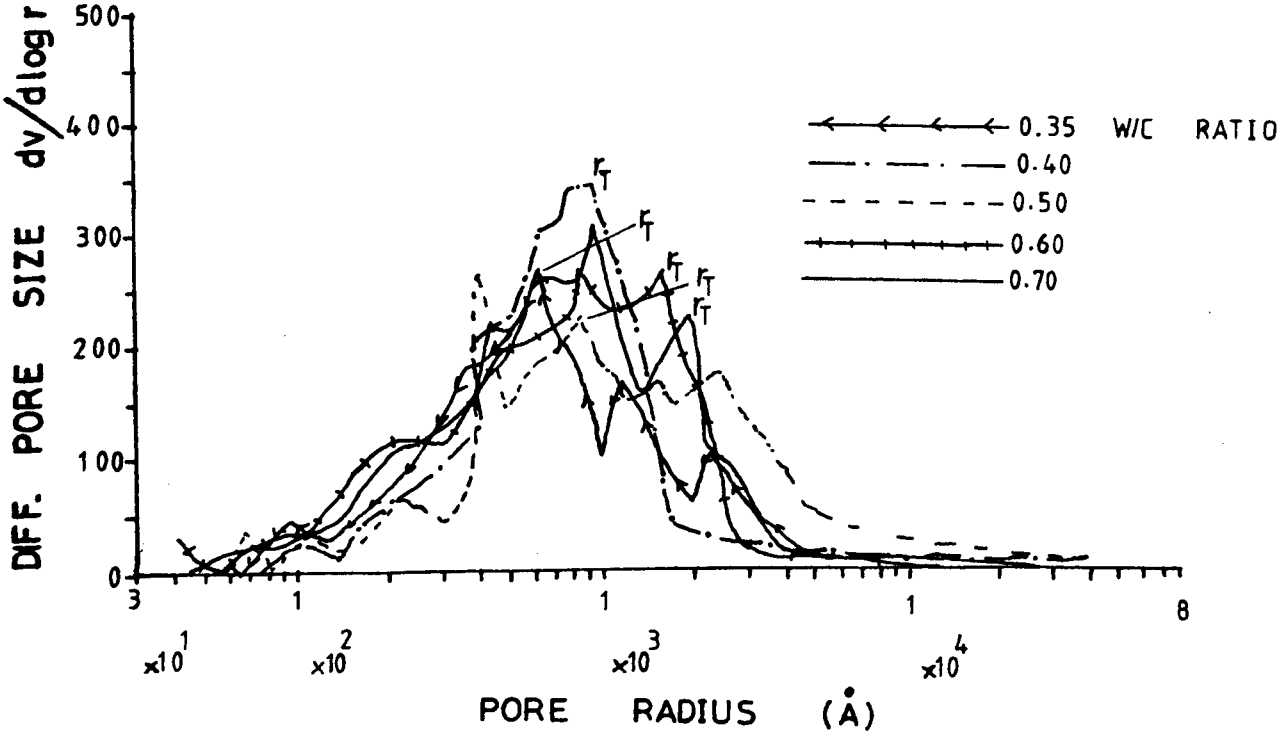

FIG 6.24 DIFFERENTIAL PORE SIZE FOR VARYING W/C RATIO (1:1 CEMENT: SAND RATIO 28 DAYS CURING)

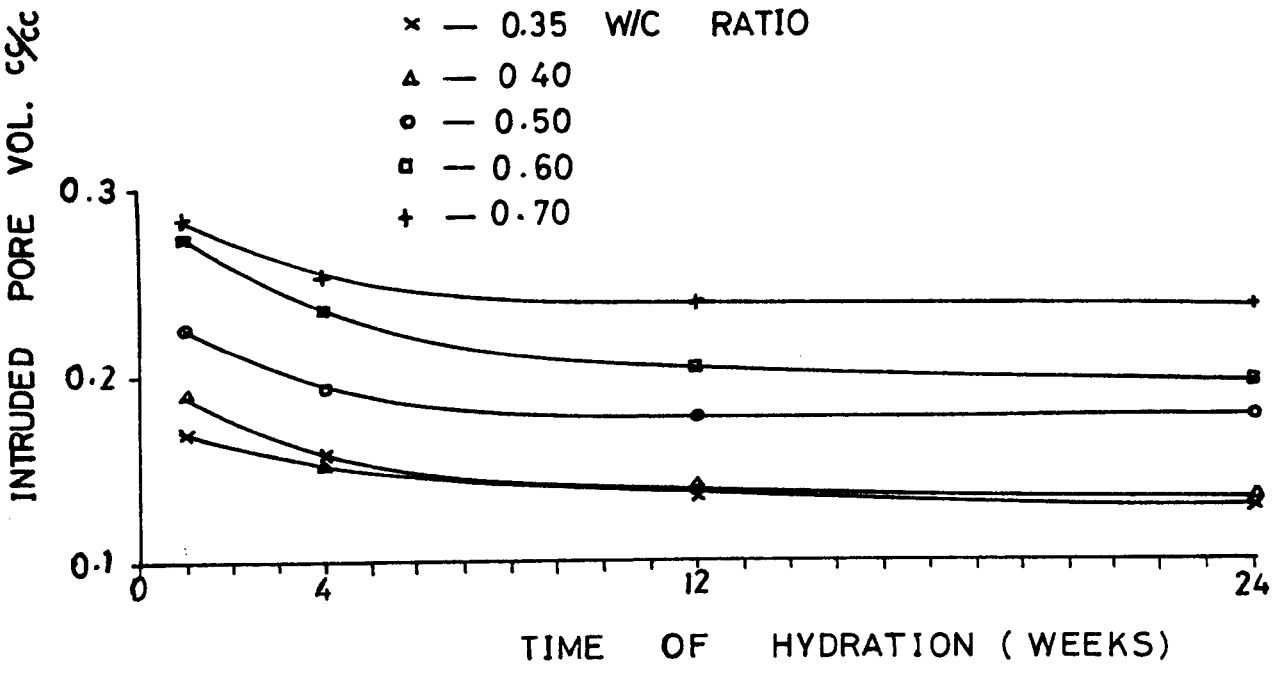

FIG 6.25 VARIATION OF TOTAL INTRUDED PORE VOLUME WITH TIME OF HYDRATION AND W/C RATIO FOR 1:1 CEMENT: SAND RATIO (MORTAR)

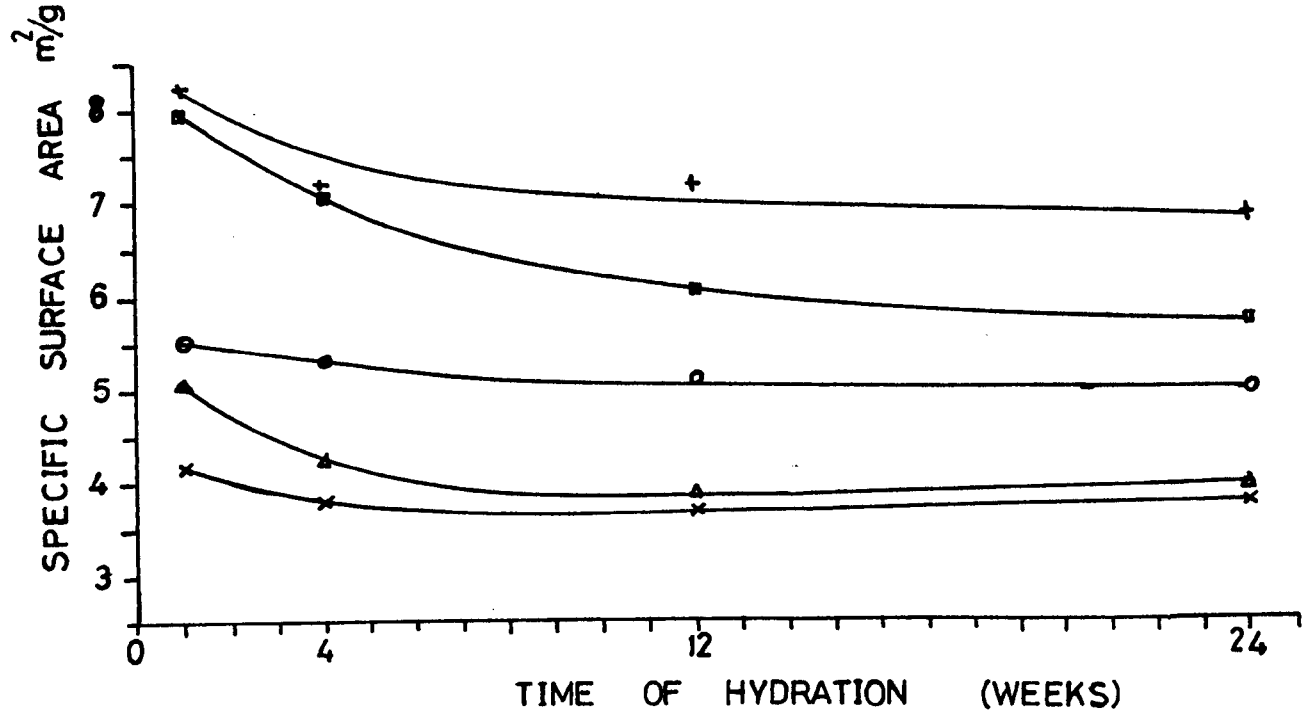

FIG 6.26 VARIATION OF SURFACE AREA OF MORTARS WITH TIME OF HYDRATION (1:1 CEMENT:SAND RATIO)

2. The total intruded pore volume decreases with increasing aggregate volume concentration (Figs. 6.21 and 6.22 and Table 6.8). For w/c = 0.50, after 28 days curing, intruded pore for HCP (1:0 cement/sand ratio) is 1.48 times intruded pore for 1:1 mortar which is 1.04 times that for 1:1½ mortar, which is 1.19 times that of 1:2 mortar which is also 1.21 times that of 1:3 (cement/sand ratio) mortar which is 6.02 times total intruded pore volume of aggregate. Aggregate tested was fine sand with properties shown in Table 3.3.

If a correction is made by determining the total pore volume, and intruded pore volume per volume of paste in the mortar, or concrete, using equation 6.19, the values of the corrected pores are shown in Table 6.8B below.

$$V_p' = \frac{V_p \times 100}{(100-V_A)} \qquad (6.19)$$

where V_p = total pore volume or intruded pore volume cc/cc

V_A = aggregate volume concentration (%)

V_p' = total pore volume per volume of paste in the mortar

		0.5 w/c RATIO		0.70 w/c RATIO	
CEMENT/ SAND RATIO	AGGREGATE VOL. CONC. %	TOTAL PORE VOL / VOL OF PASTE cc/cc	INTR PORE VOL / VOL OF PASTE cc/cc	TOT PORE VOL / VOL OF PASTE	INTR PORE VOL / VOL OF PASTE cc/cc
HCP	0.0	0.436	0.283	0.470	0.335
1:1	36.0	0.425	0.298	0.519	0.392
1:1½	46.0	0.415	0.339	0.578	0.481
1:2	53.0	0.443	0.328	0.545	0.498
1:3	63.0	0.432	0.343	0.584	0.470

TABLE 6.8B Total pore volume and intruded pore volume of mortars expressed as ratios of the volume of paste in the mortar specimen (28 days curing)

The table reveals that the total pore volume/vol of paste for 0.5 w/c remains practically constant for all the aggregate volume concentrations, and approximately equal to the total porosity of the HCP, while the intruded pore volume/volume of paste, increases with aggregate volume concentration. For 0.7 w/c ratio, both the intruded pore volume and the total pore volume per volume of paste in the mortar, increased with the aggregate volume concentration.

The higher total pore volume/volume of paste, suggests that either inclusion of aggregate creates more pores in the paste or that the pores in the aggregate were inclusive in the pores calculated. If more pores were created, then it was only done at higher w/c ratios (c.f. 0.5 w/c ratio results), but if aggregate pores were included, then equal values obtained for HCP and mortar at 0.5 w/c cannot be accounted for. The increase in the intruded pore volume with aggregate volume concentration suggests strongly that pores being intruded by mercury are not necessarily pores in the paste, but could include fissures and bond cracks of the aggregate-paste interface, and would mean that these micro-cracks increase with an increase in the aggregate volume concentration.

Since mortar is being treated as a unique material irrespective of its composition, further discussion is not intended on this ratio.

3. The sharp knee which characterized the threshold region of HCP, progressively flattens out as the aggregate volume concentration increases (Fig. 6.21 and 6.22) and the distributions become closer to that of the aggregate alone. This may mean that the changes in pore size distribution with aggregate inclusion follow an addition law in a mathematical model of the composites. The effect of the flattening in the threshold region is also clearly demonstrated in the differential pore size distribution of Fig. 6.23. While HCP showed two distinct peak values (r_{mode} and r_T), the peaks obtained from mortar are less distinct. Other minor peaks are

visible and the differential pore range tends to form a plateau. This phenomenon indicates that the threshold radius, important in the change of pore structure with w/c and hydration period for HCP may be less important for mortars. A possible explanation of the flattening of the threshold region and the minor peaks associated with it, is that aggregate tends to re-orientate the pore system of HCP.

6.6.3 Threshold Radius

The apparent flattening of the threshold region, makes the determination of the threshold radius highly subjective. Values obtained after very careful observations are shown in Tables 6.9 and 6.10 for varying periods of hydration, w/c ratio and aggregate inclusions. The following observations are made.

1. The threshold radius increases with w/c ratio and decreases with time of hydration as already deduced for HCP.

2. The influence of aggregate inclusions on threshold radius is not clear from the present results, but threshold radius may decrease with an increase in the aggregate volume concentration, when mortar mixes alone are considered. This does not agree with Nyame's[104] observation which was that it increases with volume concentration.

3. An important observation is that the threshold radius for mortar is generally higher than that of HCP, despite the relatively low value of the threshold radius for aggregate. This may mean that this radius in mortar, is linked to the aggregate/cement interface or even to fissures, rather than to the pore. Its continuous nature in HCP, as suggested by Winslow[80], may not be obtained in mortar, and where it is continuous, it may be highly tortuous. A possible relationship between this radius and permeability of mortar will be discussed in Chapter 8.

6.6.4 Specific Surface Area and Hydraulic Radius of Mortars

The surface area and hydraulic radii of those pores in mortars and concrete which are accessible to mercury at 2000 kgf/cm^2 are given in

		7 DAYS		28 DAYS		3 MONTHS		6 MONTHS	
Mortar Designation	w/c ratio	Threshold radius r_T (Å)	Mode pore radius r_{mode}	Threshold radius r_T	Mode pore radius r_{mode}	Threshold radius r_T	Mode pore radius r_{mode}	Threshold radius r_T	Mode pore radius r_{mode}
M35-1	0.35	6250	792	4375	653	2321	653	1583	653
M40-1	0.40	6250	601	4375	969	2750	601	2321	601
M50-1	0.50	8750	968	6250	406	3375	791	3375	517
M60-1	0.60	11250	2750	8750	1771	4375	857	4375	969
M70-1	0.70	22500	715	11250	857	4375	1035	3375	910

TABLE 6.9 Threshold pore radius and mode pore radius for mortar of varying w/c ratios (1:1 cement:sand ratio)

CEMENT SAND/RATIO	AGGREGATE VOL CONCEN. %	0.50 w/c RATIO		0.70 w/c RATIO	
		Threshold radius r_T (Å)	Mode pore radius r_{mode}	Threshold radius r_T	Mode pore radius r_{mode}
HCP	0.0	1771	455	2750	601
1:1	36.0	6250	406	11250	857
1:1.5	46.0	4375	601	8750	715
1:2	53.0	2750	1306	4375	2008
1:3	63.0	2750	601	3375	968
Aggregate	100.0	169	169	169	169
Concrete	63.0	2008	653	2750	653

TABLE 6.10 Threshold pore radius and mode pore radius for mortars of different aggregate volume concentrations (28 day curing

rows 6 to 28 of columns 6 and 7 in Tables 6.2 to 6.5. Table 6.11 and Figs. 6.26 and 6.27 illustrate the effect of w/c ratios and time of hydration on the surface area of mortar with 1:1 cement/sand ratio, and the following observations are made from the plots.

1. The surface areas of mortars are generally less than those of HCP, while the hydraulic radii are generally higher for all the corresponding w/c ratios and peridos of hydration studied. The surface area of HCP is about 3.1 to 4.54 times that of mortar of 1:1 cement/sand ratio, with the ratio increasing with an increase in the aggregate volume concentration.

2. The surface area of mortars decreases with an increase in the aggregate volume concentration and period of hydration (Fig. 6.28) and increases linearly with the w/c ratio (Fig. 6.27). A statistical analysis of the hydraulic radii, reveals that its values at various w/c ratio at a given hydration period and aggregate concentration do not vary by more than 10% (Tables 6.11 and 6.12). It follows therefore that hydraulic radius is independent of the w/c ratio. Also to a reasonable approximation, hydraulic radius (r_h) decreases with hydration but varies erratically with aggregate volume concentration as shown in Table 6.12.

The only other available information on the surface area and hydraulic radius of mortar determined using mercury porosimetry is that by Nyame[104]. He found that surface area decreased with aggregate content, but becomes practically constant after 55% aggregate volume concentration. His values range between $10 m^2/gm$ for 1:0.5 cement/sand ratio and $4 m^2/gm$ for 1:3 cement/sand ratio. These are within the range of values obtained in the present research.

6.7 Effect of Saturation with Oil on the Pore Parameters of HCP, Mortar and Concrete

The purpose of this section is to investigate the effect of oil

MORTAR DESIGNATION	w/c RATIO	7 DAYS		28 DAYS		3 MONTHS		6 MONTHS	
		SURFACE AREA m^2/g	HYDRAULIC RADIUS (Å)	SURFACE AREA m^2/g	HYDRAULIC RADIUS (Å)	SURFACE RADIUS m^2/g	HYDRAULIC RADIUS (Å)	SURFACE RADIUS m^2/g	HYDRAULIC RADIUS (Å)
M35-1	0.35	4.16	199.52	3.78	198.41	3.66	177.60	3.76	162.23
M40-1	0.40	5.05	192.08	4.22	177.78	3.89	172.24	3.94	162.43
M50-1	0.50	5.53	215.2	5.30	188.70	5.12	179.69	4.95	181.80
M60-1	0.60	7.95	193.71	7.04	184.66	6.01	181.36	5.70	178.95
M70-1	0.70	8.18	199.12	7.18	200.60	7.14	184.87	6.82	189.15
Mean			199.92		190.03		179.15		174.91
C.O.V.*			4.1%		4.48%		2.3%		6.17%

*C.O.V. = Coefficient of variation

TABLE 6.11 Surface area and hydraulic radius of mortars at varying w/c ratios (1:1 cement:sand ratio)

CEMENT/ SAND RATIO	AGGREGATE VOL CONC+ %	7 DAYS		28 DAYS		3 MONTHS		6 MONTHS	
		MEAN HYDRAULIC RADIUS Å	COEFF OF VARIATION %	MEAN HYDRAULIC RADIUS Å	COEFF OF VARIATION %	MEAN HYDRAULIC RADIUS Å	COEFF OF VARIATION %	MEAN HYDRAULIC RADIUS Å	COEFF OF VARIATION %
HCP	0.0	76.86	8.10	80.40	9.20	78.90	9.40	71.48	5.60
1:1	36.0	199.92	4.09	190.03	4.48	179.15	2.30	174.91	6.17
1:1.5	46.0	219.34	6.20	211.83	3.13	201.90	7.71	188.52	6.43
1:2	53.0	205.19	3.50	200.07	3.34	183.26	4.00	184.92	1.92
1:3	63.0	215.40	1.65	213.92	1.03	221.52	6.21	178.96	3.51
Concrete 1:1.5:1.5	63.0	212.41	9.88	203.18	9.06	189.57	6.84	176.30	8.10

Aggregate surface area = 0.97 m^2/g, Hydraulic radius = 85.1Å

+ The aggregate volume concentration is for mortar at 28 day curing 0.50 w/c ratio

TABLE 6.12 Hydraulic radius of mortars

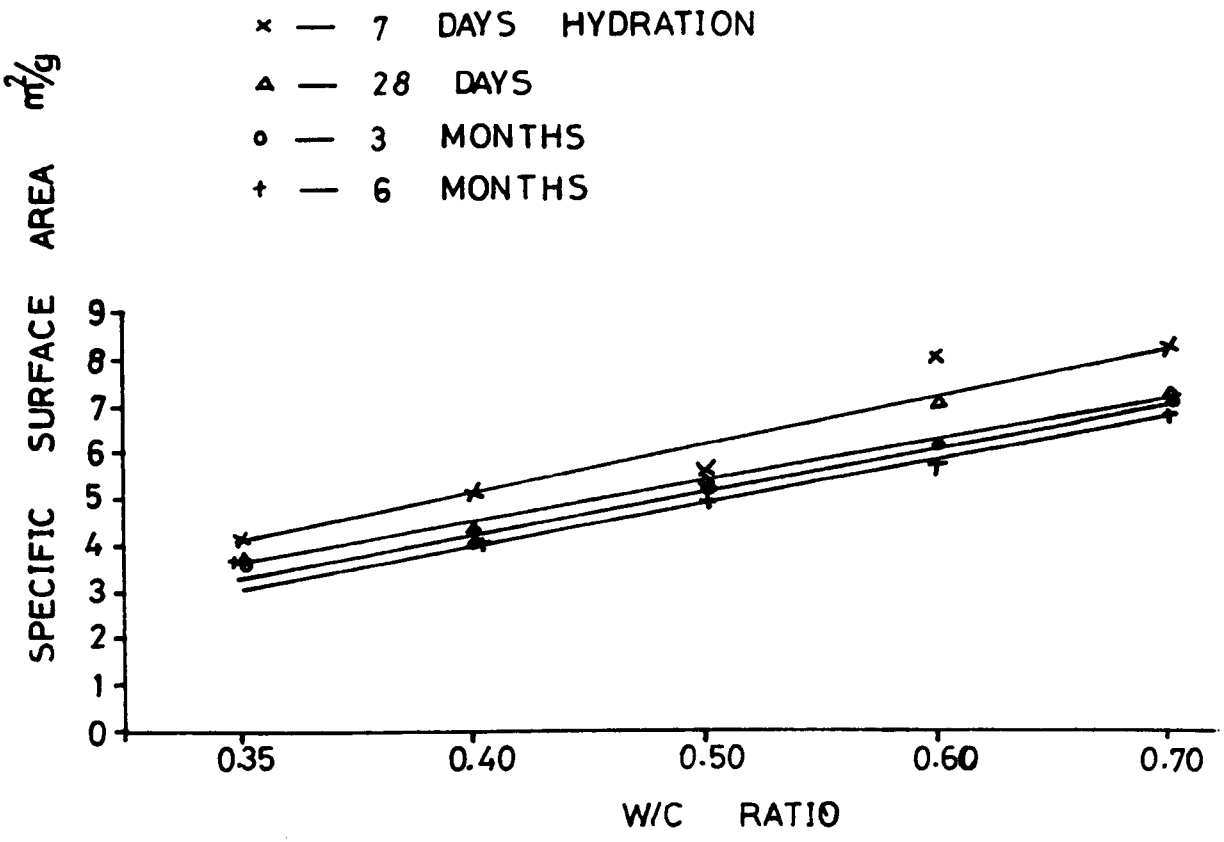

FIG 6.27 VARIATION OF SURFACE AREA OF MORTARS WITH W/C RATIO (1:1 CEMENT : SAND RATIO)

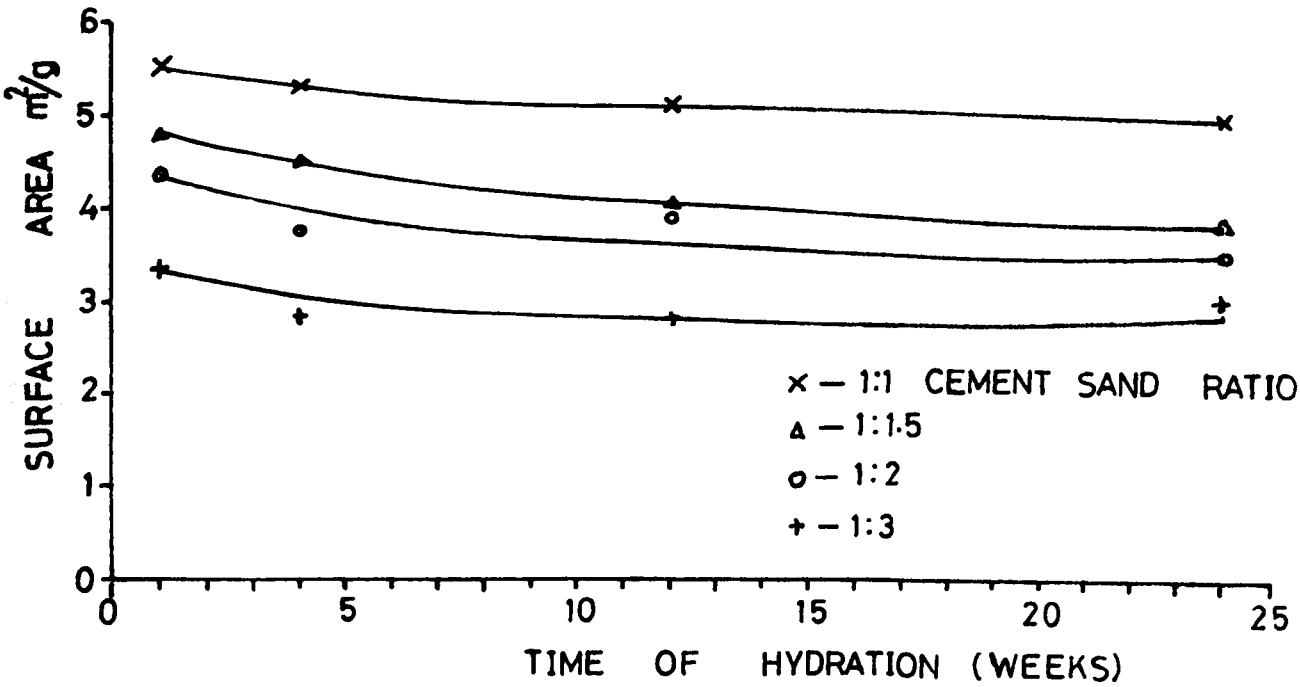

FIG 6.28 VARIATION OF SURFACE AREA OF MORTARS WITH TIME OF HYDRATION AND AGGREGATE VOLUME CONCENTRATION (0.50 W/C RATIO)

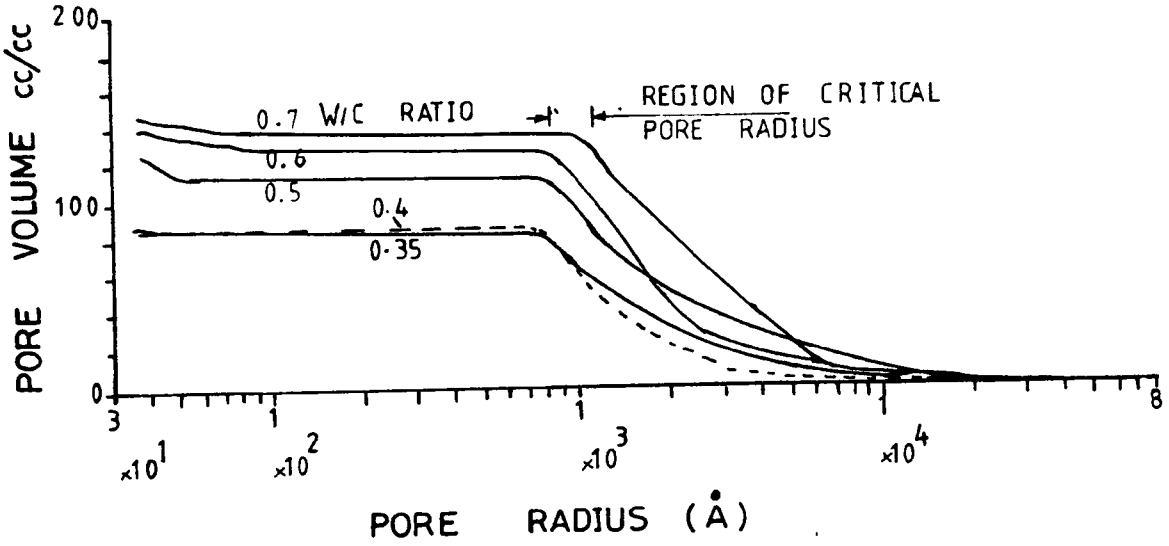

FIG 6 29 PORE SIZE DISTRIBUTIONS FOR NORTH SEA CRUDE OIL SATURATED MORTAR AT VARYING W/C RATIO (1:1 CEMENT: SAND RATIO 28 DAYS CURING)

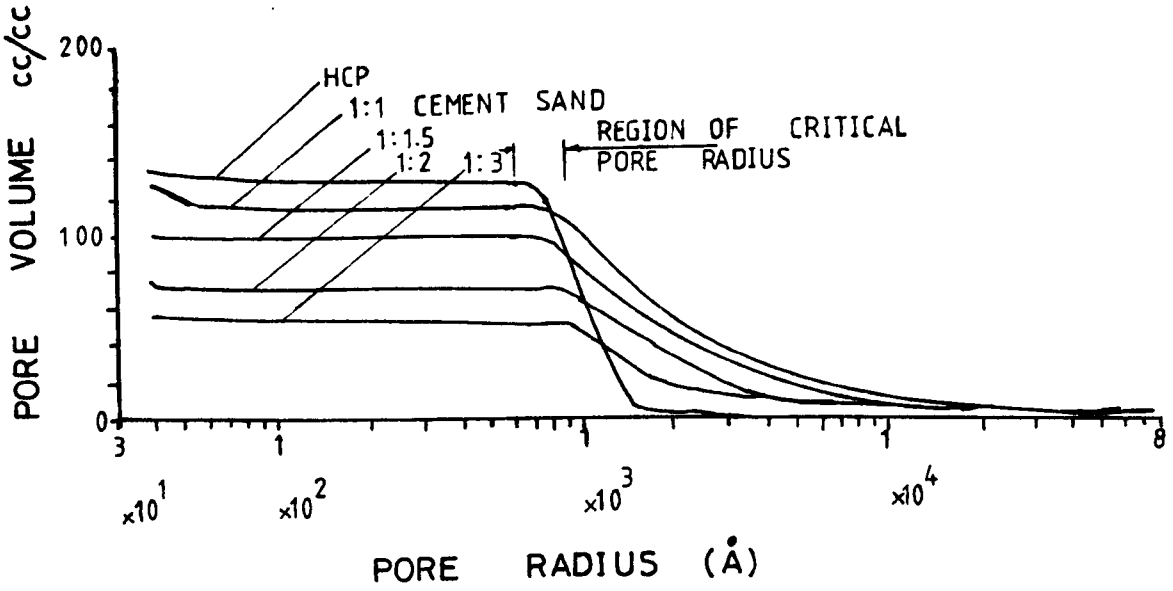

FIG 6.30 EFFECT OF NORTH SEA CRUDE OIL SATURATION OF MORTARS ON THEIR PORE SIZE DISTRIBUTIONS

(28 DAYS CURING, 0.50 W/C RATIO)

on the pore parameters of HCP, mortar and concrete. This is necessary, since the specimens were initially saturated in oil (section 3.8.2) before the permeability test is carried out. As a result, some of the pores may have been affected by the saturation, and therefore could effect the permeability result.

The 25mm cubes used for these tests were saturated in various types of oil (KU, NS, PA, DE and H_2O) and dried as described in section 6.2 prior to test. Resaturation in water was done on a control specimens. Pore parameters obtained after this treatment are shown in Tables 6.13 to 6.15 and are discussed briefly below.

6.7.1 Pore Size Distribution

Typical pore size distributions are shown in Fig. 6.29, for mortars of 1:1 cement/sand ratio, Fig 6.30 for HCP and mortar of various aggregate volume concentration, all saturated in the North Sea oil and Fig. 6.31, for HCP, saturated in the five liquid types. Fig. 6.32 shows typical differential pore size distribution for mortar (1:1 cement/sand) saturated in N.S. Observations from these plots are.

1. The distributions for HCP, mortar and concrete saturated in diesel (DE) and parafin (PA) took the usual distribution pattern for unsaturated specimen with increasing cumulative pore volume as the radius decreases, Fig. 6.33. For North Sea (NS), and Kuwait oil (KU) saturated specimens, the cumulative pore volume remained constant for all the radii less than 650 $\overset{0}{A}$. The differential pore size distribution (Fig. 6.32) clearly identified this radius. It is possible therefore that the wax in the crude oils, which does not exist in DE, PA and H_2O, closed all the pores less than 650 $\overset{0}{A}$. The minor peaks for pores <650 $\overset{0}{A}$ shown in Fig. 6.32, could be due to compression of the wax at very high intrusion pressures.

This revelation may be of great importance to saturated permeability studies, for it follows that as long as the HCP, mortar and

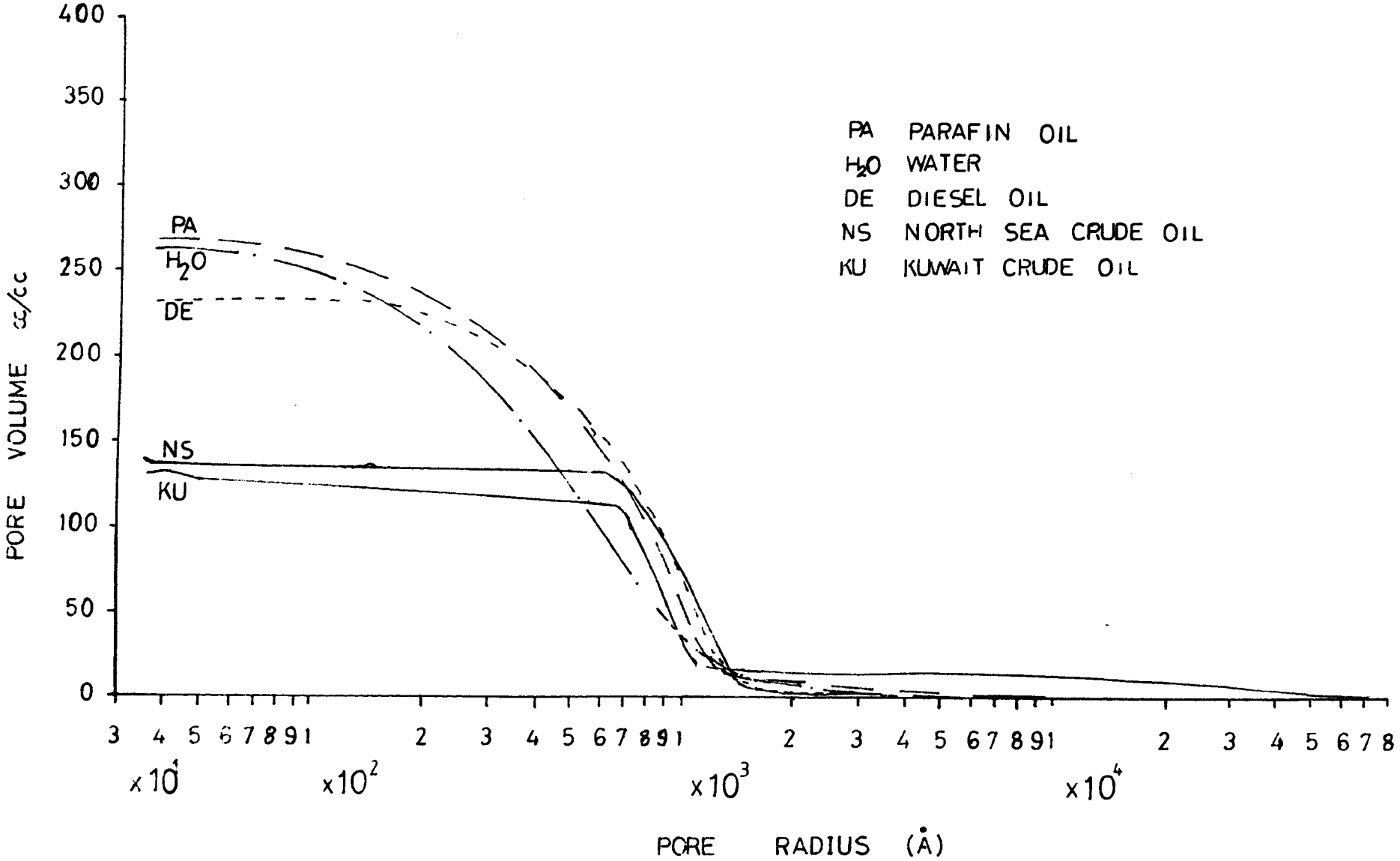

FIG 6.31 EFFECT OF DIFFERENT OIL SATURATIONS ON THE PORE SIZE DISTRIBUTIONS IN HCP (0.5 W/C RATIO, 28 DAYS CURING)

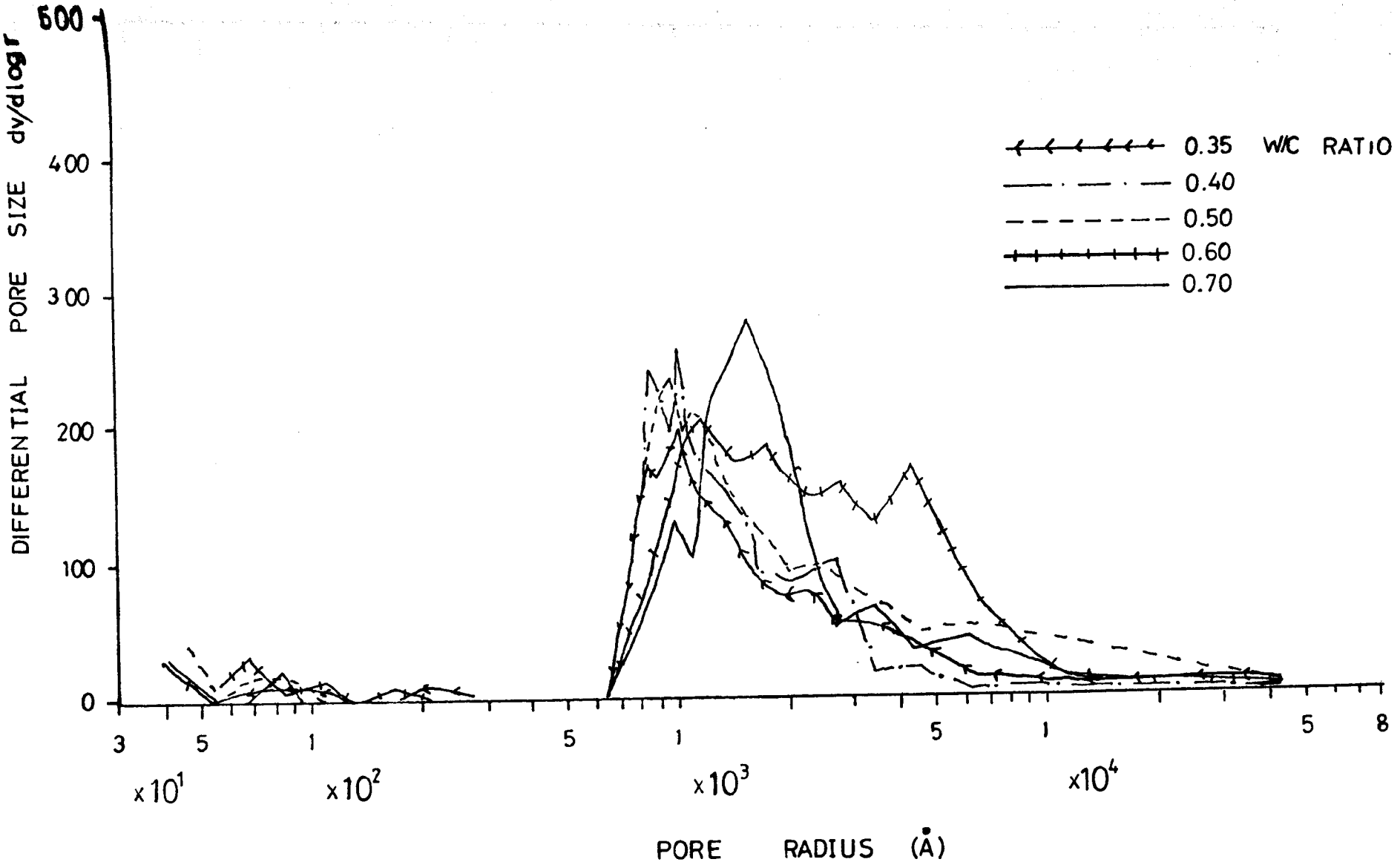

FIG 6.32 DIFFERENTIAL PORE SIZE DISTRIBUTIONS FOR NORTH SEA CRUDE OIL SATURATED MORTAR (1:1 CEMENT: SAND RATIO)
28 DAYS CURING

1	2		3		4	5	6	7	8	9	10
SPECIMEN DESIG NATION	TOTAL INTRUDED PORE VOLUME cc/cc	cc/g	PORE VOL >650Å cc/cc	cc/g	%AGE OF INTRUDED PORE >650Å	%AGE OF TOTAL PORE AREA >650Å	SURFACE AREA OF INTR. PORE m^2/g	SURFACE AREA OF PORES >650Å	HYDRAULIC RADII OF INTRUDED PORE Å	HYDRAULIC RADII OF PORES >650Å Å	THRESHOLD RADII Å
OP35	0.106	0.060	0.106	0.060	100.0	28.8	2.58	0.79	232.5	759.5	1036
OP40	0.115	0.070	0.112	0.068	97.4	28.7	3.30	0.98	212.1	693.4	1036
OP50	0.122	0.081	0.115	0.077	94.3	26.4	5.11	1.08	158.5	703.7	1583
OP60	0.122	0.087	0.117	0.083	95.9	25.7	5.76	1.33	151.0	624.1	1770
OP70	0.136	0.100	0.130	0.095	95.6	27.66	6.12	1.66	163.4	572.3	2008
M35-1	0.090	0.043	0.085	0.041	94.4	44.32	1.48	0.53	290.5	773.6	3375
M40-1	0.087	0.043	0.087	0.043	100.0	39.71	2.44	0.63	176.2	682.5	4375
M50-1	0.127	0.065	0.114	0.059	90.0	49.29	3.25	0.67	200.0	880.6	6250
M60-1	0.142	0.080	0.130	0.062	91.54	45.20	2.94	0.71	272.1	873.2	6250
M70-1	0.149	0.083	0.137	0.074	91.9	34.36	4.64	0.90	178.9	822.2	11250
M35-1.5	0.078	0.037	0.076	0.036	97.4	43.2	1.28	0.46	289.1	782.6	2750
M40-1.5	0.082	0.039	0.079	0.038	96.3	41.1	1.29	0.59	302.3	644.1	3350
M50-1.5	0.096	0.048	0.094	0.047	97.9	42.0	2.42	0.61	198.3	770.5	3350
M60-1.5	0.116	0.060	0.113	0.058	97.4	41.5	2.83	0.68	212.0	852.9	4815
M70-1.5	0.123	0.066	0.121	0.065	98.4	38.8	3.93	0.84	167.9	773.8	8750
M35-2	0.064	0.030	0.063	0.029	98.4	41.15	0.82	0.35	365.9	828.6	2321
M40-2	0.074	0.036	0.071	0.035	95.9	46.67	1.06	0.40	339.6	875.0	2750
M50-2	0.084	0.040	0.082	0.039	97.6	40.38	1.08	0.54	370.4	722.2	2750
M60-2	0.110	0.056	0.106	0.053	96.4	44.01	1.52	0.63	368.4	841.3	3350
M70-2	0.112	0.060	0.108	0.057	96.4	41.07	1.82	0.80	329.7	712.5	6250
M50-3	0.056	0.027	0.053	0.025	92.9	35.53	0.57	0.31	473.7	806.5	2008
M60-3	0.066	0.033	0.062	0.031	93.9	31.88	0.83	0.37	397.6	837.8	2321
M70-3	0.076	0.038	0.072	0.036	94.7	33.39	0.88	0.43	431.8	837.2	3375
C40-1.5	0.077	0.034	0.069	0.031	90.80	42.50	1.29	0.37	263.6	837.8	2008
C50-1.5	0.086	0.039	0.084	0.038	97.67	48.65	1.34	0.46	291.0	826.1	2321
C60-1.5	0.097	0.045	0.089	0.041	91.75	45.32	1.70	0.50	264.7	820.0	2750
C70-1.5	0.124	0.059	0.119	0.056	95.97	52.43	2.23	0.66	264.6	848.5	4375

TABLE 6.13 Test results for North Sea oil saturated HCP, mortar and concrete

1	2		3		4	5	6	7	8	9	10
SPECIMEN DESIG NATION	TOTAL INTRUDED PORE VOLUME		PORE $_0$ VOL >650Å		%AGE OF INTRUDED $_0$ PORE >650Å	%AGE OF TOTAL PORE $_0$ AREA >650Å	SURFACE AREA OF INTR. PORE m^2/g	SURFACE AREA OF PORES $_0$ >650Å	HYDRAULIC RADII OF INTRUDED PORE $_0$ Å	HYDRAULIC RADII OF PORES $_0$ >650Å $_0$ Å	THRESHOLD RADII Å
	cc/cc	cc/g	cc/cc	cc/g							
KUWAIT CRUDE OIL SATURATED											
OP40	0.122	0.074	0.113	0.068	92.62	28.49	7.47	1.08	99.1	629.6	969
OP50	0.132	0.088	0.114	0.076	86.36	24.19	8.55	1.42	102.9	535.2	1036
OP60	0.136	0.096	0.124	0.088	92.65	27.10	10.44	1.58	92.0	557.0	1113
OP70	0.145	0.106	0.133	0.097	91.72	26.39	9.90	1.78	107.1	544.9	1202
M40-1.5	0.086	0.041	0.079	0.038	91.86	41.12	1.50	0.41	256.3	926.8	2321
M50-1.5	0.096	0.048	0.090	0.045	93.75	39.87	1.69	0.60	284.0	750.0	2750
M60-1.5	0.111	0.058	0.107	0.055	96.40	38.95	1.85	0.63	313.5	873.0	4375
M70-1.5	0.130	0.069	0.126	0.067	96.92	43.51	2.22	0.93	310.8	720.4	6250
C40-1.5	0.074	0.033	0.067	0.030	90.54	42.45	1.32	0.35	250.0	857.1	2008
C50-1.5	0.087	0.040	0.084	0.038	96.55	49.43	1.34	0.45	298.5	844.4	2321
C60-1.5	0.096	0.045	0.086	0.040	89.58	43.38	1.68	0.49	267.9	816.3	3375
C70-1.5	0.124	0.059	0.118	0.056	95.16	61.82	2.32	0.66	254.3	848.5	4375
DRIED AND RESATURATED IN WATER											
OP40	0.224	0.136	0.098	0.059	43.76	24.56	17.35	1.22	78.4	483.6	1201
OP50	0.264	0.175	0.102	0.068	38.64	23.33	26.12	1.27	75.0	535.4	1306
OP60	0.283	0.201	0.108	0.077	38.16	23.34	26.95	1.44	86.1	534.7	1432
OP70	0.326	0.238	0.121	0.088	37.12	26.12	33.33	1.54	71.4	571.4	1583
M40-1.5	0.154	0.074	0.076	0.037	49.35	39.71	3.99	0.50	185.5	740.0	2008
M50-1.5	0.177	0.089	0.077	0.039	43.50	34.55	6.28	0.60	141.7	650.0	2321
M60-1.5	0.210	0.108	0.095	0.049	45.24	34.88	7.59	0.73	142.3	671.2	3375
M70-1.5	0.236	0.126	0.106	0.056	44.92	33.83	9.60	1.00	131.3	660.0	6250
C40-1.5	0.120	0.053	0.048	0.021	40.0	31.31	3.21	0.31	165.1	677.4	1113
C50-1.5	0.130	0.059	0.061	0.028	46.90	36.40	3.69	0.44	159.9	636.4	1770
C60-1.5	0.137	0.064	0.067	0.031	48.90	37.92	4.33	0.46	147.8	673.9	2008
C70-1.5	0.144	0.068	0.074	0.035	51.4	38.25	4.06	0.54	167.5	648.1	3375

TABLE 6.14 Test results for Kuwait crude oil and dried and resaturated in water (HCP, mortar and concrete) specimens

1	2		3		4	5	6	7	8	9	10
SPECIMEN DESIGNATION	TOTAL INTRUDED PORE VOLUME cc/cc	cc/g	PORE VOL >650Å cc/cc	cc/g	%AGE OF INTRUDED PORE >650Å	%AGE OF TOTAL PORE AREA >650Å	SURFACE AREA OF INTR. PORE m^2/g	SURFACE AREA OF PORES >650Å	HYDRAULIC RADII OF INTRUDED PORE Å	HYDRAULIC RADII OF PORES >650Å Å	THRESHOLD RADII Å
DIESEL SATURATED											
OP40	0.216	0.131	0.154	0.094	71.29	39.02	10.10	1.70	129.7	552.9	910
OP50	0.233	0.156	0.166	0.110	72.53	32.14	15.31	2.08	101.9	528.8	969
OP60	0.288	0.205	0.174	0.123	60.42	37.65	19.71	2.16	104.0	569.4	1113
OP70	0.307	0.224	0.180	0.131	58.63	38.96	19.96	2.41	112.2	543.6	1202
M40-1.5	0.143	0.069	0.101	0.049	70.63	52.57	3.53	0.76	195.5	644.7	2321
M50-1.5	0.158	0.079	0.108	0.054	68.35	48.71	4.21	0.86	187.6	627.9	2750
M60_1.5	0.182	0.094	0.131	0.068	71.98	48.11	4.52	1.05	208.0	647.6	4375
M70-1.5	0.216	0.115	0.159	0.085	73.61	50.83	4.94	1.31	232.8	648.9	6250
C40-1.5	0.108	0.048	0.051	0.022	47.22	47.15	2.48	0.44	193.5	500.0	2008
C50-1.5	0.117	0.053	0.071	0.032	60.68	42.20	2.40	0.58	220.8	551.7	2321
C60-1.5	0.128	0.060	0.075	0.035	58.59	42.50	2.92	0.64	205.5	546.9	3375
C70;-.5	0.152	0.072	0.103	0.049	67.76	49.85	3.25	0.77	221.5	636.4	6250
PARAFIN SATURATED											
OP40	0.229	0.133	0.133	0.081	58.08	33.72	12.18	1.60	66.50	506.3	910
OP50	0.263	0.175	0.146	0.097	55.51	33.47	23.85	1.87	73.4	518.7	969
OP60	0.281	0.199	0.152	0.107	54.09	33.19	26.22	2.01	75.9	532.3	1306
OP70	0.307	0.224	0.164	0.120	53.42	35.64	25.49	2.20	87.9	545.5	1770
M40-15	0.160	0.077	0.097	0.047	60.62	50.65	4.23	0.70	182.0	671.4	2750
M50-1.5	0.167	0.084	0.100	0.050	59.88	44.43	5.07	0.83	165.7	602.4	2750
M60-1.5	0.213	0.110	0.121	0.068	56.80	44.33	5.56	1.09	197.8	623.9	3375
M70-1.5	0.251	0.134	0.142	0.086	56.57	45.57	7.01	1.42	191.2	605.6	6250
C40-1.5	0.114	0.050	0.057	0.025	50.00	37.66	3.14	0.42	159.2	595.2	2321
C50-1.5	0.128	0.058	0.066	0.030	51.56	38.94	3.79	0.52	153.0	576.9	2750
C60-1.5	0.140	0.065	0.072	0.033	51.43	40.89	3.70	0.60	175.7	550.0	2750
C70-1.5	0.170	0.081	0.91	0.043	53.52	47.36	4.46	0.71	181.6	605.5	6250

TABLE 6.15 Test results for diesel and parafin oil saturated HCP mortar and concrete

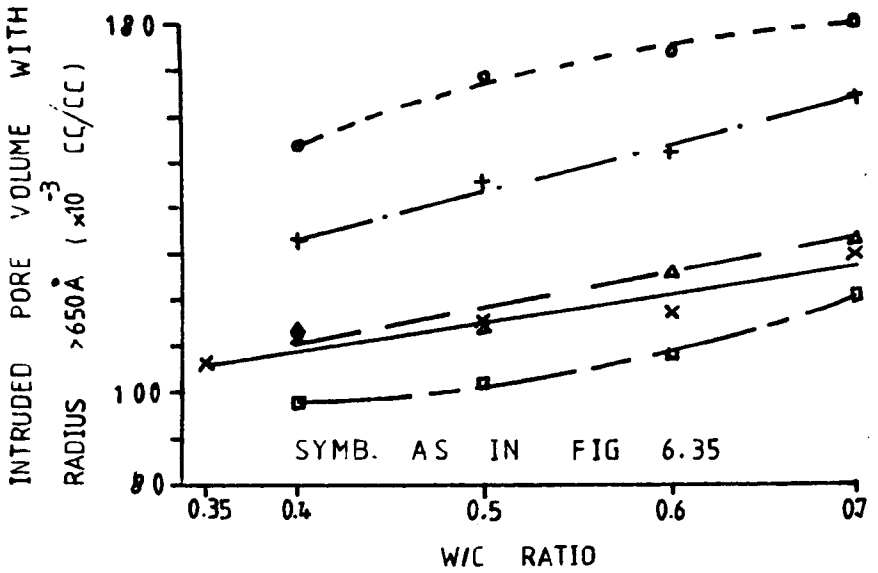

FIG 6.33 VAR. OF INTR. PORE VOL. OF RAD. >650Å WITH W/C RATIO FOR HCP

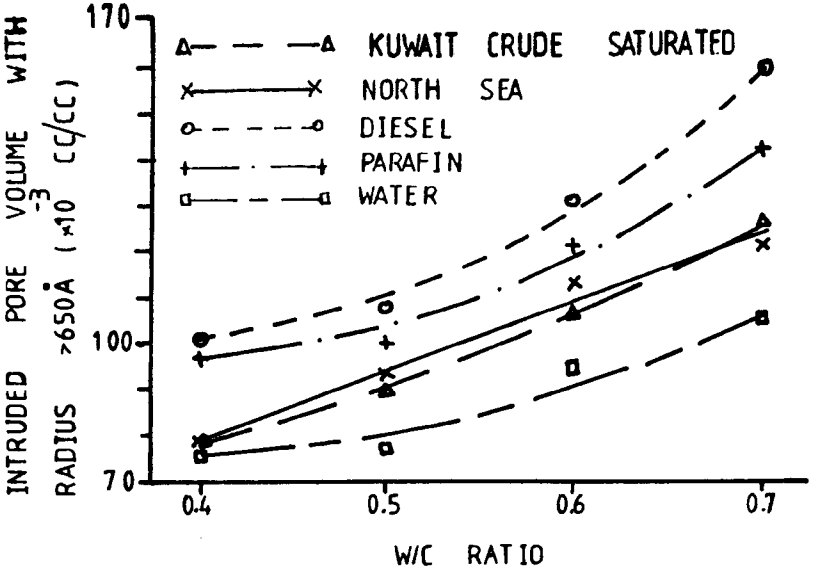

FIG 6 35 VARIATION OF INTR. PORE VOLUME OF RADIUS >650Å WITH W/C RATIO FOR MORTAR

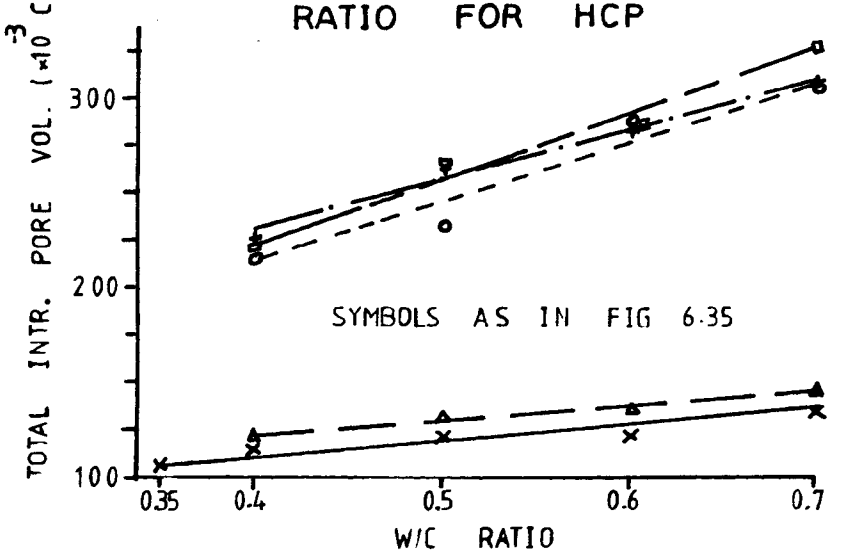

FIG 6.34 VARIATION OF TOTAL INTRUDED PORE VOLUME WITH W/C RATIO FOR DIFF. LIQUID SATURATIONS (HCP)

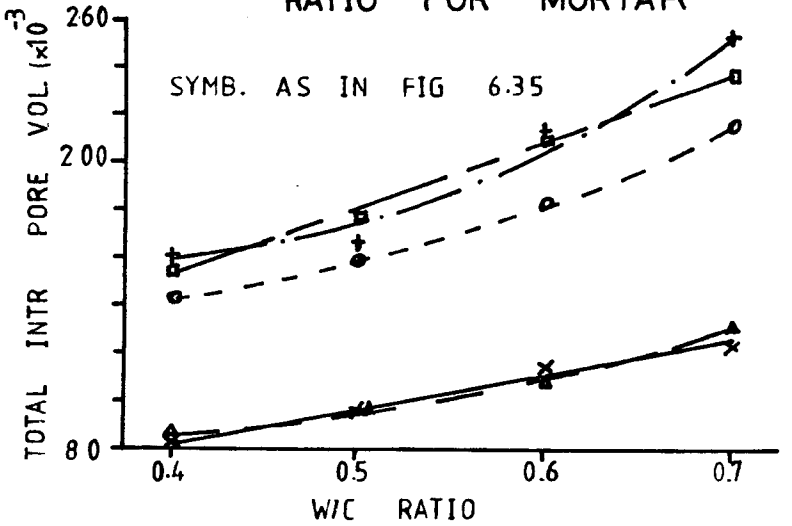

FIG 6.36 AS GIVEN IN FIG 6.34 BUT FOR MORTAR OF 1:1 CEMENT:SAND RATIO

concrete specimens were saturated in the crude oil before the permeability tests, pores in the specimens <650 $\overset{0}{A}$ have negligible effect on the crude oil permeability through them. This pore radius of 650 $\overset{0}{A}$ is therefore called the critical pore radius P_{cr}, for crude oil permeability. The pore parameters, such as surface area and hydraulic radius, associated with pores ≥ 650 $\overset{0}{A}$, will be investigated further in this section, while the influence of these parameters on permeability is studied in Chapter 8.

It has been reported[182] that impurities can increase or decrease the contact angle between mercury and pore walls. This is expected to shift the pore size distribution, but not change the size of pores penetrated by the mercury. Therefore the total closing of pores <650 $\overset{0}{A}$, must have been brought about by the oil as discussed earlier.

2. Effect of the oil saturation on the distribution before the critical pore radius is not apparent. The usual sharp knee at the threshold region of HCP and the flattening of the threshold region of mortar are observed. These distributions have been discussed earlier in section 6.5.2.4

6.7.2 Total Intruded Pore Volume and Intruded Volume of Pores with radii $>P_{cr}$

The total intruded pore volume and the volume of pores with radii greater than 650 $\overset{0}{A}$ are given in columns 2 and 3 respectively of Tables 6.13 to 6.15 for NS, KU, DE, PA and H_2O saturated specimens and in Fig.6.33-6.35 The observations are discussed below.

1. Table A below gives the range of ratios of total intruded pores of HCP, mortar and concrete saturated in NS, KU, DE and PA in relation to water resaturated specimens which were the control specimens. Table B, gives the ratio of total pores >650 $\overset{0}{A}$ for these oil saturated specimens in relation to water saturated.

Table A, shows that saturation in North Sea and Kuwait crude oil

	H_2O/H_2O	KU/H_2O	NS/H_2O	DE/H_2O	PA/H_2O
HCP	1.0	0.44-0.54	0.42-0.51	0.88-1.02	0.94-1.06
Mortar (1:1.5)	1.0	0.53-0.56	0.52-0.54	.92-0.93	.94-1.06
Concrete (1:1½:1½)	1.0	0.62-0.86	0.63-0.86	0.90-1.06	0.95-1.18

TABLE A: Ratio of total intruded pore volume

	H_2O/H_2O	KU/H_2O	NS/H_2O	DE/H_2O	PA/H_2O
HCP	1.0	1.10-1.15	1.07-1.14	1.49-1.61	1.36-1.43
Mortar (1:1½)	1.0	1.04-1.19	1.04-1.22	1.33-1.40	1.27-1.34
Concrete (1:1½:1½)	1.0	1.28-1.59	1.33-1.61	1.06-1.39	1.07-1.23

TABLE B: Ratio of pores with radii >650 $\mathring{A}$

greatly reduced the total intruded pore volume, probably as a result of blocking of pores <650 $\mathring{A}$ (section 6.7.1). The Diesel and Parafin saturation appear not to affect the total intruded pore volume. Pores with radii >650 $\mathring{A}$ have ratios greater than 1 for all types of oil saturation, in relation to the water saturated specimens (Table B). This means that hydration, which continued in specimens under water, subdivided and reduced the larger pore sizes but that hydration did not occur in specimens in oil. The fact that DE and PA have much lower ratios for pores up to 37 $\mathring{A}$ than for pores >650 $\mathring{A}$, appear to suggest that some unidentified properties of diesel and parafin affects the volume of finer pore sizes, or that water resaturated specimens had a greater number of pores between 37 $\mathring{A}$ to 650 $\mathring{A}$ to match the reduction of pores >650 $\mathring{A}$.

2. The fact that HCP has a lower percentage of pores >650 $\mathring{A}$ (between 24 to 36%) than mortar (38-50%) and concrete (36-53%), column 5 of Tables 6.13 to 6.15, shows that mortar and concrete have coarser pores than HCP.

3. The total intruded pore volume and pores of radii >650 $\overset{0}{A}$, were both found to increase with an increase in w/c ratio as shown in Figs. 6.33 and 6.34 for HCP, Figs. 6.35 and 6.36 for mortar of 1:1 cement/sand ratio. Water saturated specimens, retained the usual non-linear increase in the total intruded pore volume while other specimens saturated in different types of oil, increased erratically especially for HCP. For mortar, the intruded pore volume of pores of radii >650 $\overset{0}{A}$ increased non-linearly with an increase in the w/c ratio. The shape of the curves resemble that of permeability versus w/c ratio (Chapter 7), and may be important in determining the pore parameters that most influence permeability.

The influence of aggregate inclusion on the pores of radii >650 $\overset{0}{A}$ was studied using North Sea oil saturated specimens and the result is shown in Fig. 6.37. The pore volume of pores with radii >650 $\overset{0}{A}$ reduces rapidly when aggregate is added, and the rate of reduction is almost constant with the range of mortars studied. It has been shown in section 6.6 that aggregate inclusion reduces the total intruded pore volume. It appears that saturation in North Sea crude oil does not influence the behaviour of pores >650 $\overset{0}{A}$ in relation to aggregate inclusion, but only closes pores <650 $\overset{0}{A}$ as earlier deduced.

The two previous paragraphs reveal that an increase in w/c ratio, increases pores of radii >650 $\overset{0}{A}$, while an increase in aggregate volume, reduces the pores of radii >650 $\overset{0}{A}$. In relation to permeability (Chapter 7), increase in w/c ratio or aggregate value increases the permeability. This suggests that change in those pores above the critical pore radius, produced by changes in w/c ratio, relates to permeability, while the change produced by aggregate inclusion may not.

6.7.3 Specific Surface Area

The surface area of the total intruded pores and intruded pores with radii >650 $\overset{0}{A}$ are shown in columns 6 and 7 of tables 6.13 to 6.15 for

various liquid saturations. Table C gives the ratio of surface area of the intruded pores for HCP, mortar and concrete saturated in NS, KU, DE and PA to that saturated in water, while Table D gives the ratio of surface area for pores of radii >650 $\overset{0}{A}$.

	H_2O/H_2O	KU/H_2O	NS/H_2O	DE/H_2O	PA/H_2O
HCP	1.0	0.30-0.43	0.18-0.21	0.58-0.75	0.70-0.97
Mortar (1:1½)	1.0	0.23-0.40	0.32-0.41	0.51-0.88	0.73-1.06
Concrete (1:1½:1½:)	1.0	0.36-0.57	0.36-0.55	0.65-0.80	0.85-1.10

TABLE C Ratio of surface area of intruded pores

	H_2O/H_2O	KU/H_2O	NS/H_2O	DE/H_2O	PA/H_2O
HCP	1.0	0.89-1.16	0.80-1.08	1.39-1.64	1.31-1.47
Mortar (1:1½)	1.0	0.82-1.00	0.84-1.18	1.31-1.52	1.38-1.49
Concrete(1:1½:1½)	1.0	1.13-1.22	1.19-1.22	1.32-1.42	1.18-1.35

TABLE D: Ratio of surface area of pores of radii >650 $\overset{0}{A}$

The table reveals that there is a substantial reduction in the total pore surface area as a result of North Sea and Kuwait crude oil saturation. Diesel saturated specimens had some reductions, but had a much higher ratio than NS and KU. Parafin saturated specimens were unaffected. The very low value of total pore surface area for NS and KU saturated specimens is associated with the closure of pores <650 $\overset{0}{A}$ by waxy deposits of the crude oils as mentioned in section 6.7.1. The lower value of total surface area of DE saturated HCP, mortar and concrete, when compared with H_2O saturated suggests, a mechanism or reaction of diesel oil which affect the pore parameters of cement composites. Table D

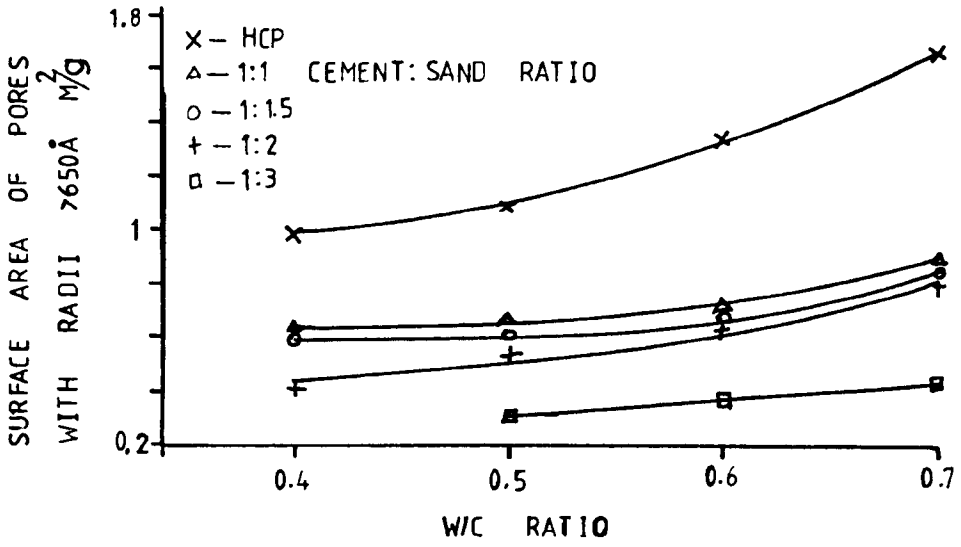

FIG 6.37 VAR. OF SURFACE AREA OF PORES, RADII >650Å WITH W/C RATIO FOR NS SATUR. SPEC.

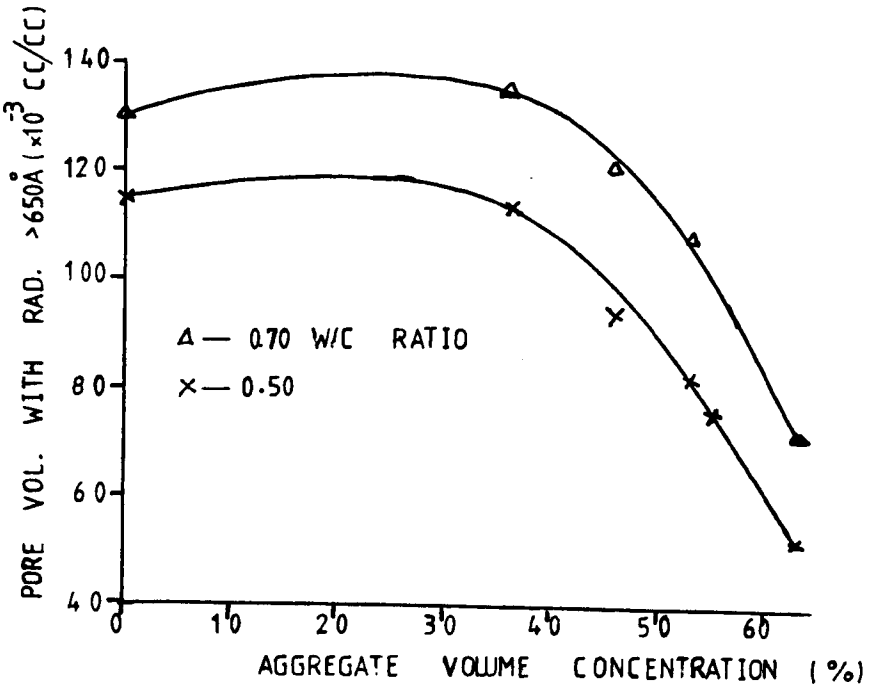

FIG 6.38 VAR. OF PORE VOL. WITH RAD. >650Å WITH AGG. VOL. CONCEN. FOR NS SAT. SPECIMENS

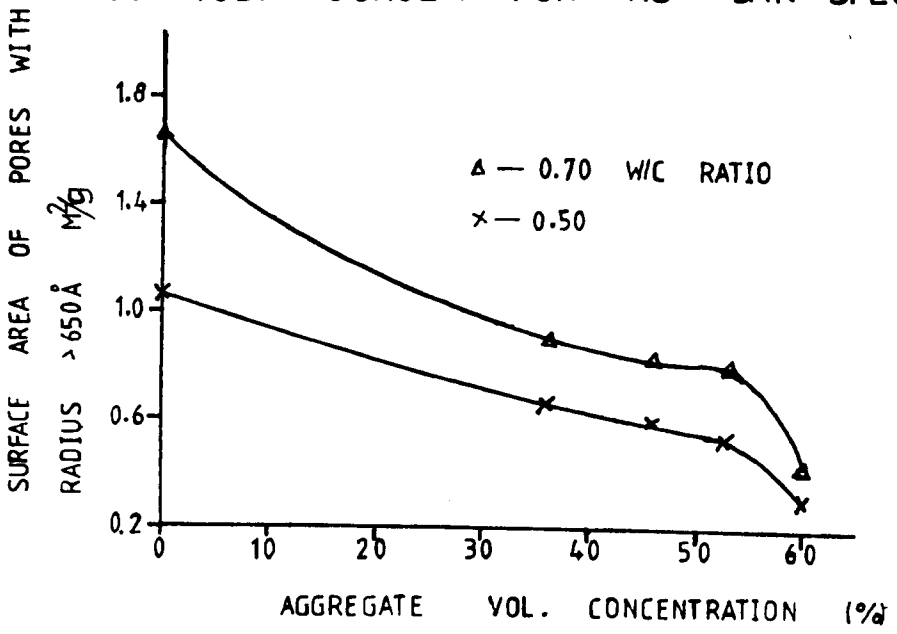

FIG 6.39 VAR. OF SURFACE AREA OF PORES WITH RADI >650A WITH AGGRE. VOL. CONCENTRATION FOR NORTH SEA OIL SATURATED SPECIMENS

reveals that the ratio of surface area of pores with radii >650 $\overset{0}{A}$ are not greatly affected by North Sea and Kuwait crude oil. Higher ratios (i.e. greater than 1.0) are obtained for DE and PA saturated specimens. This suggests that both waxy deposits in NS and KU and hydration of water saturated specimens equally reduced the surface area of pores >650 $\overset{0}{A}$ in these specimens, while DE and PA saturated specimens are unaffected.

Further study of the changes in pore surface area for pores with radii >650 $\overset{0}{A}$ reveals that (1) the surface area for NS saturated specimens decreases non-linearly with the aggregate volume concentration and falls sharply after about 53% aggregate volume (Fig. 6.39). The reason for this fall is not clear, but may show a critical point where the aggregate dominates the paste. (2) The pore surface area increases non-linearly with w/c ratio, for all the liquids.

6.7.4 Threshold and Hydraulic Radii

The threshold pore radii for various specimens saturated in NS, KU, DE, PA and H_2O are given in column 10, and the hydraulic radii for the total intruded pores and for pores >650 $\overset{0}{A}$ are given in columns 8 and 9 respectively of Tables 6.13 to 6.15. The following observations are made.

1. The hydraulic radii of the total intruded pores for NS, KU. DE and PA saturated HCP, mortar and concrete specimens were found to be generally higher than those of H_2O saturated specimens. Table E shows the ratio of average r_h for NS, KU, DE and PA saturated to that of H_2O saturated HCP, mortar and concrete. For pores with radii >650 $\overset{0}{A}$, the ratio of the average hydraulic radius is shown in Table F, for KU and NS saturated specimens, the hydraulic radius is generally higher than those of H_2O saturated for both HCP, mortar and concrete, while DE and PA saturated specimens appear to be approximately equal to those saturated in water.

The higher values of hydraulic radii obtained for NS, DE, KU and PA

saturated specimens, suggest that renewed hydration for water soaked specimen causes a reduction in the average width of the pores (i.e. the hydraulic radii), while the r_h for oil saturated specimens are unaffected, since oil does not encourage hydration. The hydraulic radius (r_h) of pores with radii >650 Å in KU and NS saturated specimens (Table F) shows the same trend but DE and PA saturated specimens do not. The reasons for this are not clear.

	H_2O/H_2O	KU/H_2O	NS/H_2O	DE/H_2O	PA/H_2O
HCP	1.0	1.29	2.20	1.44	0.98
Mortar (1:1½)	1.0	1.94	1.47	1.37	1.23
Concrete (1:1½:1½)	1.0	1.67	1.69	1.31	1.05

TABLE E: Ratio of average hydraulic radius of total intruded pores

	H_2O/H_2O	KU/H_2O	NS/H_2O	DE/H_2O	PA/H_2O
HCP	1.0	1.07	1.22	1.03	0.99
Mortar (1:1½)	1.0	1.20	1.41	0.94	0.92
Concrete (1:1½:1½)	1.0	1.28	1.26	0.85	0.88

TABLE F: Ratio of average hydraulic radius of pores with radii >650 Å

	H_2O/H_2O	KU/H_2O	NS/H_2O	DE/H_2O	PA/H_2O
HCP	1.0	0.76-0.81	0.86-1.27	0.74-0.78	0.74-1.12
Mortar (1:1½)	1.0	1.0-1.30	1.40-1.67	1.0-1.30	1.0-1.37
Concrete (1:1½:1½)	1.0	1.30-1.80	1.30-1.80	1.31-1.85	1.37-2.09

TABLE G: Ratio of threshold radius

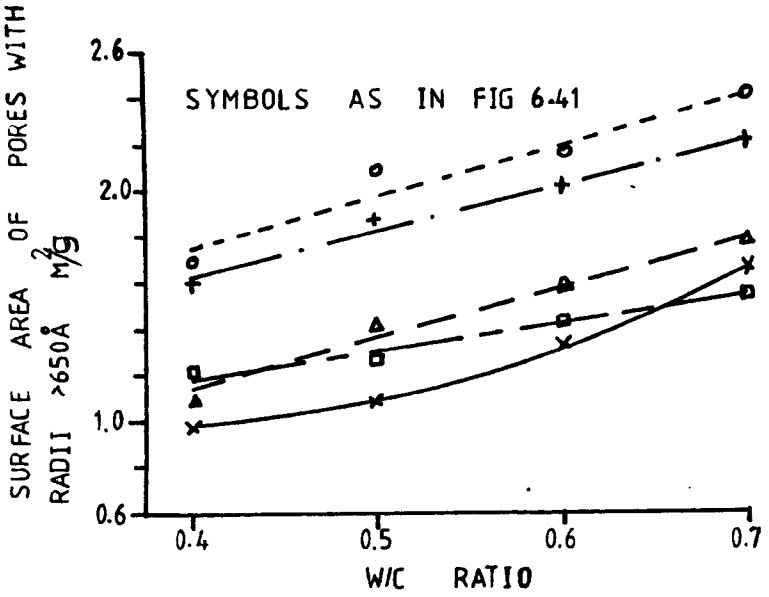

FIG 6.40 HCP SPECIMENS

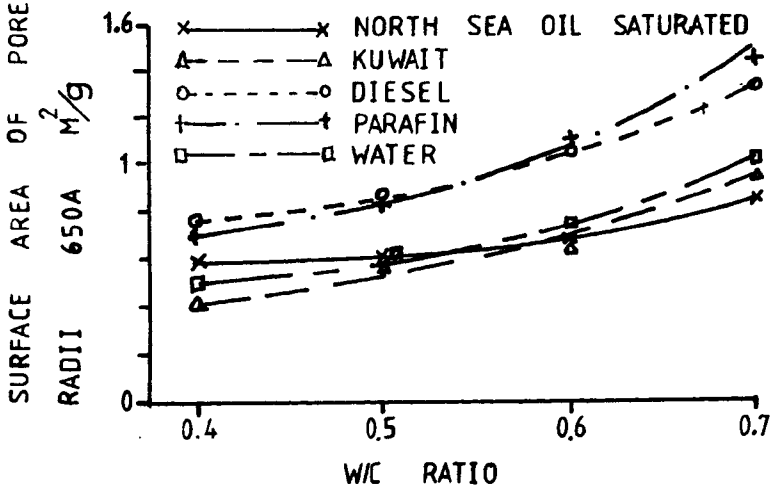

FIG 6.41 MORTAR SPECIMENS

FIG 6.40 & 6.41 VARIATION OF SURFACE AREA OF PORES OF RADII >650A WITH W/C RATIO FOR DIFFERENT LIQUID SATURATION

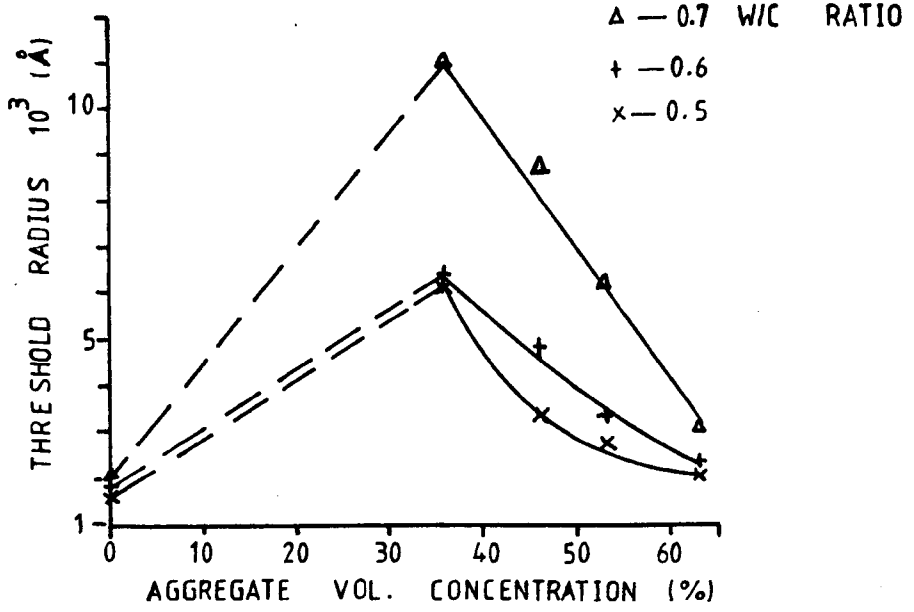

FIG 6.42 VARIATION OF THRES. RAD. WITH AGGRE. VOL. CONCENTRATION FOR NORTH SEA OIL SAT. SPECIMENS

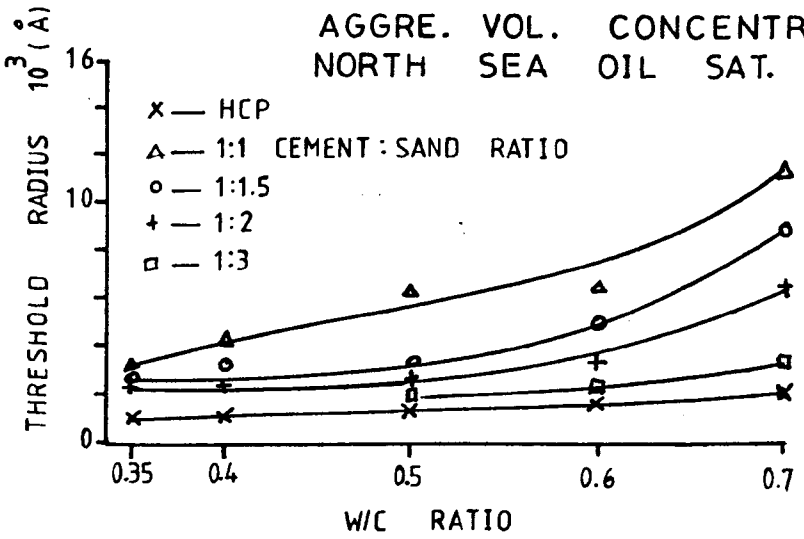

FIG 6.43 VARIATION OF THRES. RADIUS WITH W/C RATIO FOR NORTH SEA OIL SATURATED SPECIMENS

Table G, shows the range of ratios of the threshold radii r_T after NS, KU, De and PA saturation, for HCP, mortar, and concrete compared with H_2O saturattion. The results reveal that the threshold radius of HCP is reduced after saturation in all the four oil types, while the threshold radius of mortar and concrete increased in relation to water saturated. The reduction in r_T for HCP after KU and NS saturation, could be due to a partial closure of the pores by the waxy deposits, in which case this outweighted the renewed hydration in the water soaked pastes. The reason for the reduction in r_T after DE and PA saturation is not clear. The higher ratios (> 1.0) obtained for mortar and concrete tends to suggest that in these specimens, effect of hydration outweighs the effect of the waxy deposits. This is probably because the crude oil molecules bound together by these waxy deposits were not large enough to close these threshold radii found in mortar and concrete which were generally higher than those in HCP specimens.

Further exploration of the behaviour of threshold radius for HCP and mortar after saturation in North Sea crude oil (Fig. 6.42 and 6.43) reveals that (1) addition of small amount of aggregate to HCP increases the threshold radii, but further addition of aggregate reduces the threshold radius. The decrease in r_T is non-linear at lower w/c ratio (Fig. 6.42), but approximates to a linear relationship at greater w/c ratios. This may mean that at lower w/c ratios, the pores are highly non-uniform, but at higher w/c ratios, more uniform pores and flow channels are created. (2) The threshold radius increases non-linearly with w/c ratio for all the cement composites considered. These observations are the same for non-oil saturated specimens (section 6.5.2.7) and suggests that the pattern of behaviour of threshold radius with aggregate inclusion and w/c ratio is not affected by saturation in oil.

A statistical analysis of the hydraulic radius of total intruded

pores and pores with radii >650 Å (Tables 6.16 and 6.17) for HCP, mortar and concrete specimens showed a coefficient of variation of less than 10% after liquid saturation. This means that the hydraulic radius is independent of w/c ratio as earlier observed in section 6.5.2.7. This suggests therefore that the behaviour of hydraulic radius in relation to w/c ratio is unaffected by saturation in oil.

6.8 Effect of Curing Condition on the Pore Structure of HCP and Mortar

The preparation and casting of these specimens were as detailed in section 3.4. After demoulding, the specimens were stored in the constant temperature room (CTR or dry cured), at 16 $\pm$0.05°C, 50 $\pm$ 1% R.H., for the specific curing periods of 7 days, 28 days, and 3 months, prior to test. The pore parameters obtained from these HCP and mortar specimens are given in Table 6.18, for varying curing periods, and brief discussions of these are given below.

6.8.1 Total Intruded Pore Volume and Compressive Strength

The dry cured specimens contain more intruded pores than the wet cured (cured in fog room at 21 $\pm$ 1%, 99 $\pm$ 1% R.H.) specimens as shown in Table 6.19. This is not surprising since hydration cannot continue under the dry condition because there is insufficient water. After 7 days curing the intruded pores are approximately equal for the two curing conditions but as curing continued, the difference becomes larger, because hydration only continued in the wet room, at the normal rate, while the rate decreased greatly in the dry room. This is clearly shown in the results after 3 months curing. In addition, the CTR specimens developed micro-cracks which are also intrudable by mercury. This is more apparent in the HCP specimens and is detectable with a hand microscope of 40x magnification. The larger increase in the volume of pores for the 0.4 w/c specimens, even after 7 days curing, shows that hydration ceased earlier in these dry cured specimens because of lack of water.

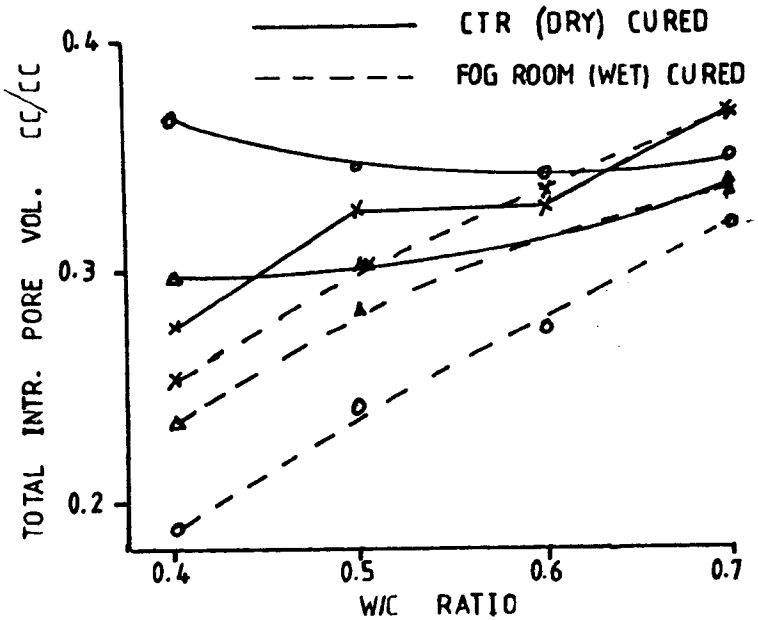

FIG 6.44 HCP SPECIMEN

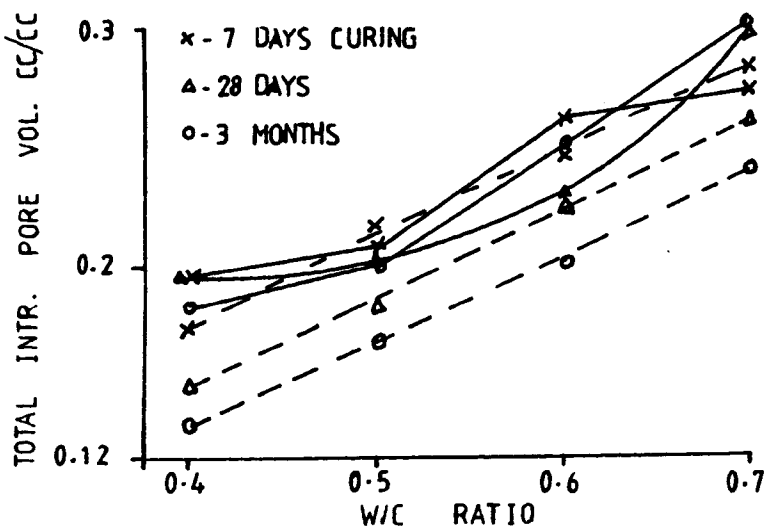

FIG 6.45 MORTAR 1:1.5 CEMENT:SAND

FIG 6.44 & 6.45 VARIATION OF TOTAL INTRUDED PORE VOLUME WITH W/C RATIO

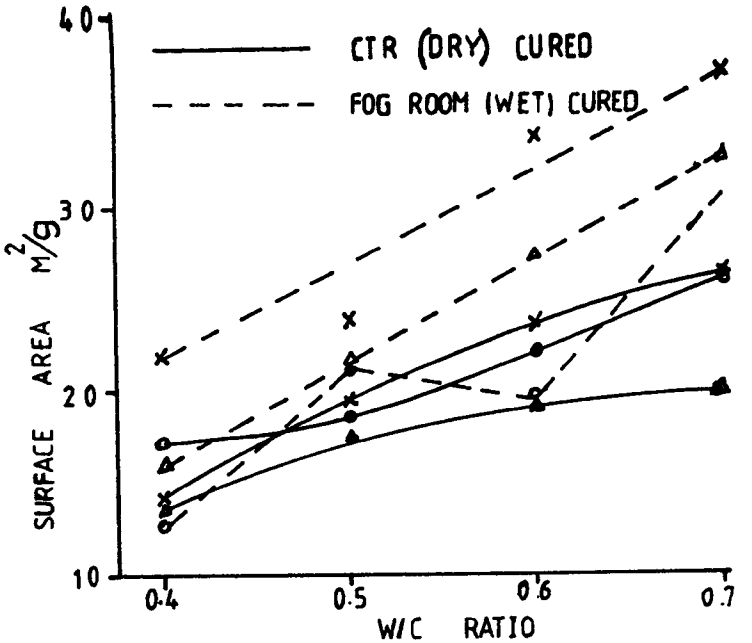

FIG 6.46 HCP SPECIMEN

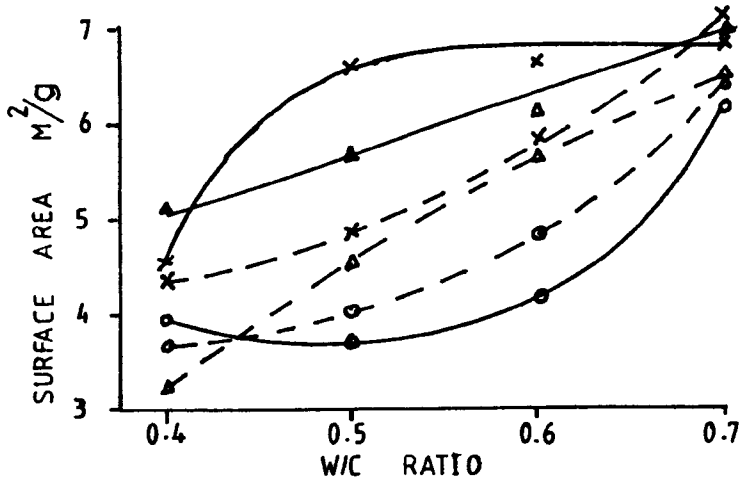

FIG 6.47 MORTAR 1:1.5 CEMENT:SAND RATIO

FIG 6.46 & 6.47 VARIATION OF SPECIFIC SURFACE AREA WITH W/C RATIO

CEMENT/SAND RATIO	HYDRAULIC RADII OF TOTAL INTR. PORES (A)	C.O.V. FOR THE TOTAL INTR PORES %	HYDRAULIC RADII OF PORES >650(A) (A)	C.O.V. FOR PORES >650 (A) %
HCP	183.5	17.74	670.6	9.74
1:1	223.5	21.57	806.42	9.05
1:1.5	233.9	22.48	764.8	8.82
1:2	354.8	4.73	795.9	8.29
1:3	434.4	7.16	827.2	1.77
concrete 1:1.5:1.5	271.0	4.27	833.1	1.31

TABLE 6.16 Hydraulic radii of mortar saturated in North Sea crude oil

TYPE OF LIQUID SATURATION	HYDRAULIC RADII OF TOTAL INTRUDED PORES	COEFF OF VARIATION %	HYDRAULIC RADII OF PORES >650Å	C.O.V
HCP				
North Sea	183.5	17.75	670.6	10.26
Kuwait	100.3	5.54	566.7	6.55
Diesel	112.0	9.78	548.7	2.69
Parafin	76.1	8.70	525.7	2.79
Water	77.7	7.00	531.3	5.89
MORTAR 1:1.5				
North Sea	233.9	22.48	764.8	8.82
Kuwait	291.2	7.96	817.6	10.42
Diesel	206.0	8.31	642.3	1.31
Parafin	184.2	6.54	625.8	4.40
Water	150.2	13.88	680.3	5.19
CONCRETE				
North sea	273.07	4.65	833.1	1.31
Kuwait	267.7	7.09	841.6	1.82
Diesel	210.3	5.53	558.8	8.80
Parafin	167.4	6.97	559.4	6.61
Water	160.1	4.75	659.0	2.62

TABLE 6.17 Hydraulic Radii of HCP, mortar and concrete saturated in different types of oil

1	2		3		4	5	6	7	8	9
SPECIMEN DESIGNATION	TOTAL INTRUDED PORE VOL cc/cc	cc/g	INTRUDED PORE VOL >650A cc/cc	cc/g	%AGE OF THE INTRU. PORE >650A	SURFACE AREA OF INTRUDED PORE m^2/g	SURFACE AREA OF PORES >650A m^2/g	HYDRAULIC RADII OF INTRUDED PORES A	HYDRAULIC RADII OF PORES ≥650A A	THRESHOLD RADII A
7 DAYS CURING HARDENED CEMENT PASTES										
OP40	0.276	0.171	0.161	0.100	58	14.34	1.9542	119.2	511.7	2009
OP50	0.327	0.223	0.205	0.140	62	19.44	2.10	114.7	666.7	3375
OP60	0.326	0.240	0.186	0.137	57	23.68	2.096	101.4	653.6	3375
OP70	0.370	0.274	0.215	0.160	58	26.24	2.3096	104.4	692.8	6250
28 DAYS CURING										
OP40	0.298	0.181	0.195	0.118	65	13.71	2.11	132.0	559.2	2009
OP50	0.303	0.202	0.198	0.132	65	17.78	2.02	113.6	653.5	2750
OP60	0.312	0.222	0.174	0.124	56	19.35	1.80	114.7	688.9	3375
OP70	0.339	0.248	0.204	0.149	60	19.87	1.83	124.8	814.2	6250
3 MONTHS CURING										
OP40	0.366	0.211	0.238	0.137	65	17.26	2.22	122.3	617.8	3375
OP50	0.346	0.220	0.228	0.145	66	18.56	2.10	118.5	690.5	3375
OP60	0.342	0.220	0.188	0.121	55	22.10	1.83	99.6	660.6	3375
OP70	0.349	0.235	0.191	0.128	54	26.25	1.85	89.5	691.9	4375
7 DAYS MORTAR (1:1.5 CEMENT:SAND RATIO)										
M40-1.5	P.197	0.096	0.125	0.061	63	4.51	0.83	212.9	734.9	6250
M50-1.5	0.208	0.128	0.123	0.066	59	6.58	0.92	194.5	717.4	11250
M60-1.5	0.260	0.139	0.172	0.092	66	6.62	1.10	210.0	836.4	11250
M70-1.5	0.272	0.156	0.191	0.110	70	6.81	1.29	229.1	852.7	11250
28 DAYS										
M40-1.5	0.197	0.099	0.125	0.063	63	5.12	0.86	193.4	732.6	6250
M50-1.5	0.208	0.108	0.136	0.065	67	5.66	0.91	190.8	714.3	6250
M60-1.5	0.229	0.118	0.160	0.083	70	6.11	1.06	193.1	783.0	11250
M70-1.5	0.298	0.159	0.233	0.119	75	6.95	1.41	228.8	844.0	45000
3 MONTHS										
M40-1.5	0.184	0.088	0.121	0.058	66	3.98	0.90	221.1	644.4	6250
M50-1.5	0.202	0.100	0.134	0.066	66	3.73	1.00	268.1	660.0	6250
M60-1.5	0.251	0.128	0.192	0.092	76	4.59	1.36	278.9	720.6	11250
M70-1.5	0.301	0.161	0.243	0.129	81	6.07	1.92	265.2	671.9	45000

TABLE 6.18 Pore parameters for HCP and mortar specimens cured in a constant temperature room (CTR) at $16 \pm 0.05^{\circ}C$, 55% RH

SPECIMEN DESIGNATION CON.	7 DAYS CURING			28 DAYS CURING			3 MONTHS CURING		
	TOTAL INTRUDED PORE VOLUME cc/cc		%AGE INCREASE IN INTR. PORE VOL	TOTAL INTRUDED PORE VOLUME cc/cc		%AGE INCREASE IN INTR. PORE VOL	TOTAL INTRUDED PORE VOLUME cc/cc		%AGE INCREASE IN INTR. PORE VOL
	FOG ROOM CURED $21\pm1\ ^{o}C$ $99\pm1\%RH$ V_F	CTR CURED $16\pm0.5\ ^{o}C$ $55\pm1\%RH$ V_C	$\frac{V_C-V_F}{V_F}\times100$	FOG ROOM CURED V_F	CTR CURED V_C	$\frac{V_C-V_F}{V_F}\times100$	FOG ROOM CURED V_F	CTR CURED V_C	$\frac{V_C-V_F}{V_F}\times100$
OP40	0.253	0.276	9	0.235	0.298	27	0.189	0.366	78
OP50	0.302	0.327	8	0.283	0.303	7	0.243	0.346	42
OP60	0.334	0.326	-2	0.314	0.312	-1	0.274	0.342	25
OP70	0.368	0.370	1	0.335	0.339	1	0.322	0.349	8
M40-1.5	0.172	0.197	12	0.150	0.197	31	0.134	0.184	37
M50-1.5	0 217	0.208	-4	0.183	0.203	11	0.168	0.202	20
M60-1.5	0.246	0.262	7	0.226	0.229	1	0.201	0.251	25
M70-1.5	0.282	0.272	-4	0.260	0.298	15	0.240	0.301	25

TABLE 6.19 Total intruded pore volume for the fog room and CTR cured HCP and mortar

w/c RATIO	HCP			MORTAR 1:1.5			CONCRETE 1:1.5:1.5		
	COMPRESSIVE STRENGTH		%AGE DECREASE IN STRENGTH $\frac{F_F-F_C}{F_F}\times100$	COMPRESSIVE STRENGTH N/mm^2		%AGE DECREASE	COMPRESSIVE STRENGTH N/mm^2		%AGE DECREASE
	FOG ROOM CURED F_F	CTR CURED F_C		FOG ROOM CURED F_F	CTR CURED F_C		FOG ROOM CURED F_F	CTR CURED F_C	
0.40	72.6	53.5	26	74.6	56.2	25	72.6	56.0	23
0.50	52.0	41.6	20	63.0	50.6	20	61.4	50.2	18
0.60	45.4	35.5	22	50.0	44.1	12	50.8	35.2	31
0.70	40.2	28.8	28	40.0	27.6	31	36.0	23.3	35

TABLE 6.20 Compressive strength of fog room ($21\pm1\ ^{o}C$, $99\pm1\%$ RH) and CTR ($16\pm0.5\ ^{o}C$ $55\pm1\%$ RH) cured HCP, mortar and concrete (28 days curing)

The compressive strength of the dry cured specimens is generally lower than those of the wet cured specimens, (Table 6.20). This reduction in strength could be as a result of weak bonding due to insufficient hydration products or greater internal micro-cracking due to drying shrinkage.

The total intruded pore volume for wet cured specimens increased reasonably linearly with w/c ratio, for the curing periods and for both HCP and mortar, while for the dry cured HCP and mortar, the intruded pore volume increases erratically with w/c ratio (Fig. 6.44 and 6.45). This is probably because while hydration or lack of it, controls the subdivision of pores in the wet cured as well as dry cured, micro-cracking causes additional spaces in dry cured specimens.

6.8.2 Specific Surface Area

As earlier stated in section 6.5.2.6, the surface area increases erratically with the w/c ratio for both curing conditions and for HCP and mortar specimens (Fig. 6.46 and 6.47). This erratic behaviour of the surface area with w/c ratio is difficult to explain, but may be associated with the presence of micro-cracks produced during drying of the specimens.

6.8.3 Hydraulic and Threshold Radii

The hydraulic radius and the threshold radius of wet cured HCP and mortar specimens are generally lower than those of dry cured, for all the w/c ratios, (Table 6.21 and 6.22). The hydraulic radius (r_h) for dry cured HCP is up to 1.59 times that of wet cured, while for mortar it is up to 1.36 times. The threshold radius r_T for the dry cured HCP is between 1.13 to 4.29 times that of wet cured, while for mortar, it is between 1.85 to 7.20 times.

As discussed earlier in section 6.5.2.5, the hydraulic radius is independent of the w/c ratio, while the threshold radius increases with an increase in w/c ratios, for both curing conditions.

PERIOD OF HYDRATION	FOG ROOM CURED				CTR CURED			
	MEAN HYDRAULIC RADII OF TOTAL INTR. PORES (Å)	COEFF. OF VARIATION %	MEAN HYDRAULIC RADIUS OF PORES >650Å	COEFF. OF VARIATION	MEAN HYDRAULIC RADII OF TOTAL INTR. PORES (Å)	COEFF. OF VARIATION	MEAN HYDRAULIC RADIUS OF PORES >650Å	COEFF. OF VARIATION
HCP								
7 days	76.86	8.10	485.1	7.27	109.9	6.62	631.2	11.16
28 days	80.40	9.20	464.1	5.66	121.3	6.25	678.9	13.45
3 months	78.90	9.40	419.0	7.93	107.5	12.5	665.0	4.56
6 months	71.48	5.60	391.2	9.90	-	-	-	-
MORTAR 1:1½ CEMENT/SAND RATIO								
7 days	219.34	6.20	594.5	6.17	211.6	5.80	785.4	7.61
28 days	211.83	3.13	564.4	7.36	201.6	7.83	768.5	6.55
3 months	201.90	7.71	516.6	9.41	258.3	8.55	674.2	4.23
6 months	188.52	6.43	464.9	3.11	-	-	-	-

TABLE 6.21 Mean hydraulic radius for total intruded pores and for pores of radii >650Å

	FOG ROOM CURED				CTR CURED		
	7 days	28 days	3 months	6 months	7 days	28 days	3 months
HCP							
OP35	1583	910	910	858	-	-	-
OP40	1771	1306	910	792	2009	2009	3375
OP50	2750	1771	1036	910	3375	2750	3375
OP60	2750	2320	1112	969	3375	3375	3375
OP70	3375	2750	1306	969	6250	6250	6250
MORTAR 1:1.5 (CEMENT:SAND RATIO)							
M35-1.5	2750	2008	1583	1432	-	-	-
M40-1.5	3375	3375	2009	2009	6250	6250	6250
M50-1.5	6250	4375	2750	2321	11250	6250	8750
M60-1.5	6250	6250	3375	3375	11250	11250	11250
M70-1.5	11250	8750	6250	4815	11250	45000	45000

TABLE 6.22 Threshold pore radii for HCP and mortar (1:1.5 cement:sand ratio) for fog room and CTR cured specimens

The threshold radius decreases with the curing period for wet cured HCP and mortar, but increases for the dry cured specimens (Table 6.18). The effect of the curing period on the threshold radius for wet cured specimens has earlier been discussed in section 6.5.2.5. The reverse behaviour of the dry cured specimens could be due to lack of hydration as a result of insufficient water and the development of micro-cracks over longer curing periods.

The present Chapter, dealt with the influence of w/c ratio, hydration and aggregate inclusion on the pore structure of HCP, mortar and concrete. In Chapter 8, efforts will be made to establish a functional relationship between some of these pore parameters and the saturated permeability of mortar. Also the significance of the critical pore radius will be considered.

6.9 Summary of Test Results to Determine the Pore Structure of HCP, Mortar and Concrete

1. The changes in pore structure of HCP and mortar with the w/c ratio of the mix and period of hydration of the specimen can be measured by changes in total porosity, intruded pore volume and a single point value in pore size distribution, called the threshold radius. Care is needed in the measurement and interpretation of the threshold radius in mortar mixes.

2. An increase in the initial w/c ratio increases the total pore volume, the pore surface area, the total intruded pore volume and the threshold radius but decreases the density and has no noticeable effect on the hydraulic radius.

3. An increase in the period of hydration decreases the total pore volume, the pore surface area, the threshold radius, the total intruded pore volume, and the hydraulic radius but increases the density of both HCP and mortar.

4. Aggregate inclusions reduce the total pore volume of the bulk specimen, the pore surface area and the intruded pore volume, but increases the density. If considered per volume of paste in the mortar, then the inclusion of aggregate increases the total pore volume and the intruded pore volume. The addition of a small volume of aggregate to HCP increases the threshold radius, but further increase in aggregate volume gradually reduces the threshold radius.

5. Wax deposits from the crude oils (North Sea and Kuwait) appear to block all pores with less than 650 $\mathring{A}$ radius. This pore radius of 650 $\mathring{A}$ is called a critical pore radius (P_{cr}), and is believed to be the minimum pore that could influence the permeability of crude oil through HCP, mortar and concrete.

6. Dry curing at 16 $\pm$ 0.5°C, 50$\pm$1% R.H., increases the intruded pore volume, the threshold radius and the hydraulic radius, when compared with wet cured specimen (21 $\pm$ 1°C, 99 $\pm$ 1. R.H.) of the same age, but decreases the strength. For the dry cured specimens, no unique relationship was found between the initial w/c ratio or the period of hydration on the pore structure. The development of micro-cracks in dry cured specimens, was thought to have greatly distorted the pore system.

CHAPTER 7

PERMEABILITY OF HCP, MORTAR AND CONCRETE TO NORTH SEA CRUDE OIL

7.1 Introduction

Permeability is one of the very important properties of concrete which determines its durability and has obvious applications for the storage of liquids. The movement of fluids in HCP, mortar or concrete takes place in the continuous flow channels which depends on the number and size of connected pores. The overall permeability of mortar or concrete is a function of the paste permeability, the permeability of aggregate particles and the integrity of the bond between the two[152].

This chapter presents the measured permeability of HCP, mortar and concrete to North Sea crude oil. OPC was used for all the mixes and the properties of each mix, the aggregates and the North Sea crude oil are given in Chapter 3. The changes in permeability produced by variations in the w/c ratio, hydration period and aggregate inclusions are investigated in this chapter.

The mix proportions for these tests are given in table 6.1 and section 5.2 describes the permeability apparatus and the analytical techniques employed. The coefficient of permeability, K, was calculated using equation 2.21. Unless otherwise stated, the permeability coefficients are calculated for North Sea crude oil flowing through disc specimens 100 mm dia. x 25 mm thick as detailed in section 3.4.1.1

7.2 Permeability of HCP and Mortar Specimens

Drying the HCP specimens made from ordinary portland cement, prior to saturation in crude oil, often produced cracking, despite all the effort made to avoid it (section 3.8.2) and the specimens fell apart when being set up in the permeability cell. The results for the specimens with minor cracks are reported in table 7.1. A critical look at these few results suggest that

PASTE DESIGNATION	W/C RATIO / APP PRESSURE m	SATURATED PERMEABILITY K x 10^{-13} m/s				
		33.2	49.8	66.4	83.0	99.6
DRIED TO 55°C						
OP35	0.35	23.0	28.0	27.2	30.8	31.2
OP40	0.40	40.3	39.0	54.4	61.6	62.4
OP50	0.50	23.0	33.6	41.1	41.6	48.4
OP60	0.60	27.3	22.3	30.5	38.6	43.5
OP70	0.70	34.5	36.3	39.2	51.3	57.2
DRIED TO 105°C						
OP35	0.35	30.0	33.3	40.75	43.3	115.1
OP40	0.40	12.10	14.14	16.40	15.06	24.54
OP50	0.50	48.4	49.0	51.0	59.5	58.4
OP60	0.60	22.5	30.0	33.3	35.2	36.2
OP70	0.70	6.4	12.1	15.06	14.54	24.2

TABLE 7.1: Saturated Permeability of HCP to Crude Oil.

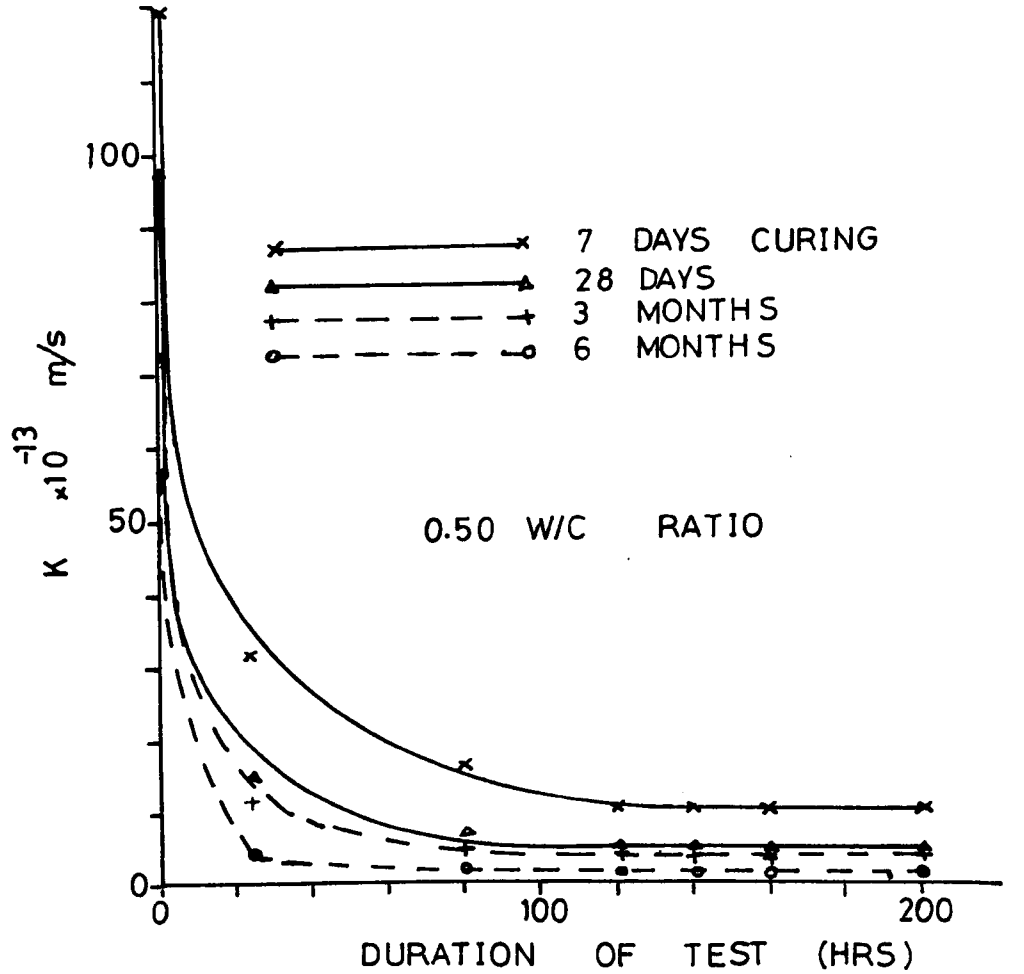

FIG 7.1 VARIATION OF K WITH DURATION OF TEST FOR MORTAR OF 1:1 CEMENT : SAND RATIO (49.8 METRE HEAD OF OIL)

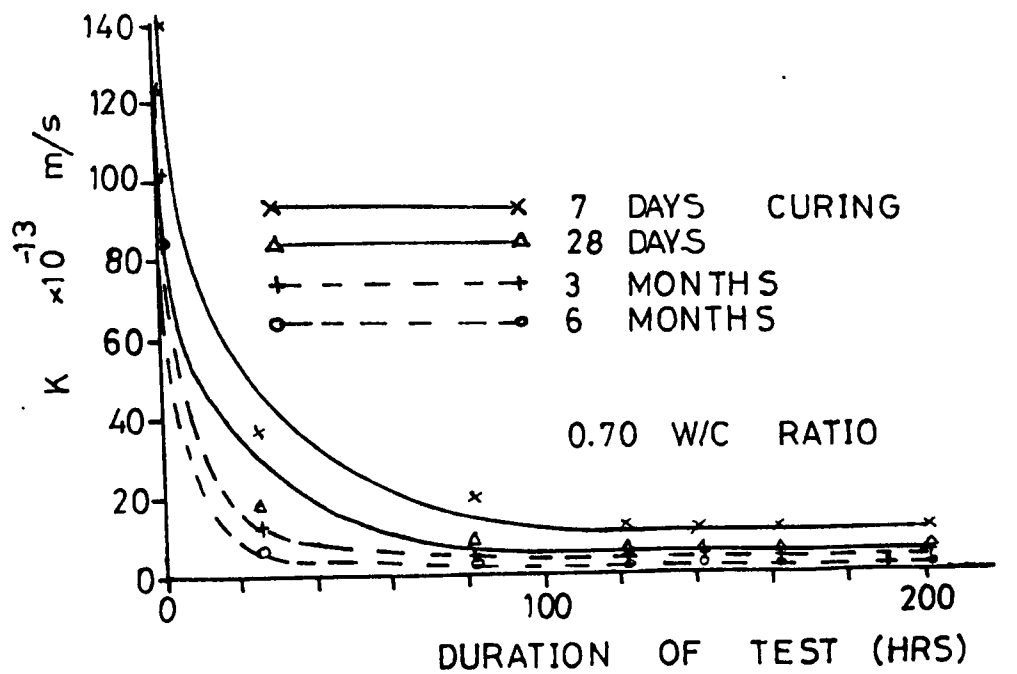

FIG 7.2 VARIATION OF K WITH DURATION OF TEST FOR MORTAR OF 1:1 CEMENT: SAND RATIO (49.8 METRE HEAD OF OIL)

they are highly unreliable, and permeability tests on dried HCP specimens were discontinued. Water permeability tests on undried HCP to determine the effect of specimen dimensions on the coefficient of permeability K, is reported later in section 7.2.1 .7.

The mortar specimens did not appear to crack during drying even when oven dried up to 105°C. A stereo-microscope (up to 400 x magnification) was used to look for possible cracks in the mortar and concrete specimens, but none was found. It was therefore concluded that there will be no cracks provided gradual drying as described in sections 3.8.1 and 3.8.2, is carried out. Most permeability results were obtained on mortar specimens with w/c ratio varying from 0.35 to 0.70, period of hydration from 7 days to 6 months and cement/sand ratio from 1:1 to 1.3. The effect of addition of coarse aggregate to mortar on permeability was studied using concrete of 1:1½:1½ (cement:sand:coarse aggregate) ratio by weight, with a maximum size of coarse aggregate of 6.30 mm.

The treatment of the specimens before being placed in the permeability cell and the testing procedures have been fully described in chapter 5. Most specimens were tested at five oil pressures VIS: 0.827, 0.690, 0.552, 0.414 and 0.276 N/mm^2 corresponding to crude oil heads of 99.60, 83.0, 66.4, 49.8 and 33.2 meters respectively. At each pressure, the test was continued until the flow rate became almost constant which normally occurred within 120 hrs. (section 7.2.1.1).

7.2.1 Factors affecting the Permeability of Mortars

7.2.1.1 Duration of test

The variation of the coefficient of permeability with time through out the test period is illustrated in figs. 7.1 and 7.2, at a pressure head of 49.8 m of oil (0.414 N/mm^2) using mortar of 1:1 cement/sand ratio after hydration of up to 6 months. Other mortar ratios and pressure heads exhibit the same characteristics, hence only typical plots are presented and discussed below.

1. The coefficient of permeability K, and hence the rate at which oil flows through the mortar decreased rapidly with time during the test period up to 120 hrs., after which it remained practically constant, throughout the remaining test period of up to 200 hrs. For 1:1 cement/sand ratio, and 0.5 w/c ratio, the reduction in K in the 24 hrs., 120 hrs. and 200 hrs. was between 3.84 - 14.25, 11.90 - 45.60 and 11.90 - 57.90 respectively. For 0.7 w/c ratio, the reduction was between 3.8 - 12.7, 7.49 - 38.48 and 7.64 - 41.56 in the 24 hrs., 120 hrs., and 200 hrs. periods (fig. 7.1 and 7.2). The range of values depends on the period of hydration.

For these mortar specimens, the outflow after 120 hrs. was between 35 - 75% of the inflow values, and after 200 hrs. the outflow was between 75 to 90% of the inflow, depending on the w/c ratio and cement/sand ratio. Despite the low outflow/inflow ratio at 120 hrs., the steady state flow is assumed to have been attained at this time since there is no significant increase in the permeability coefficient after this time. Hence all reported K values (unless otherwise stated) are the values obtained after 120 hrs.

The reduction in the rate of flow (i.e., reduction in K) could be partly due to reduction in the pores, caused by the deposits of wax from the crude oil and partly as a result of partial drying of the oil from the outer surfaces of the specimens while preparing the specimens prior to test. A similar reduction was observed by Oyeka[17] for oil flow through HCP, and Kirillov[175] for water flow through concrete.

7.2.1.2 Water/cement ratios

W/c ratio controls, to a large extent, the spacing of unhydrated cement grains after the mortar has set, and hence has significant effect on the properties of cement composites[114]. The variation in permeability with w/c ratio at varying cement/sand ratios (1:1, 1:1½, 1:2 and 1:3) and four hydration periods (7 days, 28 days, 3 months and 6 months) is given in table 7.2. Typical plots of K versus w/c ratio, after 28 days and 6 months hydration are shown in figs. 7.3 and 7.4 respectively, for varying

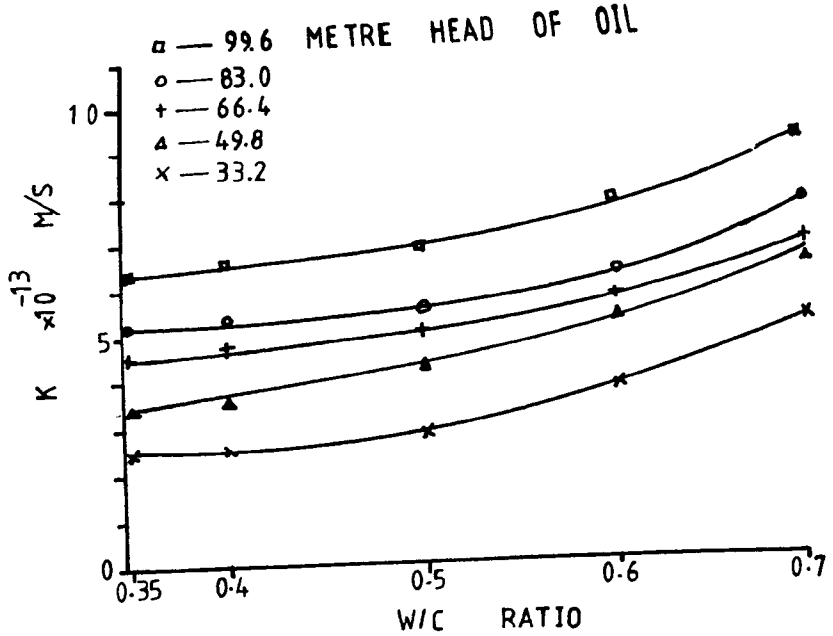

FIG 7.3 VARIATION OF K WITH W/C RATIO 28 DAYS HYDRATED MORTAR OF 1:1 CEMENT: SAND RATIO

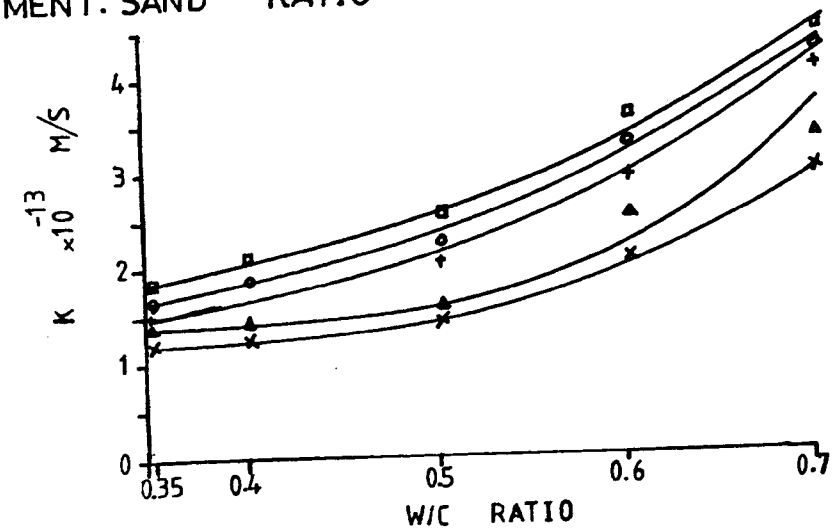

FIG 7.4 VARIATION OF K WITH W/C RATIO, 6 MONTHS HYDRATED MORTAR OF 1:1 CEMENT: SAND RATIO

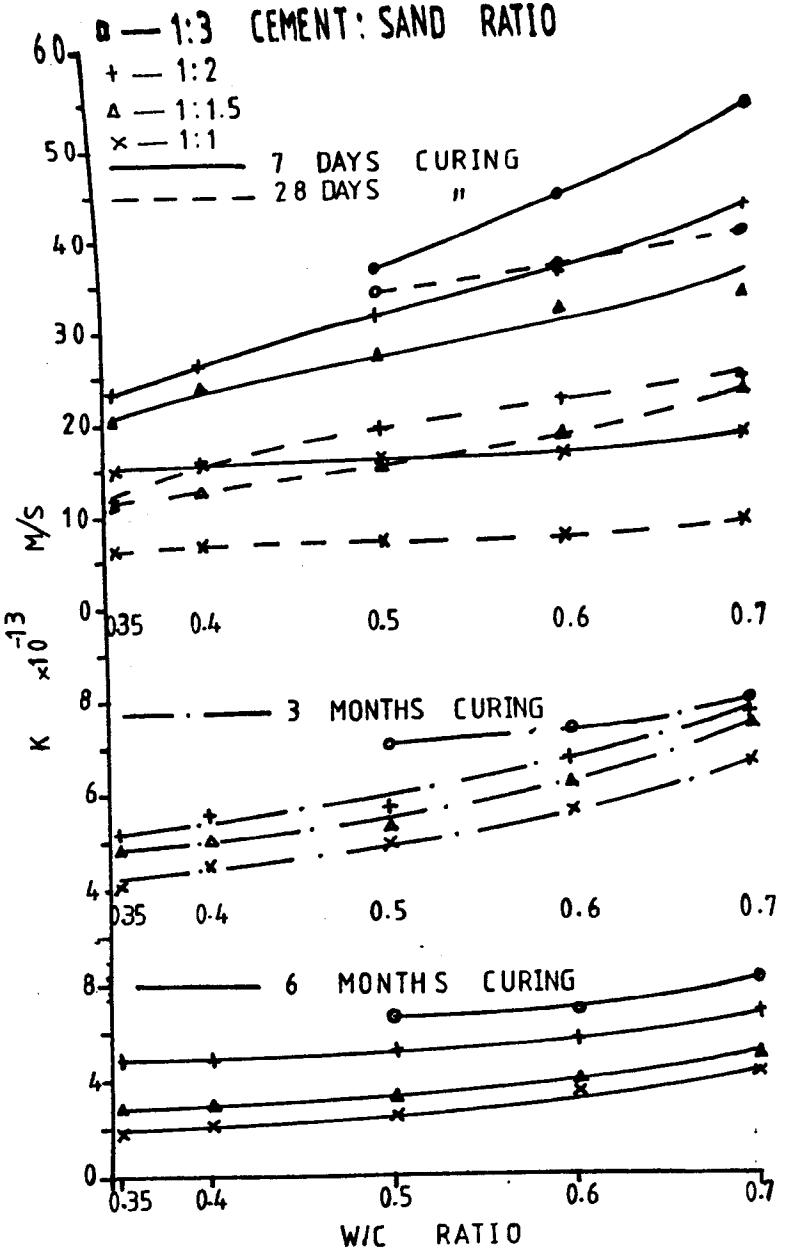

FIG 7.5 VARIATION OF K WITH W/C FOR FOUR HYDRATION PERIODS, CEMENT SAND RATIOS AND AT 99.6 METRES OF OIL

TIME OF HYDRATION	PERMEABILITY OF MORTAR AND CONCRETE K x 10^{-13} M/S																			
	7 DAYS					28 DAYS					3 MONTHS					6 MONTHS				
SPECIMEN DESIGNATION / APPLIED PRESSURE (M)	33.2	49.8	66.4	83.0	99.6	33.2	49.8	66.4	83.0	99.6	33.2	49.8	66.4	83.0	99.6	33.2	49.8	66.4	83.0	99.6
M35-1	7.60	9.60	11.40	11.80	14.6	2.40	3.40	4.55	5.20	6.31	2.01	2.95	3.15	3.80	4.0	1.20	1.40	1.50	1.65	1.85
M40-1	7.71	9.70	12.50	13.20	15.3	2.55	3.51	4.75	5.35	6.60	2.15	3.20	3.35	4.08	4.50	1.27	1.45	1.83	1.90	2.11
M50-1	8.15	10.30	13.30	14.10	16.15	2.90	4.24	5.01	5.5	6.85	2.40	3.78	4.05	4.75	4.95	1.41	1.55	2.01	2.15	2.50
M60-1	8.85	10.90	13.90	14.50	16.4	3.70	5.30	5.75	6.25	7.85	3.35	4.50	4.90	5.45	5.65	2.06	2.50	2.90	3.25	3.55
M70-1	9.91	12.00	16.60	15.60	18.6	5.10	6.37	6.80	7.70	9.10	4.56	5.76	6.25	6.50	6.65	2.93	3.30	4.0	4.15	4.35
M35-1½	13.80	17.60	18.90	19.60	20.2	6.30	8.30	8.50	11.20	11.20	3.01	3.42	3.94	4.40	4.85	1.67	2.02	2.51	2.56	2.94
M40-1½	15.20	20.00	23.60	24.50	24.6	6.50	9.00	9.10	12.0	12.5	3.21	3.78	4.36	4.56	5.01	1.92	2.06	2.60	2.78	3.02
M50-1½	19.70	24.20	26.00	27.4	27.5	7.50	10.0	12.0	13.9	15.45	3.55	4.62	4.86	5.12	5.33	1.96	2.15	2.27	3.24	3.44
M60-1½	21.90	26.40	28.40	31.0	32.7	10.0	13.0	14.5	16.0	19.0	4.15	5.13	5.81	6.17	6.24	2.33	2.50	3.65	4.10	4.10
M70-1½	25.60	28.60	31.20	32.9	33.9	12.5	17.5	19.1	22.9	23.5	4.84	6.15	6.86	7.25	7.50	2.95	3.10	4.67	4.98	5.05
M35-2	18.1	20.2	21.2	22.8	23.2	9.5	9.7	10.5	11.15	11.57	3.53	4.54	4.59	4.85	5.15	3.05	3.21	3.56	4.05	4.80
M40-2	19.0	21.9	22.4	24.8	26.4	15.3	15.5	16.64	16.73	16.75	3.61	4.61	4.85	4.95	5.55	3.10	3.32	3.63	4.15	4.85
M50-2	22.5	27.3	28.3	31.3	31.7	17.9	18.6	19.50	19.90	19.96	4.23	5.23	5.25	5.50	5.70	3.35	3.70	4.01	4.32	5.30
M60-2	26.7	28.8	33.2	34.1	36.5	20.1	20.15	21.0	22.30	22.51	4.91	5.90	6.07	6.45	6.75	3.75	4.20	4.40	4.75	5.70
M70-2	36.8	38.2	40.0	41.9	43.5	21.6	21.7	22.5	24.16	24.79	5.88	6.90	7.30	7.65	7.70	4.50	5.15	5.26	5.46	6.80
M50-3	24.9	29.1	31.1	32.8	36.9	24.4	27.8	31.0	32.0	34.3	6.01	6.44	6.81	7.02	7.05	4.85	5.43	5.75	6.15	6.72
M60-3	27.5	34.9	38.9	41.5	44.5	27.0	32.5	34.1	37.0	37.1	6.45	6.81	7.05	7.23	7.40	5.21	5.47	5.83	6.25	6.92
M70-3	31.6	43.7	49.2	52.6	54.7	30.0	36.3	37.7	40.5	41.0	7.02	7.55	7.75	7.85	8.00	6.22	6.21	6.50	7.20	8.25
C35-1½	9.3	10.1	13.0	14.2	14.2	7.4	8.8	9.1	10.9	11.6	7.16	7.70	8.20	9.20	9.94	4.99	4.72	6.15	6.54	6.61
C40-1½	11.6	12.2	14.0	16.6	17.2	7.5	9.5	10.0	11.2	12.5	7.60	8.01	8.65	9.53	10.46	5.42	5.33	6.13	6.63	6.30
C50-1½	14.3	14.5	16.5	18.9	19.5	9.3	11.0	11.5	12.5	13.0	8.30	8.85	9.72	10.30	11.60	5.76	5.63	6.50	7.10	7.52
C60-1½	18.6	18.1	21.5	24.0	24.5	11.0	14.0	15.0	16.0	16.0	9.25	9.50	10.45	11.40	12.65	6.50	6.53	7.59	8.34	8.98
C70-1½	23.5	24.5	27.5	30.1	31.1	15.0	18.0	20.0	21.0	22.5	10.70	10.98	12.10	12.58	14.30	8.74	7.64	8.86	10.43	11.01

TABLE 7.2: Saturated Permeability of Cement, Mortar and Concrete to Crude Oil.
(see table 6.1 for the mix proportions)

pressure heads. Fig. 7.5 shows K versus w/c at 99.6 metre head of oil for the four hydration periods. Table 7.3 illustrates the values of K, total porosity and dry density obtained from six specimens prepared from the same mix. These six identical specimens were obtained for each w/c ratio (0.35, 0.40, 0.50, 0.60 and 0.70) and each hydration period (7 days, 28 days, 3 months and 6 months) and tested for permeability at 99.6 m, pressure head of oil. The test was to investigate the extent of variation in total porosity, dry density and coefficient of permeability within a particular mix. The various observations from the results are discussed below.

1. Table 7.3 shows that porosities are within ±0.02 cc/cc of each other for a particular mix, and dry densities are within ±0.05 g/cc for each w/c ratio and period of hydration. The coefficients of variation (C.O.V) for both porosity and dry density are below 5%. It is therefore sensible to suggest that the samples are representative with respect to w/c ratio. The permeability results have a C.O.V. between 20 to 30% at each w/c ratio and hydration period. Fig. 7.6 and 7.7 illustrate the extent of scatter in the K values. It can be seen from the vertical lines drawn through the minimum and maximum values of K, joined with dotted lines to form the variation envelope, that the scatter is quite large. The scatter may be due to clogging of the pores by the wax in the oil. Close inspection of the surfaces of the specimens which had been exposed to the inlet oil pressure revealed a greasy texture with layers of heavy oil particles. The layer varies from sample to sample and could have reduced the quantity of oil entering the pores. It was observed that the oil in the outlet tube has a much lighter texture indicating that a filteration process has been occurring. To obtain reasonable results, the surface exposed to the inlet pressure are cleaned of these deposits prior to tests at 120 hrs.

The smaller variations in total porosity and dry density when compared with those of permeabiltiy for a given w/c ratio, indicates that permeability is more sensitive to mix variations. Since the test is carried

W/C RATIO	0.35			0.40			0.50			0.60			0.70		
TESTED AFTER HYDRATING IN FOG ROOM FOR 28 DAYS	K x 10^{-13} m/s	TOTAL POROSITY cc/cc	DENSITY g/cc	K x 10^{-13} m/s	TOTAL POROSITY cc/cc	DENSITY g/cc	K x 10^{-13} m/s	TOTAL POROSITY cc/cc	DRY DENSITY g/cc	K x 10^{-13} m/s	TOTAL POROSITY cc/cc	DRY DENSITY g/cc	K x 10^{-13} m/s	TOTAL POROSITY cc/cc	DRY DENSITY g/cc
	3.36	0.204	2.08	5.12	0.228	2.01	4.86	0.252	1.97	6.05	0.312	1.82	7.19	0.326	1.73
	5.52	0.186	2.05	5.35	0.218	2.04	5.23	0.260	1.94	6.98	0.331	1.79	7.34	0.328	1.74
	5.94	0.192	2.10	5.84	0.220	2.00	6.12	0.272	1.91	6.43	0.311	1.80	8.22	0.328	1.76
	6.24	0.200	2.07	6.47	0.220	2.06	6.76	0.280	1.90	7.99	0.320	1.79	9.15	0.332	1.75
	7.39	0.186	2.08	7.56	0.226	2.01	7.35	0.278	1.90	8.12	0.310	1.78	9.22	0.336	1.75
	9.41	0.184	2.10	9.26	0.232	2.00	10.78	0.290	1.90	11.53	0.336	1.76	13.48	0.342	1.77
MEAN	6.31	0.192	0.208	6.60	0.224	2.02	6.85	0.272	1.92	7.85	0.320	1.79	9.10	0.332	1.75
C.O.V. (%)	29.11	3.94	0.83	21.70	2.25	1.11	28.5	4.62	1.38	23.1	3.18	1.02	23.3	1.67	0.74

HYDRATION PERIOD	7 DAYS			28 DAYS			3 MONTHS			6 MONTHS		
0.5 W/C RATIO	K x 10^{-13} m/s	TOTAL POROSITY cc/cc	DENSITY g/cc	K x 10^{-13} m/s	TOTAL POROSITY cc/cc	DENSITY g/cc	K x 10^{-13} m/s	TOTAL POROSITY cc/cc	DENSITY g/cc	K x 10^{-13} m/s	TOTAL POROSITY cc/cc	DENSITY g/cc
	12.00	0.262	1.91	4.86	0.260	1.97	3.72	0.248	1.95	1.66	0.248	1.98
	14.10	0.285	1.90	5.23	0.260	1.94	4.47	0.248	1.93	1.83	0.256	1.99
	15.76	0.280	1.89	6.12	0.274	1.91	4.58	0.252	1.93	2.13	0.250	1.97
	16.23	0.280	1.89	6.76	0.280	1.90	4.89	0.248	1.91	2.54	0.244	1.95
	18.10	0.287	1.88	7.35	0.278	1.90	5.85	0.256	1.87	2.90	0.250	1.91
	20.41	0.286	1.87	10.78	0.280	1.90	6.19	0.260	1.87	3.94	0.240	1.90
MEAN	16.15	0.280	1.89	6.85	0.272	1.92	4.95	0.252	1.91	2.50	0.248	1.95
C.O.V.	16.50	3.03	0.68	28.50	3.20	1.38	17.0	1.83	1.60	30.7	1.75	2.03

TABLE 7.3: Crude oil permeability, total porosity and dry density of Mortar (1:1 cement/sand ratio), tested for permeability at 99.6 metres pressure head of oil.

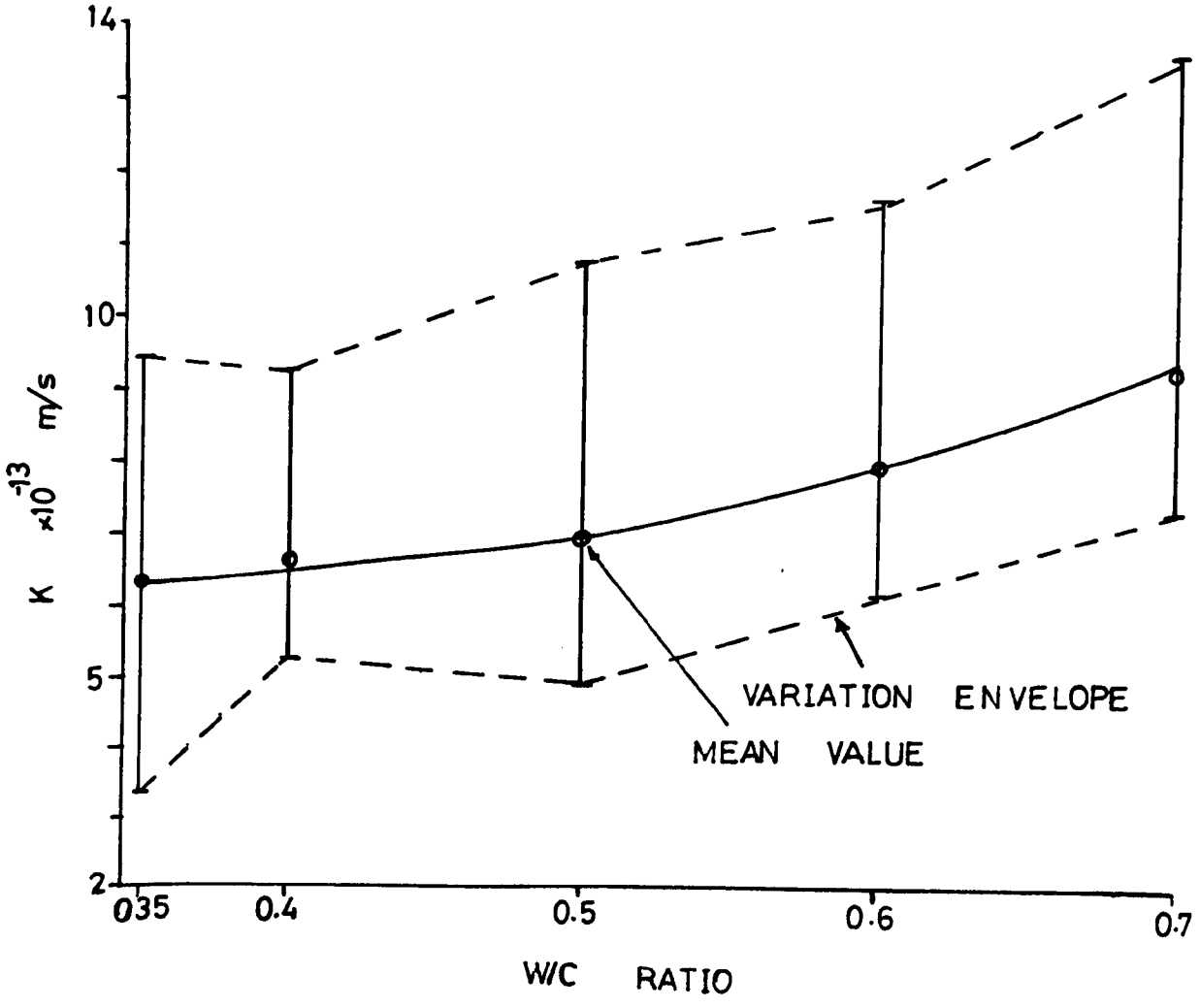

FIG 7.6 GRAPH OF K VS W/C RATIO SHOWING THE EXTENT OF SCATTER OF K FOR A GIVEN W/C RATIO (1:1 CEMENT: SAND RATIO, 28 DAYS CURING, 99.6 METRE HEAD OF OIL)

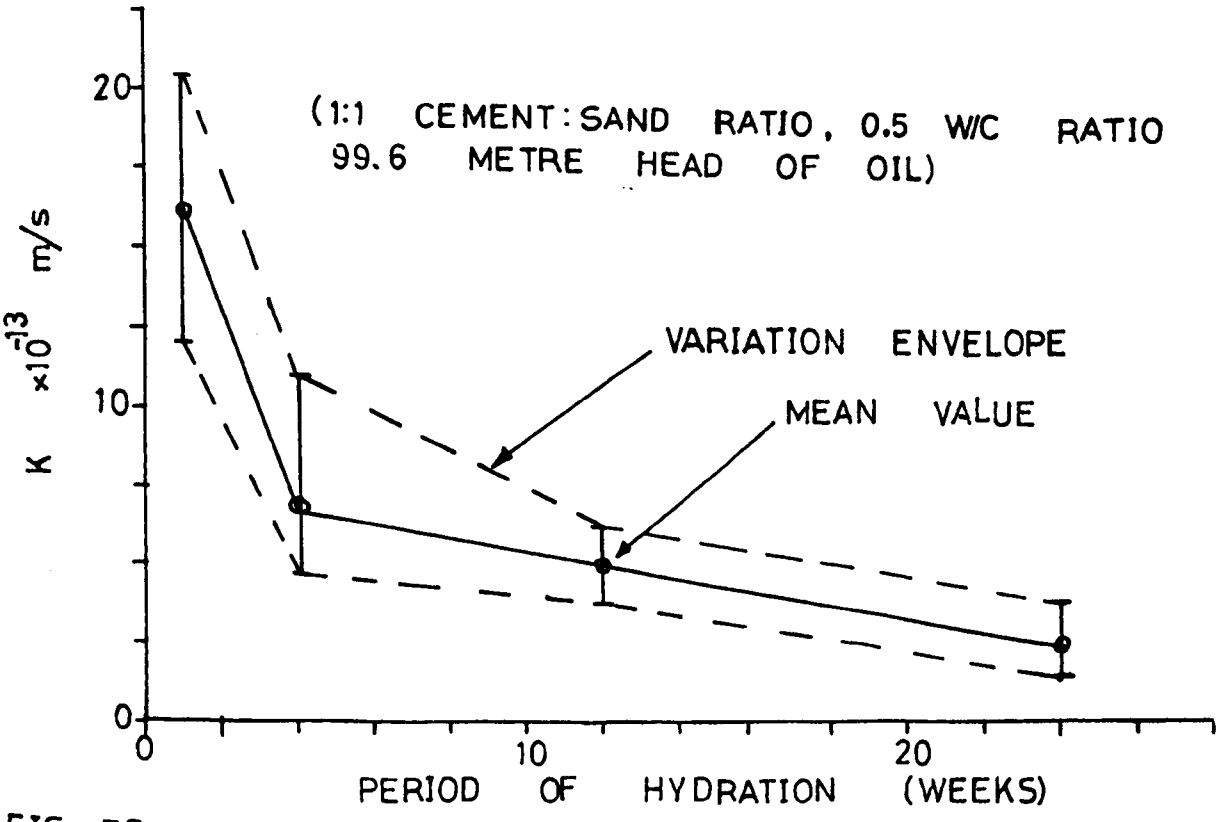

FIG 7.7 GRAPH OF K VS HYDRATION PERIOD SHOWING THE EXTENT OF SCATTER OF K FOR GIVEN AGE

out in a constant temperature room (CTR), the effect of temperature and humidity variations are not considered.

2. The permeability increases exponentially with an increase in the w/c ratio (table 7.2) and can be represented by an equation of the form

$$K = K_o(\exp)^{a\ w/c} \qquad (7.1)$$

where K_o is a theoretical coefficient of permeability at zero w/c ratio. K_o and a are constants, table 7.4, and were determined regressionally. Oyeka's[17] equation for Kuwait crude oil flow through HCP is similar but the constants of regression are different.

2. Under 83.0 m, pressure head of oil, K after 28 days curing has increased 1.40 times for 1:1 mortar, 1.65 times for 1.1½ mortar, 1.21 times for 1:2 and 1:3 mortar, as the w/c ratio was increased from 0.50 to 0.70. These are very low values compared with more than a hundred fold increase for water flow through HCP[114] and may be again as a result of wax deposition from the oil.

7.2.1.3 Period of hydration

The main values of K at various ages are given in table 7.2. Typical plots of K versus time of hydration are given in figs. 7.8 and 7.9 for 1:1 cement/sand ratio and oil heads of 49.8 and 83.0 metres respectively. Fig. 7.10 and 7.11 show the variation of K with hydration for four mortars with 0.50 and 0.70 w/c ratios under 49.8 and 99.6 metre head of oil. The following observations are made from the plots.

1. Permeability generally decreases rapidly at the initial stages of hydration. For 1:1 mortar, a rapid decrease occurred in K, in the first 28 days and then remained about constant for up to 6 months. For 1:1½ and 1:2 cement/sand ratio, some reduction in K continued up to 6 months while for 1:3 mortar, K reduced in the first 3 months of hydration. A further decrease in K after 3 months was found to be very small for all the mortar mixes (figs. 7.8 to 7.11).

With a 1:1 mortar, enough cement paste is available so that smaller

HYDROSTATIC PRESSURE HEAD (M)	7 DAYS CURING			28 DAYS CURING			3 MONTHS CURING			6 MONTHS CURING		
	$K_o \times 10^{-13}$	a	r	$K_o \times 10^{-13}$	a	r	$K_o \times 10^{-13}$	a	r	$K_o \times 10^{-13}$	a	r
1:1 CEMENT/SAND RATIO												
33.2	5.72	0.754	0.983	1.11	2.06	0.970	0.832	2.35	0.978	0.451	2.566	0.971
49.8	7.57	0.634	0.987	1.71	1.87	0.995	1.507	1.88	0.996	0.519	2.564	0.958
66.4	9.41	0.649	0.965	3.00	1.12	0.978	1.547	1.96	0.996	0.582	2.694	0.985
83.0	9.64	0.701	0.952	3.44	1.07	0.945	2.225	1.52	0.998	0.635	2.660	0.987
99.6	11.82	0.614	0.963	4.33	1.02	0.976	2.517	1.37	0.994	0.768	2.483	0.994
1:1.5 CEMENT/SAND RATIO												
33.2	7.62	1.766	0.988	2.93	2.03	0.985	1.86	1.35	0.996	1.00	1.48	0.968
49.8	12.50	1.232	0.940	3.83	2.09	0.982	1.96	1.63	0.995	1.27	1.19	0.953
66.4	13.20	1.272	0.947	3.68	2.33	0.997	2.29	1.55	0.996	1.29	1.78	0.986
83.0	13.29	1.363	0.948	5.49	1.93	0.974	2.56	1.46	0.992	1.29	1.92	0.997
99.6	13.19	1.426	0.960	5.36	2.11	0.995	3.05	1.23	0.975	1.64	1.56	0.989
1:2 CEMENT/SAND RATIO												
33.2	8.67	1.979	0.984	5.83	2.01	0.880	2.03	1.49	0.994	2.01	1.10	0.975
49.8	11.06	1.720	0.982	6.07	1.96	0.871	2.88	1.22	0.992	1.96	1.33	0.986
66.4	10.96	1.854	0.998	6.84	1.83	0.861	2.86	1.29	0.987	2.36	1.10	0.983
83.0	12.71	1.700	0.992	6.78	1.94	0.904	2.94	1.33	0.988	2.96	0.83	0.970
99.6	12.94	1.742	0.997	6.53	2.02	0.942	3.45	1.12	0.978	3.32	0.97	0.972
1:3 CEMENT/SAND RATIO												
33.2	13.63	1.19	0.995	14.55	1.03	0.996	4.07	0.78	0.998	2.56	1.24	0.971
49.8	10.45	2.03	0.998	14.38	1.33	0.995	4.29	0.79	0.986	3.81	0.67	0.890
66.4	9.86	2.29	0.998	18.99	0.98	0.998	4.88	0.65	0.966	4.17	0.61	0.913
83.0	10.07	2.36	0.996	17.92	1.18	0.991	5.26	0.56	0.965	4.06	0.79	0.909
99.6	13.75	1.97	0.996	21.88	0.89	0.997	5.11	0.63	0.991	3.93	1.03	0.925
CONCRETE 1:1½:1½ CEMENT/SAND/GRAVEL												
33.2	3.97	2.56	0.995	3.45	2.03	0.985	4.82	1.11	0.996	2.92	1.46	0.958
49.8	4.46	2.40	0.994	4.18	2.04	0.993	5.41	0.98	0.993	3.05	1.29	0.987
66.4	5.91	2.16	0.994	4.06	2.22	0.990	5.62	1.07	0.995	4.03	1.07	0.964
83.0	6.96	2.07	0.995	4.56	2.13	0.985	6.66	0.90	0.997	3.92	1.32	0.963
99.6	6.96	2.12	0.993	5.93	1.77	0.950	6.95	1.02	0.998	3.76	1.48	0.983

TABLE 7.4: Constants of Regression for eqn. (7.1) K vs w/c Ratio.

FIG 7.8 & 7.9 VARIAT. OF K WITH TIME OF HYDRATION AT VARYING W/C RATIO

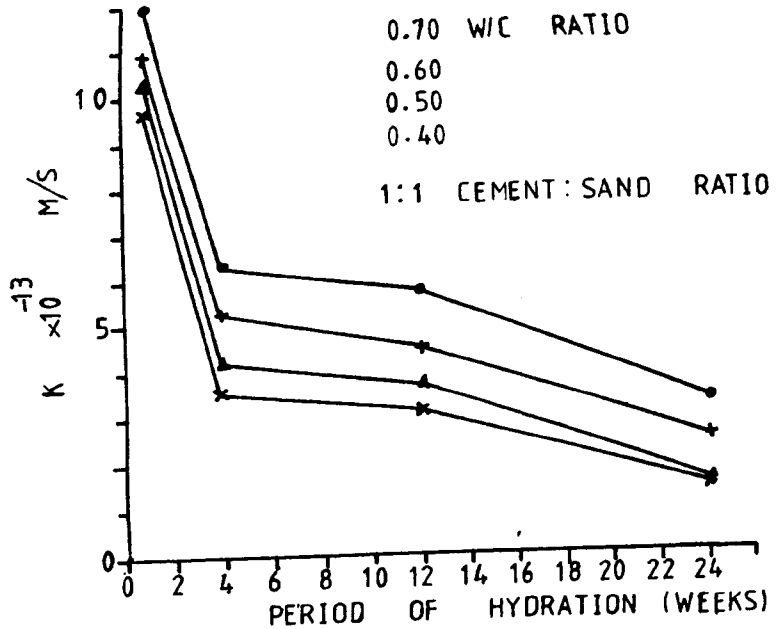

FIG 7.8 FOR 49.8 METRES PRESSURE HEAD OF OIL

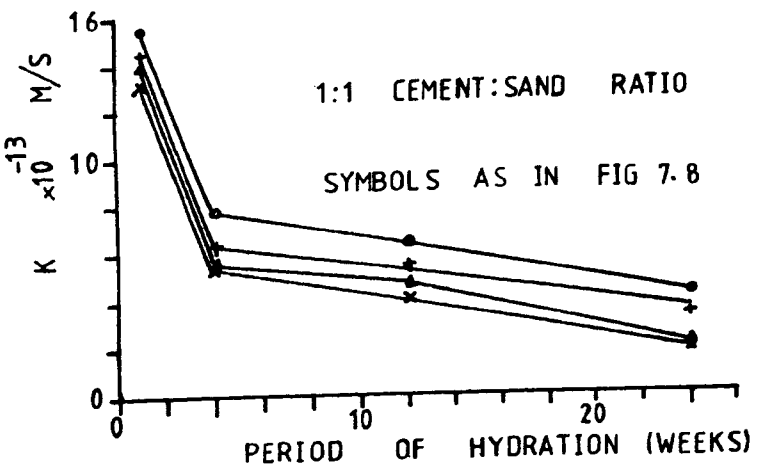

FIG 7.9 FOR 83.0 METRES PRESSURE HEAD OF OIL

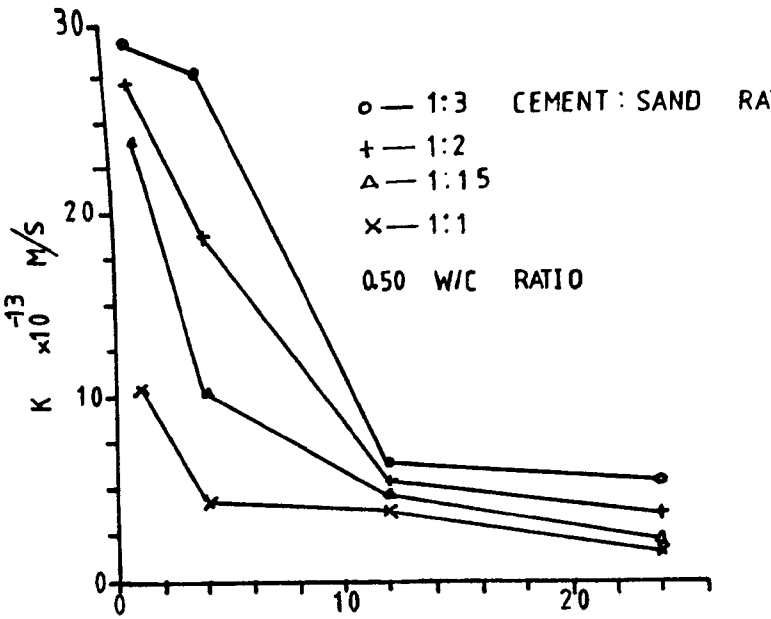

FIG 7.10 49.8 METRE HEAD OF OIL

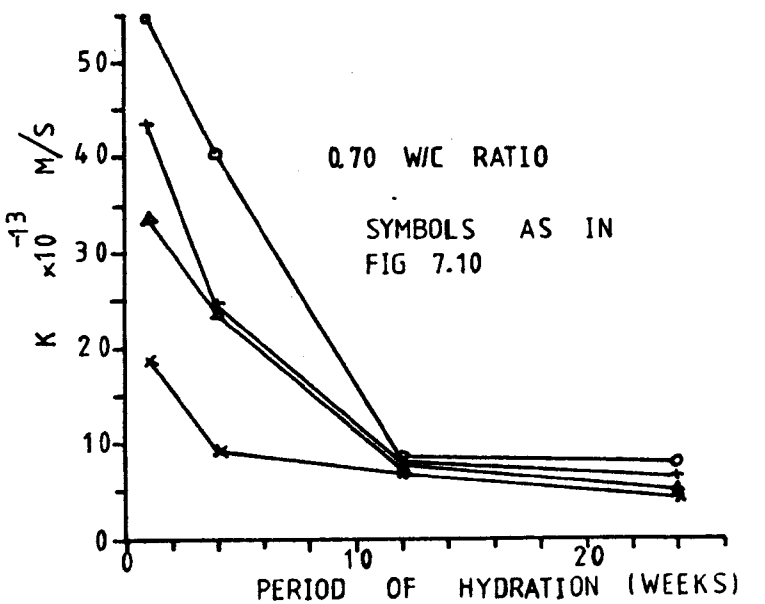

FIG 7.11 99.6 METRE HEAD OF OIL

FIG 7.10 & 7.11 VARIATION OF K WITH TIME OF HYDRATION AT VARYING CEMENT : SAND RATIO

pore sizes are formed rapidly in the first 28 days. Most of these pore sizes are blocked by the waxy deposits of the crude oil (section 6.7), consequently permeability is rapidly reduced to a constant level. As the aggregate content is increased, and cement content reduced, the pores are larger at a given age and it takes longer for the wax to reduce the flow. Total porosity reduces with hydration, but not as rapidly as permeability, suggesting that total porosity may not relate uniquely to permeability. This will be discussed further in chapter 8.

2. Under 99.6 metre head of oil pressure, K decreased with hydration from 7 days to 28 days (0.5 w/c ratio) by 2.36 times for 1:1 mortar, 1.78 times for 1:1½, 1.59 times for 1:2 and 1.08 times for 1:3 mortar. These are very low figures compared with values of about 65 times for water flow through HCP[114]. This is an obvious difference between oil and water flow, for both mortar and HCP.

7.2.1.4 Applied hydrostatic pressure

The variations of K with the applied hydrostatic head are illustrated in fig. 7.12, for 1:1 cement/sand ratio and fig. 7.13 for the four cement/sand ratios and four hydration periods, at 0.5 w/c ratio. These results are also given in table 7.2, and the following observations are made.

1. The coefficient of permeability increased approximately linearly with an increase in the applied hydrostatic pressure. The rate of increase varied erratically with w/c ratio and the period of hydration. For 1:1 mortar, with w/c ratio = 0.50, after 7 days hydration, increasing the pressure from 33.2 to 49.8, 66.4, 83.0 and 99.6 metre head of oil, increases K by 1.26, 1.63, 1.73 and 1.98 times the K value at 33.2 metres pressure head of oil respectively. For w/c = 0.7, the increases in K were 1.26, 1.47, 1.57 and 1.85, as the oil pressure increased. The increases for other hydration periods for 0.50 w/c ratio were as follows: after 28 days hydration, 1.46, 1.73, 1.90 and 2.36; after 3 months hydration, 1.58, 1.69, 1.98 and 2.06 and after 6 months hydration, increases in K is 1.10, 1.43, 1.52

FIG 7.13 VARIATION OF K WITH APPLIED PRESSURE FOR THE FOUR HYDRATION PERIODS AND W/C RATIOS

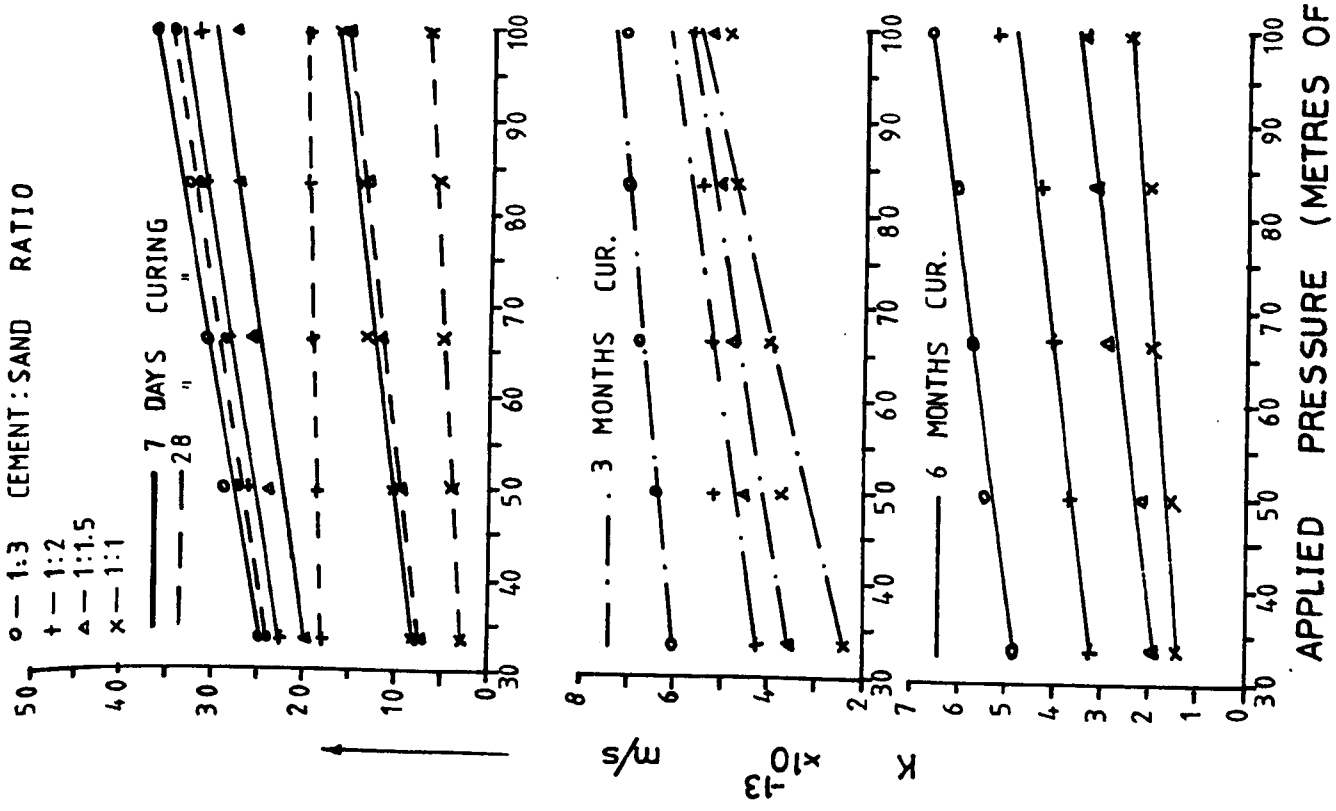

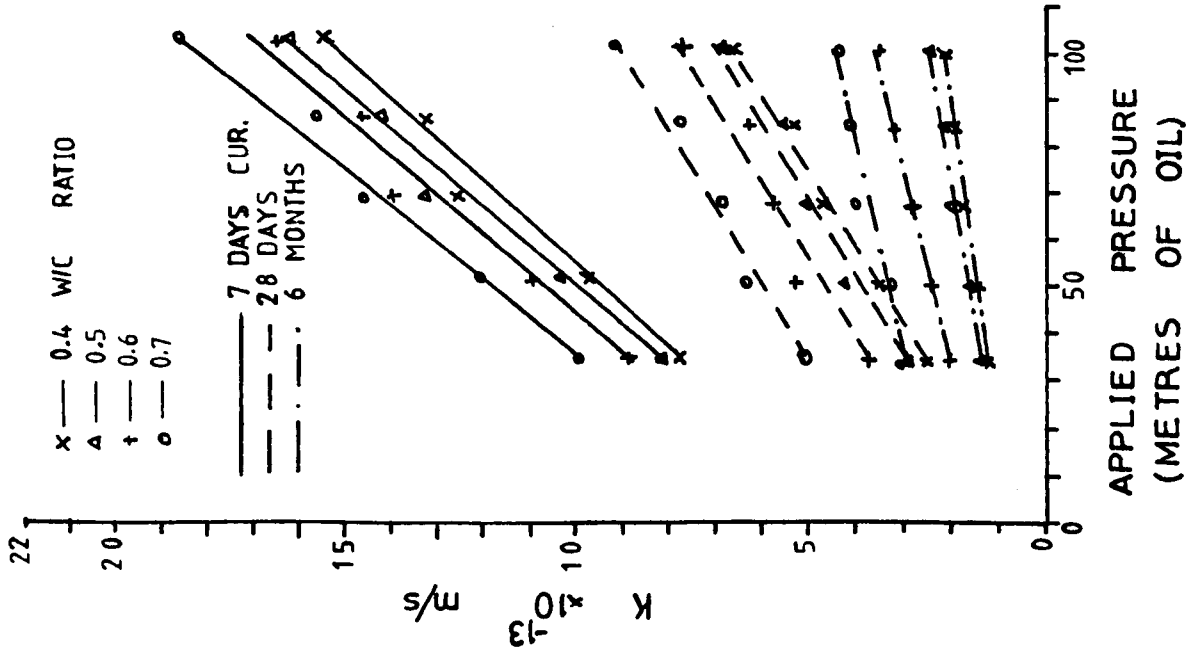

FIG 7.12 VARIAT. OF K WITH APPLIED PRESSURE FOR MORTAR OF 1:1 CEMENT: SAND RATIO

and 1.77 as the oil pressure increased from 33.2 metres to 49.8, 66.4, 83.0 and 99.6 metres respectively.

3. For mortars of varying cement/sand ratios, the relationship between K and the applied hydrostatic head (h) can be expressed with an equation of the form:

$$K = Dh+C \qquad (7.2)$$

The constants D and C were determined by regression analysis and are given in table 7.5.

The increase in K with applied pressure could be because some of the waxy deposits that blocked the pores below 650 Å (the critical pore radius) were flushed away at higher oil pressures to increase the permeability. Alternatively, high pressures may destroy the pore partitions and create more flow channels, or the high pressures forced oil through smaller pore sizes. The relative importance of these effects is not known and may be of interest in further investigations.

The increase in K with applied pressure was also observed by Oyeka[17] for crude oil flow through HCP. In contrast, Nyame[114] observed a decrease in K with applied pressure for water flow through HCP, hydrated for 7 days. However, these tests took 3 weeks with the specimens in water, and further hydration may have occurred[114].

7.2.1.5 Effect of aggregate volume concentration

The effects of aggregate volume concentration were studied by varying the cement/sand ratio up to 1:3 as shown in table 6.1. Table 7.6 and figs. 7.14 and 7.15 give the variations of K with aggregate volume concentration for 28 days cured mortars at 49.8 and 83.0 metres pressure head of oil. The following observations are made.

1. Comparing table 7.1 with 7.2, indicates that the additions of sand to HCP reduces the permeability, but this result needs further investigation since the cracking of HCP during the oven drying makes the results rather unreliable.

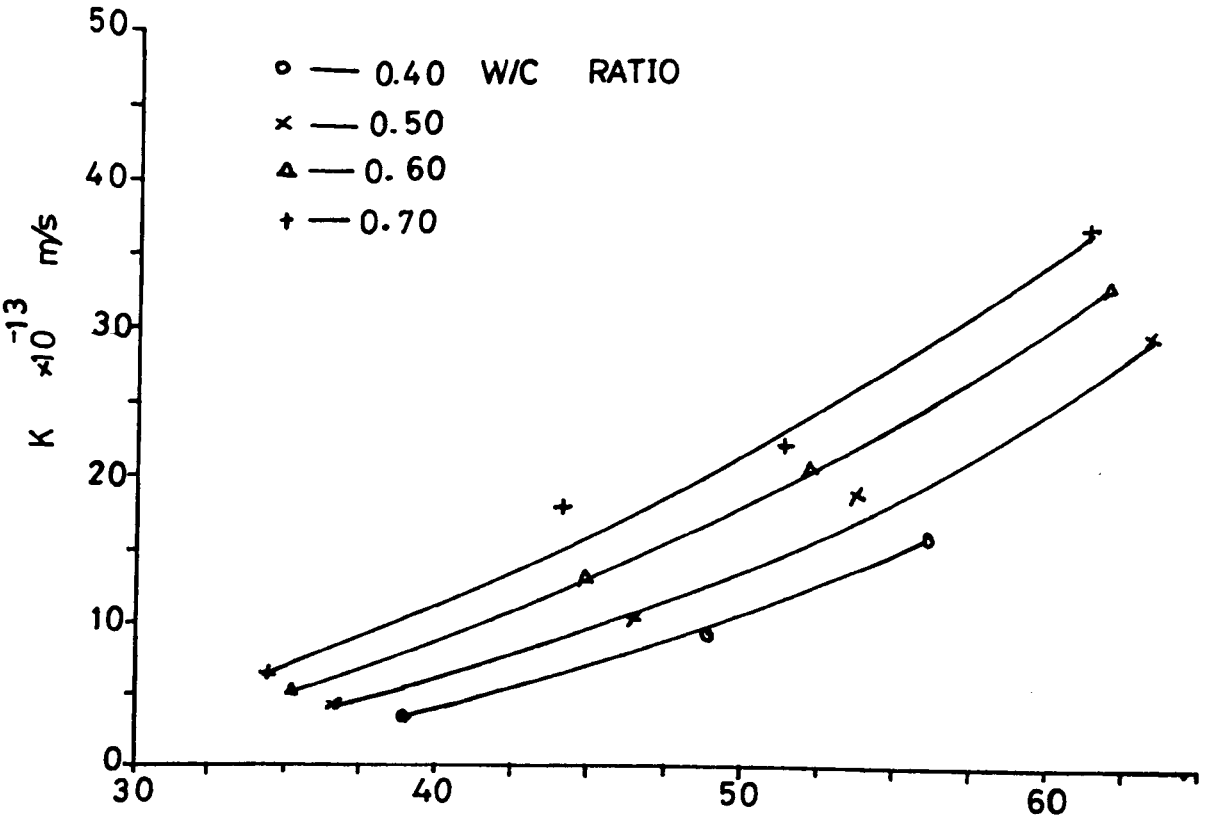

FIG 7.14 AT 49.8 METRES, PRESSURE HEAD OF OIL

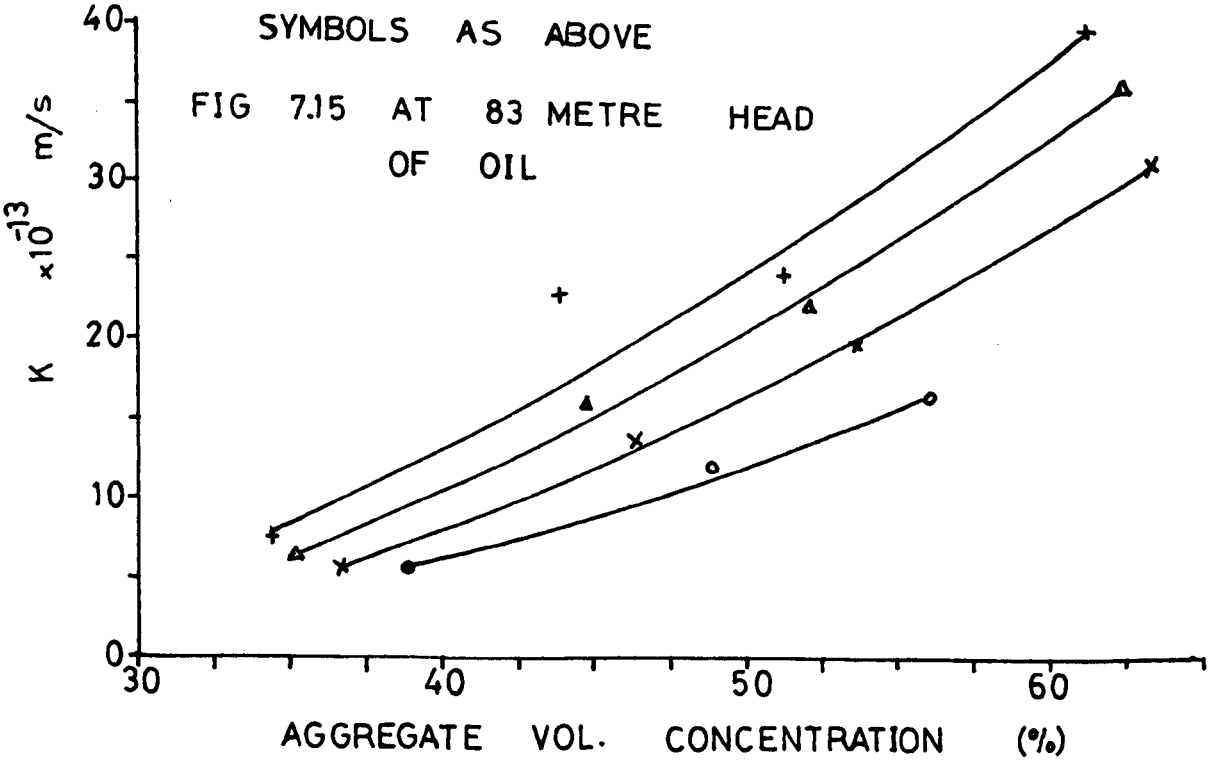

FIG 7.14 & 7.15 EFFECT OF AGGREGATE VOLUME CONCENTRATION ON PERMEABILITY OF MORTARS, CURED FOR 28 DAYS

W/C RATIO	7 DAYS CURING			28 DAYS CURING			3 MONTHS CURING			6 MONTHS CURING		
	$D \times 10^{-15}$	$C \times 10^{-13}$	r	$D \times 10^{-15}$	$C \times 10^{-13}$	r	$D \times 10^{-15}$	$C \times 10^{-13}$	r	$D \times 10^{-15}$	$C \times 10^{-13}$	r
1:1 CEMENT/SAND RATIO												
0.35	9.76	4.52	0.981	5.80	0.52	0.997	2.91	1.25	0.970	0.93	0.90	0.994
0.40	11.25	4.21	0.988	5.98	0.58	0.995	3.36	1.22	0.977	1.28	0.86	0.981
0.50	11.93	4.48	0.982	5.52	1.24	0.987	3.66	1.56	0.951	1.68	0.81	0.986
0.60	11.27	5.43	0.983	5.57	2.07	0.972	3.34	2.55	0.960	2.25	1.36	0.997
0.70	12.64	5.75	0.992	5.62	3.28	0.986	2.96	3.97	0.926	2.22	2.27	0.967
1:1.5 CEMENT/SAND RATIO												
0.35	8.92	12.10	0.918	7.65	4.02	0.956	2.81	2.06	0.998	1.86	1.11	0.980
0.40	12.83	13.48	0.857	9.04	3.82	0.965	2.64	2.43	0.988	1.76	1.31	0.981
0.50	11.33	17.44	0.920	11.93	3.85	0.996	2.44	3.06	0.927	2.44	1.13	0.968
0.60	15.78	17.60	0.983	12.65	6.10	0.990	3.14	3.41	0.945	3.10	1.28	0.942
0.70	12.59	22.08	0.981	16.51	8.14	0.969	3.87	3.95	0.950	3.66	1.72	0.926
1:2 CEMENT/SAND RATIO												
0.35	7.71	15.98	0.978	3.37	8.25	0.987	2.14	3.11	0.920	2.61	2.00	0.968
0.40	10.66	15.82	0.984	2.49	14.53	0.906	2.54	3.03	0.943	2.61	2.08	0.975
0.50	13.49	19.26	0.954	3.29	16.99	0.960	1.93	3.90	0.896	2.72	2.33	0.961
0.60	15.00	21.90	0.982	4.20	18.42	0.959	2.55	4.32	0.954	2.68	2.78	0.960
0.70	10.30	33.24	0.998	5.33	19.31	0.927	2.64	5.33	0.930	2.96	3.47	0.920
1:3 CEMENT/SAND RATIO												
0.50	16.68	19.88	0.986	14.46	20.30	0.983	1.60	5.60	0.956	2.69	4.00	0.995
0.60	24.45	21.22	0.974	14.88	23.66	0.941	1.40	6.06	0.986	2.53	4.26	0.984
0.70	33.19	24.32	0.943	15.78	26.62	0.937	1.68	6.58	0.955	3.04	4.86	0.921

TABLE 7.5: Constants of Regression in eqn. (7.2) K vs applied hydrostatic pressure (h).

PASTE DESIGNATION	AGGREGATE VOLUME CONCENTRATION (%)	COEFFICIENT OF PERMEABILITY K x 10^{-13} m/s AT VARYING METRE HEAD OF OIL				
		m → 33.20	49.80	66.40	83.00	99.60
0.35 W/C RATIO						
M35-1	40.64	2.40	3.40	4.55	5.20	6.31
M35-1.5	50.66	6.30	8.30	8.50	11.20	11.20
M35-2	57.79	9.50	9.70	10.50	11.50	11.57
0.40 W/C RATIO						
M40-1	38.82	2.55	3.51	4.75	5.35	6.60
M40-1.5	48.77	6.50	9.00	9.11	12.01	12.50
M40-2	55.93	15.30	15.50	16.64	16.73	16.75
0.50 W/C RATIO						
M50-1	36.59	2.90	4.24	5.01	5.50	6.85
M50-1.5	46.39	7.50	10.00	12.02	13.90	15.45
M50-2	53.57	17.90	18.61	19.50	19.90	19.98
M50-3	63.38	24.40	27.80	31.00	32.00	34.30
0.60 W/C RATIO						
M60-1	35.16	3.70	5.30	5.75	6.25	7.85
M60-1.5	44.86	10.00	13.00	14.50	16.03	19.00
M60-2	52.03	20.10	20.15	21.01	22.30	22.51
M60-3	61.93	27.00	32.50	34.10	37.00	37.10
0.70 W/C RATIO						
M70-1	34.51	5.10	6.37	6.80	7.70	9.10
M70-1.5	44.15	12.50	17.50	19.10	22.90	23.51
M70-2	51.31	21.60	21.70	22.53	24.16	24.79
M70-3	61.25	30.00	36.30	37.70	40.50	41.00

TABLE 7.6: Influence of Aggregate Volume Concentration on Permeability of Mortars, 28 days hydration.

2. An increase in the aggregate volume concentration in mortar produces a non-linear increase in permeability (figs. 7.14 and 7.15).

3. For mortars hydrated for 28 days, the relationship between the percentage aggregate volume concentration and K can be represented with an exponential equation of the form

$$K = K_o(exp)^{b_1(AV)} \qquad (7.3)$$

Where AV = Aggregate volume concentration (%)

K_o = theoretical coefficient of permeability at zero aggregate volume concentration

b_i is a constant

K_o and b_1 are determined regressionally and are given in table 7.7.

Aggregates will reduce the number of flow channels per unit cross-sectional area and lengthen the flow paths, which may cause a reduction in permeability. Alternatively fissures and bond cracks around the aggregate particles, may increase the flow. No literature clarifying the relative importance of these opposing effects on permeability of mortars and concrete has been found. Comparing HCP and mortar, it is seen that, when sand is added in small amounts, the permeability reduces, indicating that the first effect is dominant. When larger amounts of sand are added, then permeability increases, perhaps because the second effect is now dominant. More work is however required to clarify this point.

Powers et al[141], state that since the paste forms a continuous phase surrounding the aggregate particles, the permeability of mortars and concrete will depend on that of the paste, the permeability of the aggregate and the relative proportion of the two. Neville[27], stated that for a fully hydrated concrete, it is the permeability of the paste which has the greatest effect on the permeability of the concrete. If Neville's deduction is correct, then a reduction in permeability would occur with an increase in the aggregate volume concentration (since a smaller quantity of cement paste is available). This has not been found to be the case, hence fissures in

APPLIED HYDROSTATIC PRESSURE HEAD (M)	$K_o \times 10^{-14}$	b_1	r
0.35 w/c RATIO			
33.2	0.923	0.0813	0.991
49.8	2.844	0.0629	0.959
66.4	6.281	0.0496	0.984
83.0	7.955	0.0482	0.922
99.6	15.035	0.0368	0.929
0.40 W/C RATIO			
33.2	0.436	0.1041	0.997
49.8	1.210	0.0873	0.998
66.4	2.756	0.0728	0.997
83.0	4.021	0.0677	0.989
99.6	8.698	0.0535	0.995
0.50 W/C RATIO			
33.2	1.614	0.0823	0.973
49.8	3.451	0.0713	0.985
66.4	4.619	0.0680	0.988
83.0	5.861	0.0647	0.983
99.6	8.816	0.0585	0.988
0.60 W/C RATIO			
33.2	3.001	0.0761	0.964
49.8	5.589	0.0672	0.986
66.4	6.541	0.0654	0.983
83.0	7.248	0.0650	0.982
99.6	12.632	0.0557	0.973
0.70 W/C RATIO			
33.2	5.842	0.0668	0.975
49.8	8.620	0.0626	0.970
66.4	9.770	0.0612	0.963
83.0	12.547	0.0583	0.944
99.6	17.194	0.0529	0.952

TABLE 7.7: Constants of Equation (7.3) K vs Agg. Vol. Concentration.

in the mortar may be responsible for the increase in permeability.

The aggregate permeability was not measured in this work but tests on the porosity of the aggregate showed a much lower value (table 6.8) than for the paste. If permeability increases with porosity (fig. 8.2) and ref. (17, 27), then it would be expected that the permeability of the aggregate is negligible. The two major parameters influencing the permeability of mortars therefore appear to be (1) The development of fissures and bond cracks - this is thought to increase with an increase in the aggregate volume concentration; (2) The relative proportion of paste to aggregate. The process of the development of fissures and bond cracks with an increase in aggregate proportions, and its relationship to permeability, is not studied further in this work.

7.2.1.6 Effect of drying temperature

The effect of drying temperatures on the oil permeability of mortar was studied with 3 months hydrated mortar, of 1:1 cement/sand ratio and w/c ratios of either 0.50 or 0.70 (figs. 7.16 and 7.17). Since complete expulsion of evaporable water cannot be achieved at temperatures lower than 105°C, the K values obtained at lower temperatures must have been influenced by the presence of this water, hence a more complex mathematics, which is beyond the scope of this study may be required to obtain equivalent K values. To obtain a more reliable result, water permeability was used. The K values for the oil flow through mortar of 1:1 cement/sand ratio, hydrated for 3 months, and water flow through mortar (1:1½ cement/sand) and concrete (1:1½:1½ cement/sand/gravel) hydrated for 28 days are given in table 7.8. Variations of log K (for water flow) with dry temperature are given in fig. 7.18, while figs. 7.19 to 7.21, illustrate the variations of K with w/c ratios at different drying temperatures of 0°C, 55°C, 80°C and 105°C for water flows. The drying procedures are as detailed in sections 3.8.1 and 3.8.2, and the following observations are made.

1. The flow of both oil and water increased exponentially with an

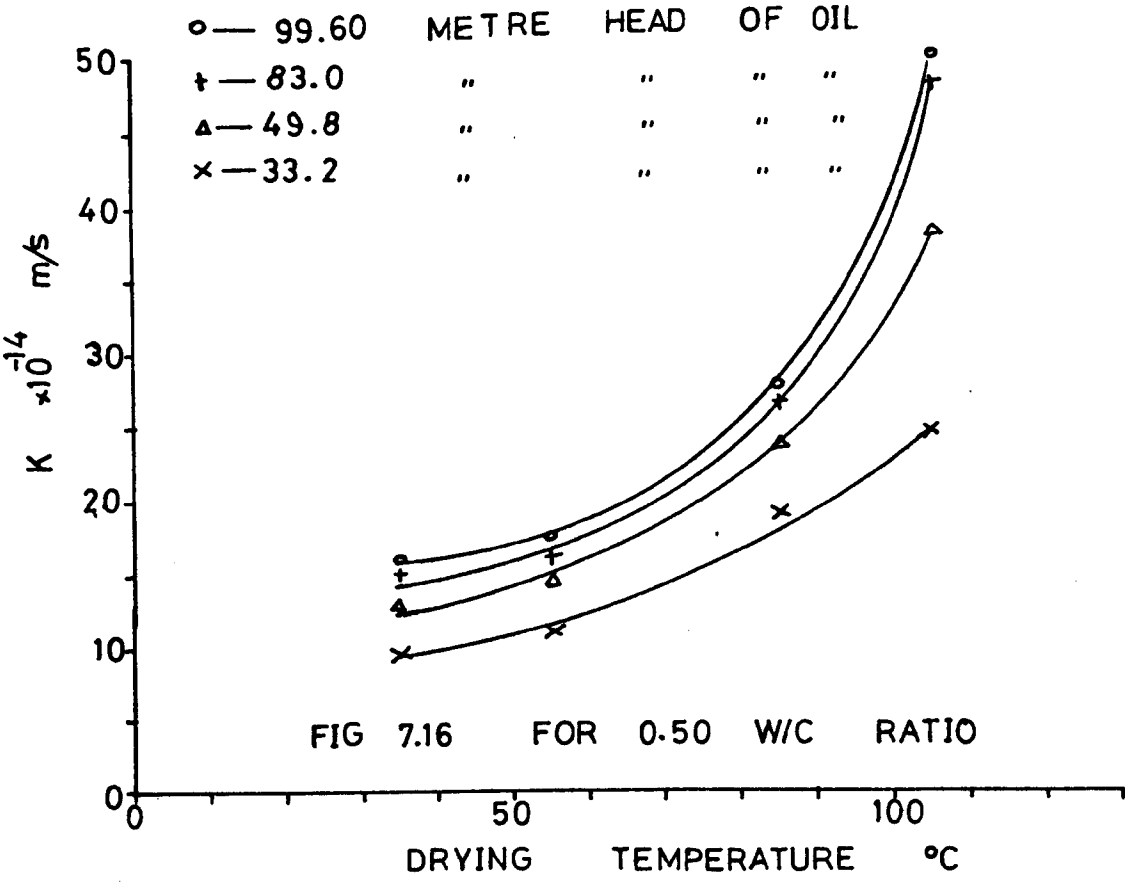

FIG 7.16 FOR 0.50 W/C RATIO

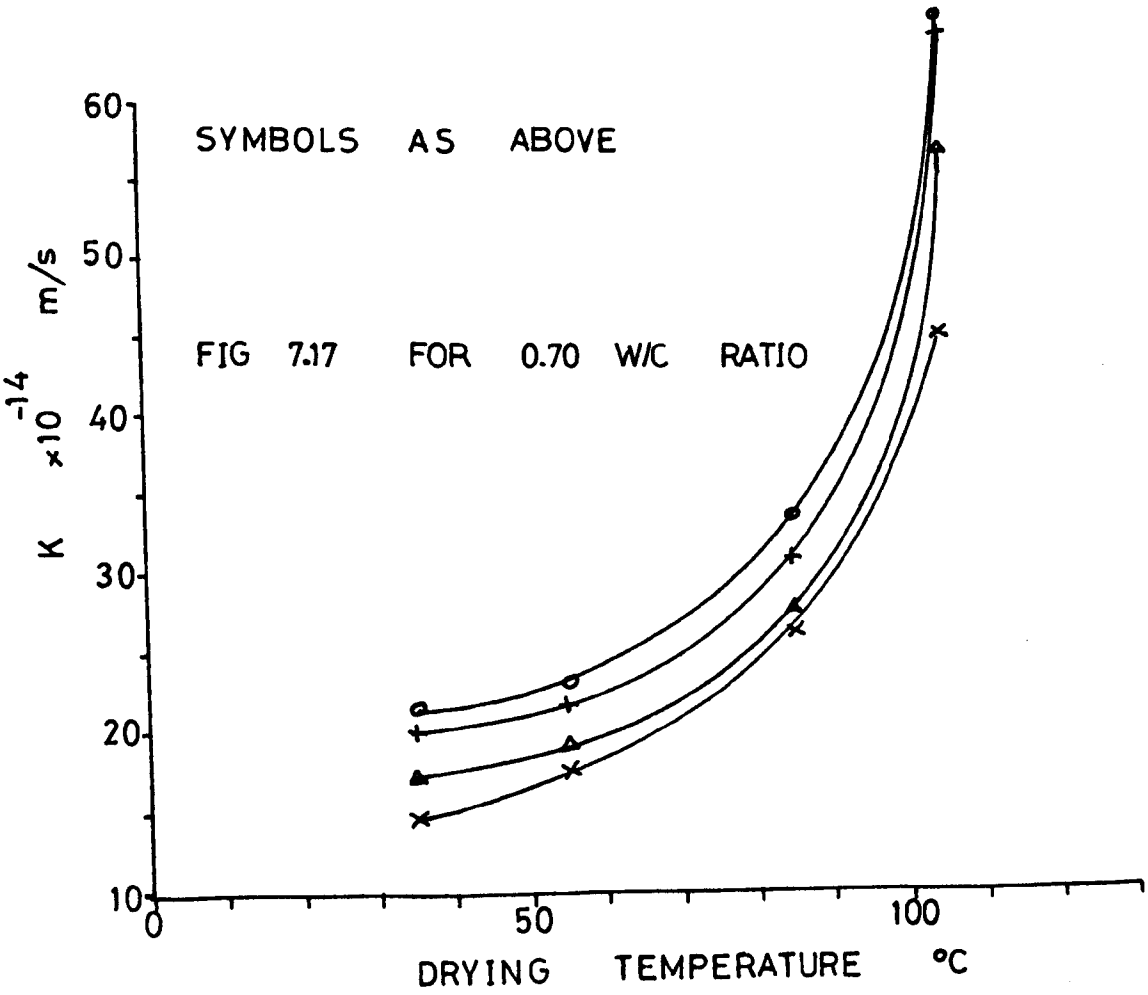

FIG 7.17 FOR 0.70 W/C RATIO

FIG 7.16 & 7.17 EFFECT OF DRYING TEMPERATURE O
CRUDE OIL PERMEABILITY OF MORTAR
1:1 CEMENT: SAND RATIO 3 MONTH CU

SATURATED PERMEABILITY OF MORTAR TO WATER (28 DAYS CURING)																				
		NO DRYING K x 10^{-14}					55°C K x 10^{-13}					80°C K x 10^{-13}					105°C K x 10^{-12} m/s				
		33.2	49.8	66.4	83.0	99.6	33.2	49.8	66.4	83.0	99.6	33.2	49.8	66.4	83.0	99.6	33.2	49.8	66.4	83.0	99.6
M35-1½		5.0	10.0	26.5	32.0	30.0	6.94	10.01	12.5	13.2	14.9	25.0	30.8	36.5	45.1	52.5	1.75	3.25	4.01	4.75	6.5
M40-1½		7.0	13.8	30.5	33.8	36.2	7.12	13.0	16.4	15.5	17.7	28.5	32.9	38.0	48.6	55.4	3.05	4.5	5.0	6.0	8.0
M50-1½		9.33	16.1	36.6	41.1	41.3	12.9	20.2	24.6	24.8	31.0	34.2	37.0	43.5	55.5	65.7	8.02	9.3	10.6	13.2	14.5
M60-1½		18.67	26.5	50.0	54.5	58.1	25.4	32.7	45.5	51.2	57.5	42.5	51.2	53.2	70.0	76.5	20.01	23.0	30.5	32.7	33.9
M70-1½		36.1	46.2	74.5	78.7	80.5	49.0	55.5	71.8	89.2	92.5	55.0	57.6	76.0	90.3	94.9	52.5	56.5	62.5	71.5	79.5
SATURATED PERMEABILITY OF CONCRETE TO WATER (28 DAYS CURING)																				
C35-1		3.05	5.5	8.0	10.01	12.5	8.5	11.02	12.6	15.8	18.2	4.95	12.5	21.5	25.5	35.8	5.0	6.1	7.0	7.4	8.1
C40-1		4.5	6.03	10.4	12.4	14.0	10.2	13.6	14.8	16.8	21.0	5.5	14	23.9	27.5	38.7	5.7	7.6	8.1	8.4	8.9
C50-1		7.01	11.0	16.4	18.0	19.5	21.5	25.6	26.3	28.0	31.5	9.8	21.6	31.9	36.7	51.6	6.4	9.1	10.0	11.0	11.5
C60-1		14.0	17.4	23.4	25.9	27.4	35.0	39.1	41.9	44.8	52.5	16.5	29.5	43.0	48.4	67.0	13.0	20.0	21.6	23.2	23.8
C70-1		23.5	27.89	34.8	38.0	39.8	55.5	57.5	58.5	67.5	84.5	27.0	44.7	59.8	68.8	92.8	21.6	39.3	44.4	46.5	48.4
SATURATED PERMEABILITY OF MORTAR TO OIL (3 MONTHS HYDRATION) K x 10^{-12} m/s																				
		35°C					55°C					85°C					105°C				
M50-1		7.32	12.74	13.37	14.96	15.98	10.87	14.48	14.98	15.78	17.01	18.80	23.16	24.76	26.12	27.20	24.0	37.8	40.5	47.5	49.5
M70-1		14.76	17.37	18.24	20.16	21.46	17.76	19.47	21.78	21.84	23.22	26.41	27.90	28.66	30.76	33.67	45.6	57.6	62.5	65.0	66.5

TABLE 7.8: Effect of Drying Temperature on K for both Water and Oil.

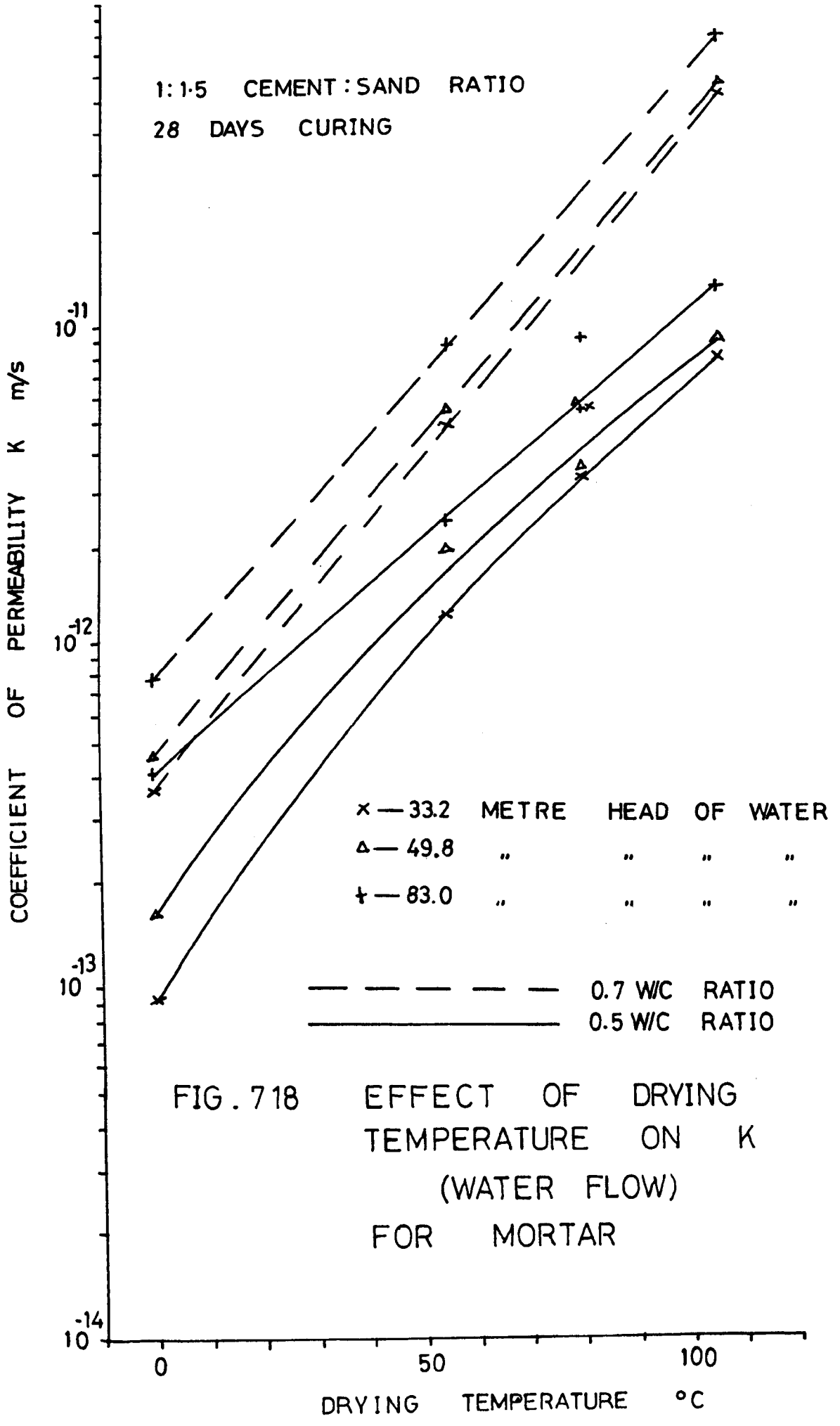

FIG. 7.18 EFFECT OF DRYING TEMPERATURE ON K (WATER FLOW) FOR MORTAR

increase in the drying temperature. The flow of water however showed a higher rate of increase than did oil. For water flow through mortar, (1:1½ cement/sand ratio) with 0.5 w/c ratio, with 99.6 m pressure head, K at 105°C is 2.9 times K at 55°C. The increase in K with drying temperature could be due to micro-cracking resulting from drying shrinkage. The differential temperature between the inner and outer surfaces of the specimens may have set up stresses which could crack the specimens[183]. The drying procedure adopted tried to minimise these stresses. These specimens were resaturated after drying prior to test, so all were carried out under steady state flow condition.

2. Figures 7.19 to 7.21 shows that K increases exponentially with w/c ratio for all the drying temperatujes. The shape of the curves suggests that drying has very little effect on the variation of K with w/c ratio.

3. For mortars of 1:1½ cement/sand ratio, hydrated in the fog room for 28 days, the relationship between the drying temperature T and water permeability coefficient K_w can be represented by an exponential equation of the form

$$K_w = K_o(\exp)^{aT} \qquad (7.4)$$

Where T = drying temperature °C

K_w = coefficient of permeability for water flow m/s

K_o = a theoretical coefficient of permeability at zero drying temperature. The value of K_o should be close to the value of K obtained experimentally on an undried specimen

a = constant

K_o and a are determined regressionally and are given in table 7.9.

7.2.1.7 Effect of specimen dimensions on permeability

Previous investigators have used different specimen sizes in permeabiltiy tests. Powers et al[139] used 25 mm diameter truncated cones of HPC. Cook[184] used 368 mm dia. x 380 mm high concrete cylinders. Oyeka[17] used 150 mm dia. x 50 mm thick concrete discs, and 100 mm dia. x

FIG 7.19
NO DRYING

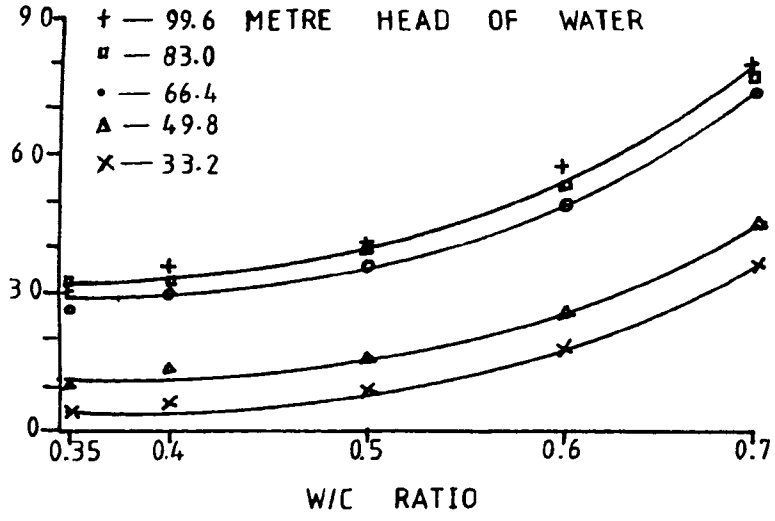

FIG 7.20
DRIED TO
55°C & 80°C

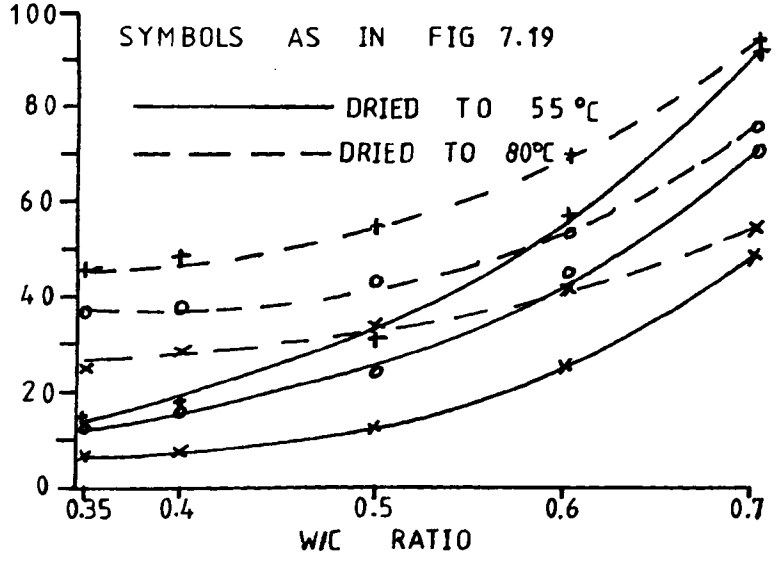

FIG 7.19 & 7.20 VARIATION OF K WITH W/C RATIO FOR MORTAR 1:1·5, 28 DAYS CURING (WATER)

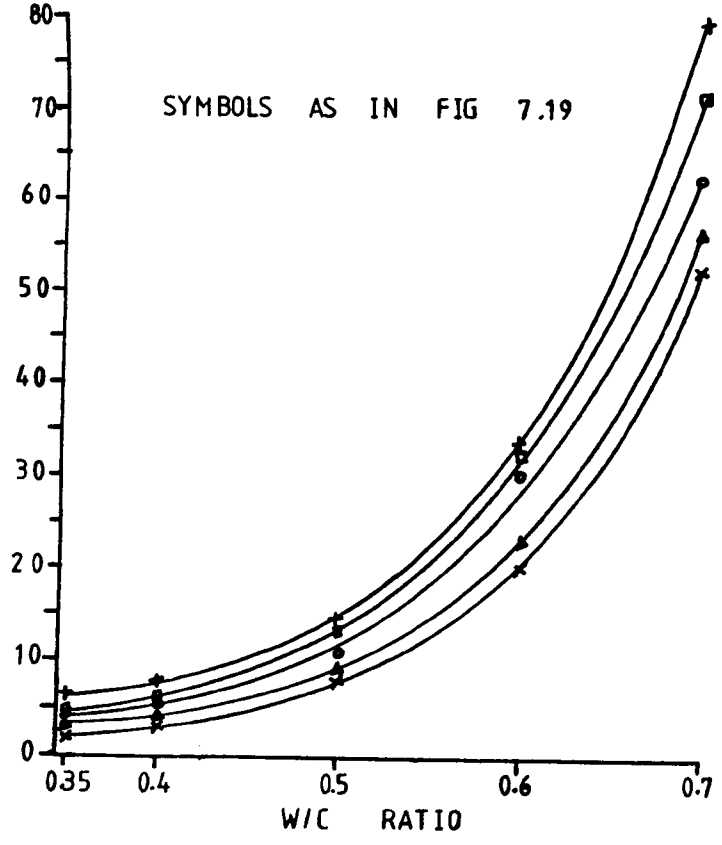

FIG 7.21 VARIATION OF K WITH W/C RATIO FOR MORTAR 1:1·5 CEMENT: SAND RATIO DRIED TO 105°C BEFORE TEST (28 DAYS CURING, WATER FLOW)

APPLIED HYDRO-STATIC PRESSURE (M)	MORTAR 1:1.5 CEMENT/SAND RATIO			CONCRETE 1:1.5:1.5 CEMENT/ SAND/COARSE AGG.		
	$K_o \times 10^{-13}$	a	r	$K_o \times 10^{-13}$	a	r
	0.35 W/C RATIO			0.35 W/C RATIO		
33.2	0.6690	0.0372	0.945	0.3508	0.04439	0.943
49.8	1.2019	0.03532	0.974	0.6296	0.04287	0.979
66.4	2.8334	0.02760	0.980	0.9004	0.04186	0.992
83.0	3.3582	0.02764	0.975	1.1620	0.04043	0.990
99.6	3.0738	0.03101	0.984	1.4624	0.03990	0.992
	0.40 W/C RATIO			0.40 W/C RATIO		
33.2	0.8096	0.03841	0.977	0.5043	0.04170	0.934
49.8	1.6062	0.03455	0.986	0.6982	0.04380	0.975
66.4	3.3215	0.02775	0.989	1.15236	0.04056	0.992
83.0	3.4807	0.02895	0.985	1.3889	0.03945	0.992
99.6	3.6520	0.03073	0.991	1.6557	0.03962	0.990
	0.50 W/C RATIO			0.50 W/C RATIO		
33.2	1.0298	0.04286	0.997	0.9236	0.03947	0.921
49.8	1.8217	0.03844	0.994	1.3844	0.04008	0.962
66.4	3.8017	0.03164	0.998	1.9591	0.03809	0.980
83.0	4.0771	0.03292	0.998	2.1350	0.03829	0.983
99.6	4.3345	0.03345	0.998	2.3876	0.03885	0.985
	0.60 W/C RATIO			0.60 W/C RATIO		
33.2	1.8978	0.04331	0.991	1.7140	0.03920	0.924
49.8	2.7298	0.0409	0.991	2.0162	0.04207	0.959
66.4	4.8854	0.03657	0.975	2.1643	0.04146	0.991
83.0	5.4464	0.0370	0.985	2.9287	0.04076	0.977
99.6	5.9374	0.03687	0.985	3.2591	0.04133	0.983
	0.70 W/C RATIO			0.70 W/C RATIO		
33.2	3.4155	0.04388	0.968	2.8305	0.03908	0.926
49.8	4.3149	0.04204	0.962	3.0172	0.04347	0.958
66.4	6.9414	0.03875	0.962	3.6242	0.04313	0.972
83.0	7.6245	0.03960	0.964	4.0675	0.04295	0.973
99.6	7.7145	0.04030	0.964	4.5586	0.04359	0.978

TABLE 7.9 Constants of equation 7.4, for mortar and concrete K vs Drying Temperature (Watch flow).

25 mm thick HCP specimens. These different specimens, may have to some extent, influenced the values of K. This section however does not intend to search for any standard dimension, but to draw attention to the need to establish a standard specimen for easy comparison of the results.

K values for three different mortar discs (100 mm dia. x 25 mm thick, 150 mm dia. x 25 mm thick and 150 mm dia. x 50 mm thick) cast from 1:1½ cement/sand ratio and hydrated in the fog room for 28 days are presented in table 7.10. The K values are for oil and water flows. The mortar used in the oil permeability tests were dried in an oven to 105°C as described in chapter 3, prior to saturation in crude oil. Those tested for water permeability were left undried. Figures 7.22 and 7.23 illustrate the variation of K with w/c ratios for oil and water flows using 49.8 and 83.0 metre head of oil and water respectively. K values were determined as described in section 5.2. The following observations are made from the plots and tables.

1. The permeability coefficient K, varies with the specimen dimensions. The K values decreased in the following order of specimen; 150 mm dia. x 50 mm thick, 100 mm dia. x 25 mm thick and finally 150 mm dia. x 25 mm thick.

2. For a constant depth of specimen, K decreased with an increase in the area of cross-section (compare 100 mm dia. x 25 mm thick and 150 mm dia. x 25 mm thick). For a constant diameter, K increased with an increase in the depth (compare 150 mm dia. x 25 mm thick and 150 mm dia. x 50 mm thick) because the pressure difference $^{dh}/_{dl}$ decreases, as clearly exhibited in equation 7.5

$$K = \frac{Q}{A} \times \frac{1}{dh/dl} \qquad (7.5)$$

The specimen dimensions do not appear to alter the general behaviour of fluid flow in mortar specimens. For example, all specimens showed an exponential increase in K with w/c ratio, and a linear increase in K with applied hydrostatic pressure for oil flow no matter what the size. This

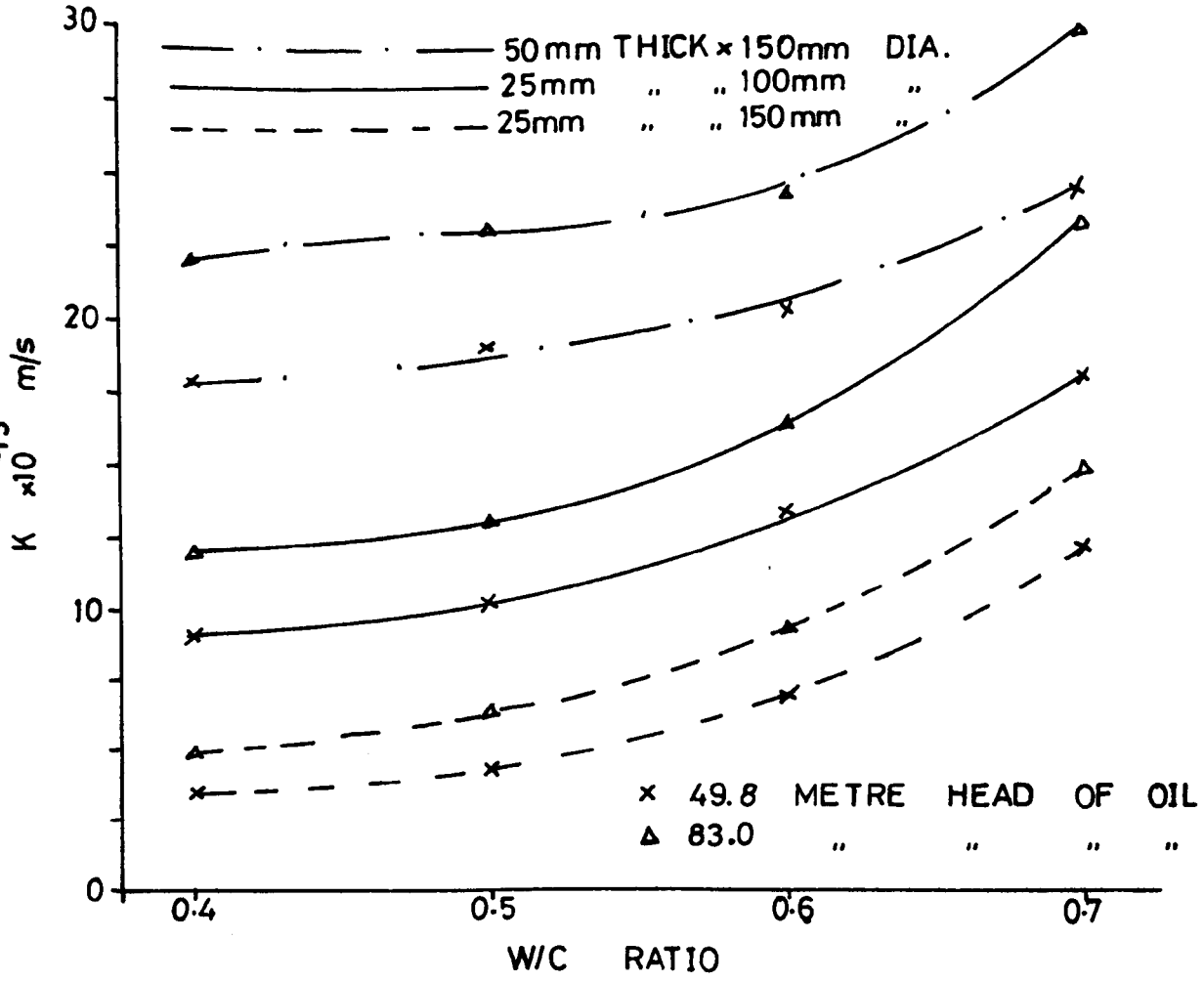

FIG 7.22 EFFCT OF SPECIMEN DIMENSION ON THE PERMEABILITY AT VARYING W/C RATIO DRIED TO 105°C, 28 DAYS CURING (OIL FLOW)

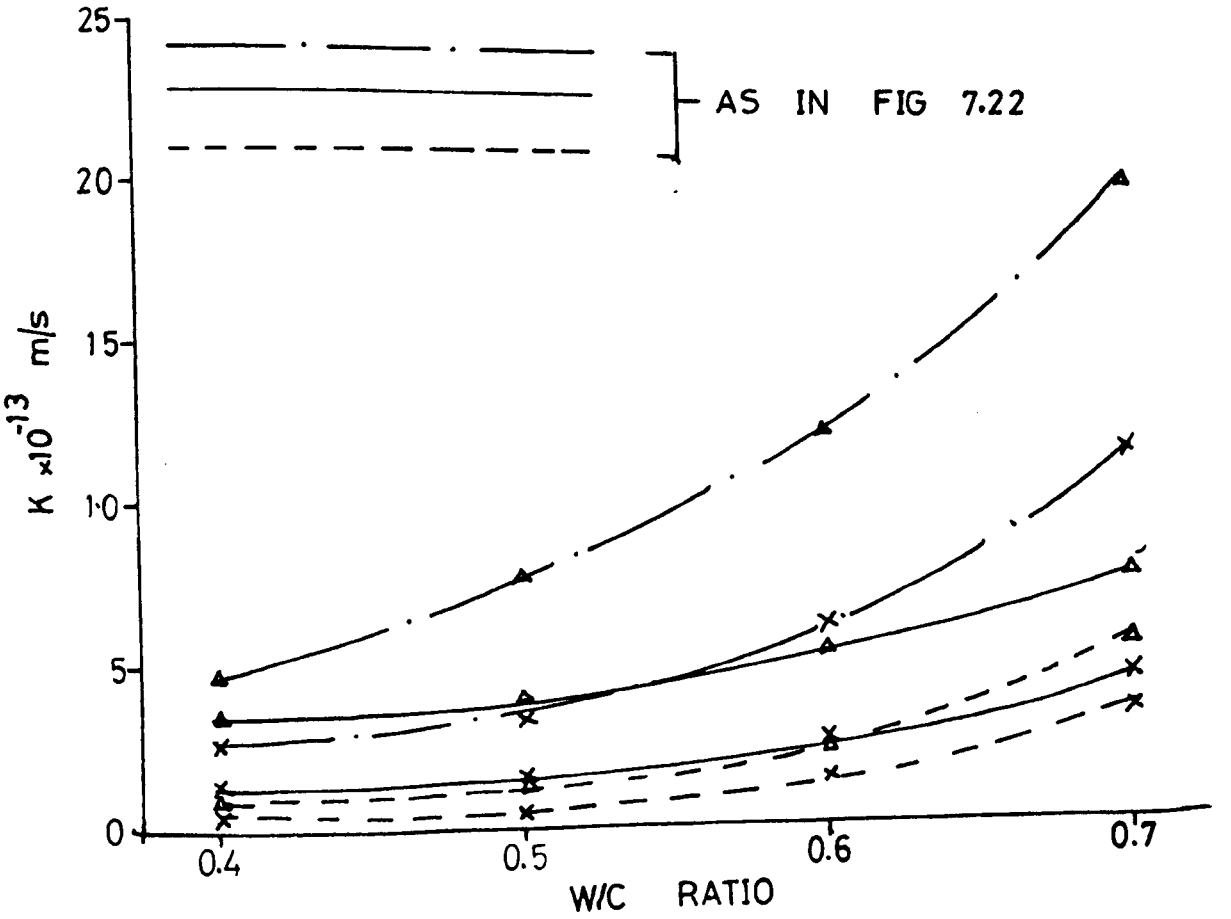

FIG 7.23 EFFECT OF SPECIMEN DIMENSION ON K, AT VARYING W/C RATIO, UNDRIED, 28 DAYS CUR. (WATER FLOW

		EFFECT OF SPECIMEN DIMENSION (28 DAY CURING)														
		PERMEABILITY OF MORTAR K x 10^{-13} M/S														
		25 mm thick x 100 mm ϕ					25 mm thick x 150 mm ϕ					50 mm thick x 150 mm ϕ				
		33.2	49.8	66.4	83.0	99.6	33.2	49.8	66.4	83.0	99.6	33.2	49.8	66.4	83.0	99.6
		DRIED AT 105°C AND SATURATED WITH OIL														
M40-1½	K x 10^{-13} M/S (OIL)	6.5	9.0	9.1	12.0	12.5	3.04	3.42	4.41	4.95	5.89	16.80	17.80	18.20	22.1	23.15
M50-1½		7.2	10.0	10.0	12.9	13.4	3.72	4.15	5.01	6.22	7.36	18.80	18.90	18.90	23.0	24.30
M60-1½		10.0	13.0	14.5	16.0	19.0	6.21	6.63	7.40	9.1	10.60	19.60	20.00	20.6	24.80	27.00
M70-1½		12.5	17.5	19.1	22.9	23.5	10.94	11.60	11.80	14.40	15.30	23.50	23.80	24.40	29.50	31.80
		NO DRYING														
M40-1½	K x 10^{-13} (WATER)	7.0	13.8	30.5	33.8	36.2	2.51	2.98	7.45	9.95	15.75	12.50	25.2	35.2	48.9	79.2
M50-1½		9.33	16.1	36.6	41.1	41.3	4.17	4.78	11.63	15.78	22.59	18.30	32.1	51.4	78.6	117.5
M60-1½		18.67	26.5	50.0	54.5	58.1	12.19	13.46	20.72	25.77	35.81	48.5	66.4	91.6	120.4	150.5
M70-1½		36.1	46.2	74.5	78.7	80.5	26.5	33.03	45.82	56.73	63.57	99.4	115.6	160.5	200.5	225.5

TABLE 7.10: Effect of Specimen Dimension on the Crude Oil and Water Permeability of Mortar.

suggests that the specimen dimensions change permeability only quantitatively. It is therefore of practical importance to have standardised specimen dimensions.

7.3 Permeability of Concrete

The flow of oil through concrete is given in table 5.2 for flows parallel and perpendicular to the directions of casting. The tests used 150 mm dia. x 50 mm thick discs with a 10 mm maximum size of aggregate. Discs of 100 mm dia. x 25 mm thick with 6.30 mm maximum size of aggregate were used for other tests to compare with the results from mortar specimens. Table 7.2 gives the variation of K with w/c ratio, applied pressure and period of hydration, while table 7.8 gives the effect of drying temperatures on the permeability of mortar and concrete. Figures 7.24 to 7.27 show the variations of K with w/c ratio, applied pressure and period of hydration for concrete and mortar of equal aggregate volume concentrations of approximately 63% while fig. 7.28 gives the effect of drying temperature on the permeability of concrete, using water flow. The following observations are made from these plots.

1. The w/c ratio, period of hydration, applied pressure and drying temperature have a similar influence on concrete as on mortar specimens. For example, (compare with sections 7.2.1.2 and 7.2.1.6) K for concrete increases exponentially with w/c ratio and drying temperature, increases approximately linearly with applied hydrostatic pressure but decreases with an increase in the hydration period. The decrease in K with hydration was very rapid at early ages, but decreased as hydration continued. Possible reasons for this behaviour have already been given in sections 7.2.1.2 to 7.2.1.6 for mortar specimens.

2. From fig. 7.27 and table 7.2, K values for 1:3 mortar and K values for 1:1½:1½ concrete, i.e., approximately equal aggregate volume concentrations, show that the mortar was more permeable up to 28 days, then it becomes

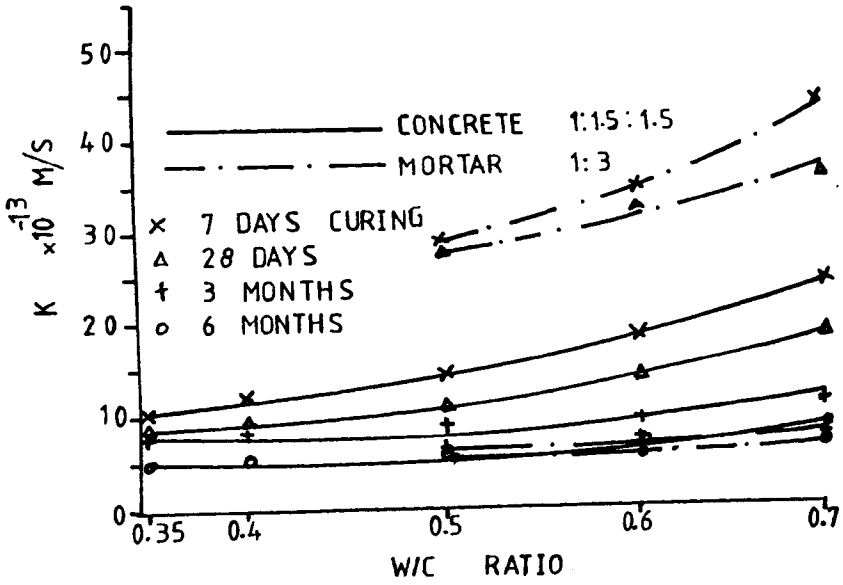

FIG 7.24 49.8 METRES HEAD OF OIL

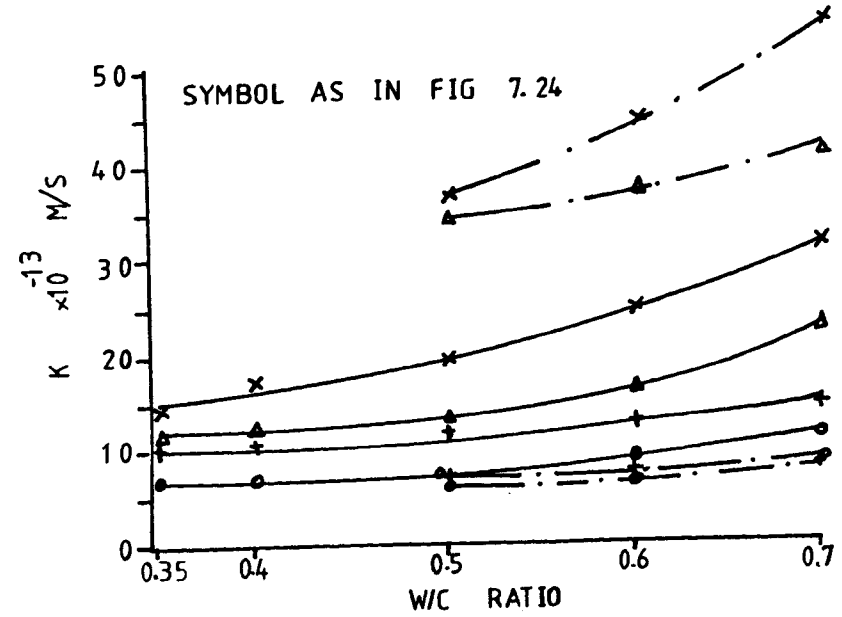

FIG 7.25
99.6 METRES
HEAD OF OIL

FIGS. 7.24 & 7.25 VARIATION OF K WITH W/C RATIO FOR MORTAR & CONCRETE OF EQUAL AGG. VOL. CONCENTRATION

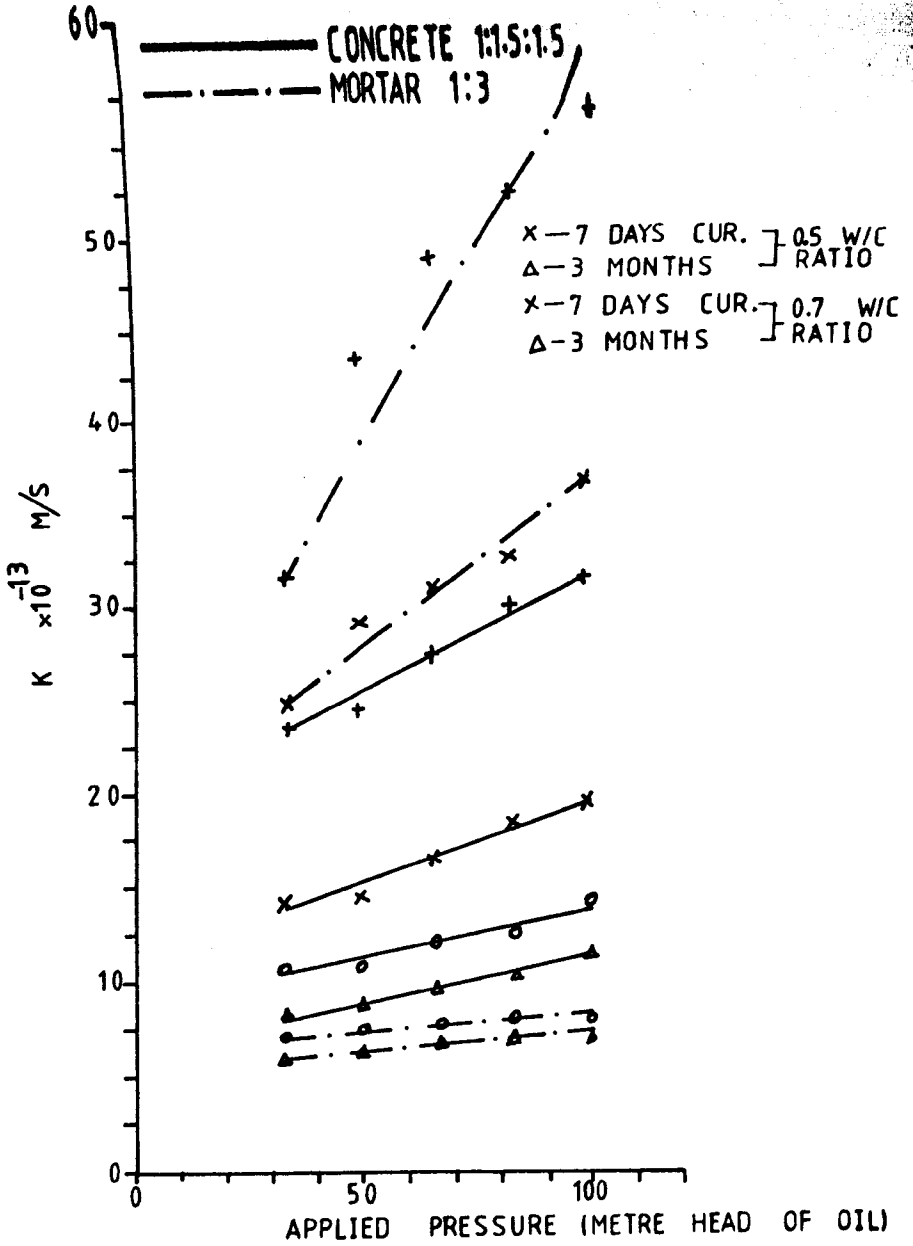

FIG 7.26 VARIATION OF K WITH APPLIED PRESSURE FOR MORTAR AND CONCRETE OF EQUAL AGG. VOL. CONCENTRATION

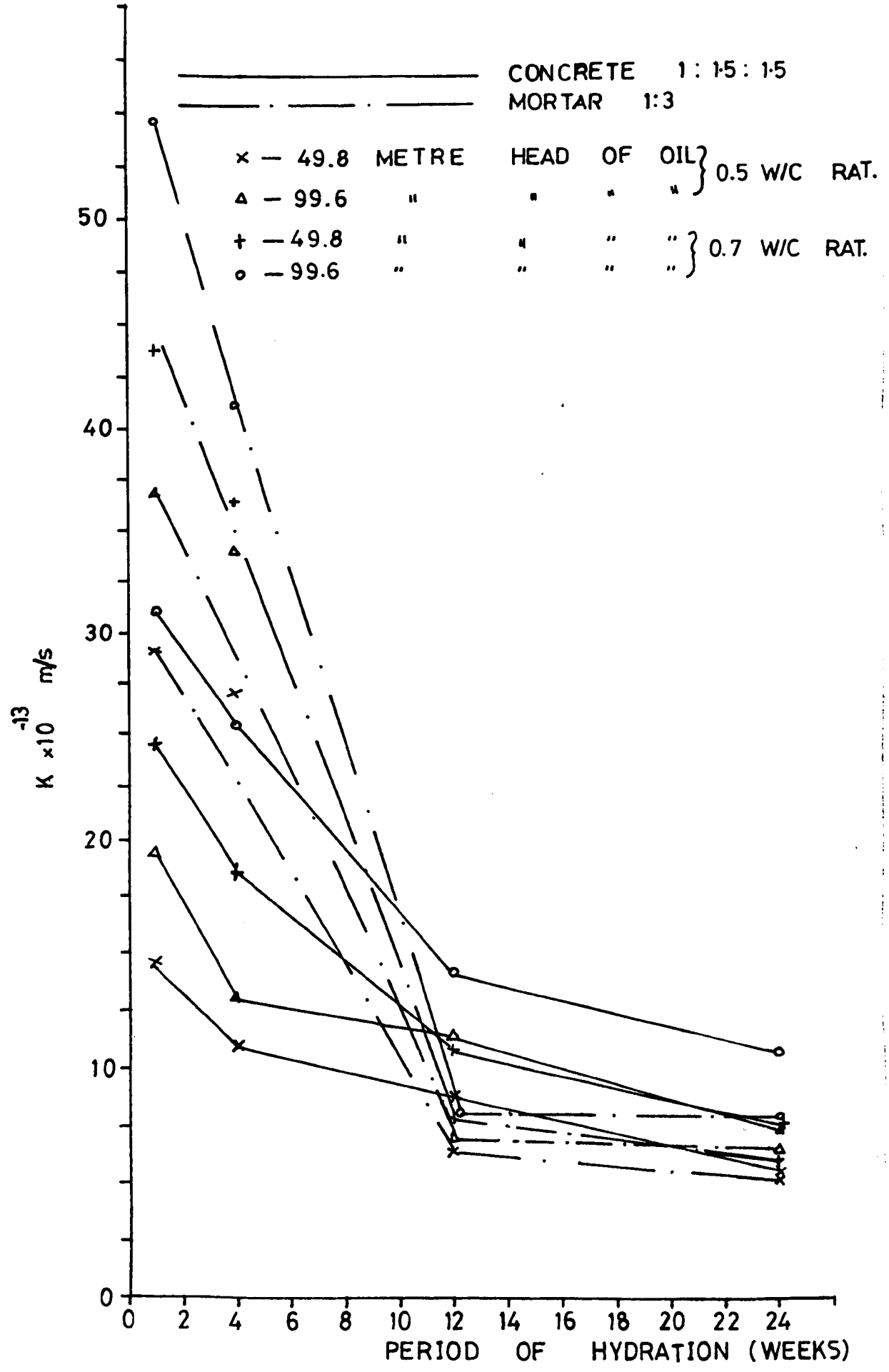

FIG 7.27 VARIATION OF K WITH PERIOD OF HYDRATION FOR CONCRETE AND MORTAR OF EQUAL AGGREGATE VOLUME CONCENTRATION

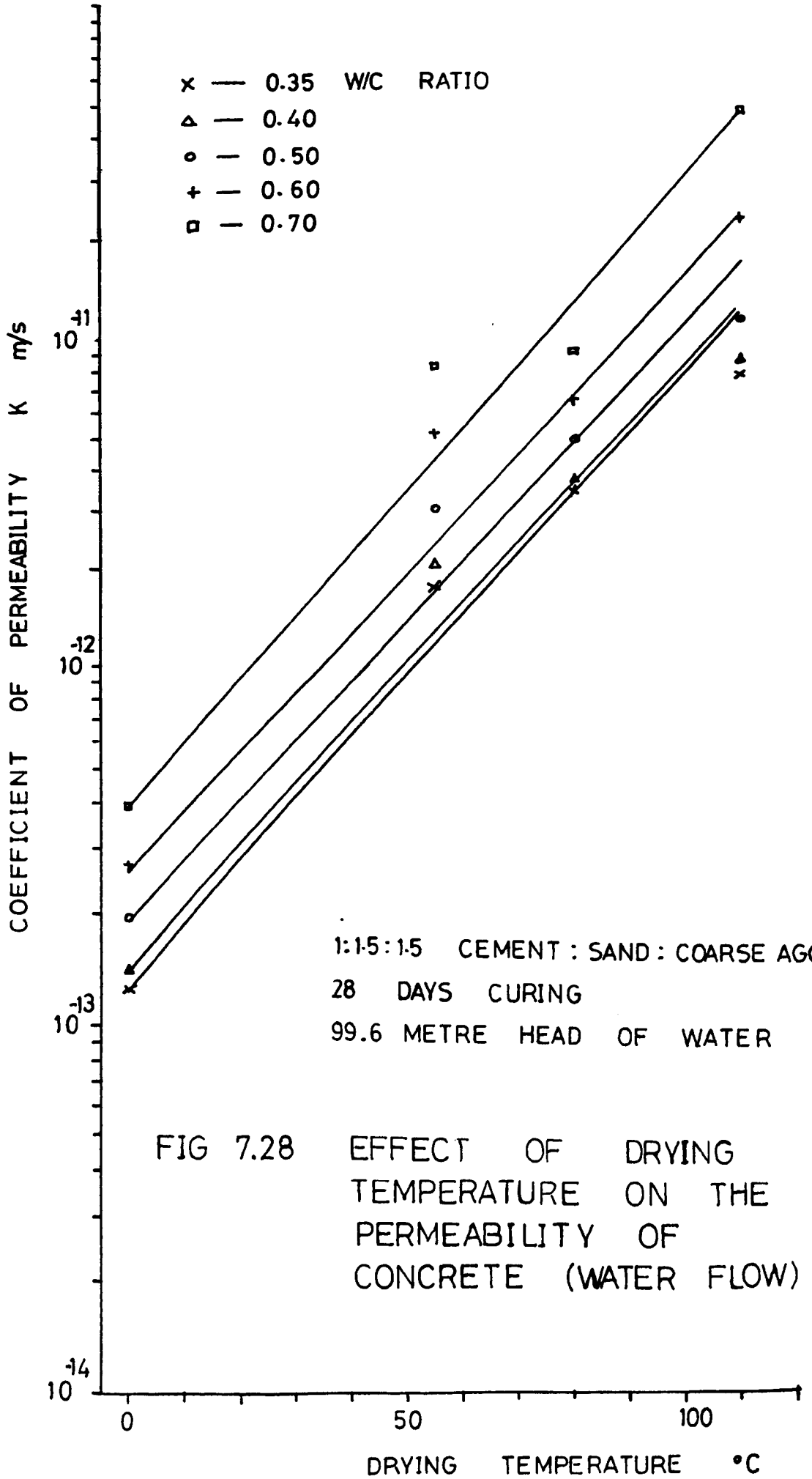

FIG 7.28 EFFECT OF DRYING TEMPERATURE ON THE PERMEABILITY OF CONCRETE (WATER FLOW)

less permeable than concrete after 3 months hydration. Mortar (1:3) with 0.70 w/c ratio under 99.6 metres, pressure head of oil has at 7 days, a K = 1.76 times the K for concrete. After 28 days, 3 months and 6 months respectively, the K for mortar (1:3 cement/sand ratio) is 1.82, 0.56 and 0.75 times the K for concrete. The reason for this behaviour is not clear, but it may be that at the initial stages, the packing of the sand grains in the matrix create flow channels which are more easily bridgeable with hydration products. Alternatively, the bonding between sand and hydration products may be stronger than between larger particles and hydrated cement, so that drying at 105°C could cause fewer bond cracks in mortar than in concrete. Further evidence of this comes from the fact that when mortar and concrete were heated to 1000°C for 2 hrs., then on cooling the concrete crumbled more than the mortar and showed an almost total loss of bond.

3. The exponential increase in K with w/c ratio can be represented by equation 7.1 while the exponential increase in K with drying temperature can also be represented by equation 7.4. K_o and a for equation 7.1, and K_o and a for equation 7.4 are determined regressionally for mortar and concrete and are given in tables 7.4 and 7.9 respectively.

CHAPTER 8

PORE STRUCTURE AND PERMEABILITY OF MORTARS

8.1 Introduction

Efforts were made to investigate the changes in pore structure of HCP, mortar and concrete (Chapter 6), and in permeability of the same materials (Chapter 7) as effected by changes in w/c ratio, hydration and aggregate inclusions. The present Chapter attempts to discuss the inter-relationships between the measured pore parameters and the saturated permeability of mortars to oil. Some functional relationships are developed and the pore parameters which most closely relate to permeability are indenitified.

8.2 Influence of Total Porsoity, Surface Area of Intruded Pores Threshold Radius, Hydraulic Radius and Pore Continuity on Oil Permeability of Mortars

It was stated[27] that permeability of concrete is not a simple function of its porosity, but depends also on the size, distribution and continuity of pores. There is a general acceptance that continuity of pores in a porous media, such as cement mortar is essential if the material is to be permeable[141, 165, 185] yet not until recently has an experimental definition of the continuity of pores been achieved for HCP[81, 111, 114]. Powers and Brownyard[54] distinguished between capillary and gel porosity of HCP, and found a good correlation between the capillary porosity and permeability. Winslow and Diamond[80], in their studies of pore size distributions and fracture surface of HCP, observed that HCP contains spaces between hydration products which are neither capillary nor gel pores. They identified the threshold radius of cement paste pores and interpreted it as corresponding to the minimum geometrically continuous pore radius thereby providing a means of identifying pore continuity in HCP. Nyame and Illston[111] identified this threshold radius as "continuous pore radius" and noted it as being representative of pores through which

water flows, while the work of Mehta et al[109] indicated that the threshold diameter is very important in relation to permeability.

The total porosity and threshold radius of mortar used in the present work, as obtained from the experiments, is given in Chapter 6, and the saturated permeability of these specimens in Chapter 7. The relationship between K and total porosity are illustrated in Figs. 8.1 and 8.2, while K versus threshold radius for 1:1 cement/sand (c/s) ratio is shown in Fig. 8.3. The following observations are made.

For a given c/s ratio but with different w/c ratios and hydration periods, K increases non-linearly with total porosity and linearly with threshold radius. The non-linear relationship of K with porosity varies with the period of hydration, while the linear relationship of K with threshold radius is independent of hydration after 7 days. This may mean that porosity does not uniquely relate to permeability.

After 7 days curing, the hydration products may not have sufficiently covered the aggregate particles in the mortar, hence flow probably occurred partly through flow channels (i.e. interconnected pores), and partly through the interface between aggregate and unhydrated pastes. As hydration continued, the aggregate is fully covered[27], allowing the flow to take place along interconnected pores only. The idea that threshold radius controls the oil flow may therefore be considered a useful conception for cement mortar, after the initial hydration period of 7 days, as Fig. 8.3 indicates. There is however doubts that oil flow in mortar is controlled by the threshold radius because as the aggregate volume concentration increased, the threshold radius decreased (Table 6.10), but K increased (Table 7.6). The increase in K despite the decrease in threshold radius, may mean that with the addition of more sand, the hydration products may be insufficient to cover the sand particles completely and so flow parts may be created on the interface. Hence the correspondence between threshold radius and permeability appear to be established for HCP[114], but not yet for mortar. In addition to

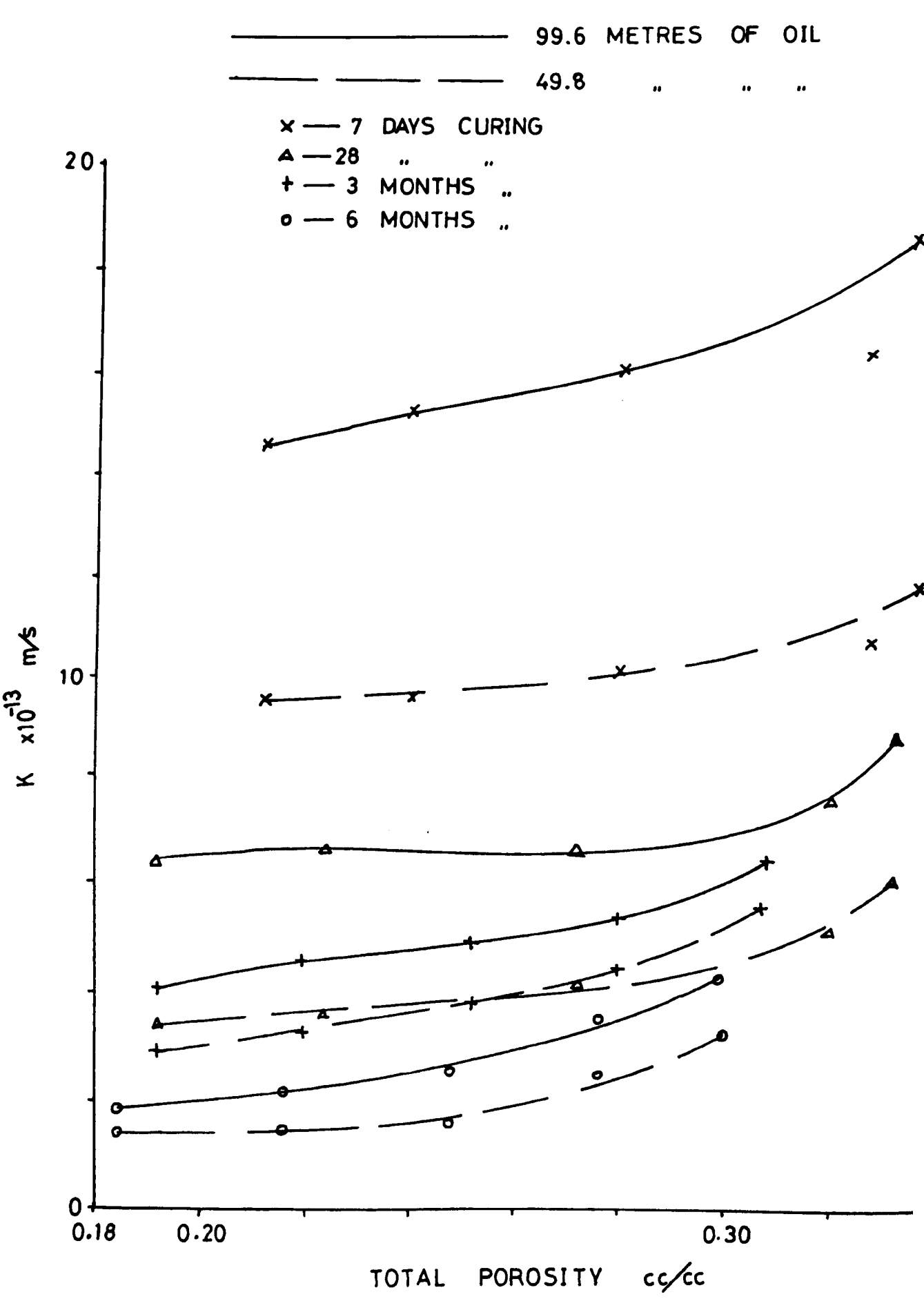

FIG 8.1 VARIATION OF K WITH TOTAL POROSITY FOR MORTAR (1:1 CEMENT: SAND RATIO)

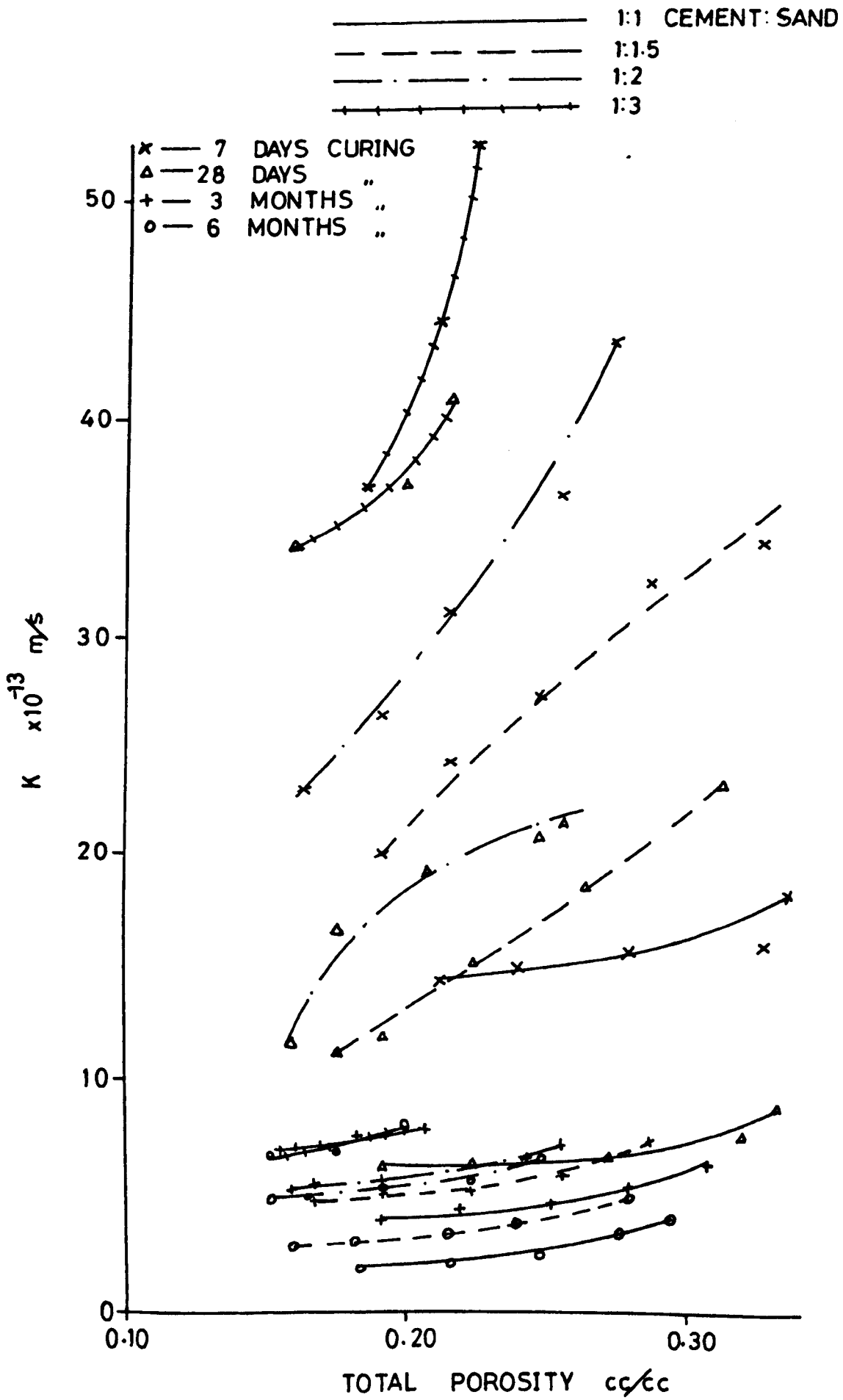

FIG 8.2 VARIATION OF K WITH TOTAL POROSITY FOR MORTARS OF VARYING C/S RATIO (K AT 99.6 METRES OF OIL)

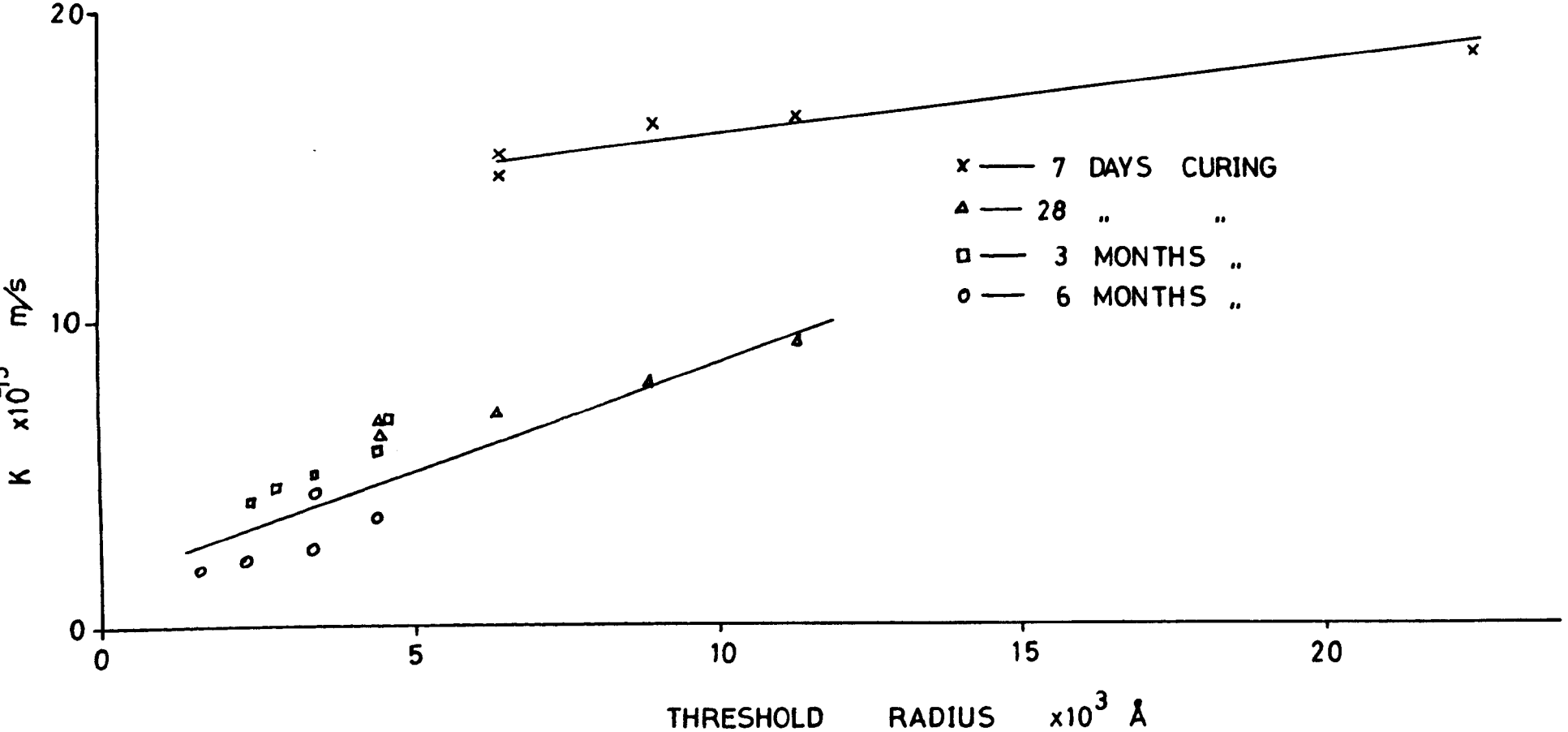

FIG 8.3 VARIATION OF K WITH THRESHOLD RADIUS FOR MORTAR, 1:1 C/S RATIO (K FOR 99.6 METRE HEAD OF OIL)

threshold radius, the influence of cement/aggregate interface characteristics and microcracks on permeability should be considered and is recommended for future work.

The plot of K versus intruded pore surface area (Fig. 8.4) suggests a linear relationship for any given hydration period, with the slope of the lines approximately equal for all the curing periods. The surface area measures the surfaces of pores, responsible for the retarding effect due to viscous drag on the flow of fluid. If it is assumed that the oil flow occurs through the total pore network and is not confined to distinct flow channels, then the greater the surface area, the greater the retarding effect hence a decrease in K. Two opposing behaviour of K with surface area are observed. For a given mortar mix with various w/c ratios, K increases with an increase in the surface area (Fig. 8.4) while for various aggregate volume concentrations, at a given w/c ratio, K increases with a decrease in the surface area (Tables 6.2 and 7.2). These opposing behaviours suggest that oil flow occurs partly through the interconnected pores and partly through the aggregate paste interface.

The probability that pores smaller than 650 $\overset{0}{A}$ in radius were totally closed by the waxy deposits of the crude oil indicates that only pores larger than this influence permeability. The pore parameters such as porosity, surface area and pore size etc are therefore only important for pores larger than 650 $\overset{0}{A}$, in relation to permeability. These are therefore called the "effective" pore parameters. Relationships between these pore parameters and permeability will be discussed in the next section. The pore parameters influencing permeability were investigated by Robson[185], who postulated the "unit pore flow" concept. This calculation required the subdivision of the measured flow rates through HCP, mortar and concrete. From this the average pore flow is deduced from an estimated number of pores and the unit pore flows calculated. From a statistical analysis, Robson suggested that permeability depends on the probability of continuous channels

developing in mortars and concrete (i.e. some pores being interconnected throughout the specimen) and is not a function of total porosity. More recently, Nyame[114] deduced that the flow of water in HCP is confined to distinct continuous channels and that the total surface area of pores in cement paste is not a good indicator of resistance to flow. This resistance would probably result from only a fraction of the total surface area which is that bounding the main continuous channels. Oyeka[17] using the water vapour adsorption method of pore structure analysis, deduced a relationship between the wide pore volume and permeability. He consequently called it the effective pore volume.

In a given mortar mix with constant hydration period but various w/c ratios, the hydraulic radius (r_h) remains practically constant, but the permeability increases. However at varying hydration period, K varies non-linearly with r_h (Fig. 8.5). It is surprising that a functional relationship appears to exist between K and r_h because the r_h values are far below the critical pore radius of 650 $\overset{0}{A}$ (section 6.7). Supposedly, the hydraulic radius is a measure of the average width of the pores and is expected to directly influence the oil permeability. The permeability increases with an increase in the aggregate volume concentration (Table 7.6), but the hydraulic radius remains almost constant (Table 6.12). This means that the changes in pore structure produced by aggregate inclusion, does not change the hydraulic radius.

8.3 Influence of the Intruded Pore Volume, Surface Area and Hydraulic Radius of Pores with Radii >650 $\overset{0}{A}$, on Oil Permeability of Mortars

The effective pore space for mortar as defined in this investigation is that portion of the pore system with radius greater than 650 $\overset{0}{A}$. The reason for the choice of this figure has been explained in sections 6.7 and 8.2.

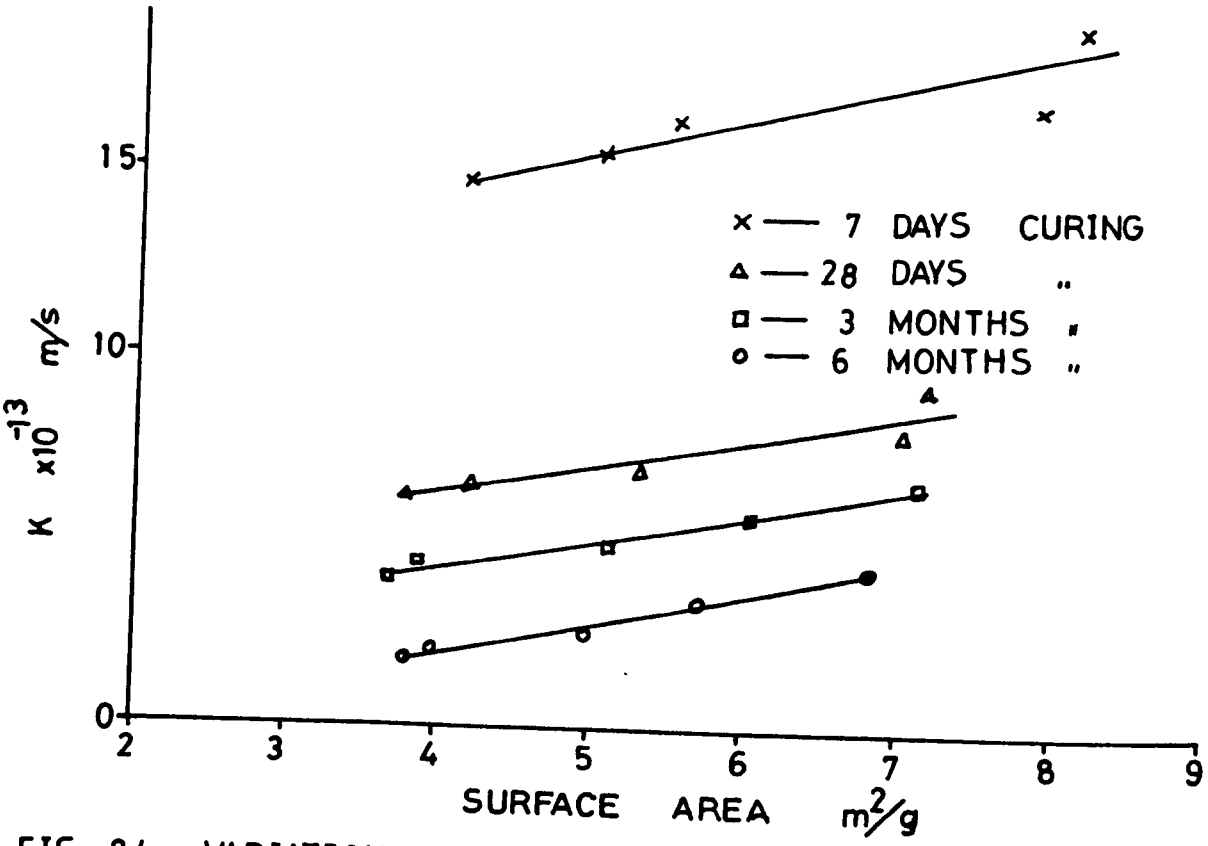

FIG 8.4 VARIATION OF K WITH SURFACE AREA OF TOTAL INTRUDED PORE FOR MORTAR 1:1 C/S RATIO (K AT 99.6 METRES OF OIL)

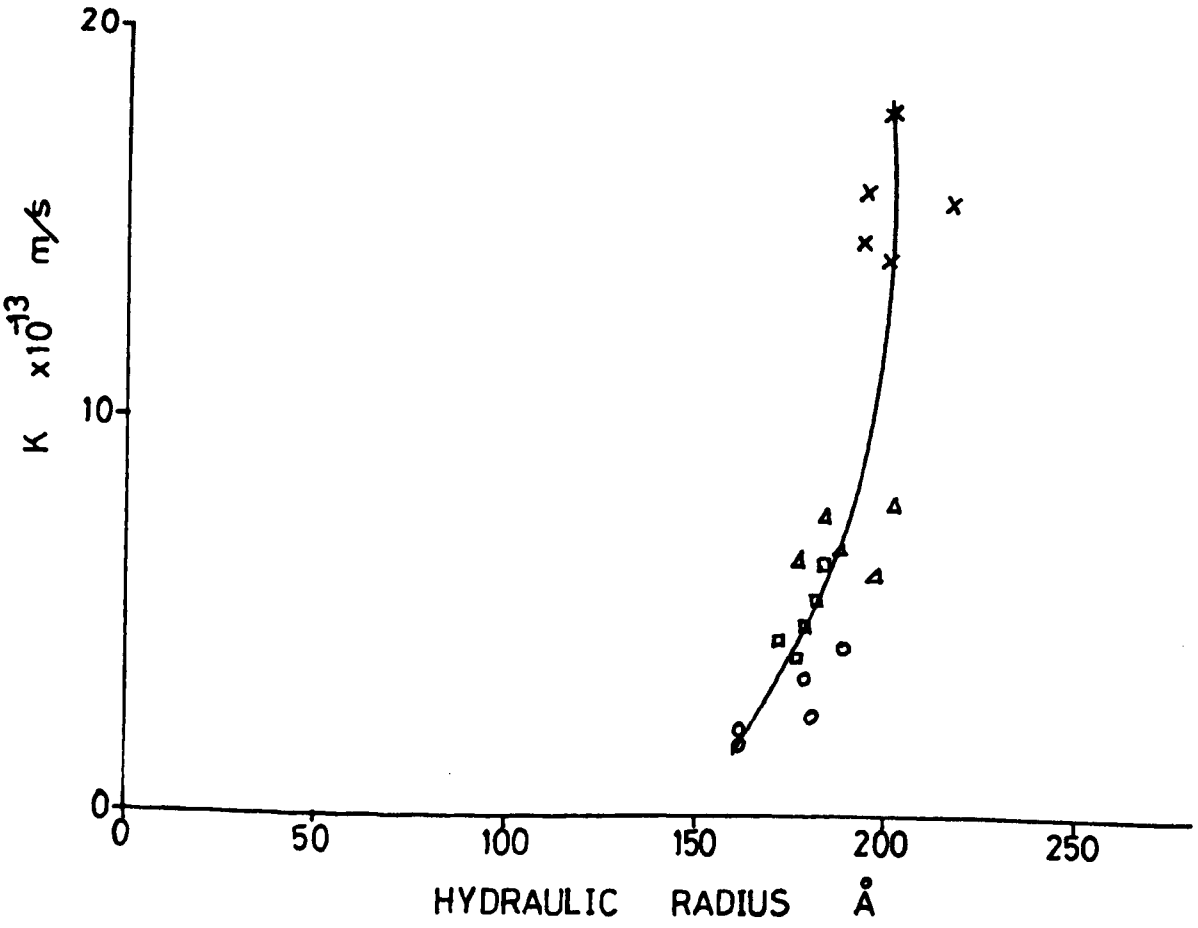

FIG 8.5 VARIATION OF K WITH HYDRAULIC RADIUS OF TOTAL INTRUDED PORE FOR MORTAR 1:1 C/S RATIO (K AT 99.6 METRES OF OIL)

The object of this section is to investigate the influence of those pores with radii >650 $\mathring{A}$ on permeability. Unless otherwise stated, all pore parameters to be discussed in this section will therefore refer to the effective pores.

The variation of K with the effective pore volume is illustrated in Fig. 8.6 for mortars of 1:1 and 1:3 cement/sand ratio. The plots for 1:1½ and 1:2 mixes show the same behaviour as the 1:1 mix. Typical plots of K versus hydraulic radius (r_{eh}) and surface area (S_e) are shown in Figs. 8.7 and 8.8 respectively for the 1:1 c/s ratio. The other mortar mixes exhibited the same behaviour.

All the 7 days cured specimens, except those from the 1:3 mortar, show a linear relationship between effective porosity and K which is unique for that hydration period. The 28 days to 6 months cured specimens show a non-linear relationship and this behaviour appers to be independent of the hydration period after 7 days curing. This may mean that after about 28 days hydration, unique flow channels have been established within the pores of radii above 650 $\mathring{A}$. Further hydration may reduce the width of these flow channels but not close them completely and the tortuous nature of the path may be retained. All the pores wider than 650 $\mathring{A}$ radius would therefore never be fully closed by hydration, but could be subdivided into smaller pores which may later be closed by the wax in the crude oil, with consequent reduction in K with hydration period.

The relationship between K and the effective pore volume can be described with the equations below

$$K = A + B\varepsilon_e \tag{8.1}$$

$$K = K_o \varepsilon_e^{B_1} \tag{8.2}$$

where K = saturated permeability cm/s

ε_e = effective porosity cc/cc

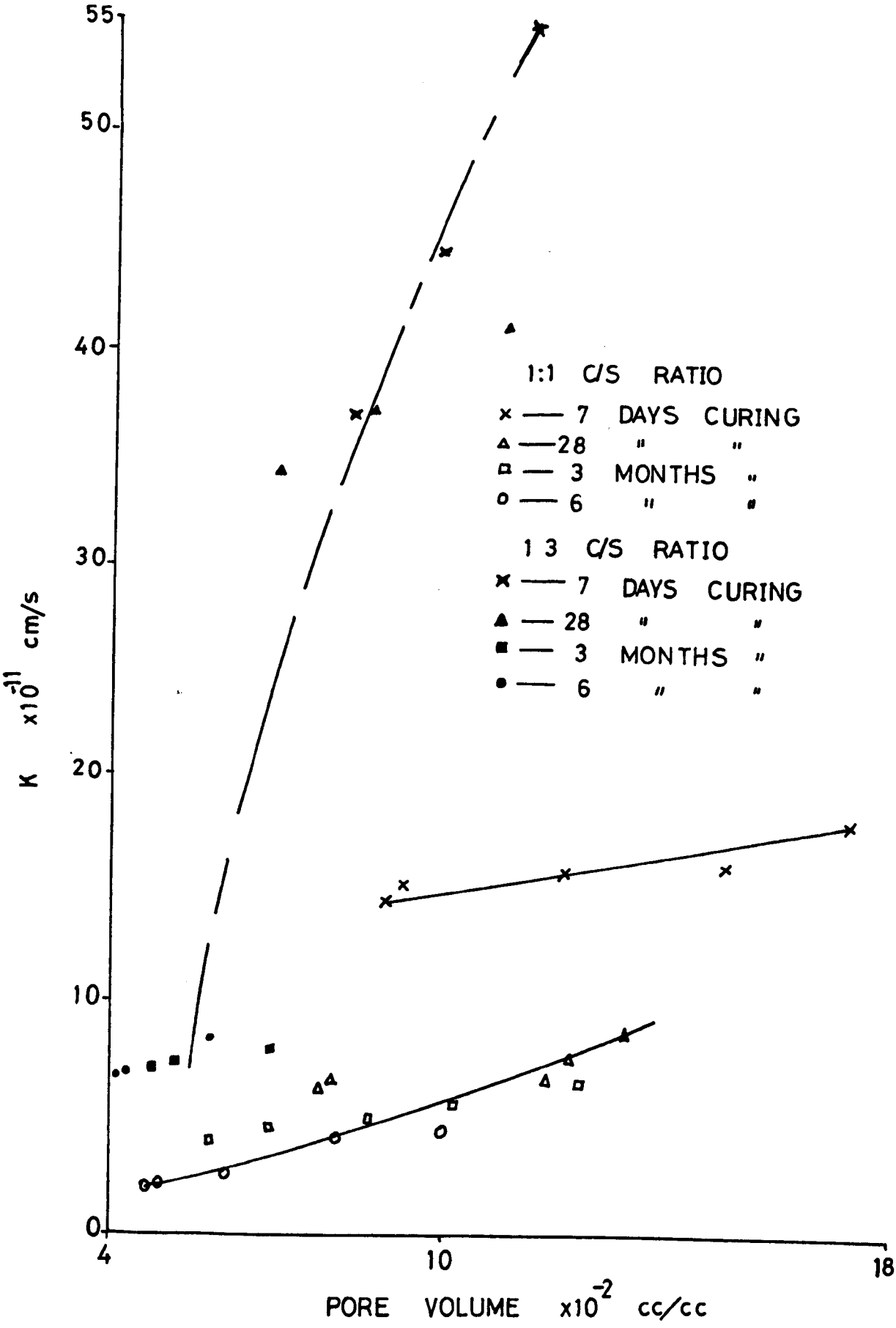

FIG 8.6 VARIATION OF K WITH PORE VOLUME OF RADIUS >650Å (K AT 99.6m PRESSURE HEAD OF OIL)

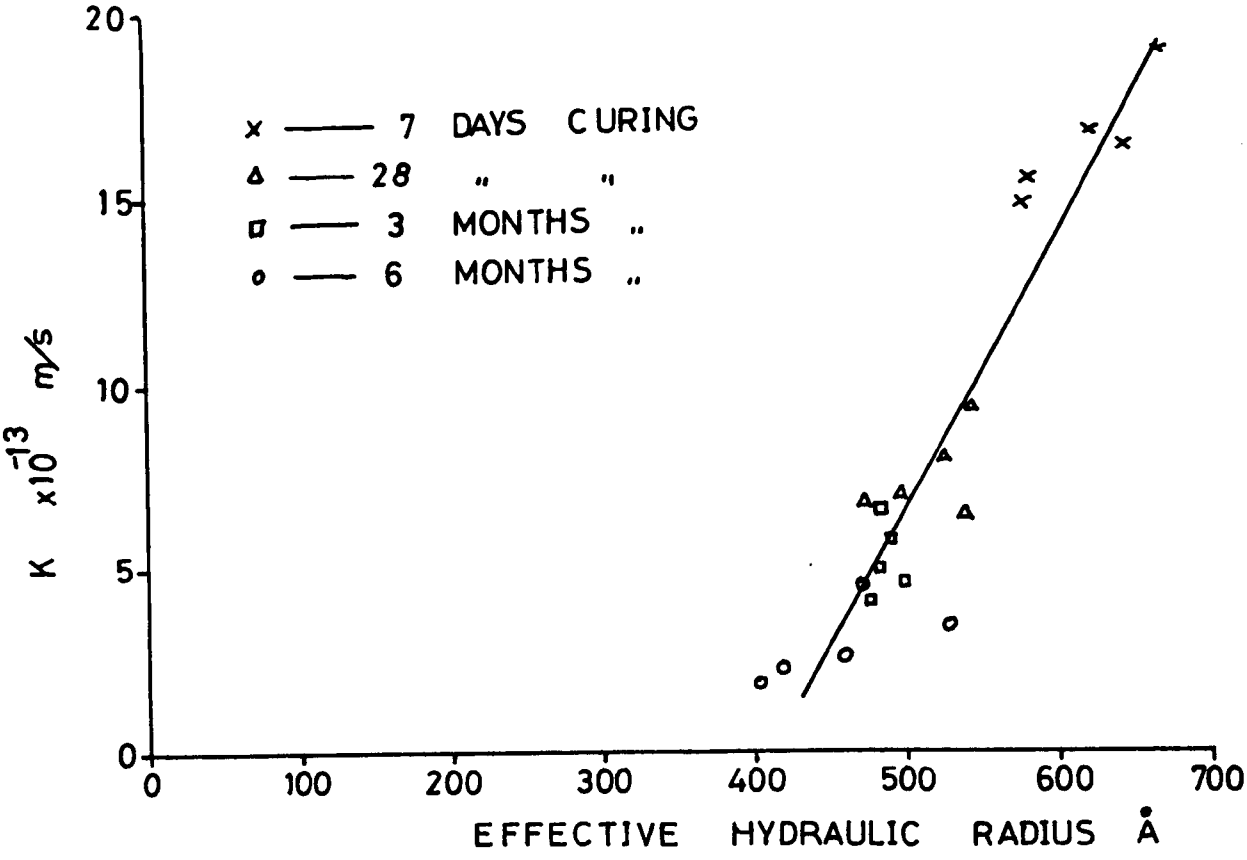

FIG 8.7 VARIATION OF K WITH HYDRAULIC RADIUS OF PORES OF RADII >650Å FOR MORTAR, 1:1 C/S RATIO (K AT 99.6m PRESSURE HEAD OF OIL)

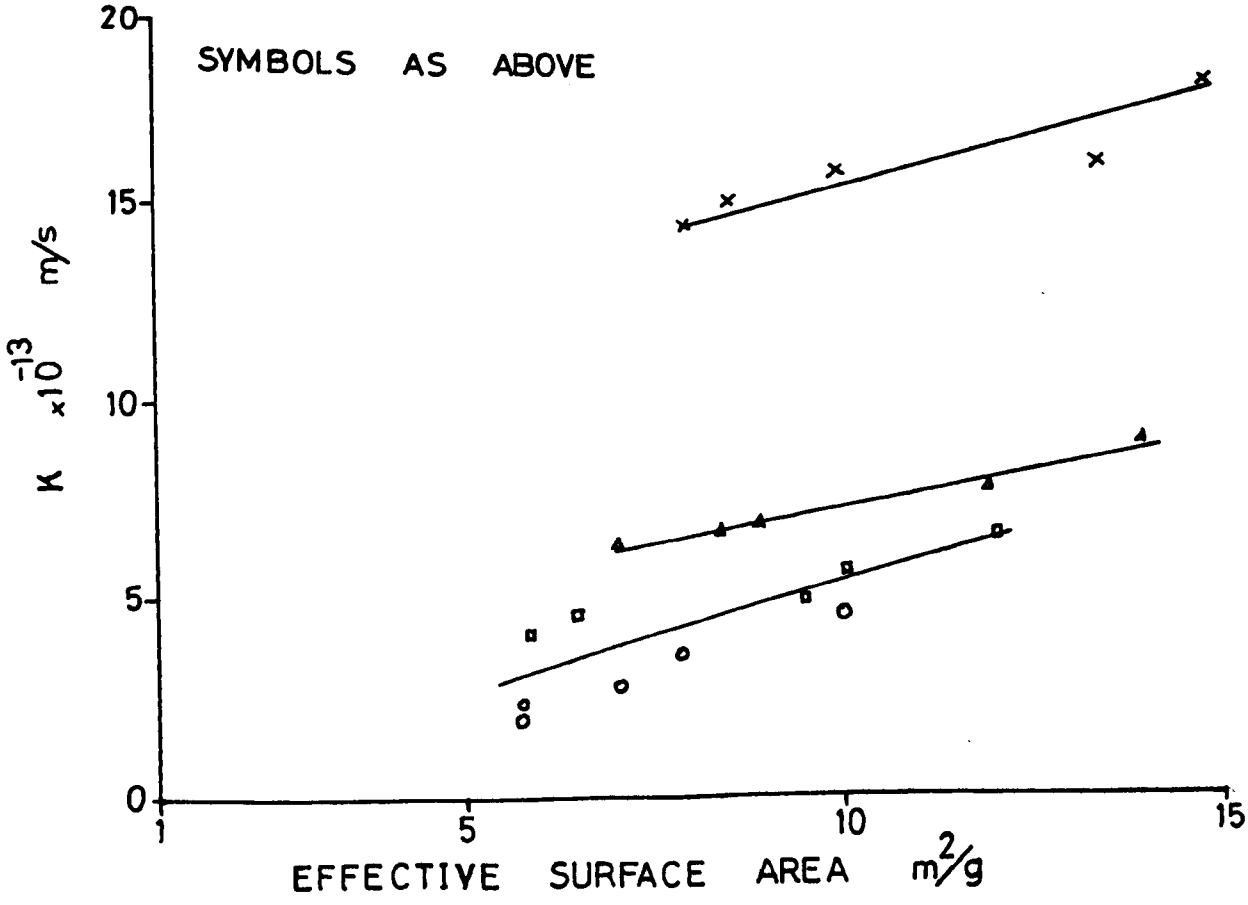

FIG 8.8 VARIATION OF K WITH SURFACE AREA OF PORES OF RADII >650A FOR MORTAR 1:1 C/S RATIO (K AT 99.6m PRESSURE HEAD OF OIL)

A, B, B_1 and K_o are constants.

The linear equation 8.1 is for 7 days hydrated mortars of 1:1, 1:1½ and 1:2 c/s ratio, while the power law equation 8.2, is for 28 days to 6 months hydrated mortars (1:1. 1:1½ and 1:2 mixes) and 7 days to 6 months hydrated mortar of 1:3 c/s ratio. A, B, B_1 and K_o were determined regressionally and are given in Table 8.1.

Permeability appears to decrease linearly with a decrease in the effective hydraulic radius (r_{eh}) as hydration continued. For a given hydration period, r_{eh} remains practically constant but K increases as the w/c ratio is increased. A lower value of r_{eh}, means higher value of effective surface area (S_e) per unit, ε_e, (since $r_{eh} = \frac{\varepsilon_e}{S_e}$) and therefore a higher resistance to flow. It follows therefore that although hydration reduces the overall surface area (Tables 6.2 to 6.5), it produces a higher effective surface area per effective unit pore volume and may have reduced the permeability. The permeability therefore appears to be more closely related to effective than to total surface area measured by porosimetry.

The variation of K with r_{eh} can be represented with an equation of the form

$$K = a + b\, r_{eh} \qquad (8.3)$$

where K = coefficient of permeability m/s

r_{eh} = effective hydraulic radius $\overset{0}{A}$

a and b are constants

a and b are determined regressionally and are given in Table 8.2.

A plot of K versus effective surface area (S_e), reveals that K varies linearly with S_e. The variation is unique for both 7 days and 28 days hydrated mortars, but remains approximately constant from 3 months to 6 months (Fig. 8.8). The variation of K with S_e can be represented with an equation of the form

CEMENT/ SAND RATIO	$Ax10^{-10}$	$Bx10^{-10}$	r
	7 DAYS HYDRATION		
1:1	1.128	3.922	0.937
1:1.5	0.611	18.11	0.987
1:2	1.162	20.73	0.919
1:3	-	-	-
	$K_o x10^{-9}$	B_1	r
	28 TO 6 MONTHS HYDRATION 7 TO 6 MONTHS HYD. 1:3 MORTAR		
1:1	1.016	1.240	0.878
1:1.5	2.810	1.457	0.871
1:2	3.426	1.368	0.826
1:3	77.601	2.280	0.9132

TABLE 8.1 Constants of regression for equations 8.1 and 8.2, K Versus effective porosity (K at 99.6 metre head of oil)

CEMENT/ SAND RATIO	$ax10^{-12}$	$bx10^{-15}$	r
1:1	-2.758	6.826	0.929
1:1.5	-5.246	12.394	0.878
1:2	-4.493	10.507	0.818
1:3	-7.279	16.19	0.871

TABLE 8.2 Constants of regression for equation 8.3, K versus effective hydraulic radius (K at 99.6 metre head of oil)

$$K = C + D\,S_e \tag{8.4}$$

where K = coefficient of permeability m/s

S_e = effective surface area m^2/g

C and D are constants, which were determined regressionally and are given in Table 8.3.

One of the most widely used theories linking permeability and the internal structure, such as surface area and porosity of a porous material is the Kozeny theory of equation 2.32. A general form is given as[140]

$$K = \frac{C\,\varepsilon_e^{\,3}}{T\,S_e^{\,2}} \tag{8.5}$$

where C = constant

T = tortuosity factor defining the degree of the uniformity of the flow path

ε_e = effective pore volume (defined previously)

S_e = effective surface area.

The effective values of pore volume and surface area are the values obtained for pores of radii >650 $\mathring{A}$. A linear relationship is obtained for the plot of K versus $\varepsilon_e^{\,3}/S_e^{\,2}$ as shown in Fig. 8.9 for mortar of 1:1 c/s ratio. Other mortar mixes (i.e. 1:1½, 1:2 and 1:3) were found to exhibit such relationships. A linear regression analysis of K and $\varepsilon_e^{\,2}/S_e^{\,2}$ gives the following functional relationship

$$K = T_1\,\varepsilon_e^{\,3}/S_e^{\,2} + T_2 \tag{8.6}$$

ε_e in cc/cc, S_e in cm^2/cm^3

where T_1 and T_2 are constants and are given in Table 8.4. T_1 is equivalent to C/T of equation 8.5 and is related to the tortuosity and degree of uniformity of the mortar. The values of T_2 are quite low and could be attributable to minor variations in the specimens during preparation.

The increase in T_1 with an increase in aggregate volume concentration (i.e. decrease in c/s ratio) may mean that the addition of sand

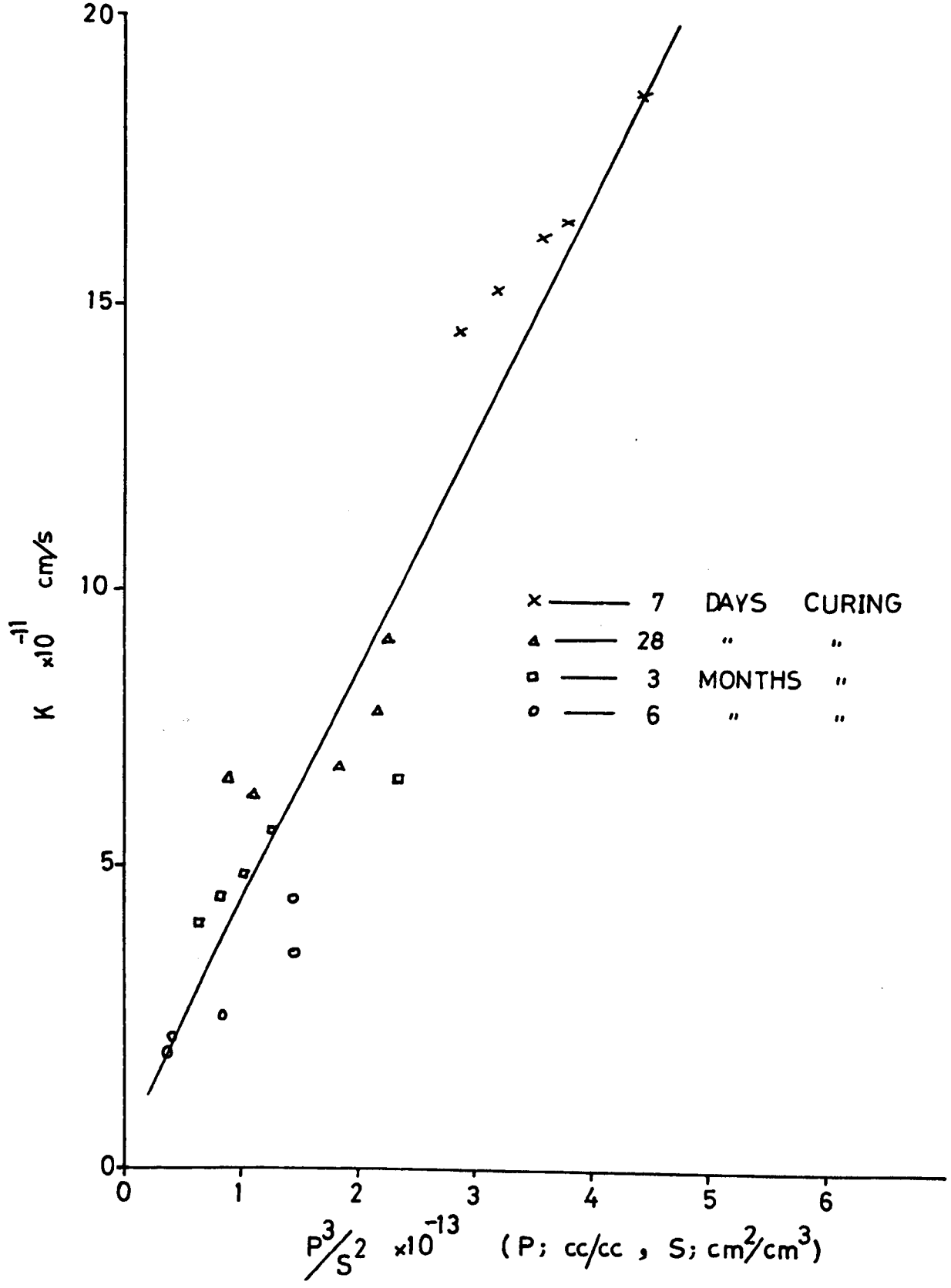

FIG 8.9 COMPARISON OF PERMEABILITY DATA WITH KOZENY'S THEORY FOR MORTAR, 1:1 C S RATIO USING EFFECTIVE PORE PARAMETERS. (K AT 99.6m PRESSURE HEAD OF OIL)

CEMENT SAND RATIO	$Cx10^{-13}$	$Dx10^{-13}$	r
	7 DAYS HYDRATION		
1:1	11.167	4.560	0.913
1:1.5	15.394	10.874	0.954
1:2	10.367	28.122	0.955
1:3	8.018	49.102	0.991
	28 DAYS HYDRATION		
1:1	3.327	3.985	0.986
1:1.5	-0.0981	17.234	0.988
1:2	5.343	17.290	0.942
1:3	18.701	24.317	0.902
	3 to 6 MONTHS HYDRATION		
1:1	-0.424	5.453	0.815
1:1.5	2.112	3.620	0.816
1:2	3.103	3.909	0.867
1:3	3.614	5.531	0.834

TABLE 8.3 Constants of regression for equation 8.4, K versus effective surface area (K at 99.6 metre head of oil)

APPLIED HYDROSTATIC HEAD m	$T_2 \times 10^{-12}$	T_1	r
	1:1 CEMENT/SAND RATIO		
33.2	-0.444	22.56	0.962
49.8	0.595	28.02	0.958
66.4	-0.303	34.51	0.951
83.0	2.712	35.68	0.949
99.6	1.156	42.24	0.946
	1:1.5 CEMENT/SAND RATIO		
33.2	3.25	87.44	0.896
49.8	-4.04	109.40	0.896
66.4	-4.01	117.41	0.886
83.0	-4.25	127.82	0.903
99.6	-4.36	132.98	0.912
	1:2 CEMENT/SAND RATIO		
33.2	1.60	110.53	0.944
49.8	1.23	116.10	0.940
66.4	1.53	124.57	0.945
83.0	1.27	130.13	0.942
99.6	1.26	134.65	0.946
	1:3 CEMENT/SAND RATIO		
33.2	0.67	168.60	0.906
49.8	3.49	228.91	0.940
66.4	4.49	252.30	0.947
83.0	4.99	272.44	0.948
99.6	4.99	284.24	0.948

TABLE 8.4 Constants of regression for equation 8.6 (Permeability data and Kozeny's theory)

produces (1) more tortuous flow channels (2) less uniformity in the specimens due to insufficient cement particles (3) combination of the two.

If point 1 applies, then an increase in the aggregate volume concentration means a decrease in the permeability, which is not the case (Tables 7.2 and 7.3). Other forms of flow channels such as microcracks or weak and open interfaces between sand and cement and/or wide flow channels must then be created with further addition of sand, although there is a decrease in threshold radius with an increase in the aggregate volume concentration (Table 6.10). An increase in the aggregate volume concentration would be expected to reduce the number of flow channels (i.e. interconnected pore spaces) because the aggregates are relatively less permeable than the cement paste they displace. The maximum pore radius of the aggregates is only 400 $\overset{0}{A}$ (Fig. 6.22) and the threshold radius 169 $\overset{0}{A}$, (Table 6.10). The most likely cause of the increased permeability would therefore seem to be microcracking, accentuated by drying of the specimen, and weakly bonded interfaces. Further research is necessary to establish the extent of the effects of these parameters. If the specimens became less uniform as the aggregate volume concentration is increased (point 2), then the effect on flow is not clear.

A regressional analysis of K and ε^3/S^2 (where ε = total porosity, S = surface area of total intruded pores) showed a correlation coefficient below 0.80 for all the mortar mixes tested. It therefore appears that the Kozeny's theory does describe the permeability of mortars more closely, when the effective pore parameters are employed. Most pore parameters did not individually relate to permeability over the whole range of the hydration period, excepting the hydraulic radius (Fig. 8.7), which however has a lower correlation coefficient than the Kozeny's equation (compare Tables 8.2 and 8.4). This suggests that inclusion of more pore parameters improved the prediction of oil flow through mortar.

Figure 8.9, shows some scatter between Kozeny's equation and the measured K, especially at lower permabilities. Considering the assumptions made in deriving this theory[140] i.e. (a) the flow channels are of definite length (b) there is no tangential component of the fluid velocity (c) the conical flow in the non-uniform flow channels is neglected, one would expect that exact correlation is not likely. So it has to be accepted that Kozeny's theory adequately describes the oil flow characteristics through mortars. The discrepancy between theory and measured results is therefore accounted for by the tortuosity factor T_1 in equation 8.6. Equation (8.6) is also based on the coefficient of permeability expressed in cm/s, which does not allow for the effect of changes in the viscosity of oil with various pore sizes as discussed in section 2.4.2.1. The scatter therefore could be due to these changes especially at low permeabilities, obtained as a result of reduction in pore sizes.

Equation (8.6) cannot be used at every applied hydrostatic pressure (h), unless the values of T_1 are specified for those pressures (Table 8.4). It has been shown that K increases approximately linearly with h (section 7.2.1.4). The factor T_1 was related to the applied pressure for each mortar mix and the equation below was obtained

$$T_1 = w_1 h + w_2 \qquad (8.7)$$

where w_1 and w_2 are constants.

A linear regression was carried out and the values of w_1 and w_2 are given in Table 8.5 for the four mortar mixes.

CEMENT/SAND RATIO	w_1	w_2	r
1:1	0.283	13.79	0.985
1:1.5	0.660	71.21	0.966
1:2	0.375	98.28	0.995
1:3	1.655	131.37	0.950

TABLE 8.5 Constant of regression for equation 8.7 (T_1 in terms of applied hydrostatic pressure head)

The following conclusions can be made from the forgoing discussions.

1. Kozeny's theory describes the flow behaviour of crude oil through mortars provided effective pore parameters are used.

2. Discrepancies between this theory and measured permeabilities of mortars are observed especially at low permeabilities. These discrepancies probably occur because of the assumptions made in deriving the theory, limitations of the measurements and/or changes in the viscosity of the oil in the flow channels.

3. Effective pore parameters, such as effective pore volume and surface area related more closely to permeability than did the threshold radius (Fig. 8.3), which was considered continuous in HCP. This might indicate that flow through mortars is not confined to distinct flow channels in the hydrating and hydration products (i.e. interconnected pores), but also occur along the surfaces of the aggregates and microcracks.

4. The effective pore parameters obtained from pore size distribution data, were found to have a closer relationship with permeability of crude oil through mortars than the total pore parameters. Kozeny's mathematical model also uses pore size distribution data as the input.

CHAPTER 9

CONCLUSIONS

9.1 Conclusions

The overall objectives in this investigation were (a) study some of the features and properties of concrete that affect the performance of concrete oil storage tanks (b) study the internal structure of HCP, mortar and concrete, and investigate relationships between pore parameters and the saturated permeability. The general conclusions are given in the following sections.

9.1.1 Flow Through Cracks in Concrete

1. The flow of water through cracks in concrete is generally greater than the flow of crude oil through the same cracks. This is so for any crack width, shape or applied liquid pressure and any crack impermeable to water is likely to be impermeable to crude oil.

2. Both oil and water flow more rapidly through a crack between concrete and reinforcement than through a joint of same width in concrete. Both also flow most slowly through cracks in the concrete matrix. For a crack width of 0.1mm, around the periphery of a steel bar, the flow velocity ranges between 4.09 m/s to 14.93 m/s (water flow) and 1.09 m/s to 5.31 m/s (oil flow) under a pressure head of 8.3 to 83.0 metres. For a 0.1mm wide sinusoidal joint and the same pressure head, the flow velocities were 1.55 m/s to 7.85 m/s (water flow) and 0.16 m/s to 1.31 m/s (oil flow). For a 0.1mm wide natural crack and the same pressure ranges, the velocities were 0.475 m/s to 1.4 m/s (water) and 0.19 m/s to 0.75 m/s (oil).

3. The flow velocity increased with an increase in applied pressure or crack width for all crack types. Both oil and water flow velocities were inversely proportional to the depth of crack. For a circular crack of width 0.10 mm, increasing the crack depth from 50mm to 125mm, decreases the water flow velocity from 4.09 m/s to 2.04 m/s at a water pressure head of 83.0 metres.

4. The measured flow velocities in the test samples Table 4.1, are higher than would be expected in concrete structures because in the test samples the artificial cracks are of constant width and no autogeneous healing occurred.

5. The flow velocity can be related reasonably accurately to the applied hydrostatic pressure with an empirical equation of the form

water flow: $$V = A_w h^{0.75} + V_w$$

oil flow: $$V = A_o h^{0.75} + V_o$$

where A_w, V_w and A_o, V_o are constants for water and oil flow respectively for a given crack width and shape.

6. Except for oil flow through natural cracks, oil and water flow through cracks is expected to obey the Reynolds law of similitude and the dimensionless ratio of equation 2.16, could apply to that. Equation 2.17 has a wider application than those given above.

7. The flow of oil or water through cracks in concrete is influenced by the fluid properties, such as density, molecular size, viscosity and wax content, and the surface characteristics, such as surface roughness and frictional resistance.

9.1.2 Absorption and Permeability - Effects of Liquid Properties and Concrete Direction of Casting on Fluid Flow

1. The flow through the tank wall (horizontal flow perpendicular to the direction of casting) is between 1.06 and 1.81 times the flow through the tank floor (vertical flow, parallel to the direction of casting), with a mean of 1.38 and a standard deviation of 1.26, and is represented reasonably accurately by the equation of the form

$$K_V = 1.718\ K_H - 5.99$$

where K_V is the permeability coefficient for the vertically cast specimens

(tank wall) and K_H is the permeability coefficient for the horizontally cast specimens (tank floor).

2. Sorptivity ($m/s^{\frac{1}{2}}$) i.e. volume of liquid absorbed per unit area (m^3/m^2), versus square root of time, can predict the flow of liquids through HCP, mortar and concrete, provided the test is carried out for a short period to minimize gravitational attractions (sections 2.4.2.2.7 and 5.5) and also provided a good representative sample of the specimen is used. The assumption of the test is that the porous solid is homogeneous.

3. The sorptivity of vertically cast specimens (tank wall) is generally higher than the sorptivity of horizontally cast specimens (tank floor) for all the liquid types tested (i.e. water, North Sea crude oil, Kuwaite crude oil, Diesel and Parafin) and was represented by the equation of the form

$$S_V = 1.19S_H + 0.08$$

where S_V is sorptivity for the vertically cast specimens and

S_H is sorptivity for the horizontally cast specimens.

4. The sorptivity of HCP is greater than that of mortar (1:1½ c/s ratio), which is greater than that of concrete (1:1½:1½ cement/sand/coarse aggregate ratio), for any given w/c ratio and liquid type. For a given mix, the sorptivity of the liquids tested are in the following descending order of magnitude, water, parafin, diesel, North Sea crude oil and Kuwait crude oil.

5. The flow behaviour of water should be studied using water of different properties to avoid misinterpretation of data when compared with crude oil and its distillates.

6. No specific oil property appears to control the flow of oil through HCP, mortar or concrete. All of these properties are important - density, kinematic viscosity, average molecular size and wax content. An increase in the density, kinematic viscosity and average molecular size, decreased the flow of oil through HCP, mortar and concrete. The variation

of these properties with sorptivity is reasonably represented by an equation of the form

$$S = S_o(\exp)^{C_1 M_s \nu \rho^2}$$

where S = sorptivity ($m/s^{\frac{1}{2}}$), M_s = molecular size, ν = kinematic viscosity (m^2/s), ρ = density (kg/m^3) and S_o and C_1 are constants.

7. Tanks designed to store water can adequately hold crude oil, but not lighter distillates such as diesel or parafin.

9.1.3 Pore Structure of HCP, Mortar and Concrete

1. The intruded pore volume of HCP after 28 days curing measured by mercury intrusion porosimetry on pastes, oven dried at 105°C, was between 0.175 and 0.335 cc/cc. The total porosity measured by finding the weight loss after drying a SSD paste to a constant weight at 105°C was between 0.368 and 0.470 cc/cc, for w/c ratios ranging from 0.35 to 0.70.

2. Increasing the w/c ratio increases the total porosity, the intruded pore volume, the pore surface area and the threshold radius but it decreases the density and has no noticeable effect on the hydraulic radius.

3. Increasing the age of a HCP specimen (w/c = 0.7) from 7 days to 6 months, decreases the total porosity, the intruded pore volume, the pore surface area, the threshold radius and the hydraulic radius by 12%, 17% 19%, 71% and 9% respectively of the value at 7 days, but increases the density by 13%. The same trend is observed for mortar and concrete but by different percentages.

4. Adding aggregate to form a mortar, reduces the total pore volume and intruded pore volume and the pore surface area, but increases the density. The reduction in the paste volume due to the aggregate inclusion is greater than the reduction in the total pore volume and the intruded pore volume, which indicates that the aggregate and/or aggregate paste interfaces are also porous. Addition of a small volume of aggregate to HCP, increases the threshold radius, but a further increase in aggregate

volume generally reduces the threshold radius.

5. The total pore volume and the intruded pore volume of mortar and concrete were thought to comprise not only the pores in the paste, but fissures and bond cracks at paste/aggregate interface. These fissures and bond cracks appear to increase with an increase in the aggregate volume.

6. Wax deposits from the crude oil (North Sea and Kuwait) appears to block all pores less than 650 $\mathring{A}$ in radius, and 650 $\mathring{A}$ radius of pore is therefore called the "critical pore radius" (P_{cr}). It is believed to be the minimum pore radius that could influence the permeability of HCP, mortar and concrete to crude oil.

7. Saturation in crude oil appears to alter the internal structure of concrete. The intruded pore volume and the pore surface area were decreased. The hydraulic radius was increased and there was no noticeable effect on the threshold radius of either HCP, mortar or concrete. After saturating HCP in North Sea crude oil, the intruded pore volume and surface area were decreased by 46-56% and 57-70% respectively but the hydraulic radius was increased by 29% for w/c ratio of 0.35 to 0.70.

8. Dry curing at $16 \pm 0.5^{o}C$ and $50 \pm 1\%$ RH, increased the intruded pore volume, the threshold radius and the hydraulic radius, but decreased the strength and has no specific effect on pore surface area, when compared with wet cured (at $21 \pm 1^{o}C$, $99 \pm 1\%$ RH), specimens of the same age. Dry curing of HCP for 28 days increased the intruded pore volume, the threshold radius and hydraulic radius by 1-27%, 54-127% and 51% respectively, but decreased the compressive strength by 20-26% for w/c ratios of 0.40 to 0.70. For the dry cured specimens, no unique relationship was found between the initial w/c ratio or the period of hydration and the pore structure. The development of micro-cracks in the dry cured specimens, was thought to have greatly distorted the pore system.

9.1.4 Permeability of Mortar and Concrete

1. The coefficient of permeability K, for both mortar and concrete

decreased rapidly with time during the initial test period up to 120 hours. After 120 hours, it remained practically constant for up to 200 hours, which was the total test period. For 1:1 c/s ratio, and 0.7 w/c ratio, K decreases by between 3.8 and 12.7 times in the first 24 hours and by a further 1.97 to 3.03 times in the next 97 hours and between 1.02 and 1.08 times in the final 80 hours.

2. K increases exponentially with w/c ratio, approximately linearly with applied hydrostatic pressure but decreases rapidly during the initial stages of hydration up to 3 months and then very slowing in the next 3 months. At an oil pressure head of 83 metres, the K for 28 days cured mortar (1:1 c/s ratio) increased 1.40 times when the w/c is increased from 0.5 to 0.70. For the same 28 day mortar with w/c = 0.5, K increased by 1.36 times as the applied pressure was increased from 33.2 metre head of oil to 99.6 metres. Under a 99.6 metres pressure head of oil, from 7 days to 28 days (0.5 w/c ratio) K decreased by 2.36 times for 1:1 c/s ratio mortar.

3. Increasing the aggregate volume concentration in mortar produces a non-linear increase in K, which can reasonably be represented by the equation below, for 28 days cured mortars

$$K = K_o(\exp)^{b_1(AV)}$$

where AV is the aggregate volume concentration (%) and b_1 and K_o are constants, K is the saturated permeability coefficient for North Sea crude oil flow.

It was thought that fissures and bond cracks did develop in mortars and may have increased the permeability.

4. K for both oil and water flow increases exponentially as the drying temperature of mortar and concrete was increased. For mortar of 1:1½ c/s ratio, 0.5 w/c ratio and at 99.6 metres pressure head of liquid, K (water) for specimens dried to 105°C is 5 times K (water) for specimens

dried to 55°C. For oil flow K is 2.9 times larger for the same change in drying condition.

5. Specimen dimension influences the K values for both oil and water flow. For oil flow under 99.6 metrees pressure head, with 1:1½ c/s ratio, 0.7 w/c ratio mortar, K for 150mm dia. x 50mm thick discs is 1.35 times K for 100mmdia. x 25mm thick disc, which is 1.54 times K for 150mm dia x 25mm thick disc. No detailed explanation for this is offered but clearly standard specimens should be used.

6. K values for mortar and concrete of approximately equal aggregate volume suggests that mortar is more permeable for the first 28 days after which it falls rapidly and becomes less permeable after about 3 months.

7. Pores of radii >650 Å are most effective in determining the permeability of mortar. Using the effective pore volume and surface area rather than the total pore parameters improved the prediction of permeability.

8. K can be related reasonably accurately to these effective pore parameters at any applied pressure, using the Kozeny's theorem in the form

$$K = T_1 \varepsilon_e^3 / S_e^2 + T_2$$

$$T_1 = w_1 h + w_2$$

where K is the saturated permeability of mortar to crude oil (m/s), ε_e is the effective intruded pore volume, S_e is the effective surface area, h is the applied hydrostatic pressure and T_1 and T_2 are constants. T_1 is the tortuosity factor.

Pore size distribution data are used to determine the effective pore parameters and provides a better understanding of the permeability of mortar and concrete to crude oil. Using the pore size distribution data in Kozeny's mathematical model, it is possible to calculate permeability.

9.2 Limitations of the Present Work

The limitations of the present investigations are considered to be as follows.

9.2.1 Materials

1. Saturated permeability at constant temperature was done using only North Sea crude oil and very few using tap water.
2. Only one type of aggregate - natural river gravel, of 10mm and 6.30mm maximum size, and one type of cement, the ordinary portland cement were used.
3. No form of admixtures was considered.

9.2.2 Flow Through Cracks

1. All the artificial cracks were assumed to have constant width and shape which is not true for natural cracks.
2. Only water and North Sea crude oil flow through cracks of five different shapes was considered.
3. The effect of constrictions and abrupt enlargement in the "flow-cell" were not considered.
4. Only one concrete mix proportion was used.

9.2.3 Model Concrete Tank

1. No attempt was made to control the temperature.
2. Only four liquid depths were considered.

9.2.4 Pore Structure Analysis

1. Porosity was determined only by weight loss when drying a SSD specimen to a constant weight at $105^{o}C$.
2. Only the mercury porosimetry method was used in the pore structure analysis.
3. Possible micro-cracking, as a result of drying the specimen to $105^{o}C$ prior to porosimetry test was not quantified.

9.2.5 Permeability Studies

1. Tests were carried out at one temperature only i.e. $16 \pm 0.5^{o}C$,

and a relative humidity of 50 $\pm$ 1%.

2. Tests were only made on small mortar and concrete specimens.

3. To accelerate the oil saturation, samples were first dried to 105°C, which may have affected the permeability results.

9.3 Recommendations for Future Work

For a fuller understanding of the effects of crude oil on the structure and properties of HCP, mortar and concrete, the following areas need to be considered for further work.

1. Study of flow through cracks with variable widths and patterns.

2. Study of the effect of surface texture of cracks such as roughness and frictional resistance on flow.

3. Microscopic examination of the pore structure of HCP, mortar and concrete, with and without admixture and saturated with oil.

4. Study of permeability and flow through cracks in oil soaked concrete made from different aggregates.

5. Study of creep characteristics of oil saturated concrete.

6. Study of aggregate-cement paste bond in oil saturated concrete.

7. Study of the structural behaviour of reinforced and prestressed oil saturated concrete members.

8. Study of the effect of air entrainment, water reducing agents, PFA and other admixtures on the properties and permability of mortar and concrete in direct contact with crude oil.

REFERENCES

1. HAMP, E., (1977). Recent developments in the construction of Liquid tanks. FIP Note No. 67, March/April 1977, pp 11 - 16.

2. PORTLAND CEMENT ASSOCIATION, (1922). Concrete tanks for fuel oil storage, 1920. Abstracted in concrete and constructional Engineering Vol. 17, pp 32 - 35, 1922.

3. PEARSON, J. C., (1944). Tests of gasoline-resistant coatings. Proceedings A.C.I., Vol. 40, pp 281 - 292, 1944.

4. HORNIBROCK, F. B., (1944). The effectiveness of various treatment and coatings for concrete in reducing penetration of Kerosene. Proc. A.C.I., Sept. 1944.

5. GERWICK, B. and HOGNESTAD, (1973). Concrete oil storage tank placed on North Sea floors. A.S.C.E. Civil Eng. Journal, pp 81, Aug. 1973.

6. RICHARDSON, G., (1974). North Sea oil structures: Proc. symp. University of Birmingham on Concrete: can it hold water. Sept. 1974, pp 47 - 54.

7. SHARP, J. V., (1981). Concrete oil production plot forms. The Metallurgist and Materials Technologist, pp 13 - 16, 1981.

8. MARION, H. and MAHFOUZ, G., (1974). Design and Construction of the Ekofisk artificial island. Proc. I.C.E., Vol. 56, Part 1, pp 497 - 511, 635, Nov. 1974.

9. NOTE NO. C406. Concrete tanks for storing petrol. Laboratory Tests on coating and lining material. B.R.S. Technical Note No. C406.

10. MEISSNER, H. and PEARSON, J., (1944). Discussion of the paper. Tests of gasoline-resistant coatings. A.C.I. Proc., Vol. 15, No. 6, pp 292 1944.

11. HANSEN, T. C., (1971). Creep of oil saturated concrete. Proc. Int. Conference on mechanical behaviour of materials, Kyoto, pp 257 - 261, Aug. 1971.

12. LEA, F., (1970). The chemistry of cement and concrete. Edward Arnold (Publ.) Ltd, pp 659 - 665, 1970.

13. MATTI, M. A., (1974). The properties of oil soaked concrete. M. Eng. dissertation, University of Sheffield, 1974.

14. MATTI, M. A., (1976). Some properties and permeability of concrete in direct contact with crude oil. Ph.D. Thesis, University of Sheffield, 1976.

15. FAIYADH, F. J., (1976). Further investigations of the properties of oil soaked concrete. M. Eng. dissertation, University of Sheffield, 1976.

16. FAIYADH, F. J., (1980). Properties of oil saturated concrete. Ph.D. Thesis, University of Sheffield, 1980.

17. OYEKA, C. C., (1978). Pore structure and crude oil permeability of hardened cement paste and concrete. Ph.D. Thesis, University of Sheffield, 1978.

18. THOMAS, T. C. and HSU et al., (1963). Micro-cracking of plain concrete and the shape of stress-strain curve. Journal of American Concrete Institute, No. 60-14, Feb. 1963.

19. SLATE, F. O. and OLSEFSKI, S., (1963). X-rays for study of internal structure and micro-cracking of concrete. Journal of American Concrete Institute, No. 60-31, May 1963.

20. SHAH, S. P. and SLATE, F. O., (1965). Internal micro-cracking, mortar-aggregate bond and stress-strain curve of concrete. Proc. of Int. Conf. on The Structure of Concrete, London, Sept. 1965.

21. BRANDTIZAER, (1928). Study of the failure of concrete under combined compressive stresses. UIEES Bulletin 185, 1928. (University of Illinois, Engineering Experiment Station).

22. MINDESS, S. and DIAMOND, S., (1980). A preliminary SEM Study of crack propagation in mortar. Cement and Concrete Research, Vol. 10, pp 509 - 519, 1980.

23. DERUCHER, K. N., (1978). Application of the Scanning Electron Microscope to Fracture Studies of Concrete. Building and Environment, Vol. 13, pp 135 - 141.

24. BEEBY, A. W., (1978). Cracking: What are crack width limits for? Concrete: The journal of the Concrete Society, Vol. 12, No. 7, July 1978.

25. BS 5337, (1976). Code of practice for the structural use of concrete for retaining aqueous liquids.

26. ANCHOR, R. D., (1976). Structural Design to BS 5337. The Structural Engineer, Vol. 55, No. 3, March 1977.

27. NEVILLE, A. M., (1977). Properties of Concrete. Pitman Publishing Ltd., 2nd. edition.

28. DICK, J. B., (1950). The Fundamentals of natural ventilation in houses. Journal of Int. of Heating and Ventilation Engineers, June 1950.

29. HOPKINS and HANSFORD, (1974). Air flow through cracks. Building Services Engineer, Vol. 42, Sept. 1974.

30. WEBBER, N. B. Fluid Mechanics for Civil Engineers, Chapman and Hall.

31. LYDERSEN, A. L. Fluid flow and heat transfer. John Wiley and Sons.

32. KAY, J. M. An Introduction to fluid mechanics and heat transfer. Cambridge University Press.

33. DUNCAN, W. J. Physical Similarity and Dimensional analysis. Edward Arnold Publishers Ltd.

34. ETHERIDGE, D. W., (1977). Crack flow equations and scale effect. Building and Environment, Vol. 12, pp 181 - 189, 1977.

35. GLANVILLE, W. H., et al, (1947). The grading of aggregates and workability of concrete. Road Research Technical Paper No. 5, London, H.M.S.O., 1947.

36. ROY, D. and GOUDA, G., (1975). Optimization of strength in cement pastes. Cement and Concrete Research, Vol. 5, 1975, pp 153 - 162.

37. LAWRENCE, C., (1973). Porosity/strength relationships for Portland Cement Pastes. IUPAC/RILEM Int. Symp. on Pore Structure and properties of Materials, Vol. 2, Prague 1973, pp D167 - 176.

38. FELDMAN, R. F. and BEAUDOIN, J. J., (1976). Microstructure and Strength of Hydrated Cement. Cement and Concrete Research, Vol. 6, pp 389 - 400, 1976.

39. POPOVICS, S., (1969). Effect of Porosity on the strength of concrete. J. of Materials, J MLSA, Vol. 4, No. 2, pp 356 - 371, June 1969.

40. SCHILLER, K. K., (1958). Porosity and strength of brittle solids (with particular reference to gypsum). Mechanical Properties of Non-metallic Brittle Materials, pp 35 - 45. Butterworth, London, 1958.

41. KROKOSKY, E. M., (1970). Strength vs Structure: a study of hydraulic cements. Materials and Structures 3, No. 17, pp 313 - 323, Paris, Sept.-Oct. 1970.

42. RYSHKEWICH, E., (1953). Compression Strength of porous sintered alumina and Zirconia. J. American Ceramic Society, No. 36, pp 66 - 68, Feb. 1953.

43. CHATTERJI, S., (1979). Analysis of techniques of measuring physical properties of cement paste to obtain microstructural information. Ceramic Bulletin, Vol. 58, No. 2, pp 233 - 234, 1979.

44. POWERS, T. C., (1968). Mechanisms of Shrinkage and reversible creep at Hardened Cement paste. Proc. of Int. Conf. on the Structure of Cement. Cement and Conc. Ass., London, 1968.

45. FELDMAN, R. F. and SEREDA, P. J., (1968). Model for Hydrated Portland Cement Paste as deduced from Sorption-Length Changes and Mechanical Properties. Journal of Material and Structures, RILEM, Vol. 1, No. 6, pp 509 - 520, 1968.

46. CHATTERJI, S., (1976). Physical Properties and Structural Models for Portland Cement Paste. Hydraulic Cement Pastes - Their Structure and properties. Cement and Conc. Ass., London, 1976.

47. HELMUTH, R. and TURK, D., (1967). The reversible and irreversible drying shrinkage of hardened Portland Cement Paste and TriCalcium Silicate Pastes. Bulletin 215, Portland Cement Assoc., 1967.

48. FEGERLAND, G., (1973). Elastic Modulus of Concrete. IUPAC/RILEM Int. Symp. on Pore Structures and Properties of Materials, Vol. II, Prague, 1973, pp D129 - D149.

49. HELMUTH, R. and TURK, D., (1966). Elastic Modulus of hardened Portland Cement and TriCalcium Silicate Pastes: Effect of porosity. Highway Research Board, Special Report 90, 1966, pp 135 - 144.

50. POWERS, T. C., (1975). Freezing Effects in Concrete. Durability of Concrete SP-47, ACI, 1975, pp 1 - 11.

51. NEWMAN, K., (1965). The Structure and properties of Concrete - an introductory review. Proc. of Int. Conf. on the Structure of Concrete C and CA, London, Sept. 1965.

52. ISHAI, O., (1965). The time-dependent deformational behaviour of Cement paste, Mortar and Concrete. Proc. of Int. Conf. on The Structure of Concrete, C and CA, London, Sept. 1965.

53. POWERS, T. C., (1962). Physical properties of Cement paste. Proc. of the 4th. Int. Symp. on the Chemistry of Cement, Washington, 1960. Washington, National Bureau of Standards 1962, Monograph 43, Vol. II, pp 577 - 609.

54. POWERS, T. C., (1958). Structure and physical properties of hardened cement pastes. Journal of American Ceramics Society, Vol. 41, No. 1, Jan. 1958, pp 1 - 6.

55. POWERS, T. C. and BROWNYARD, (1947). Studies on the physical properties of hardened cement pastes. Proc. ACI, Vol. 43, 1947, pp 101, 249, 469, 549, 845 and 933.

56. DUBININ, M. M., (1967). Adsorption in Micropores. Journal of Colloid and Interface Science, Vol. 23, pp 487 - 499, 1967.

57. KARNAUKOV, A. P., (1973). Structure, classification and simulation of porous materials. Pore structure and Properties of Materials, RILEM/ IUPAC, Prague 1973, Vol. 1, pp A3 - A33.

58. BRANAUER, S, EMMETT, P. and TELLER, E., (BET), (1938). Adsorption of gases in multi-molecular layers. J. American Chemical Society, Vol. 10, No. 2, 1938, pp 309 - 319.

59. MIKHAIL, et al., (1964). Pore structure and surface areas of hardened Portland Cement Pastes by Nitrogen Adsorption. Canadian J. of Chemistry, Vol. 42, 1964, pp 426 - 438.

60. CARMAN, P. C., (1956). Flow of gases through porous media. Butterworths, 1956.

61. POWERS, T. C., (1964). The physical structure of Portland Cement Paste. The Chemistry of Cement, Chapter 10, Ed. HFW Taylor, Academic Press.

62. HANSEN, T. C., (1970). Physical composition of hardened cement paste. ACI, Vol. 167, pp 404 - 407, May 1970.

63. POWERS, T. C., (1949). The non-evaporable water content of hardened cement paste: Its significance for concrete research and its determination. A.S.T.M. Bulletin, No. 158, pp 68 - 76, 1949.

64. COPELAND, L. and HAYES, J., (1956). Porosity of hardened Portland Cement Pastes. Journal of American Concrete Institute, ACI, Vol. 56, pp 633 - 640, 1956.

65. BRUNAUER, I., ODLER and YUDENFREUND, M., (1970). New model of hardened Portland Cement Paste, Highway Research Record, No. 328, pp 89 - 101, 105 - 107, 1970.

66. WINSLOW, D. and DIAMOND, S., (1974). Specific surface area of hardened Portland Cement Paste as determined by small angle x-ray scattering. Journal of American Ceramics Society, Vol. 57, No. 5, pp 193 - 197, May 1974.

67. RAMACHANDRAN, V. S., FELDMAN, R. F. and BEAUDON, J. J., (1981). Concrete Science. Hayden and Sons Ltd., 1981.

68. FELDMAN, R. F., (1968). Sorption and length-change scanning isotherms of methanol and water on hydrated Portland Cement. Proc. 5th. Int. Congress on Chemistry of Cement. Tokyo, Vol. III, pp 36 - 44, 1968.

69. FELDMAN, R. and RAMACHANDRAN, V., (1971). Differentiation of Interlayer and adsorbed water in hydrated Portland Cement by thermal analysis. Cement and Concrete Research, Vol. 1, No. 6, pp 607 - 620, 1971.

70. FELDMAN, R., (1971). Assessment of experimental evidence for models of hydrated Portland Cement. Highway Research Record, No. 370, pp 8 - 24, 1971.

71. FELDMAN, R., (1972). Helium flow and density measurement of hydrated TriCalcium Silicate - water system. Cement and Concrete Research, Vol. 2, No. 1, pp 123 - 236, 1972.

72. FELDMAN, R., (1972). Mechanism of creep of hydrated Portland Cement Paste. Cement and Concrete Research, Vol. 2, No. 5, pp 521 - 540, 1972.

73. SEREDA, P. and RAMACHANDRAN, V., (1975). Prediction gap between Science and Technology of Cements. II Physical and mechanical behaviour of hydrated cements. J. of American Ceramics Society, Vol. 58, No. 5-6, pp 249 - 253, 1975.

74. HOPE, B. and BROWN, N., (1975). A model for the creep of concrete. Cement and Concrete Research, Vol. 5, No. 5, pp 577 - 586, 1975.

75. FELDMAN, R., (1972). Density and porosity studies of hydrated Portland Cements. Cement Technology, Vol. 3, pp 5 - 14, 1972.

76. MIKHAIL, R., et al., (1975). Dimensions of average pore, the number of pores and surface area of hardened Portland Cement Pastes. Cement and Concrete Research, Vol. 5, pp 433 - 442, 1975.

77. BRUNAUER, S., et al., (1970). The new model of hardened Cement Paste. Highway Research Record, No. 328, pp 89 - 101, 105 - 107, 1970.

78. FELDMAN, R., (1972). Reply to discussions by Brunauer. Cement and Concrete Research, Vol. 2, No. 4, pp 493 - 498, 1972.

79. BRUNAUER, S., (1972). Discussion of Helium flow results. Cement and Concrete Research, Vol. 2, No. 4, pp 489 - 492, Vol. 2, No. 6, pp 749 - 753, 1972.

80. WINSLOW, D. N. and DIAMOND, S., (1970). A mercury porosimetry study of the evolution of porosity in Portland Cement. Journal of Materials J.M.L.S.A., Vol. 5, No. 3, pp 564 - 585, Sept. 1970.

81. WITTMAN, F. H., (1980). Properties of hardened cement paste. 7th. Int. Congress on the Chemistry of Cement, Vol. 1, Paris, 1980.

82. WITTMAN, F. H., (1976). The structure of hardened cement paste - a basis for a better understanding of the material's properties. Proc. of Conf. on Hydraulic Cement Pastes - Their Structure and Properties, Sheffield, pp 96 - 117, 1976.

83. DIAMOND, S., (1976). Cement paste micro-structure - An overview at several levels. Proc. Conf. Hydraulic Cement Pastes - Their Structure Properties, Sheffield, pp 2 - 36, 1976.

84. BERGER, R. L., et al., (1972). Discussion of the paper's morphology and surface properties of hydrates in TriCalcium Silicate paste by M. Collepardi and B. Merchese. Cement and Concrete Research, Vol. 2, pp 633 - 636, 1972.

85. TAYLOR, H. F. W., (1979). Mechanism and products of Portland Cement hydration. Contribution to the Annual meeting of Japan Cement Assoc., 1979.

86. MIDGLEY, H. G. and PETTIFER, K., (1970). The effect of w/c ratio on the micro-structure of set Portland Cement. Micron, Vol. 1, pp 428 - 432, 1970.

87. LENTZ, C. W., (1966). The silicate structure analysis of hydrated Portland Cement Paste. Highway Research Board, Washington D.C., Special Report, No. 90, pp 209 - 283, 1966.

88. TAMAS, D. D., et al., (1976). Effect of variables upon the silylation products of hydrated cements. Proc. Conf. Hydraulic Cement Pastes - Their Structure and Properties, Sheffield, pp 55 - 72, 1976.

89. SARKAR, A. K. and ROY, D. M., (1979). A new characterization technique for trimethylsilyated products of oil cement pastes. Cement and Concrete Research, Vol. 9, pp 342 - 352, 1979.

90. LACHOWSKI, E. E., (1979). Trimethylsilylation as a tool for the study of cement pastes (1) Comparison of methods of derivation. Cement and Concrete Research, Vol. 9, pp 111 - 114, 1979.

91. LACHOWSKI, E. E., (1979). Trimethylsilylation as a tool for the study of cement pastes (2) Quantitative analysis of the silicate fraction of Portland Cement Pastes. Cement and Concrete Research, Vol. 9, pp 337 - 342, 1979.

92. DENT-GLASSER, et al., (1978). A multi-method study of C_3s hydration. Cement and Concrete Research, Vol. 8, pp 733, 1978.

93. TAMAS, J. and AMRICH, L., (1978). Layer chromotographic separation of silicate oligomeris formed during the hydration of Portland Cement II Cernento 75, pp 352 - 362, 1978.

94. FONTENAY, C. and SELLVOLD, E. J., (1978). Ice formation in hardened cement paste. 1 Water saturated paste. Proc. Int. Conf. on Durability of building materials and components, Ottawa, 1978.

95. LITVAN, G. G., (1978). Adsorption systems at temperature below the freezing point of the adsorptive. Advances in Colloid and Interface Science, Vol. 9, pp 253 - 302, 1978.

96. VIGNES-ADLER, M., (1977). On the origin of the water aspiration in a freezing dispersed medium. J. of Coll. Interface Science, No. 60, pp 162 - 171, 1977.

97. WHEELER, A., (1951). Advanced Catalysis, Vol. 3, pp 349, 1951.

98. RITTER, H. and DRAKE, L., (1945). Industrial Engineering Chemical Analysis, Vol. 17, pp 782, 1945.

99. MIKHAIL, R. SH, et al., (1968). Investigation of a complete pore structure analysis II Analysis of four silica gels. Journal of Colloid and Interface Science, No. 26, pp 54 - 61, 1968.

100. BRUNAUER, et al., (1967). Some remarks about capillary condensation and pore structure analysis. J. of Colloid and Interface Science, No. 25, pp 353 - 358, 1967.

101. HAYNES, J. M., (1973). Pore size analysis according to the Kelvin equation. Material and Construction, Vol. 6, No. 33, 1973.

102. HAGYMASSY, J., et al., (1972). Pore structure analysis by water vapour adsorption III Analysis of hydrated calcium silicate and Portland Cement. Journal of Colloid and Interface Science, Vol. 38, No. 1, 1972.

103. WEATHERWAX, R. C., (1977). Collapse of cell wall pores during drying of cellulose. Journal of Colloid and Interface Science, Vol 62, No. 3, pp 432 - 445, 1977.

104. DIAMOND, S., (1971). A critical comparison of mercury porosimetry and capillary condensation pore size distributions of Portland Cement Pastes. Cement and Concrete Research, Vol.1, pp 531 - 545, 1971.

105 DIAMOND, S., (1970). Proc. 3rd. Annual Scanning Electron Microscope Symposium, Chicago III, pp 387, 1970.

106. BENTUR, A., (1980). The pore structure of hydrated cementiticus compounds of different chemical composition. J. of the American Ceramic Society, Vol. 63, No. 7-8, pp 381-386, 1980.

107. GREGG, S. J. and SING, K. S. W., (1967). Adsorption, surface area and porosity, Academic Press, 1967.

108. LOWELL, S., (1981). Equivalence of mercury porosimetry and gas adsorption. Powder Technology, Vol. 29, pp 225 - 231, 1981.

109. MEHTA, P. K. and MANMOHAN, D., (1980). Pore size distribution and permeability of hardened cement pastes. 7th. Int. Congress on the Chemistry of Cement, Vol. III, Paris, 1980.

110. WINSLOW, D. N. and LOVELL, C. W., (1981). Measurement of pore size distribution in cements aggregates and soils. Powder Technology, Vol. 29, pp 151 - 165, 1981.

111. NYAME, B. K. and ILLSTON, J. M., (1980). Capillary pore structure and permeability of hardened cement paste. 7th. Int. Conf. on the Chemistry of Cement, Paris, VI, pp 182, 1980.

112. SELLEVOID, E. J., (1974). Mercury porosimetry of hardened cement paste cured and stored at 97°C. Cement and Concrete Research, Vol. 4, No. 3, pp 399 - 404, 1974.

113. BAGER, D. H. and SELLEVOID, E. J., (1975). Mercury porosimetry of hardened cement paste - The influence of particle size. Cement and Concrete Research, Vol. 5, pp 171 - 178, 1975.

114. NYAME, B. K., (1979). Permeability and pore structure of hardened cement paste and mortar. Thesis submitted to the University of London for the degree of Ph.D., 1979.

115. KANTRO, D. L., et al., (1967). BET surface area - methods of interpretation, Chapter 12, Vol. 1, solid-gas interface ed. E. Alison Flood, Edward Arnold, London, 1967.

116. FELDMAN, R. F., et al., (1970). A new model for hydrated Portland Cement and its practical implications. Engineering Journal, Vol. 53, No. 8/9, pp 53 - 59, 1970.

117. FELDMAN, R. F., (1973). Volume change, porosity and helium flow studies of hydrated Portland Cement. RILEM/IUPAC, Prague, 1973, pp C101 - 106.

118. DUBINNIN, M. M., (1973). On the specific surface area of micropore containing adsorbents. RILEM/IUPAC, Vol. 4, pp C27, Prague, 1973.

119. DUBINNIN, M. M., (1973). Methods of determination of pore structure: adsorption method. RILEM/IUPAC, Vol. 4, pp C5, Prague, 1973.

120. BRUNAUER, S., et al., (1967). Pore structure analysis without a pore shape model. J. of Colloid and Interface Science, Vol. 24, pp 451 - 463, 1967.

121. BRUNAUER, S., et al., (1973). Complete pore structure analysis. RILEM/IUPAC, Part 1, pp C3 - C27, 1973.

122. MIKHAIL, R., et al., (1968). Investigations of a complete pore structure analysis (I) Analysis of micropores. J. of Colloid and Interface Science, Vol. 26, pp 45 - 53, 1968.

123. DUBINNIN, M. M., (1974). On the physical feasibility of Brunauer's micropore analysis method. J. of Coll. and Inter. Science, Vol. 46, No. 3, pp 351 - 356, 1974.

124. BERING, B. P., et al., (1972). On the thermodynamics of adsorption in micropores. J. of Coll. and Inter. Science, Vol. 38, pp 185 - 194, 1972.

125. MIKHAIL, R., et al., (1975). Surface area measurements by Nitrogen and Argon Adsorption. J. of Coll. and Inter. Science, Vol. 52, No. 3, pp 572 - 577, 1975.

126. HAGYMASSY, J., et al., (1969). Pore structure analysis by water vapour adsorption; t-curves for water vapour. J. of Coll. and Inter. Science, Vol. 29, No. 3, 1969.

127. BRAKEL, J. V., et al., (1981). Mercury porosimetry: state of the Powder Technology, Vol. 29, No. 1, pp 1 - 2, 1981.

128. GOOD, R. J. and MIKHAIL, R. SH., (1981). The contact angle in mercury intrusion porosimetry. Powder Technology, Vol. 29, No. 1, pp 53 - 62, 1981.

129. CARLO-ERBA. Mercury porosimeter manual for operation, Model 200.

130. HARRIS, D. H. C., et al., (1974). Free and bound water in cement pastes. Magazine of Concrete Research, Vol. 26, No. 87, pp 65 - 72, 1974.

131. SEREDA, P. J., et al., (1980). Structure formation and development in hardened cement paste. 7th. Int. Congress on Chemistry of Cement, Vol. 1, Paris, 1980.

132. BEAUDOIN, J. J. and FELDMAN, R. F., (1978). The significance of helium diffusion measurements in studying the removal of structural water in inorganic hydrated systems. Cement and Concrete Research, Vol. 8, pp 223 - 232, 1978.

133. FELDMAN, R. F., (1971). The flow of helium into the interlayer spaces of hydrated Portland Cement Pastes. Cement and Concrete Research, Vol. 1, pp 285, 1971.

134. REUTTGERS, A., et al., (1935). An investigation of the permeability of mass concrete with particular reference to boulder dam. Proc. ACI, Vol. 31, pp 382 - 416, 1935.

135. BEAR, J. and BRAESTER, C., (1972). Fundamentals of transport phenomena in porous media. Elsevier, Amsterdam, 1972.

136. SLATTERY, J. C., (1972). Momentum, energy and mass transfer in continue. MaGraw-Hill, 1972.

137. MUSKAT, M., (1937). The flow of homogeneous fluids through porous media. McGraw-Hill, 1937.

138. CARMAN, P. C., (1956). Flow of gases through porous media. Butterworths, 1956.

139. POWERS, T., et al., (1959). Flow of water in hardened Portland Cement Paste. Highway Research Board, Special Report, No. 40, pp 308 - 323, 1959.

140. SCHEIDEGGER, A. E., (1960). The physics of flow through porous media. University of Toronto Press, 1960.

141. POWERS, T. C., et al., (1959). Capillary continuity or discontinuity in cement pastes. Portland Cement Association, Research and Development Lab., Vol. 1, No. 2, May 1959, pp 38 - 48.

142. BENNER, F. C., et al., (1943). In fundamental research on occurrence and recovery of petroleum. Published by American Petroleum Institute, 1943, pp 74.

143. FATT, I., (1956). Transaction A.I.M.E. 207, Vol. 144, 1956.

144. NYAME, B. K. and ILLSTON, J. M., (1981). Relationship between permeability and pore structure of hardened cement paste. Mag. of Concrete Research, Vol. 33, No. 116, pp 139 - 146, 1981.

145. CARMAN, P., (1941). In Symposium on New Models of Particle Size Distribution in Subsieve range. A.S.T.M. Publication, pp 24, 1941.

146. POWERS, T., (1968). The properties of fresh concrete. John Wiley and Sons, New York, 1968.

147. RIDEAL, E. K., (1941). Diffusion in and through solids. The Cambridge series of physical chemistry, Cambridge University Press, 1941.

148. HALL, C., (1977). Water movement in porous building materials I Unsaturated flow theory and its applications. Building and Environment, Vol. 12, pp 117 - 125, 1977.

149. PHILIP, J. R., (1955). Numerical solution of equations of the diffusion type with diffusivity concentration-dependent. Trans. Faraday Society, Vol. 51, pp 885 - 892, 1955.

150. PHILIP, J. R., (1969). Theory of Infiltration. Adv. hydroscience, 5, pp 215 - 296, 1969.

151. JANSSON, I., (1965). Testing the rate of water absorption. RILEM/ CIB, symposium on moisture problems in buildings, Helsinki, 1965.

152. POWERS, T. C., et al., (1954). Permeability of Portland Cement Paste. Journ. of ACI, Vol. 51, Nov. 1954, pp 285 - 298.

153. MCMILLAN, F. R. and LYSE, W., (1929). Some permeability studies of concrete. Proc. ACI, Vol. 26, 1929, pp 101.

154. HIGGINSON, E. C., (1961). Effect of steam curing on the important properties of concrete. Journ. ACI, Vol. 58, No. 3, pp 281, 1961.

155. Recommended practice for atmospheric pressure steam curing of concrete. Journal of ACI, Vol. 66, pp 629, 1969.

156. TYLER, I. L. and ERLIN, B., (1968). A proposed simple method for determining the permeability of concrete. J. of Portland Cement Association, Res. of Dev. Lab., Vol. 3, No. 3, pp 2 - 7.

157. BRACS, G., et al., (1970). Use of electrical resistance probes in tracing moisture permeation through concrete. Proc. ACI, Vol 67, No. 8, pp 642, 1970.

158. MURATA, J., (1965). Studies on the permeability of concrete. Bulletin RILEM No. 29, 1965, pp 47.

159. TOY, H. C., (1924). The permeability of concrete. ICE. selected Engineering papers, No. 20, 1924.

160. NORTON, P. T. and PIETTA, D. H., (1931). The permeability of gravel concrete. J. of ACI, Vol. 27, pp 1093, 1931.

161. WATSON, A. J. and OYEKA, C. C., (1981). Oil permeability of hardened cement pastes and concrete. Magazine of Concrete Research, Vol. 33, No. 115, pp 85 - 95, 1981.

162. POWERS, T. C., (1979). The specific surface area of hydrated cement obtained from permeability data. Materials and Construction, Vol. 12, No. 69, pp 159 - 168, 1979.

163. HANCOX, N. L., (1968). An electrical measurement of the effective cross-sectional area for conduction or flow process in cement paste. Magazine of Concrete Research, Vol. 20, No. 64, pp 171 - 175, 1968.

164. DUNAGAN, W. H., (1939). Method of measuring the passage of water through concrete. Proc. A.S.T.M., Vol. 39, pp 866, 1939.

165. PIHLAJAVAARA, S. E. and PARROL, H., (1975). On the correlation between permeability properties and strength of concrete. Cement and Concrete Research, Vol. 5, pp 321 - 328, 1975.

166. LEVITT, M., (1971). The I.S.A.T., A non-destructive test for the durability of concrete. Brit. Journ. of Non-destructive testing, Vol. 13, No. 4, pp 106 - 112, 1971.

167. FIGG, J. W., (1973). Methods of measuring the air and water permeability of concrete. Magazine of Concrete Research, Vol. 5, No. 85, pp 213 - 219, 1973.

168. LEVITT, M., (1970). Non-destructive testing of concrete by initial surface adsorption method. I.C.E. Conf. on non-destructive testing of concrete and timber, London, 1970.

169. GLANVILLE, W. H., (1931). The permeability of Portland Cement Concrete. Building Research Technical paper No. 3, 1931.

170. B.S. 1881, Part 5, (1970). Methods of testing hardened concrete for other than strength, B.S. 1881, Part 5, 1970.

171. VALENTA, O., (19-9). Kinetics of water penetration into concrete as an important factor of its deterioration and of reinforcement corrosion. RILEM, Symposium on durability of concrete, pp A-177 - A-189, 1969.

172. REDSHAW, S. C., et al., (1967). Laboratory tests for absorption and angularity of aggregates. Research Report RR/C3, Dept. of Civil Eng. University of Birmingham.

173. TEYCHENNE, D., FRANKLIN, R. and ERNTROY, H., (1975). Design of Normal Concrete mixes. Department of the Environmental B.R.E., H.M.S., London, 1975.

174. MIDGLEY, H. C., (1969). Electron microscopy of set Portland Cement Structure, solid mechanics and engineering design. Proc. of Conf. at Univ. of Southampton, Session III, pp 275, 1969.

175. KIRILLOV, A. P., (1966). The mechanism of water seepage through concrete. Hydrotechnical Construction No. 5, pp 369 - 372, March 1966.

176. HARKER, J. H. and BACKHURST, J. R., (1981). Fuel and Energy, Academic Press, 1981.

177. ORR, C., (1969). Review of the mercury porosimeter technique. Powder Technology, Vol. 3, pp 117, 1969.

178. DIAMOND, S., (1973). Pore structure of hardened cement pastes as influenced by hydration temperature. IUPAC/RILEM Int. Symposium on Pore structure and properties of materials, Vol. 1, Prague, pp B73 - 88, 1973.

179. TAPLIN, J., (1959). A method for following the hydration reaction in Portland Cement Paste. J. of Applied Science, Vol. 10, pp 329 - 345, 1959.

180. SOROKA, I. and RELIS, M., (1977). Variation in density of Portland Cement hydration products. Cement and Concrete Research, Vol. 7, pp 673 - 680, 1977.

181. HUNT, C. M., (1966). Structure of Portland Cement Paste and concrete. Highway Research Board, Special Report No. 90, pp 112 - 122. 1966

182. MOSCOV, L. and LUB, S., (1981). Practical use of mercury porosimetry in the study of porous solids. Powder Technology, Vol. 29, pp 45 - 52, 1981.

183. OKPALA, D. C., (1979). Temperature effects on bridge decks. M.Eng. dissertation, University of Sheffield, 1979.

184. COOK, H. K., (1951). Permeability of lean mass concrete. Proc. American Soc. for Testing and Materials (A.S.T.M.), Vol. 51, pp 1156 - 1165, 1951.

185. ROBSON, R. A., (1965). Mobility of water in porous media of high surface area. Bulletin RILEM No. 27, pp 65, 1965.